DEVELOPMENT OF A PERFORMANCE-BASED SEISMIC DESIGN PHILOSOPHY FOR MID-RISE WOODFRAME CONSTRUCTION

NEESWOOD

INTEGRATION OF SEISMIC PROTECTION SYSTEMS IN PERFORMANCE-BASED SEISMIC DESIGN OF WOODFRAMED STRUCTURES



By
Jayesh K. Shinde and Michael D. Symans

Technical Report MCEER-10-0003 ■ June 18, 2010

This research was conducted at Rensselaer Polytechnic Institute and was supported by the National Science Foundation under Grant No. CMMI-0529903 (NEES Research) and CMMI-0402490 (NEES Operations).

Sponsored by the
National Science Foundation
NSF Grant Number CMMI-0529903 and CMMI-0402490

Project Title
Development of a Performance-Based Seismic Design
Philosophy for Mid-Rise Woodframe Construction

Project Team
Colorado State University
University of Delaware
University at Buffalo, State University of New York
Rensselaer Polytechnic Institute
Texas A&M University

Web Site
www.engr.colostate.edu/NEESWood

DISCLAIMER

This report is based upon work supported by the National Science Foundation under Grant No. CMMI-0529903 (NEES Research) and CMMI-0402490 (NEES Operations). Any opinions, findings, and conclusions or recommendations expressed in this material are those of the investigators and do not necessarily reflect the views of MCEER, the National Science Foundation, or other sponsors.

NEESWood Report No. 6

Integration of Seismic Protection Systems in Performance-Based Seismic Design of Woodframed Structures

by

Jayesh K. Shinde[1] and Michael D. Symans[2]

Publication Date: June 18, 2010
Submittal Date: February 24, 2010

Technical Report MCEER-10-0003

NSF Grant Numbers CMMI-0529903 and CMMI-0402490

1 Graduate Student, Department of Civil and Environmental Engineering, Rensselaer Polytechnic Institute
2 Associate Professor, Department of Civil and Environmental Engineering, Rensselaer Polytechnic Institute

MCEER
University at Buffalo, State University of New York
Red Jacket Quadrangle, Buffalo, NY 14261
Phone: (716) 645-3391; Fax (716) 645-3399
E-mail: *mceer@buffalo.edu*; WWW Site: *http://mceer.buffalo.edu*

Project Overview

NEESWood: Development of a Performance-Based Seismic Design Philosophy for Mid-Rise Woodframe Construction

While woodframe structures have historically performed well with regard to life safety in regions of moderate to high seismicity, these types of low-rise structures have sustained significant structural and nonstructural damage in recent earthquakes. To date, the height of woodframe construction has been limited to approximately four stories, mainly due to a lack of understanding of the dynamic response of taller (mid-rise) woodframe construction, nonstructural limitations such as material fire requirements, and potential damage considerations for nonstructural finishes. Current building code requirements for engineered wood construction around the world are not based on a global seismic design philosophy. Rather, wood elements are designed independently of each other without considering the influence of their stiffness and strength on the other structural components of the structural system. Furthermore, load paths in woodframe construction arising during earthquake shaking are not well understood. These factors, rather than economic considerations, have limited the use of wood to low-rise construction and, thereby, have reduced the economical competitiveness of the wood industry in the U.S. and abroad relative to the steel and concrete industry. This project sought to take on the challenge of developing a direct displacement based seismic design philosophy that provides the necessary mechanisms to safely increase the height of woodframe structures in active seismic zones of the U.S. as well as mitigating damage to low-rise woodframe structures. This was accomplished through the development of a new seismic design philosophy that will make mid-rise woodframe construction a competitive option in regions of moderate to high seismicity. Such a design philosophy falls under the umbrella of the performance-based design paradigm.

In Year 1 of the NEESWood Project, a full-scale seismic benchmark test of a two-story woodframe townhouse unit that required the simultaneous use of the two three-dimensional shake tables at the University of Buffalo's NEES node was performed. As the largest full-scale three-dimensional shake table test ever performed in the U.S., the results of this series of shake table tests on the townhouse serve as a benchmark for both woodframe performance and nonlinear models for seismic analysis of woodframe structures. These efficient analysis tools provide a platform upon which to build the direct displacement based design (DDBD) philosophy. The DDBD methodology relies on the development of key performance requirements such as limiting inter-story deformations. The method incorporates the use of economical seismic protection systems such as supplemental dampers and base isolation systems in order to further increase energy dissipation capacity and/or increase the natural period of the woodframe buildings.

The societal impacts of this new DDBD procedure, aimed at increasing the height of woodframe structures equipped with economical seismic protection systems, is also investigated within the scope of this NEESWood project. Following the development of the DDBD philosophy for mid-rise (and all) woodframe structures, it was applied to the seismic design of a mid-rise (six-story) multi-family residential woodframe condominium/apartment building. This mid-rise woodframe structure was constructed and tested at full-scale in a series of shake table tests on the E-Defense (Miki) shake table in Japan. The use of the E-Defense shake table, the largest 3-D shake table in the world, was necessary to accommodate the height and payload of the mid-rise building.

The research presented in this report focuses on the unique characteristics of woodframed structures that affect the design and implementation of seismic protection systems, and approaches used to increase the performance reliability of these structures in regions of high seismic intensity. In addition, the development of simplified nonlinear analysis and design procedures for structures that incorporate seismic protection systems are discussed. Finally, the results from experimental shaking table tests and nonlinear dynamic response-history analyses are presented to clearly demonstrate the improved seismic performance that can be achieved via application of seismic protection systems to woodframed structures.

Project Team

John W. van de Lindt, Ph.D., Principal Investigator: Associate Professor, Department of Civil Engineering, Colorado State University, Fort Collins, CO 80523-1372; *jwv@engr.colostate.edu*.

Rachel A. Davidson, Ph.D., Co-Principal Investigator: Associate Professor, Department of Civil and Environmental Engineering, University of Delaware, Newark, DE 19716-3120; *rdavidso@udel.edu.*

Andre Filiatrault, Ph.D. Eng., Co-Principal Investigator: Professor Department of Civil, Structural, and Environmental Engineering, State University of New York at Buffalo, Buffalo, New York 14261; *af36@buffalo.edu*.

David V. Rosowsky, Ph.D., Co-Principal Investigator: A.P. Florence Wiley Chair Professor and Department Head, Texas A&M University, Department of Civil Engineering, College Station, TX 77843-3136; *rosowsky@tamu.edu*.

Michael D. Symans, Ph.D., Co-Principal Investigator: Associate Professor, Department of Civil and Environmental Engineering, Rensselaer Polytechnic Institute, 110 8th Street, Troy, NY 12180-3590; *symans@rpi.edu*.

ABSTRACT

The application of seismic protection systems in light-framed wood structures is virtually non-existent within the U.S. as woodframed construction has generally been considered to perform well during earthquakes. However, the 1994 Northridge Earthquake clearly demonstrated the vulnerability of such construction in that extensive, and in many cases unrepairable, damage occurred in thousands of woodframed buildings. As a result, a research project (the NEESWood project) was initiated with an emphasis on developing a seismic design approach that considers multiple levels of performance. As part of this project, the application of seismic protection systems (seismic damping and isolation systems) to woodframed buildings was investigated. The research focused on the unique characteristics of woodframed structures that affect the design and implementation of seismic protection systems and approaches used to increase the performance reliability of woodframed structures in regions of high seismic intensity. In addition, simplified nonlinear analysis and design procedures for structures that incorporate seismic protection systems were developed. The results from experimental shaking table tests and nonlinear dynamic response-history analyses were used to demonstrate the improved seismic performance that can be achieved via application of seismic protection systems to woodframed structures.

ACKNOWLEDGMENT

Technical assistance provided by the members of the "NEESWood" research team, including Dr. John van de Lindt and Dr. Hongyan Liu (Base Isolation), Dr. Andre Filiatrault (Benchmark Testing), Dr. David Rosowsky and Dr. Wei Pang (DBD), is gratefully acknowledged. We are also thankful to the undergraduate research assistants who participated in the project, including James Lucas, Frank Cook, Jasan LaSasso, Sophia Stehr, Tequisha Hendrickson, and James Knoll. We want to especially express our gratitude to Jasan LaSasso who assisted with the construction of the experimental test specimens.

Financial support for this project was provided by the National Science Foundation under Grant No. CMMI-0529903 (NEES Research) and CMMI-0402490 (NEES Operations). In addition, financial assistance from the Department of Civil and Environmental Engineering at Rensselaer Polytechnic Institute is appreciated.

The fluid viscous dampers used in the experimental tests were manufactured and donated by Taylor Devices, Inc. of North Tonawanda, NY. Technical assistance provided by Mr. Douglas Taylor (President) and Mr. John Metzger (Engineering Manager) of Taylor Devices, Inc., is gratefully acknowledged. The Friction Pendulum System isolation bearings in the experimental tests were manufactured and donated by Earthquake Protection Systems (EPS), Inc. The support of Dr. Victor Zayas of EPS is appreciated.

TABLE OF CONTENTS

TABLE OF CONTENTS (CONT'D)

TABLE OF CONTENTS (CONT'D)

TABLE OF CONTENTS (CONT'D)

TABLE OF CONTENTS (CONT'D)

TABLE OF CONTENTS (CONT'D)

LIST OF FIGURES

LIST OF FIGURES (CONT'D)

LIST OF FIGURES (CONT'D)

LIST OF FIGURES (CONT'D)

LIST OF TABLES

LIST OF TABLES (CONT'D)

1. INTRODUCTION

The application of seismic protection systems in light-framed wood structures is virtually non-existent within the U.S. as woodframed construction has generally been considered to perform well during earthquakes. However, the 1994 Northridge Earthquake clearly demonstrated the vulnerability of such construction in that extensive, and in many cases unrepairable, damage occurred in thousands of woodframed buildings. As a result, a research project (the NEESWood project) was initiated with an emphasis on developing a seismic design approach that considers multiple levels of performance. As part of this project, the application of seismic protection systems (seismic damping and isolation systems) to woodframed buildings was investigated.

The research presented in this report will focus on the unique characteristics of woodframed structures that affect the design and implementation of seismic protection systems and approaches used to increase the performance reliability of woodframed structures in regions of high seismic intensity. In addition, the development of simplified nonlinear analysis and design procedures for structures that incorporate seismic protection systems will be discussed. Finally, the results from experimental shaking table tests and nonlinear dynamic response-history analyses will be presented to clearly demonstrate the improved seismic performance that can be achieved via application of seismic protection systems to woodframed structures.

1.1 Need for Seismic Hazard Mitigation of Woodframed Structures

Although woodframed construction in the U.S. has generally been considered to perform well during earthquakes, the 1994 Northridge Earthquake (Moment Magnitude = 6.8) clearly demonstrated the seismic vulnerability of such construction (Kircher et al. 1997). The estimated property losses in woodframed buildings, majority of which includes single family residential housing, were approximately $20 billion and 24 of the 25 fatalities occurred in such buildings. Additionally, 48,000 housing units, almost all of them in woodframed buildings, were rendered uninhabitable by the earthquake underscoring the fact that the conventionally designed woodframed structures perform well with regard to life safety but suffer significant structural and non-structural damage making them uninhabitable during severe seismic events. Note that the single family residential housing in North America primarily consists of woodframed construction and accounts for the single largest investment of owners during their lifetime and thus the overall impact of a major earthquake become particularly important with regard to an economic loss. Seismic hazard mitigation of woodframed structures is very important in that regard as it will help to protect the investments of owners by reducing a seismic risk.

1.2 Role of DBD in Seismic Hazard Mitigation of Structures

For many years, performance-based seismic design (PBSD) has been outlined in design codes as a prescriptive method based on force calculations. However, due to severe damage structures experienced in recent major earthquakes, there has been a gradual

shift in focus from force-based design to displacement-based seismic design (DBD). For example, older structures that were designed according to old code guidelines have experienced major problems related to displacement-induced damage and thus DBD provides a useful design approach for retrofitting of those structures. Since the strong correlation between inter-story drift and the level of damage has been established in different structures, in the displacement-based seismic design (DBD) damage limitation requirements (i.e., performance levels) are explicitly considered at the start of design in terms of inter-story drift limits for a given hazard level. In contrast, in the force-based design, deflection calculations are done at the end of design to check safety and serviceability requirements. DBD also allows imposing multiple performance levels for multiple hazard levels to meet the collective design objective. Note that seismic protection systems can be used effectively to achieve higher design performance levels for high seismic hazard. One popular DBD procedure proposed by Priestly et al. (1998, 2007) is being extensively adopted by design practitioners and researchers and it is explicitly known as a direct displacement-based design (DDD).

1.2.1 Overview of Direct Displacement-Based Seismic Design

The fundamental difference between the force-based design and the direct displacement-based design (DDD) is that the former characterizes the structure with a constant stiffness and thus different yield displacements while the latter considers the realistic conditions of varying stiffnesses with a constant yield displacement (Priestly 2007). Since the peak inter-story drift provides a key measure of the structural and nonstructural damage in a building during an earthquake, the realistic representation of damage is only possible in the displacement-based design. The force-based design uses an initial stiffness and assumed damping (typically 5%). This damping accounts for inherent "viscous" damping through a rate-dependent damping model. The displacement dependent nature of energy dissipation in real structures is not explicitly considered. The DDD uses the secant stiffness at design displacement and associated equivalent damping. The equivalent damping is determined based on the hysteretic energy dissipation (displacement-dependent energy dissipation) at the design displacement which is often difficult to quantify for structures subjected to damage. This approach to

modeling energy dissipation is particularly relevant for woodframed structures since they exhibit highly nonlinear behavior when subjected to strong seismic excitation. Including seismic protection systems to reduce damage to the structures enables the designer to quantify damping more accurately, and thus it improves reliability of the DDD procedure.

1.3 Role of Seismic Protection Systems in Seismic Hazard Mitigation of Structures

One approach to protect structures during a large seismic event is to incorporate an advanced seismic protection system. Seismic protection system reduces the response of the structure during seismic excitations either by changing fundamental characteristics of structure (e.g., a base isolation system increases the fundamental natural period of the supported structure) or by providing additional means to absorb seismic input energy (e.g., an energy dissipation provides supplemental damping). In general, the application of seismic protection systems is helpful to achieve the following objectives:

- To mitigate damage and thus protect the investments of owners.
- To reduce the cost of insurance premiums by reducing seismic risk.
- To improve performance such that loss of life and injuries are reduced.
- To make architecturally attractive design (large openings) possible by reducing the stiffness demand on the structure.
- To retrofit old structures to meet higher performance levels.

1.3.1 Role of Energy Dissipation Systems in Seismic Protection

The amplitude of structural response tends to decrease with time when the excitation force becomes zero. This reduction is often due to various energy loss mechanisms present inherently within the structure or develop during the course of excitation. The energy loss is also known as energy dissipation or damping. The role of damping in structural response is evident from the equation of motion of dynamic system. As the damping increases, the restoring forces (developed due to the structural resistance to displacement) decrease. Seismic input energy within the structure can be dissipated through cracks, friction, and in general any inelastic response. Application of energy

dissipation systems (which provides supplemental damping to the structure) reduce seismic response of the structure by dissipating seismic input energy, thereby reducing the amount of energy dissipated via inelastic behavior and thus damage to structural members (also see Figure 1.1c). There are various types of energy dissipation system available depending on the desired dissipation mode (e.g., fluid viscous dampers, visco-elastic dampers and friction dampers).

1.3.2 Role of Base Isolation Systems in Seismic Protection

The damage potential of an earthquake is essentially due to the close match between the fundamental frequencies of vibration of the majority of structures and the frequency content of the majority of seismic excitations (i.e., similar to resonance phenomena). During earthquakes, many structures can survive by escaping the dominant frequency range of the earthquake via the period elongation caused by accumulated damage. Seismic base isolation uses the same concept of shifting the fundamental period of a structure away from the dominant period range of earthquake ground motions (majority of earthquakes have dominant periods in the range of 0.1 to 0.6 sec) and thereby decoupling a structure from its foundation to reduce the structural response during seismic excitations. Base isolation systems also provide an additional means of energy dissipation to reduce the transmitted acceleration into the superstructure. Base isolation can significantly reduce damage to the structure and its contents by reducing floor accelerations and inter-story drifts in superstructure (superstructure almost responds rigidly during seismic excitation).

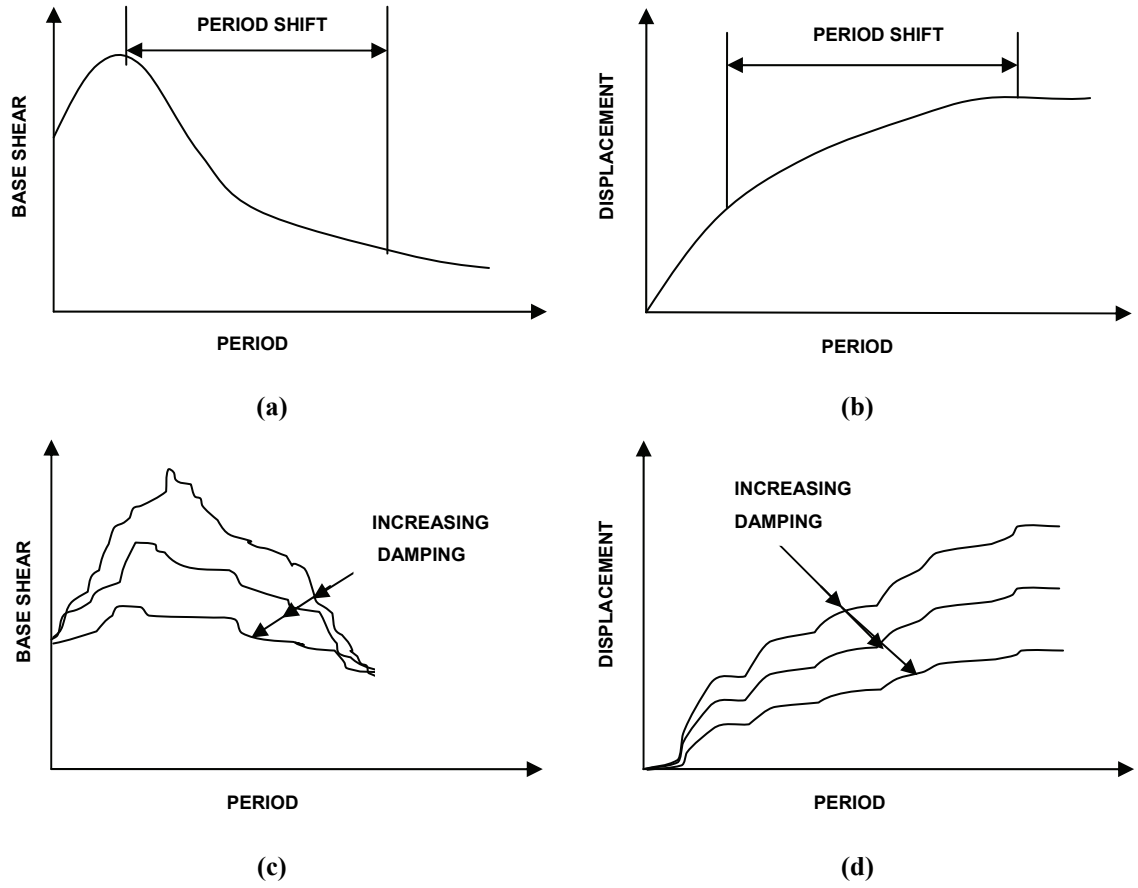

Figure 1.1 Various Aspects of Seismic Base Isolation: (a) Effect on Base Shear due to Period Lengthening (b) Effect on Isolator Displacement due to Period Lengthening (c) Effect of Damping on Base Shear (d) Effect of Damping on Displacement

Figure 1.1 shows the various aspects of seismic base isolation. The reduction in force response (and thus base shear) due to period lengthening is illustrated in Figure1.1a. Figure 1.1b shows the effect of period lengthening on displacement response. As the period increases (i.e., the flexibility of isolation system increases), the displacement across it is also increased. However, as seen in the Figure 1.1d, the displacement can be controlled by increasing damping. The increased damping also reduces the forces at a given period as shown in Figure 1.1c.

An isolation system should be able to provide vertical support to the superstructure while providing horizontal flexibility and energy dissipation capacity. The three functions could be combined into a single device or could be provided by means of different components. There are two basic types of isolation systems; elastomeric

bearings and sliding bearings. Elastomeric bearings have low lateral stiffness and thus shift the fundamental period of the structure to avoid resonance with the excitations. Sliding isolation bearings (e.g., Friction Pendulum System) allow the superstructure to slide on a surface having a relatively low level of friction to filter out damaging frequencies of the ground motion.

1.3.3 Application of Seismic Protection Systems to Woodframed Structures

There have been continuing research efforts to develop or implement seismic protection systems in woodframed buildings, particularly in Japan where different base isolation systems have been applied to residential structures. Application of seismic protection systems to light-frame wood buildings in North America has been virtually nonexistent with one exception. A comprehensive literature review on the application of advanced seismic protection systems (both base isolation and supplemental damping systems) to woodframed structures is presented by Symans et al. (2002). Therein, the only known application of a base isolation system to a light-wood framed building in North America is presented (a residential structure on a sliding isolation system). This study also clearly identified the various challenges of the application of seismic protection systems to woodframed structures. Some of these challenges for the application of energy dissipation systems are:

1) Locating the dampers within the confines of shearwall [typical width available is 139.7 mm (5.5 in) for the case of 50.8 mm x 152.4 mm (2 in x 6 in) nominal studs].
2) Constructing a suitable damper framing system and integrating within the woodframed shear wall such that inter-story drift is transferred to the dampers without any major losses (losses can be significant due to inherently flexible framing connections and joints of woodframed shearwalls).
3) A modified framing arrangement to accommodate the damper assembly if necessary [the damper assembly should be preferably located in the structural shearwalls carrying the majority of gravity loads (i.e., the shearwalls carrying floor joists along their length) and away from wall openings].

Some of these challenges for the application of base isolation systems are:

1) Low weight of woodframed structures (Lateral stiffness of isolation systems must be very low to sufficiently extend period. For elastomeric bearings, the requirement of low stiffness leads to potential bearing instability. Also, low weight on sliding bearings leads to high and unstable friction coefficients and the potential for undesirable sliding during strong windstorms).
2) Absence of stiff diaphragm at the first floor in woodframed structures (The introduction of a stiff diaphragm is important to ensure the transfer of base shear to the isolation systems while maintaining uniform motion across all bearings and thus maintain the effectiveness of isolation).
3) A need of flexible utility connections (e.g., gas, electric, telecommunications, etc.) which limit the displacement capacity of the isolation system and thus the isolation effect.

In addition to these technical challenges for application of seismic protection systems to woodframed structure, some important challenges are cost control, a lack of technical and construction expertise, the need for simple and practical design methods, and making building owners aware of the benefits of using such systems to protect their investment.

1.4 NEESWood Project

The research presented herein regarding the integration of seismic protection systems within the PBSD philosophy for design of woodframed structures was part of the NEESWood project. To date, the height of woodframed construction has been limited to approximately four or five stories, mainly due to the lack of understanding of the dynamic response of taller (mid-rise) woodframed construction, non-structural limitations such as material fire requirements, and potential damage considerations for non-structural finishes. The NEESWood project seeks to develop a performance-based seismic design (PBSD) philosophy that will provide the necessary mechanisms to safely increase the height of woodframed structures in active seismic zones of the U.S. as well as mitigating damage to low-rise woodframed structures. An impediment to the development of PBSD for woodframed buildings is the lack of a complete understanding of their seismic behavior. In addition, only a few numerical analysis models capable of

reliably predicting the global behavior of three-dimensional woodframed structures have been developed. This is mainly due to a lack of experimental test data on the seismic response of full-scale woodframed structures of realistic dimensions. Thus, the NEESWood Project started with seismic shaking table testing of a full-scale, two-story, woodframed townhouse building (the "benchmark" test structure). The results of the testing were used to provide benchmark data against which numerical models were developed and refined for use within the PBSD philosophy. This PBSD philosophy was used to design a mid-rise (six-story) woodframed apartment building which was tested using three-dimensional earthquake ground motions at the E-Defense shaking table facility in Miki City, Japan. The performance of the building was consistent with the design requirements outlined within the PBSD.

1.5 Objectives and Scope of Research

The major objective of the research presented herein is to increase the performance reliability of woodframed structures in regions of high seismic intensity through the development of simple analysis procedures and innovative ways to include seismic protection systems in woodframed structures while establishing their performance via experimental testing. This objective is met through a comprehensive experimental and numerical study that includes the following major tasks:

1) Integration of seismic protection systems within the existing numerical models and time-history analysis tools.
2) Integration of seismic protection systems within the existing PBSD procedures used for woodframed structures.
3) Development of new simplified PBSD procedures for woodframed structures with seismic protection systems.
4) Evaluation of seismic response of woodframed structure with seismic protection systems via shake table testing and thus developing an experimental database for benchmarking future numerical models.
5) Comparison of performance of different seismic protection systems and recommendations for their specific use.

1.6 Report Organization

The report is organized into five chapters. Chapter 1 provides an introduction that lays the background for the research to be presented. Chapters 2 to 4 present the main body of the research. Lastly, Chapter 5 provides a final summary and conclusions, as well as discussion on future work. Note that Chapters 2 to 4 are presented in manuscript format to be disseminated as journal publications, and thus they have some unavoidable overlap. In addition, supporting details (e.g., design program codes, figures, photos etc.) within Chapters 2 to 4 that were considered unnecessary for publication purpose are included in separate appendices provided at the end of this report. This helped in keeping notes of important details to aid in completeness of the report.

Chapter 2 presents a study consisting of a detailed evaluation of the testing of benchmark structure with dampers (Phase 2 of benchmark tests) and its displacement-based design with the application of newly designed toggle-braced damper assembly. The damping system consisted of fluid viscous dampers incorporated within modular walls which can be constructed off-site and delivered to the job site for "drop-in" installation. The displacement-based design procedure was originally developed within the NEESWood project for the design of multistory woodframed structures and in this study is further extended to include the application of a damping system. The procedure requires simple modal analysis and determination of equivalent stiffness based on the backbone response of the shearwalls. The validity of the proposed displacement-based procedure is confirmed using results from nonlinear dynamic response-history analyses.

Chapter 3 focuses on the results from shaking table tests of wood shearwalls retrofitted via toggle-braced fluid viscous dampers and its numerical modeling. Based on what was learned from Phase 2 of benchmark testing, a new design for the modular damper walls with a toggle brace configuration was developed and tested within full-scale shearwalls. Within the context of performance-based seismic design, the effect of the fluid viscous dampers on the deformation demand and hysteretic energy dissipation demand is emphasized. The results demonstrated that the retrofit provided a significant increase in the seismic resistance of the walls, allowing them to achieve high levels of performance when subjected to strong ground motions. However, the full potential of the retrofit was not realized due to losses in transmission of wall drift to the toggle-bracing

system. The study also presents a detailed evaluation of these losses to help in increasing the potential of toggle-braced modular damper walls via more efficient design.

Chapter 4 presents a study consisting of the development of two displacement-based design procedures for isolated woodframed structures and their validation via nonlinear dynamic response-history analyses and experimental results from shaking table tests of a half-scale, two-story, woodframed building supported on a sliding isolation system. One method involves a conventional direct displacement-based design procedure in which a new approach has been taken to define an equivalent single-degree-of-freedom (SDOF) model for an isolated building structure with the computation of its design inter-story drift based on the relative contribution of the isolation system displacement and the effective displacement of the equivalent SDOF fixed-base superstructure, all without the need for modal analysis. In addition, a simple and quick design procedure based on normalized modal analysis and generation of inter-story drift spectra has been developed. These practical approaches have been developed with the objective of enabling designers to efficiently evaluate various options before making the final selection of isolation system parameters.

Chapter 5 provides a summary and conclusions of the research work presented in this report, major contributions of this research to the field of structural/earthquake engineering, and recommendations for future research needed to foster implementation of seismic protection systems in woodframed structures.

2. TESTING AND DISPLACEMENT-BASED DESIGN OF TWO-STORY WOODFRAMED STRUCTURE WITH FLUID VISCOUS DAMPERS

Woodframed structures experienced significant damage during the 1994 Northridge Earthquake. One approach to improving the performance of such structures is to incorporate a seismic protection system (e.g., a seismic isolation or damping system). Such a system was recently implemented as one of the phases of the NEESWood project benchmark structure shake table testing that was conducted at the University at Buffalo NEES site. In this phase, the benchmark structure, a full-scale, two-story, woodframed townhouse, was retrofitted via implementation of modular damper walls. The testing represented the first application of such a damping system within a full-scale

woodframed building. The tests results showed that, due to a number of factors, the engagement of the dampers was limited and thus the improvement in performance of the building was modest. However, the testing demonstrated the feasibility of implementing a damping system within woodframed construction. Based on what was learned from the testing and in collaboration with an industry partner, a new design for the modular damper walls with toggle-braced linear viscous dampers was developed and tested recently. This chapter presents a detailed evaluation of the testing of benchamark structure with dampers and its displacement-based design with the application of newly designed toggle-braced damper assembly. The displacement-based design procedure was originally developed within the NEESWood project for the design of multistory woodframed structures and in this study is further extended to include the application of a damping system. The procedure requires simple modal analysis and determination of equivalent stiffness based on the backbone response of the shearwalls. The validity of the proposed displacement-based procedure is confirmed using results from nonlinear dynamic response-history analyses.

2.1 Introduction

Although woodframed construction in the U.S. has generally been considered to perform well during earthquakes, the 1994 Northridge Earthquake (Moment Magnitude = 6.8) clearly demonstrated the seismic vulnerability of such construction (Kircher et al. 1997). The estimated property losses in woodframed buildings, a majority of which includes single family residential housing, were approximately $20 billion and 24 of the 25 fatalities occurred in such buildings, underscoring the fact that conventionally designed woodframed structures perform well with regard to life safety but suffer significant structural and non-structural damage making them uninhabitable during severe seismic events. As such, the NEESWood project sought to develop a performance-based seismic design (PBSD) philosophy that will provide the necessary mechanisms to safely increase the height of woodframed structures in active seismic zones of the U.S. as well as mitigating damage to low-rise woodframed structures (van de Lindt et al. 2006). The testing phase of the NEESWood Project began with seismic shaking table testing of a full-scale, two-story, woodframed townhouse building (the “benchmark” test structure)

(Filiatrault et al. 2007 and Christovasilis et al. 2007). The results of the tests were used to develop the PBSD philosophy. This PBSD philosophy was then used to design a mid-rise (six-story) woodframed apartment building which was tested using three-dimensional earthquake ground motions at the E-Defense shaking table facility in Miki City, Japan.

One approach to protect woodframed buildings during such a large seismic event is to incorporate an advanced seismic protection system. For example, introducing a base isolation system can reduce the seismic response of a woodframed building by increasing the fundamental natural period and thereby filtering out damaging frequencies of the ground motion. Alternatively, an energy dissipation system can be used to dissipate a portion of the seismic input energy, thereby reducing the energy dissipation demand (and thus damage) on the wood framing system. In general, the application of seismic protection systems is helpful to achieve following objectives:

- To mitigate damage and thus protect the investments of owners.
- To reduce the cost of insurance premiums by reducing seismic risk.
- To improve performance such that loss of life and injuries are reduced.
- To make architecturally attractive design (large openings) possible by reducing the stiffness demand on the structure.
- To retrofit old structures to meet higher performance levels.

Note that the single family residential housing in North America primarily consists of woodframed construction and accounts for the single largest investment of owners during their lifetime and thus the overall impact of the objectives mentioned herein become particularly important with regard to economic losses during an earthquake. A comprehensive literature review on the application of advanced seismic protection systems (both base isolation and supplemental damping systems) to woodframed structures is presented by Symans et al. (2002). This study clearly identified the various challenges of the application of seismic protection systems to woodframed structures. Some of these challenges for the application of energy dissipation systems are:

1) Locating the dampers within the confines of shearwall (typical width available is 139.7 mm (5.5 in) for the case of 50.8 mm x 152.4 mm (2 in x 6 in) nominal studs).

2) Constructing a suitable damper framing system and integrating within the woodframed shearwall such that inter-story drift is transferred to the dampers without any major losses (losses can be significant due to inherently flexible framing connections and joints of woodframed shearwalls).
3) A modified framing arrangement to accommodate the damper assembly if necessary [the damper assembly should be preferably located in the structural shearwalls carrying the majority of gravity loads (i.e., the shearwalls carrying floor joists along their length) and away from wall openings].

In addition to these technical challenges, some important challenges are cost control, the lack of technical/construction expertise, the need for simple and practical design methods, and making building owners aware of the benefits of using such systems to protect their investments.

The objective of the study described herein is to experimentally evaluate the seismic response of a full-scale, two-story, three-dimensional woodframed building incorporating a supplemental damping system. The testing was conducted as Phase 2 of the NEESWood benchmark structure test program (Shinde et al. 2007). The damping system consisted of fluid viscous dampers incorporated within modular walls. A major advantage of using fluid viscous dampers is their high energy dissipation density (i.e., capability of dissipating a large amount of energy relative to their size) which allows them to fit within the relatively narrow confines of a woodframed shearwall. Studies conducted by Symans et al. (2004) and Dutil and Symans (2004) have demonstrated the potential of fluid viscous dampers to reduce the energy dissipation demand in woodframed structures. The testing of such dampers within the NEESWood benchmark structure represents the first application within a full-scale woodframed building. In that sense, one of the objectives of this study was simply to establish the feasibility of implementing a seismic damping system within a full-scale woodframed building. Due to a number of factors, including the inherent flexibility in the connections of wood framing systems, engagement of the dampers was limited during these tests and thus the full effectiveness of the dampers was not realized. Based on what was learned from this testing, a new design for the modular damper walls with a toggle brace configuration was developed and tested.

An additional objective of the study described herein is to modify a displacement-based seismic design procedure (that has been developed within the NEESWood project) to accommodate the inclusion of toggle-braced seismic dampers in woodframed buildings. The design procedure is presented using performance levels/metrics being articulated as part of the NEESWood project and the procedure is validated using results from nonlinear response-history analyses. The numerical study presented herein demonstrates the ability of an efficient energy dissipation system to achieve the desired performance level which was not clearly evident in the benchmark testing. Filiatrault and Folz (2002) presented one possible displacement-based design procedure for wood structures, with the procedure originating from one developed by Priestley (1998). This design procedure has been applied to a two-story woodframed building (Filiatrault et al. 2006). A new displacement-based design procedure has been developed by Pang and Rosowsky (2007) within the NEESWood project. The procedure requires simple modal analysis and determination of equivalent stiffness based on the backbone response of the shearwalls.

The design of seismic damping systems within the context of PBSD procedures has been discussed within the literature. Nonlinear static analysis procedures incorporating energy dissipation systems were covered in ATC-40 (ATC 1996) and FEMA 356 (ASCE 2000). Kim et al. (2003) utilized the capacity spectrum method for seismic retrofit of existing structures using viscous dampers. Kim and Choi (2006) presented a displacement-based design with dampers for seismic retrofit of framed structures. Lin et al. (2003) presented a direct displacement-based design method for steel buildings with different passive energy dissipation systems. In the study described herein, the displacement-based design procedure developed by Pang and Rosowsky (2007) has been modified for designing a damping system for seismic retrofit of an existing woodframed structure (Shinde et al. 2008a). The modification incorporates the traditional procedure of determining the size and location of energy dissipation devices (dampers) based on FEMA 356 guidelines (ASCE 2000).

2.2 Benchmark Test Structure and Experimental Setup

2.2.1 Building Configuration

The structure selected for the benchmark tests is a portion of one of the four index buildings designed within the CUREE-Caltech Woodframe Project. This building is assumed to have been built as a "production house" in either the 1980's or 1990's, located in either Northern or Southern California. The structure is a two-story townhouse building (approximately 150 m^2 (1600 ft^2)) with an attached two-car garage. The height from the first floor slab to the roof eaves is 5.48 m (18 ft). A detailed description of the test structure, experimental test setup, instrumentation, and shake table test program (test phases) is provided by Filiatrault et al. (2007).

The first and second story floor plans of the test structure are shown in Figure 2.1a and 2.1b, respectively, wherein only the structural shear walls are shown. For design purposes and in accordance with the 1997 edition of the Uniform Building Code (ICBO 1997), it is assumed that the building is located in Seismic Zone 4 and is founded on Soil Type D. The shearwalls are framed using nominal 50.8 mm x 101.6 mm (2 in x 4 in) Hem-Fir studs spaced at 406.4 mm (16 in) o.c. and sheathed on the exterior with 11 mm (7/16 in) thick OSB connected to the framing members using 8d common nails (63.5 mm (2.5 in) length x 3.3 mm (0.131 in) diameter) except in the garage walls in which nominal 50.8 mm x 152.4 mm (2 in x 6 in) studs are used. Gypsum wallboard (12.7 mm (1/2 in) thick) is used on the interior of the shearwalls and is connected with 31.8 mm (1.25 in) long #6 bugle head screws at 406.4 mm (16 in) o.c. on vertical studs only. Hold-downs are used to prevent overturning of the walls while ensuring a racking mode of deformation. Effective seismic weights of 246.9 kN (55.5 kips) and 104.5 kN (23.5 kips) are assigned to the first and second story, respectively. The edge and field spacing of sheathing-to-framing connectors for the second story shearwalls was 152.4 mm (6 in) and 304.8 mm (12 in), respectively. Three different edges spacings (76.2 mm, 101.6 mm and 152.4 mm (3 in, 4 in and 6 in)) were specified for the first-story shearwalls of the building in accordance with the 1988 Uniform Building Code (ICBO 1988).

Photographs of the test structure mounted on the dual seismic shaking tables at the University at Buffalo NEES earthquake testing facility and prior to Phase 2 and Phase 5 testing are shown in Figure 2.1c and 2.1d, respectively. The dual synchronized tri-axial

shaking tables have six degrees-of-freedom, measure 7 m x 7 m (23 ft x 23 ft), and have a combined payload capacity of 889.7 kN (200 kips).

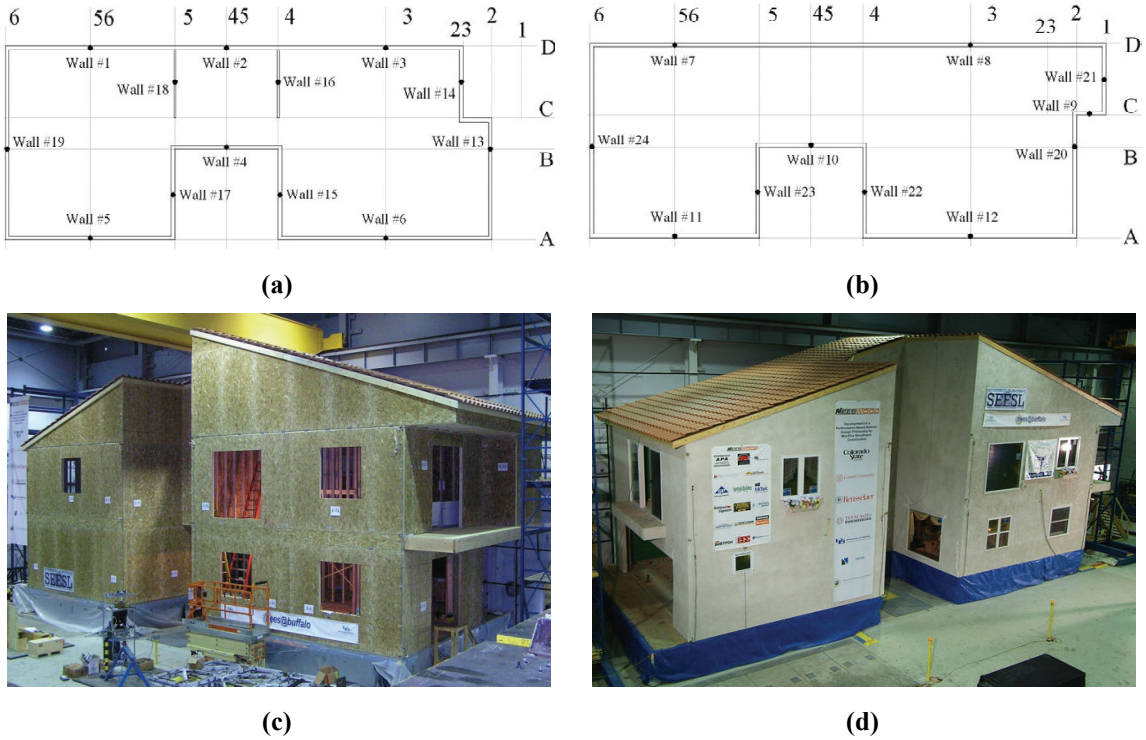

Figure 2.1 Floor Plans showing: (a) Structural Walls in First Story, (b) Structural Walls in Second Story, (c) Benchmark Test Structure Prior to Test Phase 2 and (d) Prior to Test Phase 5

2.2.2 Shake Table Test Program

2.2.2.1 Testing Phases

Various configurations of the test structure were tested in different test phases (see Table 2.1). Before the start of each test phase, the test structure was repaired in an effort to bring the lateral load-resisting system back to its original characteristics. Supplemental weight was added in the first four test phases such that the mass was the same for all test phases.

2.2.2.2 Input Ground Motions

Consistent with all other Phases of the Benchmark Structure test program, for the Phase 2 testing two historical ground motions were used for the seismic tests: an ordinary ground motion and a near-field ground motion (Christovasilis et al. 2007). The ordinary

ground motion (OGM) (i.e., far-field motion) represented a seismic hazard level corresponding to a Design Basis Earthquake (DBE) with a probability of exceedance of 10% in 50 years or a return period of 475 years. The 1994 Northridge Earthquake ground motion recorded at Canoga Park, with an amplitude-scaling factor of 1.20, was selected as the DBE. The near-field ground motion (NGM) represented a seismic hazard level corresponding to a Maximum Credible Earthquake (MCE) with a probability of exceedance of 2% in 50 years or a return period of 2,475 years. The unscaled 1994 Northridge Earthquake ground motion recorded at the Rinaldi Receiving Station was selected as the MCE. In addition to the DBE and MCE hazard levels, the Canoga Park ground motion (OGM record) was scaled down to simulate other hazard levels (see Table 2.2). Note that, in Table 2.2, the directions shown for the peak ground acceleration (PGA) values are directions that define the orientation of the test structure rather than the directions of the components of the field-recorded ground motions (e.g., the stronger component of the field-recorded Rinaldi record (component S49W) was applied along the North-South (Y) direction of the test structure). Additional details about the ground motions are provided in Section B.1. Details of shake table fidelity and instrumentation are covered in Section B.2 and B.4, respectively.

Table 2.1 Test Phases and Test Building Configurations

Test Phase	Building Configuration
1	Wood structural elements only
2	Test Phase 1 structure with passive fluid dampers installed in selected wood shear walls
3	Test Phase 1 structure with gypsum wallboard installed on structural walls
4	Test Phase 3 structure with gypsum wallboard installed on all walls and ceilings
5	Test Phase 4 structure with stucco installed on all exterior walls

Table 2.2 Ground Motions for Seismic Tests

Excitation Level	Ground Motions	Hazard Level	Scale Factor	PGA (g)		
				East-West X	North-South Y	Vertical Z
1	1994 Northridge Canoga Park	99.99%/50 years	0.12	0.04	0.05	0.06
2		50%/50 years	0.53	0.19	0.22	0.26
3		20%/50 years	0.86	0.31	0.36	0.42
4		10%/50 years	1.2	0.43	0.50	0.59
5	1994 Northridge Rinaldi	2%/50 years	1	0.47	0.84	0.85

2.3 Phase 2 Testing

For Phase 2 testing, modular (pre-fabricated) damper wall units were installed in both the first and second stories of the test structure (see Figure 2.2a). The modular damper wall units were constructed of wood framing around the perimeter and metallic chevron bracing within the central region (see Figure 2.2b). A similar configuration was utilized by Dutil and Symans (2004) in experimental shaking table tests of a single wood-framed shear wall. As shown in Figure 2.2b, the retrofitted shear wall consists of a 1.22 m (4 ft) wide modular damper wall unit that is installed within an existing wall by removal of existing studs. The modular damper wall unit includes the chevron braces, fluid damper, and a header to transfer the gravity loads to the base of the wall. The 1.22 m (4 ft) width of each modular wall unit is intended to accommodate the standard width of wood sheathing panels. Thus, the modular damper wall units can be constructed off-site and then delivered to the job site for "drop-in" installation. In fact, this was done for the Phase 2 testing (the modular wall units were constructed at Rensselaer Polytechnic Institute and transported to the University at Buffalo NEES site for "drop-in" installation in the benchmark test structure).

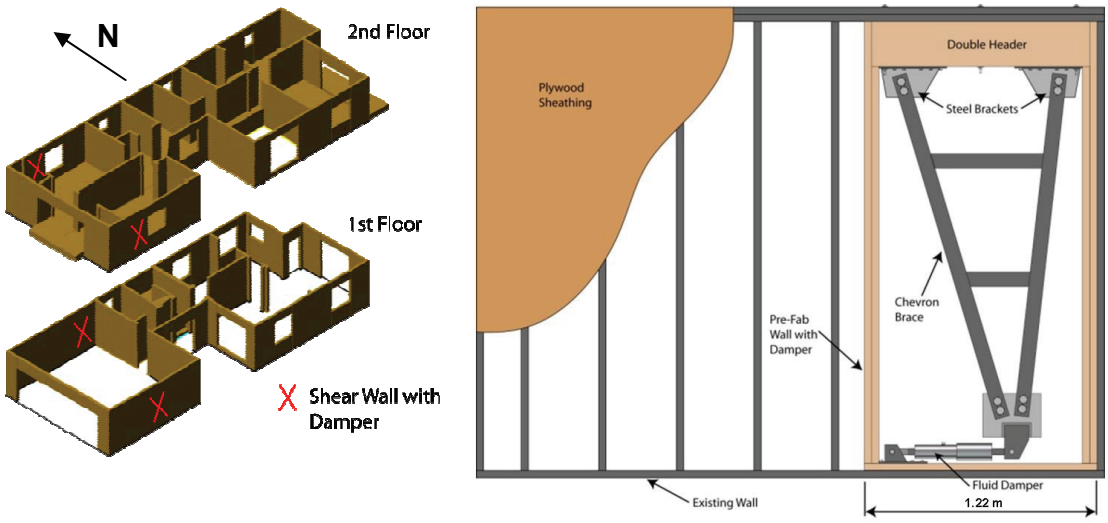

(a) (b)

Figure 2.2 (a) Isometric View of First and Second Floor Levels showing Location of Dampers and b) Schematic of Typical Shear Wall Retrofitted with Modular Damper Wall Unit

2.3.1 Numerical Modeling and Analysis

Nonlinear dynamic analysis of the benchmark structure, both with and without fluid viscous dampers installed in selected walls, was performed using the SAWS (Seismic Analysis of Wood Structures) program (Folz and Filiatrault 2004a) (see Appendix A for additional details). In this program, a three-dimensional woodframed building is degenerated to a two-dimensional "pancake" model in which the lateral load resisting system consists of shear walls that are modeled as zero-height nonlinear hysteretic spring elements and the horizontal diaphragms are assumed to have infinite in-place stiffness, resulting in three degrees-of-freedom per floor. Modifications to the SAWS program were made to allow for the inclusion of the dampers. Since the Phase 2 test structure did not include any finish materials, analysis was performed using shear wall hysteretic parameters for the wall configuration without exterior or interior finish materials. The hysteretic parameter values were obtained using the companion analysis program CASHEW (Folz and Filiatrault 2001). Data input to CASHEW includes wall geometry, shear stiffness of the sheathing panels, and the hysteretic properties of the sheathing-to-framing connections. Since testing of the benchmark structure and associated sheathing-to-framing connections had not yet begun at the early stages of the analysis, the properties of the sheathing-to-framing connections were taken from prior

testing performed at the University of California at San Diego as part of the CUREE-Caltech Woodframe Project (Isoda et al. 2001). In addition, inherent rate-dependent damping was accounted for via a Rayleigh damping formulation (based on the initial stiffness matrix) in which a damping ratio of 1% was assumed in the first and second modes.

Due to the important role story drifts play in controlling damage in wood-frame structures (Porter et al. 2001), the main criterion used in designing the damping system was to limit the story drift ratio to a prescribed value (2%). Numerical analyses using SAWS revealed that, for higher seismic levels, meeting this criterion for the transverse direction (see Figure 2.1) was particularly problematic due to short wall lengths. The short walls had relatively few anchor bolts, leading to difficulty in transferring the peak damper force through the sill plate and into the foundation. Since the installation of the modular damper walls in the benchmark structure was a seismic retrofit, additional anchor bolts could not be readily put in place. The final configuration includes four modular damper walls in the longitudinal direction (see Figure 2.2a). Given this configuration, the retrofitted structure was tested with seismic input in the longitudinal (X) and combined longitudinal and vertical (X-Z) directions.

Both linear and nonlinear fluid viscous dampers (Symans and Constantinou 1998) were considered for implementation in the modular damper walls. The dampers were designed based on a parametric analysis in which the damper force-velocity relation varied (the same relation being used for each of the four dampers) under the constraint that the predicted peak story drift ratios were less than 2% and the damper stroke and force demands were within reasonable limits. The final design of the dampers included a stroke of ±38.1 mm (1.5 in), a force capacity of 31.14 kN (7 kips), and a nonlinear force-velocity relation with a damping coefficient of 8.57 kN-(s/mm)$^{0.5}$ [1.5 kips-(s/in)$^{0.5}$]. It should be recognized that the numerical modeling used in the analyses involved a number of assumptions, including the assumption that 100% of the story drift is transferred to the damper. The degree to which such assumptions are valid depends on the actual construction of the modular damper walls and how they are installed in the structure.

2.3.2 Practical Implementation Issues

For the modular damper wall configuration shown in Figure 2.2b, a fully effective damper would be subjected to 100% of the story drift. However, during the Phase 2 testing, the displacement of the dampers was not equal to the story drift. Some likely reasons for this include:

- Manufacturing tolerances in clevis pin connections at damper ends.
- Out-of-plane displacement of dampers and steel bracing.
- Bending deformation of shear wall.
- Uplifting of modular damper walls.
- Sill plate slippage.
- Inherent flexibility of wood framing connections and joints (i.e., the wood framing system tends to deform around the modular damper walls and thus it is difficult to transfer the global structural displacements into the modular damper walls).
- A portion of the measured drift is due to global overturning, resulting in high story drifts but low shear deformations and thus low damper displacements.

In an attempt to increase the displacement of the dampers, a variety of retrofitting measures were employed. Although these measures were successful in increasing the damper displacements, further improvements were deemed necessary. A detailed displacement loss evaluation based on sensor measurements and code-based analytic formulas is presented later in the experimental results section. After the Phase 2 testing was completed, alternative modular damper wall designs were considered, including one employing a toggle brace configuration which has been constructed and tested within individual shearwalls.

2.4 Experimental Results

2.4.1 Modal Properties of Structure

System identification tests (white noise input of 0.05 g amplitude and 0.5 – 50 Hz bandwidth) were conducted between the seismic tests of each phase to determine the variations of the modal properties (natural frequencies, damping ratios, and mode

shapes) of the test structure as it experienced increasing levels of damage. The modal properties were identified from acceleration transfer functions with the half-power bandwidth method being used to determine the modal damping ratios. In this method, the modal damping ratios are dependent upon the peak values in the transfer functions. Since these peak values tend to be underestimated due to finite resolution in the transfer function data, the modal damping ratios tend to be overestimated.

Due to a number of factors, including the manufacturing tolerances in the clevis pins at the ends of the dampers, the dampers were not cycled to any significant degree under low-amplitude testing. Thus, the initial low-amplitude white noise tests (prior to any seismic testing) did not reveal any appreciable differences in the modal properties of the Phase 1 and Phase 2 test structures (see Table 2.3). Note that mode 1 primarily corresponds to motion in the transverse direction (N-S; see Fig. 2.2a) whereas modes 2 and 3 correspond to coupled longitudinal and torsional motion.

Table 2.3 Modal Properties from System Identification Tests

	Modal Period (sec)			**Modal Damping Ratio (%)**		
Test Phase / Mode	1	2	3	1	2	3
1	0.327	0.225	0.180	12.2	3.3	2.7
2	0.327	0.232	0.178	12.5	6.8	5.6

The natural periods obtained from the undamped eigenproblem (in SAWS) of the Phase 1 and 2 test structures were 0.39, 0.33, and 0.17 sec, which, for modes 1 and 2, are appreciably larger than those obtained from the experimental system identification tests. Thus, as will be shown subsequently, the numerical analyses of the Phase 1 and 2 test structures tended to overestimate the peak story drift response. Note that the natural periods mentioned above are obtained from the revised SAWS model developed based on the hysteretic parameters of cyclic nail tests (Ekiert and Hong, 2006) conducted at the University at Buffalo as part of the benchmark test program (Filiatrault et al. 2007 and Christovasilis et al. 2007).

2.4.2 Drift Response

As mentioned previously, during the modular damper wall design process, the SAWS program was used to perform numerical simulations of the benchmark test structure both

with and without dampers. The predicted peak story drifts are shown in Figure 2.3a for the structure with and without dampers (for the case with dampers, the results correspond to the final damper design). In this figure, the excitation is the field-recorded ground motion (not the shake table motion measured during testing) and the SAWS model is based on the hysteretic parameters derived from the testing performed at the University of California at San Diego (Isoda et al. 2001). The simulations clearly demonstrate the potential benefits of incorporating the modular damper walls (approximately 40% reduction in peak story drift at higher test levels) and peak drift ratios below the design criteria of 2%.

The measured peak story drift for the test structure with and without dampers is shown in Figure 2.3b. The peak responses of the test structure with and without dampers are also provided in Table B.2. Note that the peak drifts for the case without dampers (Figure 2.3b) are much less than those that were predicted from numerical simulations (Figure 2.3a). This is likely due to the inaccurate hysteretic parameters and the simplified nature of the SAWS model which does not lend itself well to analysis of the benchmark structure in the longitudinal direction (the structure is asymmetric with respect to the longitudinal axis). Furthermore, the numerical simulations were conducted using field-recorded ground motions (Figure 2.3a) whereas the measured drift response (Figure 2.3b) is due to shaking table excitation which does not exactly match the field-recorded motions.

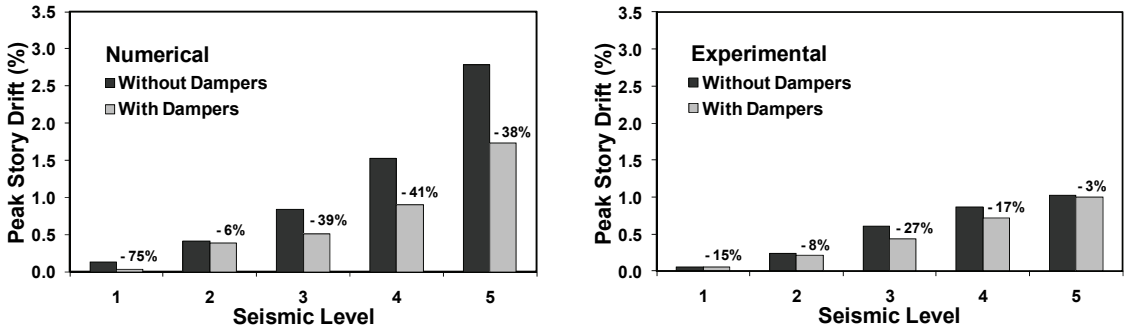

(a) **(b)**

Figure 2.3 Comparison of Seismic Response With and Without Dampers: (a) Numerical Simulations Prior to Shake Table Testing and (b) Experimental Results from Shake Table Tests

Although the measured peak drifts are small for the case without dampers (largest is approximately 1% which corresponds approximately to an Immediate Occupancy performance level) and thus one might argue that dampers are not needed, it must be recognized that the structure was tested with excitation along its stiffer direction (longitudinal direction). The benefit of the dampers would likely have been more evident if testing been conducted in the more flexible transverse direction. Also note that the floor joists in the benchmark structure were spanning along the longitudinal direction of the structure and thus limited the direct transfer of inertia forces, which would have driven the walls directly, along the longitudinal direction. As the longitudinal walls were not loaded along their length, their tendency to rock and bend was more as compared to racking in pure shear and thus resulted in additional displacement transfer losses to the dampers. In spite of this, the relative performance of the structure with and without dampers indicates that the measured drift reductions for Levels 3 and 4 are significant. The small drift reduction for Level 5 is likely due to the Level 5 ground motion (NGM) being fundamentally different from the Level 3 and 4 ground motions (OGM).

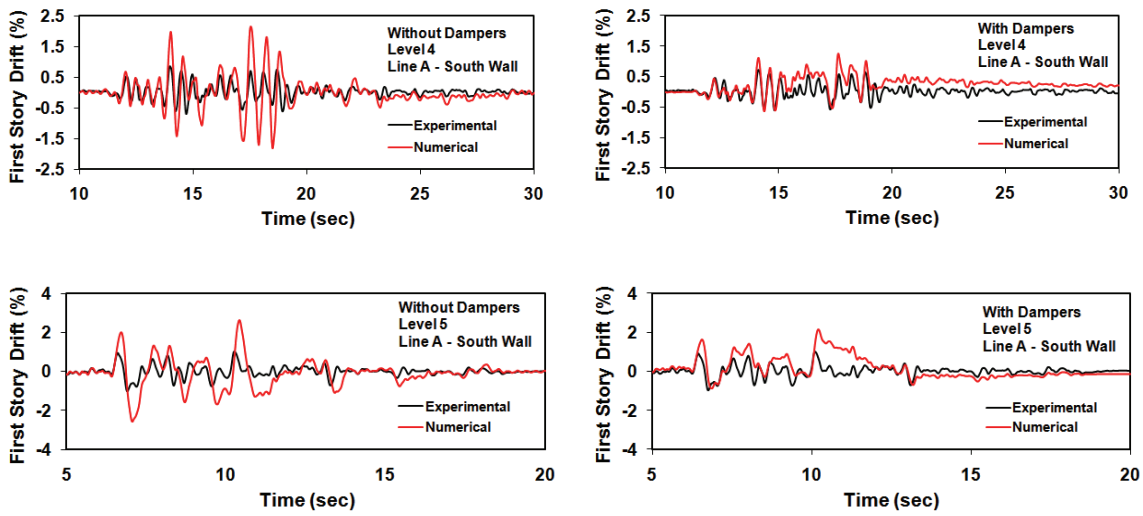

Figure 2.4 Comparison of Numerical and Experimental Drift Response History: (a) Without Dampers and (b) With Dampers

A comparison of the numerical (with the revised SAWS model) and experimental drift response histories in the South garage wall (see Figure 2.2a) are shown in Figure 2.4a (without dampers) and 2.4b (with dampers) for Level 4 and 5 Excitation. For the

numerical analysis, the measured shaking table motion is used as the excitation. The ideal displacement magnification factor of 1 (i.e., for the chevron-braced damper assembly) was used in the numerical analysis with the dampers. Note that, in all cases, the phase of the predicted response is reasonably consistent with the experimental data but the amplitude is overpredicted. Clearly, and consistent with the overall objective of testing the benchmark structure, additional work is needed to improve the ability of the numerical simulations to capture the overall characteristics of the measured response.

2.4.3 Hysteretic Response

For Excitation Levels 4 and 5, the measured global hysteretic responses (base shear vs. building drift) in the longitudinal direction of the test structure with and without dampers are shown in Figure 2.5a and the damper hysteresis loops for the damper in the first-story South garage wall are shown in Figure 2.5b. The base shear was computed by summing the inertia forces in the longitudinal direction at each level of the test structure. The building drift (2^{nd} level central displacement) was computed as the relative horizontal displacement in the longitudinal direction at the center of the roof eaves. Since the peak damper displacement was small (approximately 3.56 mm (0.14 in) for level 5 excitation), the energy dissipated by the dampers was limited and thus the influence of the dampers on the building hysteretic response was minor. Recall that the final damper design, which was based on numerical analysis using SAWS, included a damper stroke of +/- 38.1 mm (1.5 in). Thus, damper displacements that were much larger than those recorded during the experimental tests were expected. As explained previously, an alternate modular damper wall design was developed in an attempt to increase the damper displacements. The alternate design, coupled with a modified approach to installation of the modular walls, significantly increased the damper displacements and thus the effectiveness of the dampers.

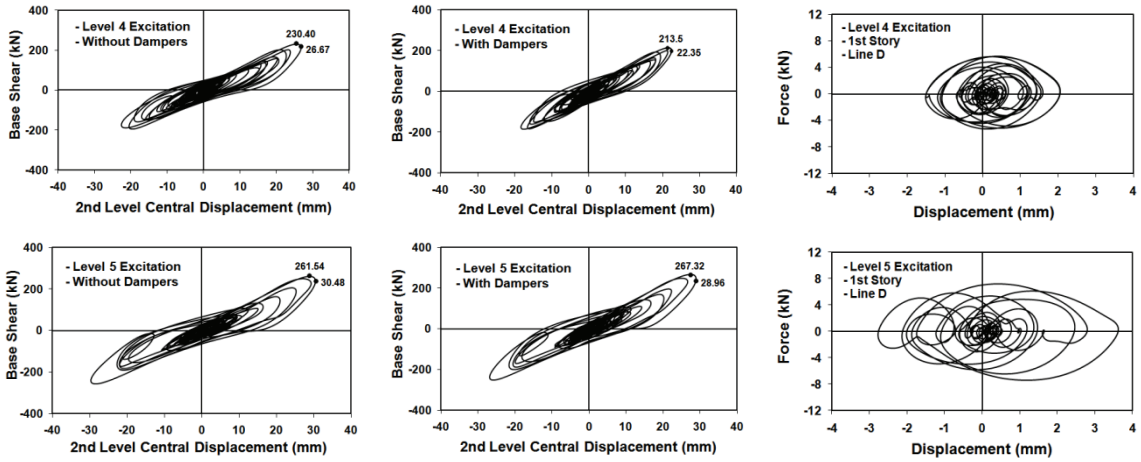

Figure 2.5 (a) Global Hysteretic Response in Longitudinal Direction and (b) Damper Hysteretic Response

2.4.4 Evaluation of Loss of Displacement Transmission to Dampers

2.4.4.1 Evaluation via Analysis of Experimentally Measured Data

Evaluation of loss of displacement transmission to the dampers was possible via analysis of sensor data that was used to measure different displacement components (i.e., slippage of sill plates, uplifting of studs, racking deformation of shearwalls and total inter-story displacement). Christovasilis et al. (2007) decomposed the first floor inter-story displacements of walls in the transverse direction into different components for different phases of testing except Phase 2. The dampers were installed in the longitudinal direction [i.e., wall lines D and A (see Figure 2.1)] and thus similar data processing was performed for decomposing first story shearwall displacements in that direction to evaluate displacement transmission losses to the dampers.

Figure 2.6 shows the displacement components of the North garage wall (Wall line D, first story). Note that the actual racking deformation of the wall (i.e., displacement component transferred to the dampers) is on the order of 50% of the total displacement. The total identifiable losses (losses that could be computed from measured experimental data), which include sill plate slippage, uplift (both sill plates and end studs), and table rotation components, are close to 10% of the total displacement. Thus, the unidentified losses are on the order of 40% of the total displacement [these include the effect of uplift of studs other than end studs, slippage of the top plate with respect to the diaphragm,

deformation of the floor joists (Christovasilis et al. 2007) and displacements due to global overturning (global bending)].

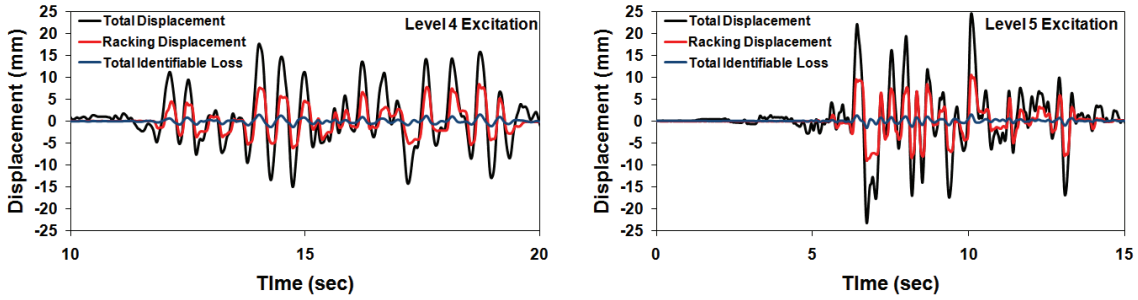

(a) (b)

Figure 2.6 Displacement Components of North Garage Wall : (a) Level 4 Excitation and (b) Level 5 Excitation

2.4.4.2 Evaluation via Code-based Analytical Equations

Equation 23-2 in IBC 2006 provides an analytical expression to predict the total deflection experienced by a shearwall during an earthquake by combining the following four types of deflection: bending (Δ_b), shear (Δ_v), nail slip (Δ_n), and anchorage slip (Δ_a) (see Appendix D for additional details). Breyer et al. (2007) provides a detailed explanation of these deflection components. The damper only has the ability to respond to shear deformations and thus the deformation of the damper is only due to the direct shear term and the shear deflection component of the nail slip deflection. Note that nail slip reduces the overall stiffness of the shearwall and thus results in additional deflection of the shearwall. This additional deflection may include bending and anchorage slip deflections which are not transferred to the dampers. Using the aforementioned analytical expression, first story shearwall deflection calculations along the longitudinal direction [i.e., wall lines D and A (see Figure 2.1)] were performed for the Phase 2 testing. The total deflection was known from the displacement data collected during the tests, and the measured acceleration at the top of first story (corresponding to the maximum deflection) was used to calculate the base shear. Note that the analytical expression for the nail slip contribution was not used herein. Instead, this contribution was computed by subtracting the deflection due to bending, shear and anchorage slip from the total measured displacement. The deflection due to anchorage slip Δ_a was

calculated by determining the chord force for the computed shear at the top of the shearwall.

The percentage contribution of each deflection component was then used to determine the amount of deflection that was transferred to the damper and the amount that was lost within the first story shearwalls in the longitudinal direction. It is assumed that only 70% of the deflection due to nail slip will be pure shear and thus contribute to the displacement transferred to the dampers. Based on these assumptions, the total displacement loss was estimated within the range of 30 to 40%. Hwang et al. (2005) reported displacement transmission losses on the order of 40% in the second story of a three-story scale-model steel-framed structure with toggle-braced dampers. Thus, it is apparent that some amount of displacement loss of the same or higher order is expected in woodframed structures, given that woodframed structures have more flexible framing members and joints than steel-framed structures.

2.5 Overview of Direct Displacement-Based Seismic Design

The fundamental difference between the force-based design and the direct displacement based design (DDD) is that the former characterizes the structure with a constant stiffness and thus different yield displacements while the latter considers the realistic conditions of varying stiffnesses with a constant yield displacement (Priestly 2007). Since the peak inter-story drift provides a key measure of the structural and nonstructural damage in a building during an earthquake, the realistic representation of damage is only possible in the displacement-based design. The force-based design uses an initial stiffness and assumed damping (typically 5%). This damping accounts for inherent "viscous" damping through a rate-dependent damping model. The displacement dependent nature of energy dissipation in real structures is not explicitly considered. The DDD uses the secant stiffness at design displacement and associated equivalent damping. The equivalent damping is determined based on the hysteretic energy dissipation (displacement-dependent energy dissipation) at the design displacement. This approach to modeling energy dissipation is particularly relevant for woodframed structures since they exhibit highly nonlinear behavior when subjected to strong seismic excitation. Classical DDD (Priestly 1998) involves the following steps:

1) Define the equivalent SDOF model by the substitute structure approach.
2) Determine the secant stiffness at the design displacement and associated equivalent viscous damping from the damping database.
3) Determine the effective period from the design displacement response spectrum corresponding to the design displacement and compute the effective lateral stiffness.
4) Compute the design base shear by multiplying the effective lateral stiffness by the design displacement.

Equivalent viscous damping used in the DDD is often difficult to quantify for structures that experience damage. Including energy dissipation systems to reduce hysteretic energy demand on the structure (and thus reduce damage) enables the designer to quantify damping more accurately, and thus it improves the reliability of the DDD procedure.

2.5.1 Displacement-Based Design using Inter-story Drift Spectra

A new displacement-based design (DBD) procedure has been developed by Pang and Rosowsky (2007) within the NEESWood project. The procedure requires simple modal analysis and determination of equivalent stiffness based on the backbone response of the shearwalls that are being considered for the design. In the design process, the acceleration response spectrum is converted into a set of inter-story drift spectra which are used to determine the minimum stiffness required for each story such that the inter-story drift is limited to specified values. A flowchart that summarizes the key steps in designing a damping system for seismic retrofit applications is shown in Figure 2.7. A detailed description of many of these key steps, including normalized modal analysis, construction of inter-story drift spectra to determine required equivalent stiffness (i.e., demand), development of wood shearwall design tables to determine actual equivalent stiffness (i.e., capacity), and computation of story shear and uplift forces, can be found in Pang and Rosowsky (2007). Note that the displacement-based design procedure described therein adopts a completely different approach as compared to the classical DDD procedure.

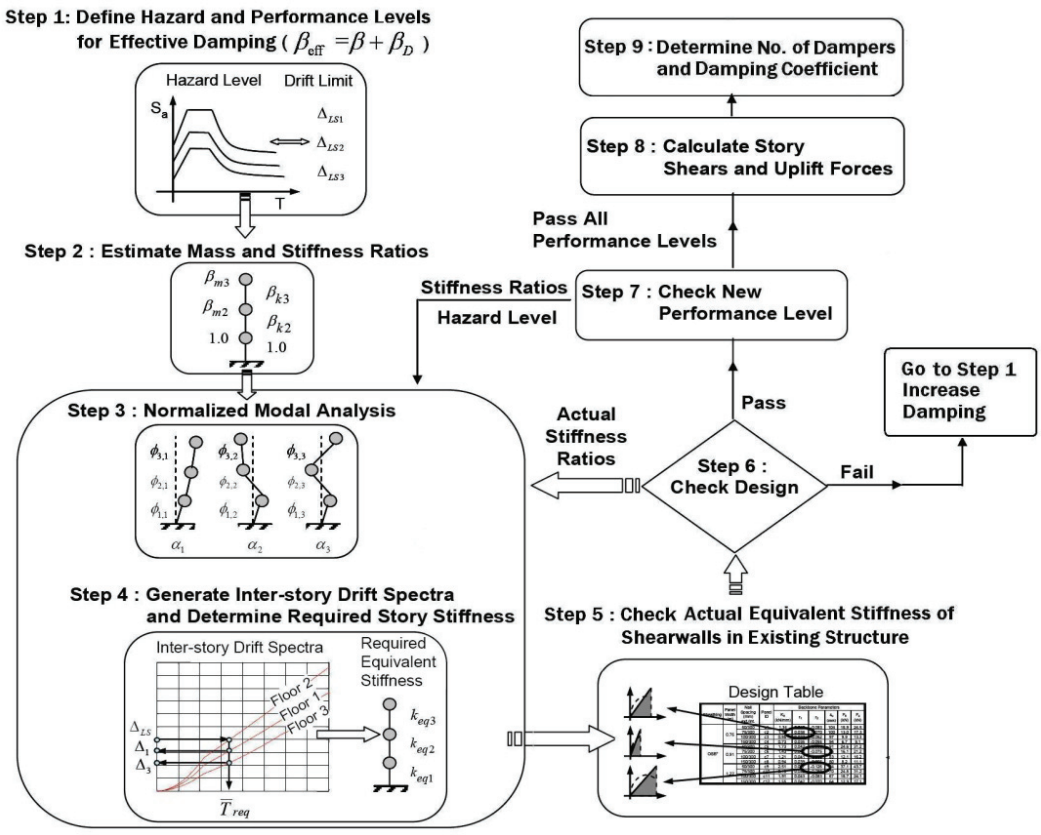

Figure 2.7 Flowchart for Designing Dampers for Seismic Retrofit of Multi-Story Buildings using Displacement-Based Design Procedure (Adapted from Pang and Rosowsky 2007)

It should be noted that the displacement-based design procedure developed by Pang and Rosowsky (2007) can be modified for design of both new and existing structures with seismic dampers. The key modifications for application to new structures are: Assume a high fundamental mode damping ratio and develop associated design acceleration response spectrum (will result in lower stiffness requirement); select shear walls that satisfy specified performance levels; for a selected number of dampers, determine their required damping coefficient; perform nonlinear response-history analysis to verify the design. For existing structures, the key modifications are: Using available test data, prepare a shearwall design table for the existing shearwalls; using a trial and error procedure, determine the level of damping required to satisfy the design performance levels; for a selected number of dampers, determine their required damping coefficient; perform nonlinear response-history analysis to verify the design.

2.6 Design Example

2.6.1 Building Configuration

The benchmark test structure was selected for the displacement-based design example presented herein. Note that the proposed displacement-based design procedure will be presented within the context of a retrofit application wherein seismic dampers (linear viscous fluid dampers with toggle-brace assembly) are incorporated within the benchmark test structure. In this study, analysis and design are performed only in the weaker direction (transverse).

The Phase 1 benchmark test structure, which includes OSB sheathing installed on the exterior sides of all structural walls was analyzed. To compare its performance with the addition of interior finish materials, the Phase 4 benchmark test structure was analyzed. The Phase 4 structure includes gypsum wallboard installed on all structural and partition walls and ceilings. Note that the Phase 5 benchmark test structure (shown in Figure 2.1d) includes exterior finish material but was not considered for the analysis herein due to the reduced reliability of the parametric values that define the hysteretic behavior of the fully finished shear walls (e.g., stucco finish is brittle and thus it is questionable to what degree it can be counted on to provide structural resistance).

2.6.2 Design Process

2.6.2.1 Target Performance Levels and Seismic Hazard Levels (Step 1 in Figure 2.7)

Table 2.4 shows performance levels and the corresponding drift limits and probability of nonexceedance (P_{NE}) for woodframed structural assemblies (modified from FEMA 356). The aforementioned benchmark structure tests indicated that the collapse prevention drift limit for a two-story building is not 3%, as specified in FEMA 356, but rather is significantly higher. In this study, the collapse prevention drift limit was taken as 4%. A study investigating the original FEMA limit states for woodframed buildings can be found in van de Lindt and Liu (2007).

The design acceleration response spectra is shown in Figure 2.8. Spectral values over a period range from 0.1 to 0.6 seconds are equal to 1.1g and 1.65g corresponding to the flat region of the 1997 Uniform Building Code design response spectrum for Los

Angeles, CA (seismic zone 4) for a 10%/50 yr and 2%/50 yr hazard level (ICBO 1997), respectively, which is consistent with the assumption that the benchmark structure is located in seismic zone 4. Note that the equations to define spectral acceleration as a function of period are based on the IBC 2006 recommendations. The design acceleration response spectrum is constructed using the damping reduction factor, B_ξ, determined in accordance with (ASCE/SEI-41 2006):

$$B_\xi = \frac{4}{5.6 - \ln\left(100\xi_{eff}\right)} \tag{2.1}$$

where ξ_{eff} is the equivalent effective viscous damping ratio. Since nonlinear hysteretic damping is explicitly considered in the analysis, the inherent viscous damping of the structure is taken as 5% in the fundamental mode to account for rate-dependant damping effect. Thus, the value of B_ξ is equal to unity.

Table 2.4 Structural Performance Levels for Woodframed Structural Assemblies

Element	Type	Structural Performance Levels		
		Collapse Prevention	**Life Safety**	**Immediate Occupancy**
Wood stud wall	Primary	Connections loose. Nails partially withdrawn. Some splitting of members and panels. Veneers dislodged.	Moderate loosening of connections and minor splitting of members.	Distributed minor hairline cracking of gypsum and plaster veneers.
	Secondary	Sheathing sheared off. Let-in braces fractured and buckled. Framing split and fractured.	Connections loose. Nails partially withdrawn. Some splitting of members and panels.	Distributed minor hairline cracking of gypsum and plaster veneers.
	Inter-story Drift Limit	**4 % transient Or permanent**	**2% transient 1% permanent**	**1% transient 0.25% permanent**
	P_{NE}	**80%**	**50%**	**50%**
Horizontal Wood Diaphragms	NA	Large permanent distortion with partial withdrawal of nails and extensive splitting of elements.	Some splitting at connections. Loosening of sheathing. Observable withdrawal of fasteners. Splitting of sheathing and framing.	No observable loosening or withdrawal of fasteners. No splitting of sheathing or framing.

2.6.2.2 Normalized Modal Analysis and Construction of Inter-Story Drift Spectra (Step 3 and 4 in Figure 2.7)

The mass ratios, β_m, (relative to the first story) are 1.0 and 0.42 for the first and second stories, respectively. The target stiffness ratio β_k must be estimated based on engineering judgment/experience. Initial values of β_k (relative to the first story) can be estimated based on the total full-height shearwall length in the direction considered and for each story. The total shearwall length for the first and second story in the weaker direction of the benchmark structure is about 15.85 m (52 ft) and 14.94 m (49 ft), respectively. Based on the shearwall length, an initial estimate of β_k = 0.94 can be assumed for the second story. However, since the inertial mass driving the second story is relatively small compared to the first story, an initial value of β_k = 2.5 for the second story was assumed (i.e., the small inertial mass results in small second story drifts and thus high equivalent stiffness). After the mass and stiffness ratios have been determined, a normalized modal analysis is performed to compute frequency parameters, α_n, and mode shapes, ϕ_n, of the n-th mode (along the transverse direction of the structure), as given by:.

$$\alpha_n^2 M\phi_n = K\phi_n \tag{2.2}$$

Knowing these parameters, the inter-story drift factors γ_{jn} are computed using:

$$\gamma_{jn} = \Gamma_n\left(\phi_{jn} - \phi_{j-1,n}\right) \tag{2.3}$$

where Γ_n is the modal participation factor corresponding to the n-th mode ϕ_{jn} and ϕ_{jn} is the mode shape amplitude at the j-th DOF(floor)in the n-th mode. The design inter-story drift spectra are then generated from the design acceleration response spectrum using:

$$\Delta_j\left(\overline{T}\right) = \frac{1}{H_j}\sqrt{\sum_n\left[\gamma_{jn}\left(\frac{\overline{T}}{2\pi\alpha_n}\right)^2 S_a\left(\frac{\overline{T}}{\alpha_n}\right)\right]^2} \tag{2.4}$$

where $\Delta_j\left(\overline{T}\right)$ is the inter-story drift for the j-th story (with contributions from all modes), H_j is the height of the j-th story, and $\overline{T}$ is the normalized first-story period. An example of the inter-story drift spectra for the structure without dampers and for a 2%/50 year hazard level, along with the parameters used for its generation, is shown in

Figure 2.9. To meet the 4% drift limit associated with the CP performance level (see Table 2.4), the maximum normalized first-story period, $\overline{T}_{req}$, is 0.41 sec. At the same hazard level, the second story will experience only 0.51% drift. Knowing the required first-story period $\overline{T}_{req}$, the required equivalent stiffness of each story is then determined using:

$$\left(k_{eq}\right)_j = \left(\frac{2\pi}{\overline{T}_{req}}\right)^2 m\beta_{kj} \tag{2.5}$$

where m is the inertial mass assigned to the first story and β_{kj} is the stiffness ratio for the j-th story).

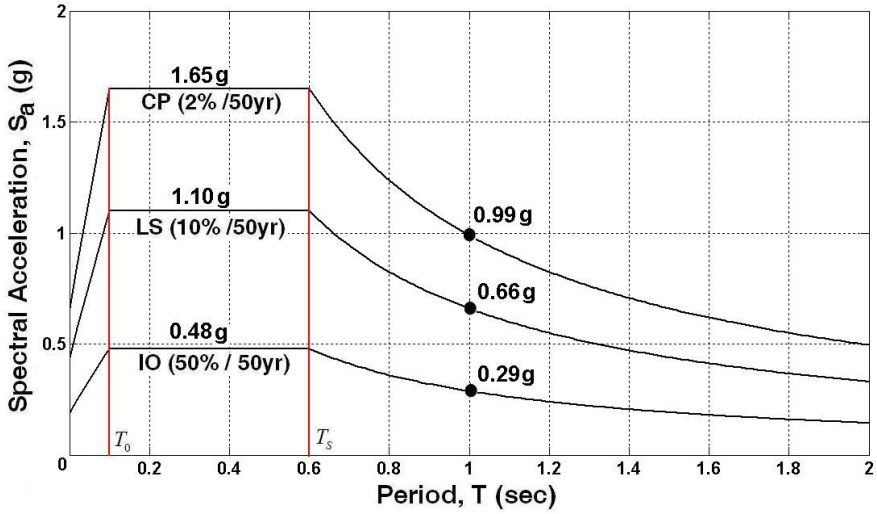

Figure 2.8 5%-Damped Design Acceleration Response Spectra for Los Angeles, California

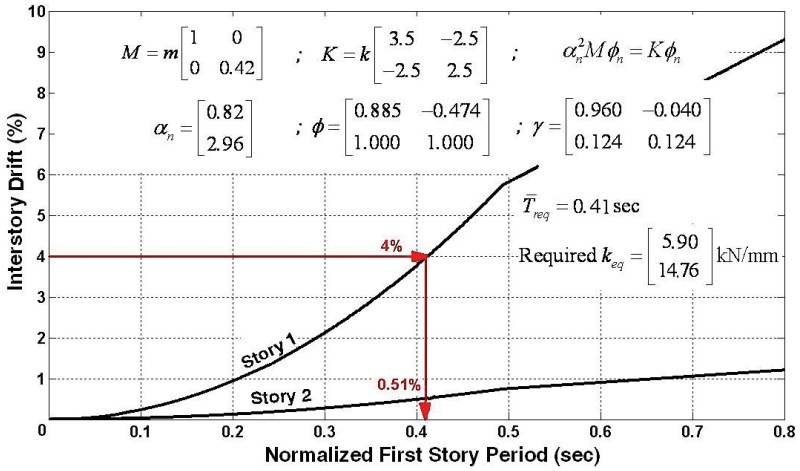

Figure 2.9 Inter-story Drift Spectra for 2%/50 year Hazard Level

2.6.2.3 Verification of Design Using Equivalent Stiffness Ratios (Step 6 in Figure 2.7)

A shearwall design table for 2.44 m (8 ft) high walls with studs spaced at 406.4 mm (16 in) on-center and OSB attached using 8d common nails is shown in Table 2.5 for Phase 1 (OSB only) and Phase 4 (OSB and GWB). The table contains the values of parameters that define the backbone curve for walls constructed with various nailing patterns and panel widths. The CASHEW program (Folz and Filiatrault 2001), along with available shearwall test data from the benchmark test, was used to generate the design table (see Section C.1 for details).

Table 2.6 summarizes the displacement-based design of the Phase 4 benchmark structure without dampers in the transverse direction and for multiple performance levels. The actual equivalent stiffness provided by the shearwalls at each story varies from the required equivalent stiffness. Another normalized modal analysis is performed (using the actual values of β_k) to determine new story drift estimates and required equivalent stiffness. Finally, the ratio of actual and required equivalent stiffness is calculated to give an indication as to whether the design meets the given performance requirements. For example, as shown in Table 2.6, the benchmark structure without dampers does not satisfy CP design limits for 2%/50 year hazard level. Note that the procedure results in equal values of stiffness ratios for all stories in the structure. The ratio of actual and required equivalent stiffness for the Phase 1 structure without dampers is also noted in the Table 2.7. As expected, these ratios are smaller for the

Phase 1 structure as compared to the Phase 4 structure as actual equivalent stiffnesses for OSB shearwalls are less as compared to OSB+GWB shearwalls. Note that new woodframed structures are traditionally designed without considering the contribution of finish materials (i.e., Phase 1 for benchmark structure). Thus, including the effect of finish materials in displacement-based design is particularly useful for retrofit applications (as done in this study) which may result in reduced retrofitting cost.

Table 2.5 Shearwall Design Table for 8 ft High Walls with Studs Spaced at 16 in On-Center and OSB Attached Using 8d Common Nails

Sheathing (Test Phase)	Panel Width (m)	Ext/ 300 (mm)*	Panel ID**	Backbone Parameters						Equivalent Stiffness, K_{eq} (kN/mm) at Target Drift				
				K_0 (kN/mm)	r_1	r_2	δ_u (mm)	F_0 (kN)	F_u (kN)	Drift (%)				
										0.25	0.50	1.0	2.0	4.0
OSB (Phase 1)	0.76	50	s1	1.34	0.040	-0.083	104	18.9	24.5	1.17	1.05	0.85	0.60	0.38
		75	s2	1.12	0.038	-0.070	100	13.0	17.3	0.96	0.83	0.65	0.45	0.27
		100	s3	0.95	0.037	-0.062	97	9.9	13.3	0.80	0.69	0.53	0.35	0.22
		150	s4	0.73	0.035	-0.055	94	6.7	9.1	0.60	0.51	0.38	0.25	0.15
	0.91	50	s5	1.73	0.042	-0.096	91	24.6	31.2	1.52	1.36	1.10	0.79	0.50
		75	s6	1.43	0.042	-0.075	85	16.1	21.2	1.22	1.06	0.83	0.57	0.35
		100	s7	1.21	0.041	-0.066	83	12.1	16.2	1.01	0.87	0.66	0.44	0.27
		150	s8	0.94	0.039	-0.055	80	8.2	11.1	0.77	0.64	0.48	0.31	0.19
	1.22	50	s9	2.51	0.037	-0.126	74	37.1	43.7	2.21	1.98	1.61	1.16	0.71
		75	s10	2.18	0.042	-0.099	70	24.8	31.2	1.86	1.62	1.26	0.87	0.51
		100	s11	1.91	0.043	-0.083	67	18.7	24.1	1.59	1.36	1.03	0.69	0.40
		150	s12	1.55	0.042	-0.070	64	12.9	17.1	1.25	1.04	0.77	0.50	0.29
OSB and GWB (Phase 4)	0.76	50	s13	1.50	0.025	-0.075	104	20.7	24.5	1.31	1.16	0.93	0.65	0.40
		75	s14	1.29	0.021	-0.061	98	14.8	17.4	1.10	0.94	0.73	0.49	0.29
		100	s15	1.13	0.017	-0.053	95	11.7	13.4	0.94	0.80	0.60	0.40	0.23
		150	s16	0.92	0.011	-0.047	91	8.5	9.4	0.75	0.63	0.46	0.29	0.17
	0.91	50	s17	2.00	0.026	-0.084	91	27.0	31.6	1.74	1.53	1.22	0.85	0.53
		75	s18	1.73	0.022	-0.064	85	18.6	21.8	1.46	1.24	0.95	0.63	0.37
		100	s19	1.52	0.018	-0.054	81	14.6	16.8	1.25	1.05	0.78	0.51	0.29
		150	s20	1.26	0.012	-0.044	77	10.7	11.8	1.00	0.83	0.60	0.38	0.21
	1.22	50	s21	2.92	0.023	-0.110	75	39.3	44.2	2.54	2.24	1.78	1.24	0.74
		75	s22	2.64	0.021	-0.084	70	27.9	31.7	2.21	1.89	1.44	0.95	0.54
		100	s23	2.40	0.017	-0.069	67	22.0	24.8	1.96	1.63	1.21	0.77	0.43
		150	s24	2.07	0.012	-0.053	63	16.3	17.8	1.63	1.33	0.94	0.58	0.31

*External/ Internal (i.e., Edge/ Field) Nail Spacing

**Highlighted Panel ID's indicate the Shearwalls used in the Benchmark Structure

Table 2.6 Displacement-Based Design of Phase 4 Benchmark Structure Without Dampers in Transverse Direction for Multiple Performance Levels

HL	PL	Drift Limit (%)	Story	Initial β_k	Drift (%)	Required K_{eq} (kN/mm)	Rounded Drift (%)	Actual K_{eq} (kN/mm)	Actual β_k	Drift (%)	Required K_{eq} (kN/mm)	Act/Req K_{eq}
2%/ 50yr	CP	4.00	1	1.00	4.00	5.90	4.00	4.66	1.00	4.00	5.90	0.79
			2	2.50	0.51	14.76	0.50	15.55	3.34	0.38	19.70	0.79
10%/ 50yr	LS	2.00	1	1.00	2.00	7.66	2.00	8.27	1.00	2.00	7.66	1.08
			2	3.34	0.19	25.59	0.25	19.00	2.30	0.28	17.62	1.08
50%/ 50yr	IO	1.00	1	1.00	1.00	6.87	1.00	12.93	1.00	1.00	6.87	1.88
			2	2.30	0.14	15.81	0.24	19.00	1.47	0.24	10.10	1.88

2.6.2.4 Displacement-Based Design of Benchmark Structure With Dampers

For the benchmark structure with dampers, new performance levels were defined as follows: LS performance for 2%/ 50 year hazard level and IO performance for 10%/ 50 year hazard level with 50% probability of nonexceedance for both hazard levels. Table 2.7 shows the ratio of actual and required equivalent stiffness for four different effective damping ratios (5%, 22.5%, 27.5%, and 32.5%) as obtained from displacement-based design analysis for the Phase 1 and 4 benchmark structure. Recall that 5% effective damping corresponds to the structure without dampers. Also note that, for a given drift level, these ratios make sense in that the required equivalent stiffness reduces with increased effective damping (and thus the equivalent stiffness ratio increases). Furthermore, these results indicate that the LS and IO performance levels can be achieved for the 2%/50 yr and 10%/50 yr hazard levels, respectively. However, a more refined nonlinear dynamic response-history analysis could be performed to confirm the results although it is expected that such analyses would yield similar inter-story drift demand results.

The effect of effective damping (15% to 35% with the increment of 2.5%) on the ratio of actual to required equivalent stiffness of Phase 1 and Phase 4 benchmark structure with dampers is also shown in Figure 2.10. Note that the effect of supplemental damping is more prominent for the lower performance level (i.e., CP performance for 2%/50 year hazard level and LS performance for 10%/50 year hazard level) as indicated by higher slopes of those lines. Also note that the ratios of actual to required equivalent stiffness are almost varying linearly with effective damping (small deviations are due to numerical rounding). The use of damping reduction factor B_ξ (approximately linearly varying over the range of effective damping ratios considered) applied to the elastic

response spectra results in this linear relationship. It is important to recognize the linear relationship in Figure 2.10 since linear interpolation can then be used to compute the ratio of actual to required equivalent stiffness.

Table 2.7 Displacement-Based Design of Benchmark Structure With Dampers in Transverse Direction for Multiple Performance Levels

Hazard Level	Perf. Level	Drift Limit (%)	K_{eq} Actual / K_{eq} Required							
			Without Dampers		With Dampers					
			ξ_{eff} = 5%		ξ_{eff} = 22.5%		ξ_{eff} = 27.5%		ξ_{eff} = 32.5%	
			Phase 1	Phase 4	Phase 1	Phase 4	Phase 1	Phase 4	Phase 1	Phase 4
2%/50 yr	CP	4.00	0.73	0.79	1.31	1.42	1.55	1.69	1.82	1.98
	LS	2.00	------	------	1.00	**1.14**	1.09	1.24	**1.17**	1.33
	IO	1.00	------	------	0.74	0.87	0.81	0.95	0.88	1.04
10%/50 yr	LS	2.00	0.95	1.08	1.50	1.71	1.63	1.86	1.76	2.00
	IO	1.00	------	------	1.12	**1.33**	1.22	1.45	**1.32**	1.57

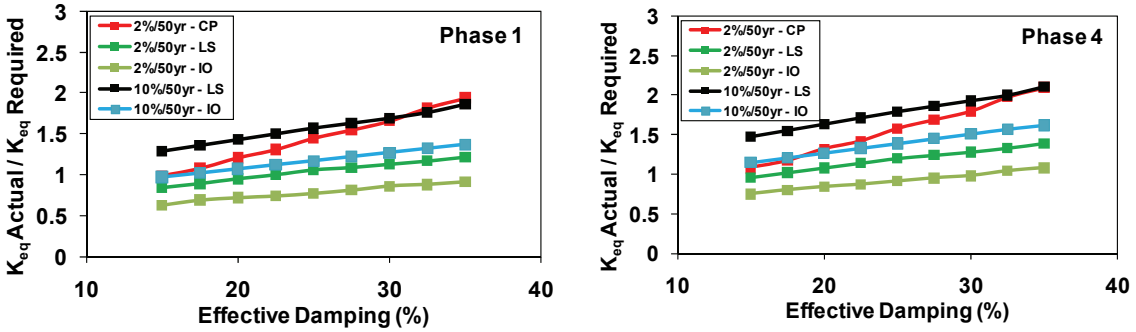

Figure 2.10 Effect of Effective Damping on Ratio of Actual to Required Equivalent Stiffness of Benchmark Structure With Dampers

The advantage of the displacement-based design is that it is much simpler than nonlinear dynamic response-history analysis while providing a reasonable prediction of structural performance for a given hazard level. For example, the results in Table 2.7 indicate that, for a 2%/50 yr hazard level, the IO performance level can not be achieved without increasing the effective damping to some value well beyond 32.5% for the Phase 1 structure. Further, for a 10%/50 yr hazard level, the IO performance level can be achieved with an effective damping ratio of 22.5% (or slightly less) for the Phase 4 structure. It is recommended that the acceptance criteria (ratio of actual to required equivalent stiffness) for selecting an optimal design be set to some value larger than

unity (say 1.1 to 1.15) to account for the various simplifying assumptions made in the displacement-based design procedure and possible discrepancies between hysteretic parameter values obtained from laboratory tests over actual field construction. Thus, based on the results in Table 2.7, an effective damping ratio of 32.5% and 22.5% was selected as suitable for achieving the desired performance for the given hazard levels for the Phase 1 and Phase 4 structure, respectively. Fine tuning of the design could be performed by conducting nonlinear dynamic response-history analyses. As the ratio of actual to required equivalent stiffness for optimal design of Phase 1 and Phase 4 structure are similar, one would expect similar results from nonlinear time history analysis (NLTHA), but as will be shown, this was not the case for the present study.

2.6.2.5 Determining the Number of Dampers and Damping Coefficient Values (Step 9 in Figure 2.7)

As mentioned previously, according to Section 1.6.1.5.3 of FEMA 356 (ASCE 2000), for structures retrofitted using seismic isolation or supplemental energy dissipation, an effective viscous damping ratio, ξ_{eff}, should be calculated using the procedure specified in Chapter 9 and utilizing the damping reduction factor B_{ξ} (see Equation 2.1). Thus, to determine the number of dampers and associated damping coefficient values, Equation 9-30 can be used:

$$\xi_{eff} = \xi + \xi_D = \xi + \frac{T\sum_j C_j \cos^2\theta_j \phi_{rj}^2}{4\pi \sum_i \left(\frac{w_i}{g}\right)\phi_i^2} \tag{2.6}$$

where ξ is the inherent structural damping ratio(taken as 5%), ξ_D is the supplemental damping ratio, T is the fundamental period of the retrofitted building, C_j is the damping coefficient of damper j, θ_j is the angle of inclination of damper j with respect to the horizontal, ϕ_{rj} is the first mode relative displacement between the ends of damper j in the horizontal direction, ϕ_i is the first mode displacement at floor level i, and w_i is the seismic weight assigned to floor level i. Having selected the number of dampers, Equation 2.6 can be used to determine the required damping coefficient for each damper.

For the optimal design presented above for the Phase 4 benchmark structure, the effective damping is 22.5% and thus the supplemental damping ratio is equal to 17.5%. Note that in Equation 2.6, $\cos\theta_j$ represents the magnification factor associated with the orientation of the damper with respect to the horizontal. An alternate damper configuration employs a toggle-brace wherein the damper displacement is amplified in accordance with the geometry of the toggle-brace assembly (Constantinou et al. 2006). In this study, a toggle-braced damper assembly is assumed to be used in the retrofit of the benchmark structure and the magnification factor is taken as 1.65 to correspond with an assembly that was tested as part of the NEESWood project (see Chapter 3). The distribution of lateral story drifts needs to be assumed to determine the number of dampers and their damping coefficient. In this case, it was assumed that the maximum story drifts are proportional to the fundamental mode shape. Alternatively, the maximum story drifts can be estimated using results from a pushover analysis. The frequencies and mode shapes were computed using the mass and initial stiffness of the benchmark structure. Assuming 4 dampers located in the first story, each having the same damping coefficient, results in damping coefficient values of 1.20 and 1.71 kN-sec/mm (0.21 and 0.3 kip-sec/in) for the Phase 1 and Phase 4 structure, respectively.

2.7 Design Appraisal

The optimal design of the damping system was determined based on the displacement-based design procedure and, as a verification step in the PBSD procedure, earthquake simulations using a suite of twenty earthquake ground motions (Krawinkler et al. 2000) were performed using SAWS. Similar to the work by Krawinkler et al. (2000), these earthquake ground motions were scaled such that their mean 5%-damped spectral values over a period range from 0.1 to 0.6 seconds is equal to 1.1g and 1.65g corresponding to the flat region of the 1997 Uniform Building Code design response spectrum for Los Angeles, CA for a 10%/50 yr and 2%/50 yr hazard level, respectively (ICBO 1997) (see Table 2.8). The approach used in the present study is consistent with ground motion scaling described in the FEMA 302 (BSSC 1997) and FEMA 356 (ASCE 2000). As mentioned previously, the same response spectra parameters were used in the

displacement-based design procedure described earlier to maintain consistency with non-linear dynamic response-history analysis.

Table 2.8 Suite of Ground Motion Records Used for Design Appraisal

Earthquake Event/Year	Notation	Peak Ground Acceleration (g)		
		Actual	Scaled	
			Life Safety	Collapse Prevention
Cape Mendocino 1992	Cm1	0.116	0.530	0.795
	Cm2	0.385	0.532	0.798
Landers 1992	Lan1	0.154	0.542	0.813
	Lan2	0.152	0.399	0.599
Loma Prieta 1989	Lp1	0.529	0.423	0.635
	Lp2	0.555	0.473	0.710
	Lp3	0.417	0.520	0.780
	Lp4	0.226	0.410	0.615
	Lp5	0.279	0.415	0.623
	Lp6	0.332	0.600	0.900
Northridge 1994	Nor2	0.416	0.470	0.705
	Nor3	0.356	0.599	0.899
	Nor4	0.357	0.472	0.708
	Nor5	0.231	0.482	0.723
	Nor6	0.273	0.609	0.914
	Nor9	0.271	0.485	0.728
	Nor10	0.157	0.472	0.708
Superstition Hills 1987	Sup1	0.116	0.604	0.906
	Sup2	0.258	0.584	0.876
	Sup3	0.186	0.398	0.597

The simulation results (with and without dampers) for the 20 motions were plotted against cumulative probability (see Figure 2.11) and a summary of results are presented in Table 2.9 and 2.10. Note that the first story drift ratio (which corresponds to the peak drift ratio of the structure) for the no damper case exceeds the 4% drift limit for both phases of the benchmark structure corresponding to the CP performance level (thus indicating collapse or incipient collapse of the structure) which is consistent with the results from the displacement-based design (see Table 2.7). Note that a drift limit of 7%, a reasonable value for defining impending instability of the structure from an analysis point of view, was imposed on the calculation of mean drift which also corresponds to the drift value defined in ATC 63 as a performance level for a 2%/50 yr hazard level. For the case with dampers and according to FEMA 302, it would be acceptable to design

to the median value of the CDF if this were a force-based design. Thus, for the Phase 4 damper design (ξ_{eff} = 22.5%), it is apparent that the LS performance level can be achieved for a 2%/50 yr hazard level as evidenced by the results (median value = 1.59% and P_{NE} = 82%). Note that the expected drift and the ratios of actual-to-required equivalent stiffness are inversely proportional and thus the drift demand of the designed structure can be estimated at each performance level by taking the ratio of the drift limit to the stiffness ratio (Pang and Rosowsky 2007). Thus, these results are consistent with that from the displacement-based design (see Table 2.10). Therefore, it can be concluded that the design of the building with dampers meets (or exceeds) the design objective for life safety for a 2%/50 yr hazard level. For the same hazard level, the Phase 1 damper design (ξ_{eff} = 32.5%) also satisfies the probability of non-exceedance criteria of 50% (median value = 1.74% and P_{NE} = 70%) as defined earlier for the structure retrofitted with dampers. Note that this approximate method of estimating drift demand was not considered to be applicable to the case without dampers for both hazard levels since many ground motions produced drift levels that exceeded the performance limit and thus the median value is not a realistic value.

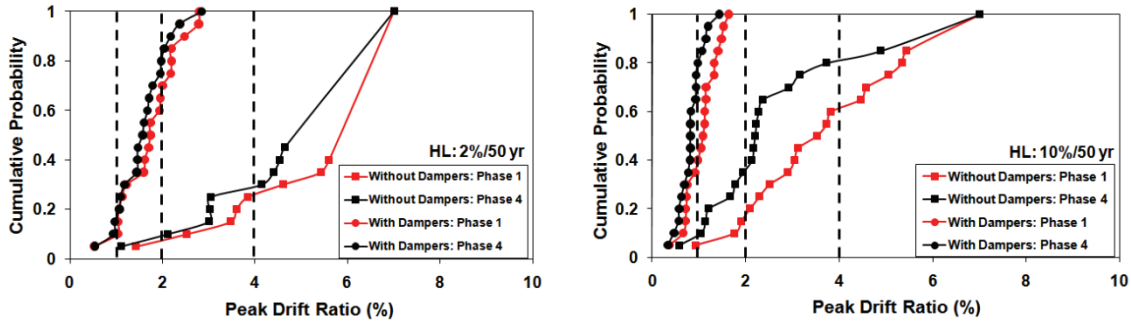

(a) **(b)**

Figure 2.11 Peak Drift Distributions from Nonlinear Dynamic Analysis of Benchmark Structure With and Without Dampers and for (a) 2%/50 yr and (b) 10%/50 yr Hazard Levels

The structure was also analyzed for the 10%/50 yr hazard level and similar conclusions can be drawn. As mentioned previously, the ratio of actual to required equivalent stiffness for optimal design of the Phase 1 and Phase 4 structure are similar and therefore one should expect similar results from NLTHA. However, the results for

the Phase 4 structure were more consistent with performance expectations from the DBD procedure (see Table 2.10). This may be due to better consistency of the hysteretic parameters defining the equivalent stiffnesses of the shearwalls in the Phase 4 structure with the hysteretic parameters used in the NLTHA modeling as compared to the Phase 1 structure (i.e., the actual equivalent stiffnesses of the Phase 1 structure (OSB only) are slightly underestimated and the actual value of the effective damping should be on the order of 35% to yield performance similar to that of the Phase 4 optimal design (ξ_{eff} = 22.5%). This discrepancy can be resolved by considering higher acceptance criteria for selecting optimal design (i.e., the ratio of actual to required equivalent stiffness of 1.2 to 1.4 may be used depending on the confidence level of designers in the estimation of actual equivalent stiffnesses of shearwalls).

Table 2.9 Summary of Results of Phase 1 and Phase 4 Benchmark Structure Without Dampers

Hazard Level	Performance Expectations			NLTHA Results			
	Perf. Level	Drift Limit (%)	P_{NE} (%)	Phase 1		Phase 4	
				ξ_{eff} = 5%		ξ_{eff} = 5%	
				Median Drift (%)	P_{NE} (%)	Median Drift (%)	P_{NE} (%)
2%/50 yr	CP	4.00	80	7.00	26	7.00	29
10%/50 yr	LS	2.00	50	3.63	18	2.21	36

Table 2.10 Summary of Results of Phase 1 and Phase 4 Benchmark Structure Retrofitted With Dampers

Hazard Level	Perf. Expectations			NLTHA Results				Expected from Design	
	Perf. Level	Drift Limit (%)	P_{NE} (%)	Phase 1		Phase 4		Phase 1	Phase 4
				ξ_{eff} = 32.5%		ξ_{eff} = 22.5%		ξ_{eff} = 32. 5%	ξ_{eff} = 22.5%
				Median Drift (%)	P_{NE} (%)	Median Drift (%)	P_{NE} (%)	Median Drift (%)	Median Drift (%)
2%/50 yr	LS	2.00	50	1.74	70	1.59	82	1.71	1.75
10%/50yr	IO	1.00	50	1.10	42	0.82	81	0.75	0.75

The reasonably good agreement between the design inter-story drifts (based on displacement-based design) and the median peak drifts obtained from response-history analyses serves to validate the proposed modifications to the displacement-based design procedure for inclusion of linear viscous dampers in seismic retrofit applications. Therefore, it can be concluded that the optimal design of the supplemental damping

system used for retrofit of the benchmark structure satisfies the specified performance objectives.

2.8 Performance Assessment

As mentioned previously, 22.5% effective damping (four toggle-braced dampers in the first story along the transverse direction) was selected as the optimal design for the Phase 4 structure. The performance improvement afforded by the dampers is now evaluated for this particular case and for selected performance measures. Figure 2.12a shows the absolute roof acceleration response history along line 6 (see Figure 2.1a) for level 4 excitation used in the benchmark test. Note that the Level 4 motion is the 1994 Northridge, Canoga Park OGM record scaled to 10%/50 year hazard level. The effect of the dampers is to reduce the peak acceleration by approximately 40%; accordingly it is expected that non-structural and contents damage of the structure would be reduced. Figure 2.12b shows the hysteretic response of wall 17 (i.e., east garage wall) with and without dampers. As expected, the peak wall displacement (drift) is significantly reduced and the energy dissipated near zero displacement is increased significantly due to the velocity-dependence of the dampers.

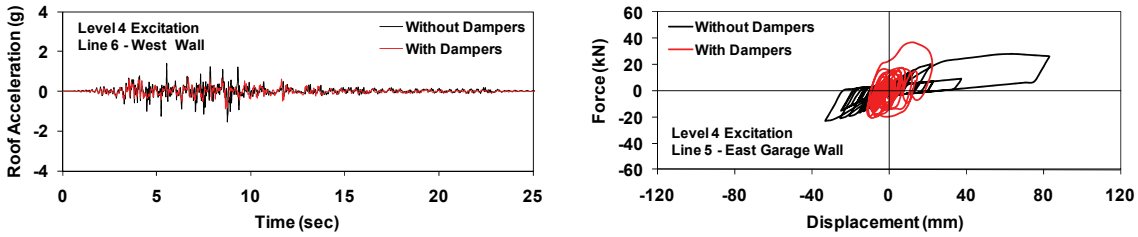

(a) **(b)**

Figure 2.12 (a) Roof Acceleration Time History and (b) Wall Hysteresis With and Without Dampers

Figure 2.13 shows a comparison of the energy distribution for the case of the structure with and without dampers (note that, for comparison purposes, the two figures are plotted to the same scale). The effect of the dampers is to reduce the hysteretic energy dissipation demand by approximately 70%. The reduced hysteretic energy dissipation demand on the wood framing system suggests that the structure with damper

walls would experience less structural damage than the structure with conventional walls.

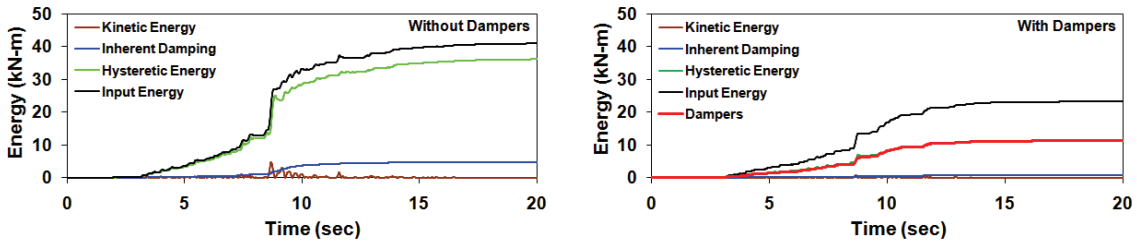

(a) **(b)**

Figure 2.13 Energy Time History for Level 4 Excitation: (a) Without Dampers and (b) With Dampers

2.9 Summary and Concluding Remarks

The research presented herein demonstrated the feasibility of implementing modular damper walls within a full-scale, three-dimensional, woodframed building. The modular damper walls contained fluid dampers within a wood framing system. Such dampers can readily fit within the dimensional restrictions of a conventional wood shearwall. Thus, the modular damper walls can be constructed off-site and delivered to the job site for "drop-in" installation. The particular application presented herein was a retrofit application.

Due to a number of factors, including the inherent flexibility in the connections of wood framing systems, engagement of the dampers was limited and thus the full effectiveness of the dampers was not realized. Furthermore, the test structure was tested in its stiffer direction, thereby limiting the need for dampers. However, a comparison of peak story drift responses with and without dampers demonstrated that the dampers offered some level of improved performance. Since peak story drift provides a key measure of damage in a building, reduction of this quantity is important. An alternate modular damper wall has been designed, with particular attention given to increasing the damper displacements. The alternate design was tested recently (see Chapter 3).

A displacement-based PBSD procedure for design of multi-story woodframed buildings with supplemental linear viscous dampers has been presented. The proposed method can be applied to the retrofit of existing structures or to the design of new

structures. The method was applied for retrofit of the NEESWood Benchmark Structure (with and without interior finish materials) with the final design being evaluated using nonlinear response-history analyses. The results demonstrated that the design inter-story drifts based on selected performance levels were in reasonable agreement with median peak inter-story drifts obtained from the nonlinear response-history analyses, thus validating the proposed displacement-based design procedure.

3. EVALUATION OF TOGGLE-BRACED FLUID VISCOUS DAMPERS FOR SEISMIC PROTECTION OF WOODFRAMED STRUCTURES

In recent years, seismic damping systems have been employed in numerous steel and concrete framed buildings. Such systems dissipate a significant portion of the seismic input energy, thereby relieving the energy dissipation demand on the structural framing system and thus reducing damage. As part of a NEESR project to develop a performance-based approach to seismic design of multi-story light-framed wood structures, the application of damping systems to such structures has been evaluated via seismic shaking table tests and numerical simulations. This chapter focuses on the results from shaking table tests of wood shearwalls retrofitted via toggle-braced fluid

viscous dampers and its numerical modeling. Within the context of performance-based seismic design, the effect of the fluid viscous dampers on the deformation demand and hysteretic energy dissipation demand is emphasized. The results demonstrated that the retrofit provided a significant increase in the seismic resistance of the walls, allowing them to achieve high levels of performance when subjected to strong ground motions. However, the full potential of the retrofit was not realized due to losses in transmission of wall drift to the toggle-bracing system. The study also presents a detailed evaluation of these losses to assist in developing more efficient designs that could increase the potential for implementation of such systems.

3.1 Introduction

Application of seismic protection systems in light-framed wood structures is virtually non-existent within the U.S. as woodframed construction has generally been considered to perform well during earthquakes. However, the 1994 Northridge Earthquake clearly demonstrated the vulnerability of such construction in that extensive, and in many cases unrepairable, damage occurred in thousands of woodframed buildings (Kircher et al. 1997). As a result, a research project (the NEESWood project) was initiated with an emphasis on developing a seismic design approach that considers multiple levels of performance (van de Lindt et al. 2006). The testing phase of the NEESWood Project began with seismic shaking table testing of a full-scale, two-story, woodframed townhouse building (the "benchmark" test structure) (Filiatrault et al. 2007 and Christovasilis et al. 2007). The results of the tests were used to develop a PBSD philosophy to design a mid-rise (six-story) woodframed apartment building which was tested using three-dimensional earthquake ground motions at the E-Defense shaking table facility in Miki City, Japan. Additionally, as part of this project, the application of seismic protection systems (seismic damping and isolation systems) to woodframed buildings was also investigated.

A comprehensive literature review on the application of advanced seismic protection systems (both base isolation and supplemental damping systems) to woodframed structures is presented by Symans et al. (2002). This study clearly identified the various challenges of the application of seismic protection systems to

woodframed structures. Some of these challenges for the application of energy dissipation systems are:

1) Locating the dampers within the confines of a shearwall.
2) Constructing a suitable damper framing system and integrating it within the woodframed shear wall such that inter-story drift is transmitted to the dampers without any major losses.
3) Developing a modified wood framing arrangement to accommodate the damper assembly.

The installation of fluid viscous dampers (Symans and Constantinou 1998) in stiff structures is often less efficient than applications to relatively flexible structures due to potentially small deformations transferred to the dampers. Also, in stiff structures, a higher damper force capacity may be needed to dissipate sufficient energy at low displacements. Note that these problems are amplified for woodframed structures where there can be significant displacement transmission losses from different sources (Shinde et al. 2007, 2010). Different displacement magnification configurations have been proposed in the literature to address the problems associated with stiff structures. Berton et al. (2004) developed a displacement amplification device that uses rack and pinion mechanisms. Taylor Devices, Inc., proposed and patented the toggle-brace damper system in 1996 (Toggle linkage seismic isolation structure," U.S. Patent Nos. 5870863 and 5934028, 1996). Constantinou et al. (2001) further verified this system via testing of a single degree of freedom steel model. Hwang et al. (2005) performed shake table tests on a scale-model of a three-story steel-framed structure with toggle-braced dampers and reported displacement transmission losses on the order of 40% and recommended that this loss be considered for field implementations.

Phase 2 of the NEESWood benchmark structure test program involved implementation and evaluation of a seismic damping system with a chevron brace configuration (Shinde et al. 2007). The testing of such dampers within the NEESWood benchmark structure represents the first application within a full-scale woodframed building. Due to a number of factors, including the inherent flexibility in the connections of wood framing systems, engagement of the dampers was limited during these tests and thus the full effectiveness of the dampers was not realized. Based on what was learned

from this testing, a new design for the modular damper walls with a toggle-braced configuration was developed. The objective of the study described herein is to experimentally and numerically evaluate the seismic response of light-framed wood shearwalls retrofitted with toggle-braced fluid viscous dampers. Within the context of performance-based seismic design, the effect of the fluid viscous dampers on the deformation demand and hysteretic energy dissipation demand is emphasized. A major advantage of using fluid viscous dampers is their high energy dissipation density (i.e., capability of dissipating a large amount of energy relative to their size) which allows them to fit within the relatively narrow confines of a woodframed shearwall. Studies conducted by Symans et al. (2004) and Dutil and Symans (2004) have demonstrated the potential of fluid viscous dampers to reduce the energy dissipation demand in woodframed structures. The results of the testing described herein demonstrated that the retrofit provide a significant increase in the seismic resistance of the walls, allowing them to achieve high levels of performance when subjected to strong ground motions. However, the full potential of the retrofit was not realized due to losses in transmission of wall drift to the toggle-bracing system. The study presented herein also includes a detailed evaluation of these losses and suggests possible retrofitting measures to reduce these losses and thus to increase the potential for future implementation of such systems.

3.2 Test Specimens and Experimental Setup

3.2.1 Test Specimen Configurations

Three test specimens (see Table 3.1) were constructed in accordance with the specifications of the 2006 International Building Code (2006 IBC) (ICC 2006). Finish material (interior gypsum board and exterior siding) was not included in any of the test specimens. The pre-test specimen was constructed with a conventional configuration to ascertain the strength and stability of the overall test setup and thus its details will not be presented. After preliminary testing with the pre-test specimen, two test specimens were constructed with and without a fluid viscous damper with toggle-braced assembly (see Figure 3.1). All shearwalls were designed to simulate the first-story shearwall in a typical two-story woodframed residential structure located in South California. Note that the walls of the pre-test specimen were constructed with two 1.22 m (4 ft) oriented

strand board (OSB) sheathing panels with 406.4 mm (16 in) stud spacing whereas a single 1.22 m (4 ft) sheathing panel was used in the actual test specimens.

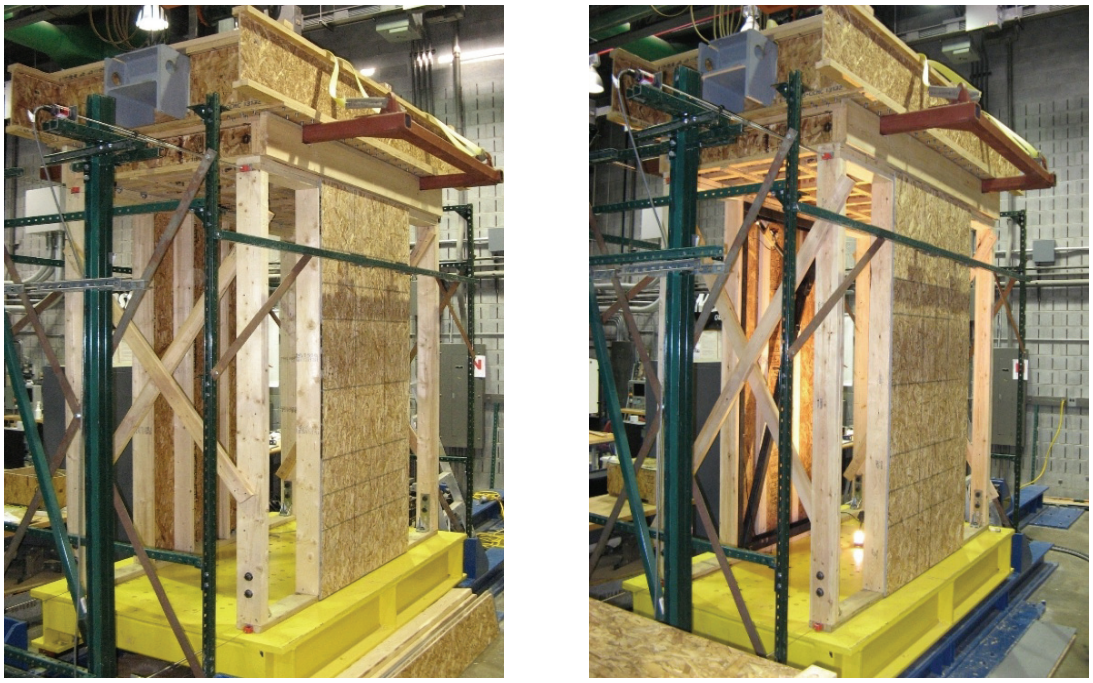

(a) (b)

Figure 3.1 Test Specimens on Seismic Shaking Table: (a) Conventional Walls and (b) Retrofitted Walls (note black steel toggle-braced framing inside of left shearwall)

3.2.2 Test Specimen Anchorage

The shearwall is usually anchored to a concrete foundation with anchor bolts passing through the sill plate and into the concrete. The shearwalls in these experiments were directly anchored to the steel platform of the seismic shaking table with A325 structural steel bolts (see Figure 3.2 and 3.3). Four 22.23 mm (7/8 in) diameter A325 steel anchor bolts were placed at 711.2 mm (28 in) spacing as shown in the Figure 3.2. The shake table and the sill plates had 25.4 mm (1 in) diameter holes, thus leaving a clearance of 1.59 mm (1/16 in.) which was sufficient to cover discrepancies in construction (such as those due to manual measurements, wood shrinkage, etc.). The position of the anchor bolts was selected considering both the location of overturning hold-downs (at both ends of the shearwalls) and anchorage locations for the toggle-braced damper assembly (which was installed at the center of the retrofitted test specimen). Due to these constraints on the anchorage locations, the resulting anchorage (four anchor bolts) was

more than necessary and thus ensured racking of the shearwalls as the primary mode of deformation. A Simpson Strong-Tie™ (Simpson) BP 7/8-3 square washer was used to transfer the anchor bolt compression force to the sill plate (the anchor bolts were passed up through the shake table platform and then through the sill plate such that the threaded end projected above the platform). This steel plate washer was 76.2 mm x 76.2 mm x 7.94 mm thick (3 in x 3 in x 5/16 in thick). Simpson Strong-Tie™ HD6A hold downs with 22.22 mm (7/8 in.) diameter A325 steel bolts were used to connect the double end studs to the shake table through the sill plate.

3.2.3 Conventional Wall Construction

The overall size of the conventional wood shear walls (framing) was 2.44 m x 2.44 m (8 ft x 8 ft). Spruce-Pine-Fir (SPF) was used for framing members [50.8 mm x 152.4 mm (2 in x 6 in)] and the interior studs (within the sheathing region) were spaced at 406.4 mm (16 in) on center and oriented perpendicular to the plane of the wall (see Figure 3.2). The wall was sheathed on one side with one 1.22 m x 2.44 m x 11.91 mm thick (4 ft x 8 ft x 7/16 in thick) OSB sheathing panel oriented vertically and nailed to the framing members with 8d common nails (63.5 mm (2.5 in) length x 3.3 mm (0.131 in) diameter). The edge and field spacing of sheathing-to-framing connectors for the test shearwalls was 152.4 mm (6 in) and 304.8 mm (12 in), respectively. The nailing of framing members (i.e., double end studs, interior studs, sill plate, and top plate) and their connections to each other was consistent with Table 2304.9.1 (fastening schedule) of IBC 2006 (see Section D.3 for a detailed drawing). Standard pre-cut studs were used such that the bottom edge of the OSB sheathing would not come into contact with the shaking table platform, thus allowing the sheathing panels to freely rotate in their own plane during the seismic excitation. Note that the tested shearwall configuration described herein is similar to segmented shearwall design (wherein the shearwall at the opening locations are neglected for design purposes). The selection of OSB thickness and spacing of nails is discussed further in the code-based design section.

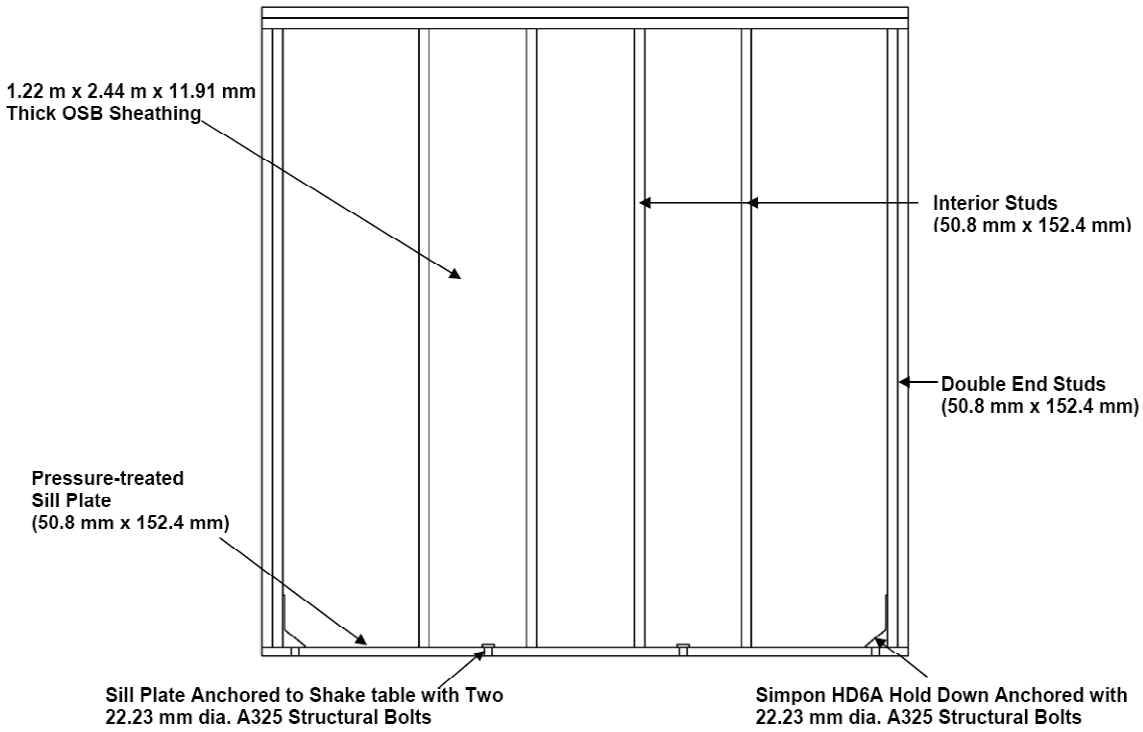

Figure 3.2 Details of Conventional Woodframed Shearwall

3.2.4 Retrofitted Wall Construction

The construction of the retrofitted shearwalls was similar to the conventional shearwalls except for the two interior studs used for field nailing at the centre of the OSB sheathing (see Figure 3.3 and Figure 3.4b). For the retrofitted wall, two 50.8 mm x 101.6 mm (2 in x 4 in) studs were used and oriented parallel to the plane of the wall, thus leaving a free space having a width of 101.6 mm (4 in) to accommodate a toggle-braced fluid viscous damper assembly. A portion of the two center studs was notched to ensure freedom of movement for the toggle bracing. The nailing of the members and sheathing in the retrofitted shearwall was the same as the nailing of the members and sheathing in the conventional shearwall with two exceptions. For the field nailing, 38.1 mm (1.5 in) long 4d common nails spaced at 228.6 mm (9 in) on center were used instead of (2.5 in) long 8d common nails spaced at 304.8 mm (12 in) on center. Also, for the toe-nailing of the interior studs to the sill plate, two 8d common nails instead of four 8d common nails were used (see Section D.3 for a detailed drawing). Note that the field nailing of the interior studs is important in that it contributes to resistance to out-of-plane buckling for

the sheathing . However, for the in-plane stiffness of the shear wall, the field nailing has relatively minor contribution as compared to the perimeter nailing.

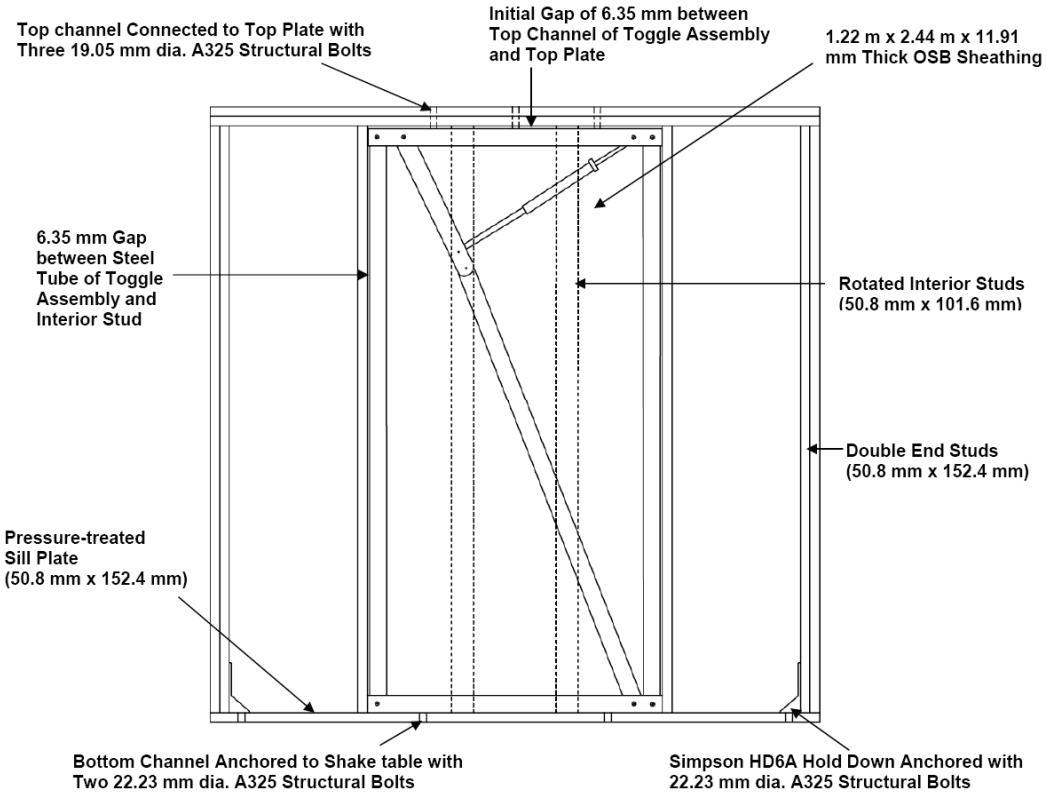

Figure 3.3 Details of Retrofitted Woodframed Shearwall

3.2.5 Applied Dead Load

To replicate the seismic loading conditions the shearwall may experience during earthquakes, gravity loading of 58.71 kN (13200 lbs) (or 12.04 kN/m (825 lb/ft)) was applied to both shearwalls. The load was applied via a typical rigid floor system consisting of wooden truss joists [TJI 230: 241.3 mm (9.5 in) deep] with blocking and connected to the top plate of the wall via Simpson A34 framing clips (see Figure 3.1 and Figure 3.4b). A wood stud [50.8 mm x 254 mm (2 in x 10 in)] was used as a rim joist connected to the truss joists spanning across the walls. The rim joist was also connected to the walls via a combination of Simpson A35 framing clips and woodscrews. The seismic mass included a 2.74m (9 ft) long steel beam (W14 x120) oriented with its web horizontal and 440 lead bricks, each weighing approximately 115.7 N (26 lbs) (see Section D.3 for detailed drawings of test setup). The lead bricks were uniformly distributed over the steel beam and TJI floor system.

3.2.6 Installation of Toggle-Braced Damper Assembly within Retrofitted Wall

Based on what was learned from the Phase 2 Benchmark structure testing (see Figure 3.4a for chevron-braced damper wall used in Phase 2 of Benchmark test), a new design for the modular damper walls with a toggle brace configuration was developed (see Figure 3.4b). The new design employs a light steel frame mechanism that surrounds a toggle-braced damper. The toggle brace provides an average displacement amplification factor, f, (assuming small displacements and rigid brace members) of 1.65 which is 65% larger than the previous damper wall design that employed a chevron-braced configuration. The dampers have nominal force capacity of 11.12 kN (2.5 kips) and a damping coefficient of 1.285 kN-sec/mm (0.225 kip-sec/in).

(a) **(b)**

Figure 3.4 Modular Damper Walls: (a) Chevron Brace Design used in Phase 2 Benchmark Tests and (b) Toggle Brace Design

As shown in Figure 3.4b, the top and bottom channel sections of the toggle-braced assembly were connected to the top plate and foundation (i.e., shaking table) using A325 structural bolts. The gap between the top channel and top plate was maintained to prevent transfer of gravity load to the toggle assembly and thus to allow free movement of the pinned joints of the toggle-braced assembly. Note that the initial gap of 6.35 mm

(1/4 in) was reduced to approximately 3.18 mm (1/8 in) due to bending of the top plate under gravity loading (since the interior studs were rotated, support across the full width of the top plate was not available). Since the toggle-braced assembly did not carry any gravity load and the pinned joints were free to rotate, the only possible mode of deformation of the toggle-braced assembly was racking. Therefore, the toggle-braced assembly is forced to deform as a unit (either in a racking mode or a rigid-body rotation mode). Thus, if the top plate displaces laterally with respect to the sill plate, the damper should deform with amplification of the lateral motion.

3.3 Shake Table Test Program

3.3.1 Testing Program

A total of three test specimens, two conventional and one retrofitted, were tested with multiple excitations (see Table 3.1). The complete details of the experimental testing program are provided in Appendix D.

Table 3.1 Description of Test Specimens Used in Experimental Test Program

Test Wall	Configuration	Purpose of Testing
Pre-test Specimen	Conventional	Evaluate overall test set-up and test specimen stability under seismic loading
Test Specimen I	Conventional	Measure seismic response of conventional test walls subjected to ordinary and near-field ground motion
Test Specimen II	Retrofitted	Measure seismic response of retrofitted test walls subjected to ordinary and near-field ground motion

3.3.2 Instrumentation

The location of sensors for the shaking table tests is shown in Figure 3.5. Nine sensors were used to measure the dynamic response of the conventional test specimen. These included four analog linear displacement and velocity transducers and five variable capacitance accelerometers. Two additional string potentiometers were utilized to measure the displacement response of the damper in each retrofitted wall (not shown in Figure 3.5). The specifications for each of these sensors are provided in Appendix D. (See Table D.3, D.4 and D.5).The signals from each of the sensors were passed through

a low-pass Butterworth filter of 25 Hz cut-off frequency. The location of the sensors and their direction of measurement are also provided in Table D.2.

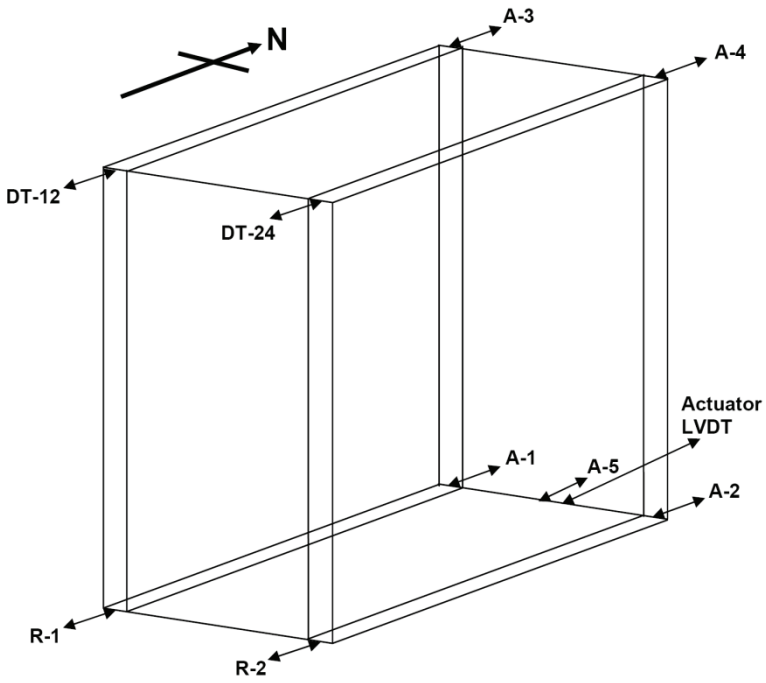

Figure 3.5 Location of Sensors for Shaking Table Tests

3.3.2.1 Location of Accelerometers

Five accelerometers were used to measure the response of each test specimen (referred to as A-1 through A-5 in Figure 3.5). Accelerometer A-5 was magnetically attached to the shaking table platform and measured the horizontal acceleration of the platform. Steel plates were glued to the end face of the top plates and sill plates to magnetically attach accelerometers. Accelerometers A-1 and A-2 were attached to the end face of the sill plate of the west and east walls, respectively, to measure acceleration input to the walls and monitor slippage between the shaking table platform and the sill plate. Accelerometers A-3 and A-4 were attached to the end face of the top plate of the west and east walls, respectively, to measure the acceleration of the top of the walls.

3.3.2.2 Location of Displacement and Velocity Transducers

Four displacement/velocity transducers were used to measure the response of each test specimen. Each sensor was capable of directly measuring displacement. The velocity was obtained via analog integration. Displacement transducers R-1 and R-2 were attached to the end face of the sill plate of the west and east walls, respectively, to measure the displacement and velocity input to the walls and monitor slippage between

the shaking table platform and the sill plate. Displacement transducers DT-12 and DT-24 were attached to the end face of the top plate of the west and east walls, respectively, to measure the displacement and velocity response of the top of the walls.

3.3.2.3 Location of String Potentiometers

Two string potentiometers were attached as shown in Figure 3.4b to measure the stroke of the dampers. The velocity across the damper was obtained by numerically differentiating the measured displacement response. The force in the damper was obtained using the measured velocity and the known force-velocity relation (the damper was experimentally tested to identify its force-velocity relation).

3.3.3 Input Ground Motions

Table 3.2 shows the input ground motions used for the Benchmark seismic shaking table tests and Table 3.3 shows the scaled input ground motions from the Benchmark tests that were used for the toggle-braced damper shaking table tests. Two historical ground motions were used for the seismic tests: an ordinary ground motion and a near-field ground motion. The ordinary ground motion (OGM) (i.e., far-field motion) represented a seismic hazard level corresponding to a Design Basis Earthquake (DBE) with a probability of exceedance of 10% in 50 years or a return period of 475 years. The 1994 Northridge Earthquake ground motion recorded at Canoga Park, with an amplitude-scaling factor of 1.20, was selected as the DBE. The near-field ground motion (NGM) represented a seismic hazard level corresponding to a Maximum Credible Earthquake (MCE) with a probability of exceedance of 2% in 50 years or a return period of 2,475 years. The unscaled 1994 Northridge Earthquake ground motion recorded at the Rinaldi Receiving Station was selected as the MCE. In addition to the DBE and MCE hazard levels, the Canoga Park ground motion (OGM record) was scaled down to simulate other hazard levels (see Table 3.2). Note that, in Table 3.2, the directions shown for the peak ground acceleration (PGA) values are directions that define the orientation of the test structure rather than the directions of the components of the field-recorded ground motions (e.g., the stronger component of the field-recorded Rinaldi record (component S49W) was applied along the North-South (Y) direction of the test structure).

Table 3.2 Ground Motions for Benchmark Seismic Shaking Table Tests

Excitation Level	Ground Motions	Hazard Level	Scale Factor	PGA (g)		
				E-W (x)	N-S (y)	Vertical (z)
1	1994 Northridge, Canoga Park	99.99%/50 years	0.12	0.04	0.05	0.06
2		50%/50 years	0.53	0.19	0.22	0.26
3		20%/50 years	0.86	0.31	0.36	0.42
4		10%/50 years	1.2	0.43	0.50	0.59
5	1994 Northridge, Rinaldi	2%/50 years	1	0.47	0.84	0.85

Table 3.3 Ground Motions for Toggle-braced Damper Shaking Table Tests

No.	Seismic Test	Scale Factor	Return Period (years)	Hazard Level
1	Level 4 (10%)	0.12	3	99.9%/50 years
2	Level 4 (33%)	0.40	38	73.2%/50 years
3	Level 5 (40%)	0.40	150	28.4%/50 years
4	Level 4 (60%)	0.72	150	28.4%/50 years

Note that, in the toggle-braced damper tests, only the y-direction (N-S) motions (stronger component) from the Benchmark Tests were used. Also, for the conventional walls, the Level 4 (60%) test was not carried out since damage in the prior seismic test (Level 5 (40%)) resulted in severe damage (test specimen appeared to be near collapse). Also note that Level 4 (60%) is considered to be equivalent to Level 5 (40%) based on the code recommendation (i.e., DBE = (2/3) MCE) and non-linear dynamic response-history analysis results from SAWS analysis. Note that Level 4 (10%) in Table 3.3 is equivalent to the Level 1 motion in Table 3.2. In addition to the seismic motions described above, each test specimen was also excited with white noise and sine sweep excitations to identify the dynamic characteristics of the test specimens both before and after each test. As shown in Table 1.3, the ground motions used in the toggle-braced damper tests were relatively weak. The rationale for using these weaker motions is as follows:

- Absence of orthogonal shear walls (i.e., test specimen was not part of a box-type test structure with walls on all four sides which can offer better seismic resistance than walls only along a single direction).

- Absence of finish materials [previous research indicates that finish materials significantly contribute to the stiffness of the walls and thus reduce the inter-story drifts (Christovasilis et al. 2007)].
- Tests were started with weaker motions to access stability and predict collapse limit. The intensity of the motions was progressively increased, thus resulting in progressive damage of the shear walls. Thus, instead of a single strong ground motion, the tests involved multiple weaker ground motions.
- The walls were designed using a code-based approach (i.e., using the spectral acceleration based on DBE and reducing the base shear via a response modification factor). Thus, the design assumes significant non-linear behavior but, for safety during testing, it is preferable to ensure a collapse margin larger than that used in practice.
- Shake table limitations (displacement and velocity limits) prevented the use of full-scale DBE and MCE motions.

3.3.4 Shake Table Fidelity

Due to the dynamics of excitation equipment (i.e., shaking table operated with hydraulic actuator), the actual displacement of the shaking table platform (i.e., output), is generally not equal to the desired servo-controller displacement command signal (i.e., input). The displacement command signal was corrected to account for these dynamics in an effort to produce the desired displacement output by pre-multiplying the inverse of the analytical shaking table transfer function by the desired displacement (Dutil and Symans 2004 and Twitchell and Symans 2003). The unloaded shaking table transfer function was used for correcting the ground motions as it was found that the loaded shaking table transfer functions did not produce better results during the testing of the pre-test specimen.

The effect of this correction can be investigated via comparison of response spectra of field motion and recorded shaking table motion. Figure 3.6 shows the 5%-damped response spectra [true (not pseudo) acceleration] up to period of 1.0 sec for the earthquake record recorded during the retrofitted wall tests. Note that woodframed structures are usually stiff and thus their response is not as strongly affected by long

period components. Thus, a 1.0 sec cutoff is deemed reasonable for the response spectra plots. It is evident that the shaking table was capable of reproducing the ground motion with reasonable fidelity for the desired range of periods. Note that a lower cutoff period of 0.07 sec (frequency = 14.29 Hz) was used in generating the spectra since the high frequency components in the recorded shake table motion (cutoff frequency of filter used in data acquisition was 25 Hz) tend to produce unrealistic values of spectral accelerations for low periods.

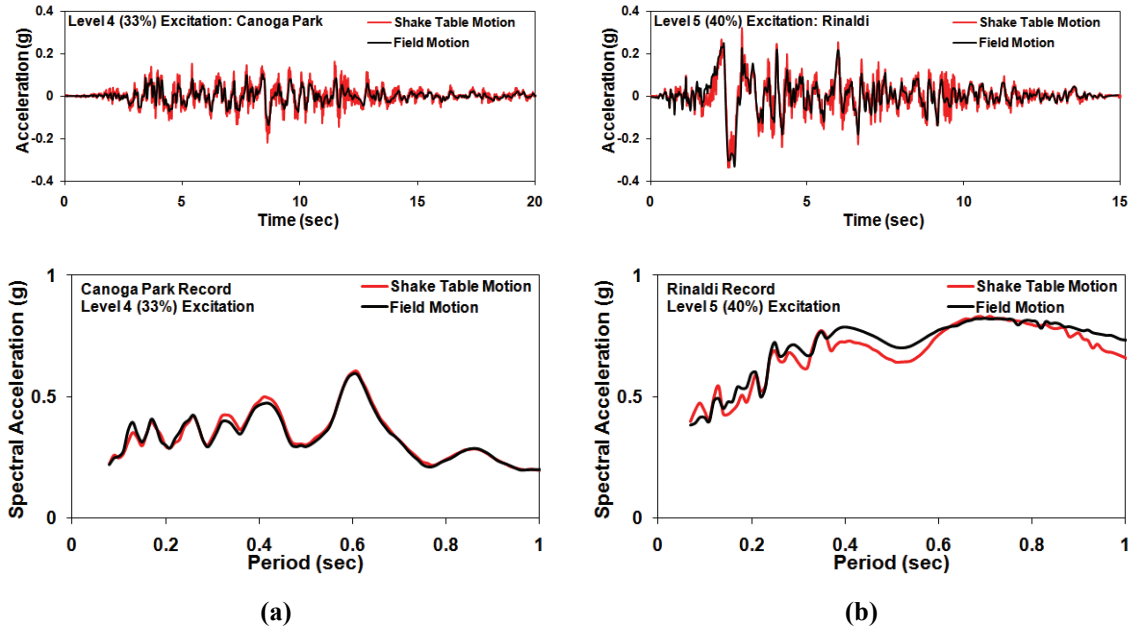

Figure 3.6 Comparison of 5%-Damped Response Spectra for Shake Table and Field Motions: (a) Level 4 (33%) Excitation (b) Level 5 (40%) Excitation

3.3.5 Practical Testing Issues

Although the test specimens were expected to be damaged during testing with the danger of losing gravity load-carrying capacity, the laboratory overhead crane was not permitted to be used as a fail-safe restraint due to concerns about impact loading on the crane. Also, due to space restriction in the lab, there was no firm lateral support constructed around the test specimens. Thus, to avoid the possibility of lateral collapse of the test specimens, a lateral support frame was constructed of steel Unistrut®. Furthermore, two 50.8 mm x 101.6 mm (2 in x 4 in) studs were used for cross-bracing at both the ends of the test specimens (see Figure 3.1). Finally, short wall segments were installed under the seismic mass to "catch" the mass if the shear walls should collapse laterally.

For the modular damper wall configuration shown in Figure 3.4b, a fully effective damper would be subjected to more than 100% of the story drift. However, during the testing, the displacement of the dampers was less than the story drift (about 60% loss was observed). Some likely reasons for this include:

- Manufacturing tolerances in clevis pin connections in toggle assembly.
- Out-of-plane displacement of dampers and steel bracing.
- Bending deformation of shear wall.
- Uplifting of modular damper walls.
- Sill plate slippage.
- Inherent flexibility of wood framing connections and joints (i.e., the wood framing system tends to deform around the modular damper walls and thus it is difficult to transfer the global structural displacements into the modular damper walls).
- A portion of the measured drift is due to global overturning, resulting in high story drifts but low shear deformations and thus low damper displacements.

Detailed displacement loss evaluation based on sensor measurements and code-based analytic formulas are presented later in the experimental results section.

3.4 Design and Analysis

3.4.1 Code-based Design

A comparison of the seismic performance of the conventional and retrofitted walls (with dampers) can be performed in two ways:

1) Designing the conventional and retrofitted walls for the same base shear and evaluating the change in structural response.
2) Designing the conventional and retrofitted walls for different base shear (i.e., retrofitted wall with lower base shear) and justifying the use of retrofitted walls by showing that the same performance objectives can be obtained even with lower stiffness of retrofitted walls for a given seismic hazard.

The first approach is often more convenient for testing and analysis purposes and thus was used in the toggle-braced damper wall testing described herein.

For design purposes and in accordance with the International Building Code (IBC 2006), the test structure is designed for a location in Southern California with stiff soil (Site Class D). The design 5%-damped spectral acceleration values for MCE hazard Level were determined in accordance with ASCE/SEI-41 (2006). The MCE spectral response acceleration for short-period, S_{MS}, value was taken equal to 1.5g and its value for one-second period, S_{M1}, was taken as 0.9g. Note that these values are higher than those based on the actual shaking table motions used for testing (see Figure 3.6b) and thus one would expect better performance of the conventional test specimen designed based on aforementioned values. However, as will be shown later, this was not the case.

The IBC 2006 provisions mention that allowable shear values are permitted to be increased to values shown for 11.91 mm (15/32 in) thick sheathing with same nailing provided for 9.53 mm (3/8 in) and 11.11 mm (7/16 in) thick OSB when (1) studs are spaced a maximum of 406.4 mm (16 in) on center, or (2) panels are applied with the long dimension across the studs. Based on this provision and the required shear carrying capacity, 9.53 mm (3/8 in) or 11.11 mm (7/16 in) thick OSB with 8d common nails and with 152.4/304.8 mm (6/12 in) spacing could be selected. Although the above condition is satisfied in the case of the test structure, for a conservative design, the aforementioned provision was not used (see Section D.1 and D.2 for details). Also, APA wood construction guide (APA 2007b) mentions that greater stiffness is required for wall sheathing when stucco (which is commonly used as a finishing material in California region) is to be applied and recommends a minimum of 11.11 mm (7/16 in) thick OSB for 406.4 mm (16 in stud spacing) for vertical panel orientation. Based on these recommendations, the final design selection had 11.11 mm (7/16 in) thick OSB with 8d common nails and with 152.4/304.8 mm (6/12 in) spacing (see Figure 3.2).

3.4.2 Numerical Modeling and Analysis with SAWS

Nonlinear dynamic analysis of the test structure, both with and without fluid viscous dampers installed in shearwalls, was performed using the SAWS (Seismic Analysis of Wood Structures) program (Folz and Filiatrault 2004a) (see Appendix A for additional details). In this program, a three-dimensional woodframed building is degenerated to a two-dimensional "pancake" model in which the lateral load resisting system consists of

shear walls that are modeled as zero-height nonlinear hysteretic spring elements and the horizontal diaphragms are assumed to have infinite in-place stiffness, resulting in three degrees-of-freedom per floor. Modifications to the SAWS program were made to allow for the inclusion of the dampers before the Phase 2 Benchmark testing. Since the test structure did not include any finish materials, analysis was performed using shear wall hysteretic parameters for the wall configuration without exterior or interior finish materials. The hysteretic parameter values were obtained using the companion analysis program CASHEW (Folz and Filiatrault 2001). Data input to CASHEW includes wall geometry, shear stiffness of the sheathing panels, and the hysteretic properties of the sheathing-to-framing connections. The initial properties of the sheathing-to-framing connections were taken from cyclic nail tests (Ekiert and Hong, 2006) conducted at the University at Buffalo as part of the benchmark test program (Filiatrault et al. 2007). In addition, inherent rate-dependent damping was accounted for via a Rayleigh damping formulation (based on the initial stiffness matrix) in which a damping ratio of 1% was assumed in the first and second modes.

3.4.2.1 Calibration of Numerical Model: Conventional Walls

As mentioned previously, the Initial Numerical Model (INM) utilized hysteretic parameter values from nailed sheathing/stud (Hem fir) connection cyclic tests conducted as part of the Benchmark structure test program. However, the constructed test specimens used Spruce Pine fir which is slightly weaker than Hem fir (comparing the specific gravity of the two lumbers species). Analysis of the INM using SAWS resulted in a natural frequency of 3.85 Hz [by coincidence, close to the natural frequency from low-amplitude system identification tests (see Table 3.5)]. Note that the SAWS program does not provide natural frequencies for uniaxial models such as the test structure. Thus, a biaxial model with very weak shearwalls in the lateral direction was used to obtain the natural frequency in the longitudinal direction. The stiffness of the walls in the lateral direction only affects the torsional frequency obtained from the SAWS analysis (since SAWS models the shearwalls in both directions independently). The INM was stiffer than the actual test structure (concluded by comparing the numerical results from INM analysis with experimental results from Level 4 (33%) excitation) and thus

underpredicted the displacement response. An Updated Numerical Model (UNM) was calibrated by reducing the initial stiffness and force intercept values in the hysteretic parameters obtained from CASHEW until the predicted displacement response reasonably matched the experimental data for Level 4 (33%) excitation (see Figure 3.14). The UNM resulted in a SAWS natural frequency of 3.33 Hz. Note that the final value of the natural frequency used in the analysis is about 15% lower than the value obtained from system identification tests (3.88 Hz) for the undamaged test structure [i.e., before any seismic excitation was applied (see Table 3.5 for values corresponding to Level 4 (10%) row. Note that Level 4 (10%) excitation was too weak to cause any damage and the dynamic properties of the test specimen remained unchanged]. This is due to the system identification testing being done at very low amplitude and the SAWS model being an idealized representation of the physical test specimen. The UNM produced reasonably accurate prediction of displacement and acceleration response for Level 5 (40%) excitation test of the conventional wall test specimen and thus validated the calibration process used herein.

3.4.2.2 Calibration of Numerical Model: Retrofitted Walls

The natural frequency of the retrofitted test specimen obtained by system identification tests was 4.50 Hz [larger than the conventional test specimen due to a different wood framing system and the presence of the steel toggle brace assembly (see Table 1.5)]. Since calibration of the conventional test specimen resulted in a natural frequency that was less than that measured in the system identification tests, the model for the retrofitted walls was taken to be the same as the Initial Numerical Model (INM) for the conventional walls which had the SAWS natural frequency of 3.85 Hz. Note that the visco-elastic behavior of the toggle-braced damper assembly cannot be accounted for directly in SAWS; rather, the damper is a pure viscous element and the elasticity of the steel framing system is accounted for via equivalent hysteretic parameters that increase the wood shearwall stiffness. A displacement magnification factor (damper displacement/structure displacement) of 0.65 was observed in tests (40% of initial value of 1.65) and was used in SAWS for analysis of the retrofitted walls. Note that there is consistency between the numerical models for the conventional and retrofitted walls in

that the value of the natural frequency of the SAWS models for both cases is about 15% less than that measured in the corresponding system identification test (i.e., the calibration procedure resulted in SAWS models that are less stiff than that measured in low amplitude system identification tests). Note that this discrepancy is consistent with the testing of a full-scale, two-story woodframed structure (without any finishing materials) tested at University of California, San Diego, within the CUREE- Caltech Woodframe Project (Folz and Filiatrault 2004b). Table 3.4 shows a summary of natural frequencies. Note that experimental natural frequencies were obtained for the undamaged test specimen [prior to seismic loading (also see Table 3.5)]. The accumulation of damage from multiple seismic tests was accounted for by subjecting the calibrated SAWS model to a train of ground motions; the SAWS model having been calibrated using one of the weaker ground motions [(Level 4 (33%)].

Table 3.4 Summary of Natural Frequencies from Experimental Testing and Numerical Modeling

	EXPERIMENTAL Frequency obtained from Low Amplitude System Identification Tests (prior to seismic testing)	**NUMERICAL Frequency of calibrated SAWS model (calibrated against measured seismic response)**
Conventional	3.88 Hz	3.33 Hz
Retrofitted	4.50 Hz	3.85 Hz

3.5 Experimental Results

3.5.1 Dynamic Properties of Structure

System identification tests [white noise input of 0.51 mm (0.02 in) amplitude and 0 – 30 Hz bandwidth and sine-sweep tests of varying amplitude and frequency bandwidth] were conducted between the seismic tests to determine the variations of the dynamic properties (natural frequency and damping ratio) of the test structure as it experienced increasing levels of damage. The natural frequency was identified from acceleration transfer functions of white noise tests, peak response frequency during sine-sweep response, and free vibration response at the end of white noise or sine-sweep signal. Table 3.5 shows the results obtained from free vibration response of the test structure after white noise or sine sweep signal. Note that Level 4 (60%) test was not carried out for conventional test structure (without dampers) due to the possibility of collapse. The

damping ratio was estimated using the maximum amplitude of the acceleration transfer function associated with the dominant natural frequency (Twitchell 1998) and the free vibration response at the end of the white noise and sine sweep tests. In the first method, the damping ratio is dependent upon the peak value in the transfer function. Since the peak value tends to be underestimated due to finite resolution in the transfer function data, especially near the dominant natural frequency where the transfer function changes rapidly, the damping ratio tends to be overestimated, Thus, the damping ratio estimated from the free vibration response is assumed to be correct and these are the values shown in Table 3.5. Note the small difference in damping ratios of the conventional and retrofitted test specimens. This can be explained as follows. The dampers were not activated during low-amplitude system identification tests and thus damping in the retrofitted wall represents low-amplitude equivalent viscous damping for a different configuration of the wood framing system (i.e. rotated inner studs and different field nailing) along with the toggle-brace framing.

Table 3.5 Influence of Retrofit on Dynamic Properties

No.	Seismic Test	Properties Measured during Post-test Free Vibration			
		Natural Frequency (Hz)		Damping (%)	
		Conventional	Retrofitted	Conventional	Retrofitted
1	Level 4 (10%)	3.88	4.50	2.37	2.57
2	Level 4 (33%)	3.38	4.38	3.42	3.81
3	Level 5 (40%)	2.00	4.37	4.74	3.94
4	Level 4 (60%)	NA	4.17	NA	4.95

The natural frequency of the retrofitted test specimen obtained by system identification tests was higher than the conventional test specimen (about 15% higher). Note that previous research also indicated an increase in natural frequency due to bracing systems (Hwang et al. 2005). Thus, the inclusion of the toggle-braced damper assembly added stiffness to the walls (this was also evident during installation of the damper assembly wherein restoring force appeared to be present). Thus, the improvement in seismic performance due to retrofitting the walls can be attributed to both added stiffness and additional energy dissipation capacity (i.e., visco-elastic behavior) due to the presence of the damper assembly.

3.5.2 Drift Response

Figure 3.7 shows that the peak wall drift (actually, peak drift ratio) is significantly reduced (63% reduction for Level 4 (33%) excitation and 78% reduction for Level 5 (40%) excitation) in the retrofitted test specimen as compared to the conventional test specimen. Figure 3.8a and 3.8b show the wall damage in the conventional and retrofitted walls (East side), respectively, after Level 5 (40%) excitation. Note the significant pullout of nails and separation of sheathing from the studs in Figure 3.8a indicating significant damage in the conventional wall (peak drift equal to 3.48%) as compared to the virtually undamaged retrofitted wall (peak drift equal to 0.77%). Due to the clear relation between story drifts and damage in wood-frame structures (Porter et al. 2001), reduction of story drifts is a key goal for seismic retrofit. The high peak drift reduction clearly indicates that the performance of retrofitted walls with the toggle-braced damper assembly is significantly improved as compared to the conventional walls.

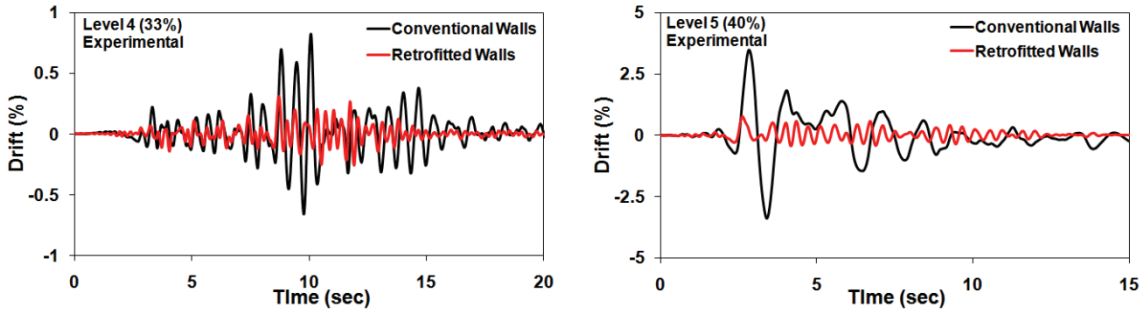

(a) (b)

Figure 3.7 Comparison of Experimental Drift Response History: (a) Level 4 (33%) Excitation and (b) Level 5 (40%) Excitation

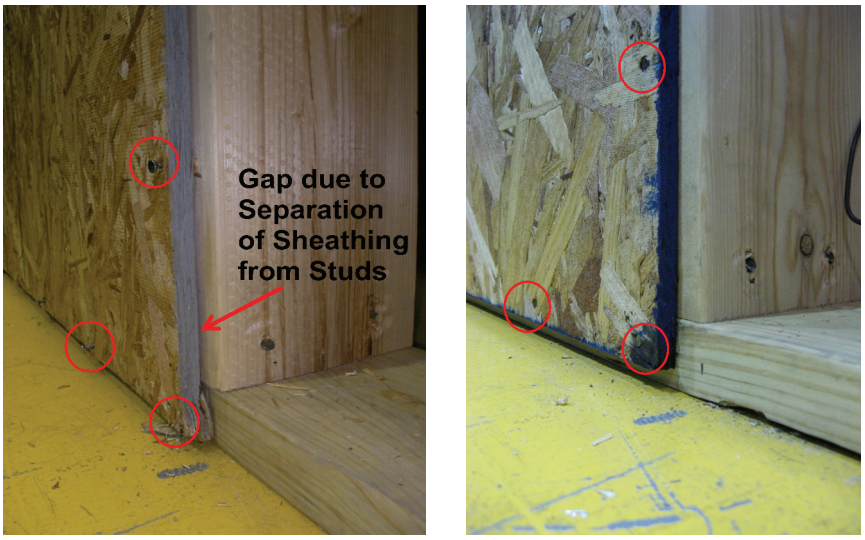

(a) (b)

Figure 3.8 Wall Damage in East Wall after Level 5 (40%) Test: (a) Conventional Wall and b) Retrofitted Wall

3.5.3 Acceleration Response

Figure 3.9a and 3.9b shows the acceleration response history for Level 4 (33%) excitation and Level 5 (40%) excitation, respectively. Note that the acceleration was significantly increased in the case of the retrofitted test specimen as compared to the conventional test specimen, especially beyond the peak response. The increase can be attributed to higher frequencies associated with the less damaged and thus stiffer retrofitted structure. As the peak acceleration is related to non-structural and contents damage of the structure, the reduction of this quantity is also desirable. The increase in acceleration observed in experimental response history is also observed in numerical simulations (see Figure 3.13). Thus, the increase in acceleration can also be attributed to the relative contribution of the toggle-braced assembly to the total structural stiffness (which is close to 32% in the testing presented herein). If this contribution is low (<< 32%; e.g., if the dampers are installed within a full size building rather than in single shear wall components), a peak acceleration reduction on the order of 40% (based on numerical simulations of a two-story woodframed building) can be expected in woodframed structures retrofitted with fluid viscous dampers (Shinde et al. 2008b). Note that the experimentally recorded acceleration response was low-pass filtered using a 25

Hz cut-off to remove higher frequency components that were not consistent with the recorded displacement response.

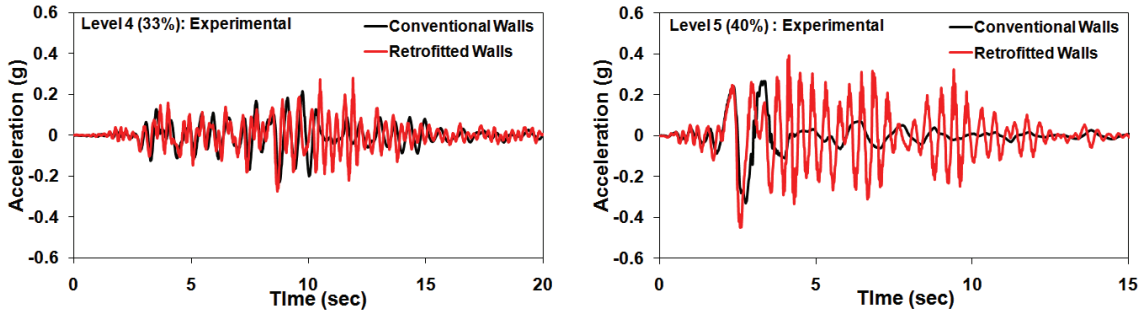

(a) (b)

Figure 3.9 Comparison of Experimental Acceleration Response History: (a) Level 4 (33%) Excitation and (b) Level 5 (40%) Excitation

3.5.4 Hysteretic Response

Figure 3.10a and 3.10b show the hysteretic response of the conventional and retrofitted test specimen for Level 4 (33%) and Level 5 (40%) excitation, respectively. As expected, the peak wall displacement (drift) is significantly reduced (78% reduction for Level 5 (40%) excitation) and the energy dissipated near zero displacement is increased significantly due to the velocity-dependence of the dampers. Note that the hysteresis loops exhibited unexpected high frequency components which were removed via application of a low-pass Butterworth filter with a cut-off frequency of 10 Hz. The effect of dampers is more pronounced in the case of strong excitation [i.e., Level 5 (40%) excitation (see Figure 3.10b)].

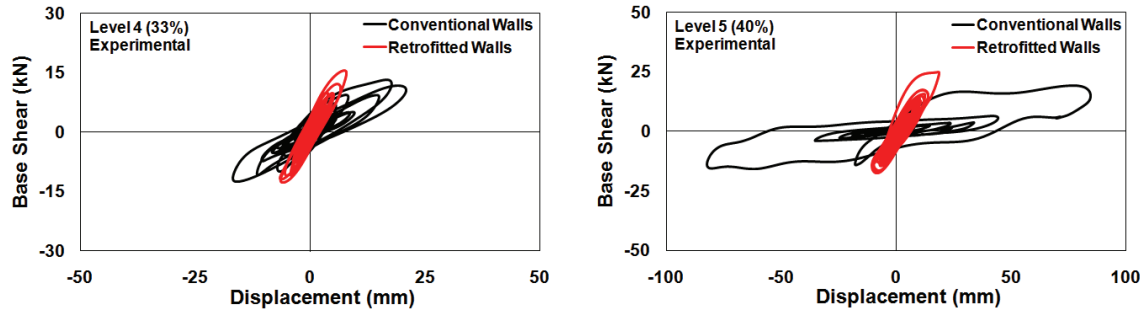

(a) (b)

Figure 3.10 Comparison of Global Hysteretic Response: (a) Level 4 (33%) Excitation and (b) Level 5 (40%) Excitation

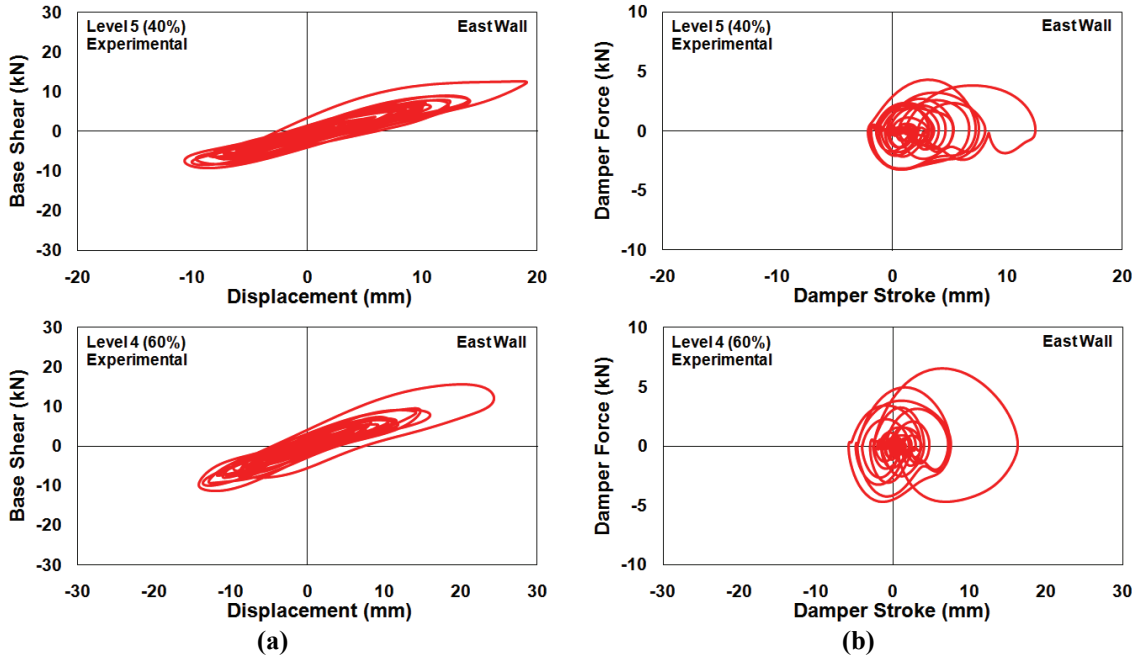

Figure 3.11 Hysteretic Response of East Wall of Retrofitted Test Specimen: (a) Global Hysteretic Response and (b) Damper Hysteretic Response

Figure 3.11 shows the hysteretic response of the retrofitted East wall specimen for Level 5 (40%) and Level 4 (60%) excitation and the associated damper hysteretic response. Note that the damper contribution to energy dissipation is most pronounced for small displacements (high velocities). Also, the shape of the damper hysteresis loops is consistent with that for a linear viscous damper (i.e., elliptical).

3.5.5 Energy Response

The seismic performance of the test specimens may also be evaluated by considering the distribution of energy within the specimens as time progresses. The energy contributions can be determined by assuming an idealized single degree-of-freedom (SDOF) representation of the test specimens (i.e., lumped mass with non-linear spring and viscous dashpot). Thus, the values of the damping ratio and natural frequency obtained from low-amplitude system identification tests were used (Table 3.5) to compute the viscous damping coefficient (for computation of inherent damping energy) and elastic stiffness (for computation of elastic strain energy). Figure 3.12 shows a comparison of the experimental energy distribution for the conventional and retrofitted test specimens for Level 5 (40%) excitation (note that, for comparison purposes, the two figures are

plotted to the same scale) along with their displacement response histories. The effect of the dampers is to reduce the hysteretic energy dissipation demand by approximately 73%. The reduced hysteretic energy dissipation demand on the wood framing system suggests that the retrofitted test specimen with dampers would experience less structural damage than the conventional test specimen (as was indeed observed in the experimental tests). Note that hysteretic energy shown in the Figure 3.12 includes both elastic and inelastic strain energy. Due to their highly non-linear hysteretic behavior, elastic strain energy is almost negligible (even less than kinetic energy) in woodframed structures and thus this quantity is not plotted separately in energy distribution plots presented herein. Also note that the hysteretic energy in the conventional test specimen gradually reduces with time due to the gradual reduction in elastic strain energy and monotonically increasing damping energy.

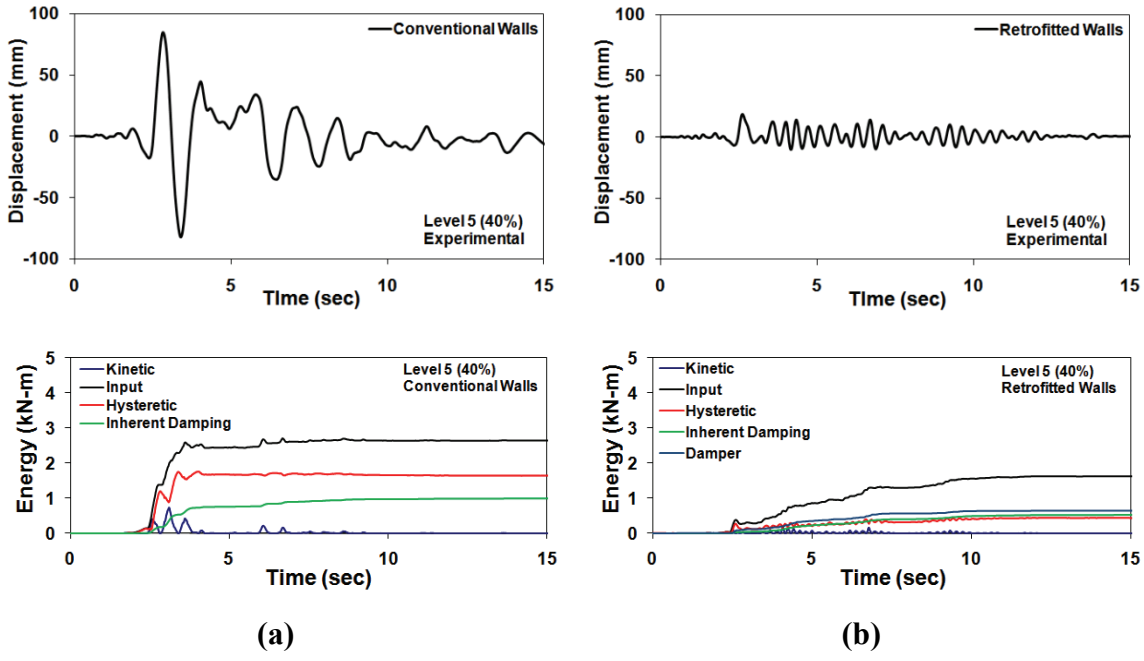

Figure 3.12 Experimental Displacement and Energy Time History for Level 5 (40%) Excitation: (a) Conventional Walls and (b) Retrofitted Walls

3.6 Comparison of Experimental and Numerical Results

Figure 3.13 and 3.14 show a comparison of the numerical and experimental acceleration and drift response history for the test specimens with the conventional and retrofitted test

specimen, respectively. Note that a good match between the numerical and experimental results for the retrofitted test specimen indicates the correct measurement of damper stroke, and thus displacement magnification factor, during experiments. Both figures show that the peak results are predicted well but that, beyond the peaks, there is poor correlation between the results, particularly for the conventional test specimen. This type of prediction (good up to the peak and poor afterwards) is not uncommon for wood structures and can be attributed to the structure being in a damaged state beyond the peak deformation (thus making it more difficult to capture the behavior beyond the peak deformation where the cyclic response is highly nonlinear).

Table 3.6 Comparison of Experimental and Numerical Peak Responses for Level 4 (33%) Excitation

	Level 4 (33%) Excitation							
	Conventional Walls				Retrofitted Walls			
	Total Acceleration (g)		Drift (%)		Total Acceleration (g)		Drift (%)	
	+ ve	- ve	+ ve	- ve	+ ve	- ve	+ ve	- ve
Experimental	0.22	0.23	0.86	0.69	0.28	0.28	0.32	0.27
Numerical	0.25	0.33	0.92	0.46	0.20	0.29	0.32	0.18
% Error	14	50	7	-33	-29	4	0	-33

Table 3.7 Comparison of Experimental and Numerical Peak Responses for Level 5 (40%) Excitation

	Level 5 (40%) Excitation							
	Conventional Walls				Retrofitted Walls			
	Total Acceleration (g)		Drift (%)		Total Acceleration (g)		Drift (%)	
	+ ve	- ve	+ ve	- ve	+ ve	- ve	+ ve	- ve
Experimental	0.27	0.33	3.48	3.39	0.39	0.45	0.77	0.43
Numerical	0.38	0.40	3.24	1.93	0.30	0.44	0.75	0.39
% Error	41	21	-7	-43	-29	-4	-3	-9

A train of seismic motions is used as an input for the SAWS analysis to account for prior damage induced by prior seismic motions. As mentioned previously, both experimental and numerical response histories show increased acceleration response in the case of the retrofitted test specimen as compared to the conventional test specimen, especially beyond the peak drift response. Also note that the numerical prediction of the acceleration response for Level 5 (40%) excitation for the conventional test specimen appears to be limited to some value after the peak value has occurred (see Figure 3.13a). This behavior may be due to the inability of the numerical model of the conventional test

specimen to resist lateral forces after significant damage occurs [peak drift more than 3% (also see Figure 3.14a)]. Table 3.6 and Table 3.7 show a comparison of experimental and numerical peak response values (both positive and negative peaks) and the corresponding percentage error. It is evident that the calibrated numerical models were able to predict the seismic response reasonably well. Notably, the percentage error between the peak experimental and numerical wall drift is less than 10% for both the test specimens and for both seismic excitations. As mentioned previously, peak story drift provides a key measure of damage in a building and thus numerical prediction of this quantity is of utmost importance.

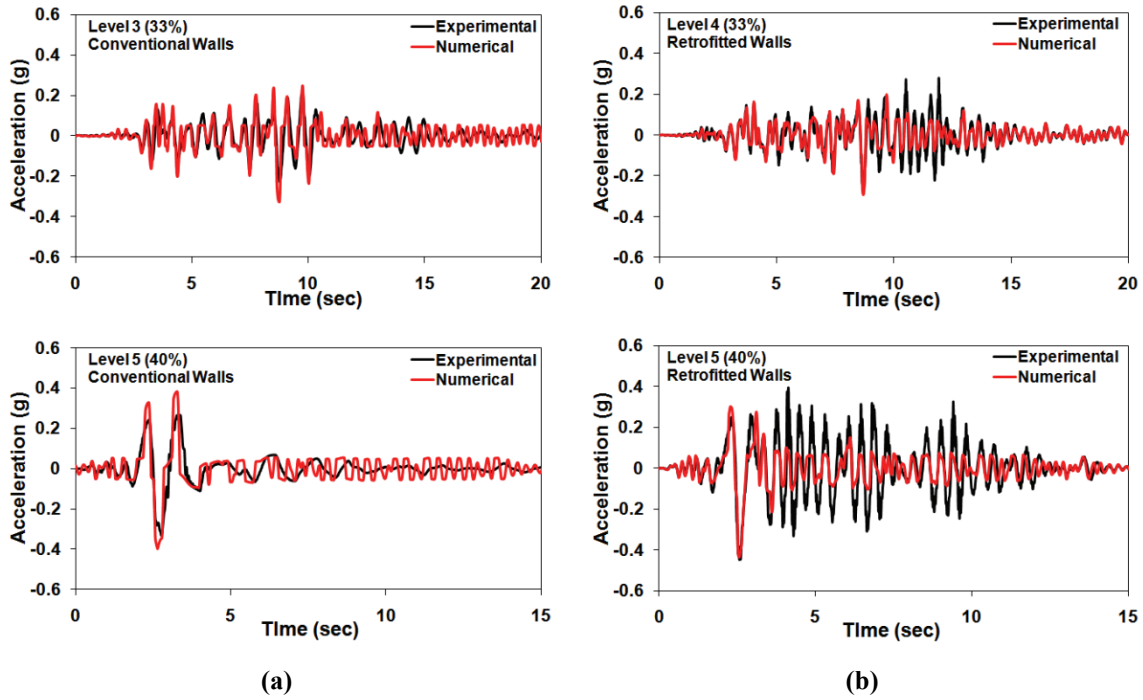

Figure 3.13 Comparison of Numerical and Experimental Acceleration Response History: (a) Conventional Walls and (b) Retrofitted Walls

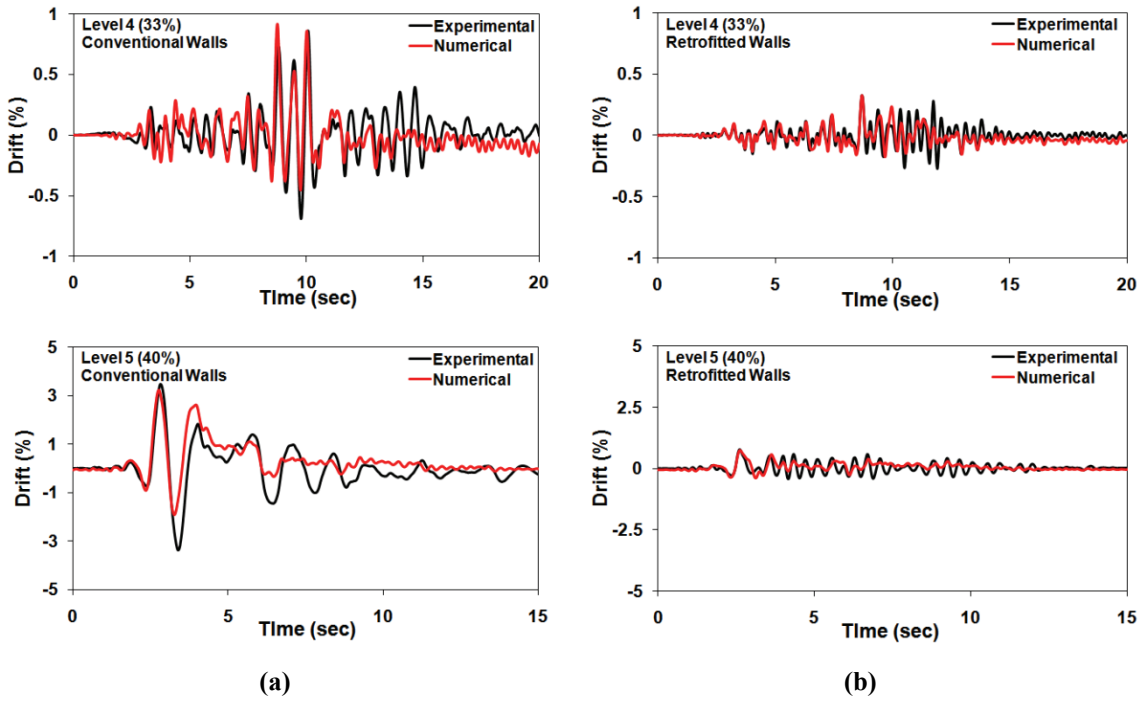

Figure 3.14 Comparison of Numerical and Experimental Drift Response History: (a) Conventional Walls and (b) Retrofitted Walls

3.7 Evaluation of Loss of Displacement Transfer to Dampers

Significant loss of displacement transmission (about 60% loss from ideal magnification of 165% to actual magnification of 65%) was observed. Figure 3.15 shows the comparison of wall displacement and damper stroke time history in the retrofitted East wall. Note that the damper stroke lagged the wall displacement during seismic excitation (approximately by 0.08 sec) and thus the top wood plate and the top channel of the damper assembly were not responding completely in phase (suggesting some displacement loss at the top channel connection). Figure 3.16 shows a direct comparison of wall displacement and damper stroke wherein the damper stroke has been shifted in time by 0.08 sec to facilitate evaluation of displacement losses. The lines representing the wall with ideal chevron-braced configuration (f = 1.0), ideal toggle-braced configuration (f = 1.65) and actual toggle-braced configuration (f = 0.65) are also shown in the figure. The actual displacement magnification factor (f = 0.65) is

calculated directly as the ratio of the maximum damper stroke to the maximum wall displacement.

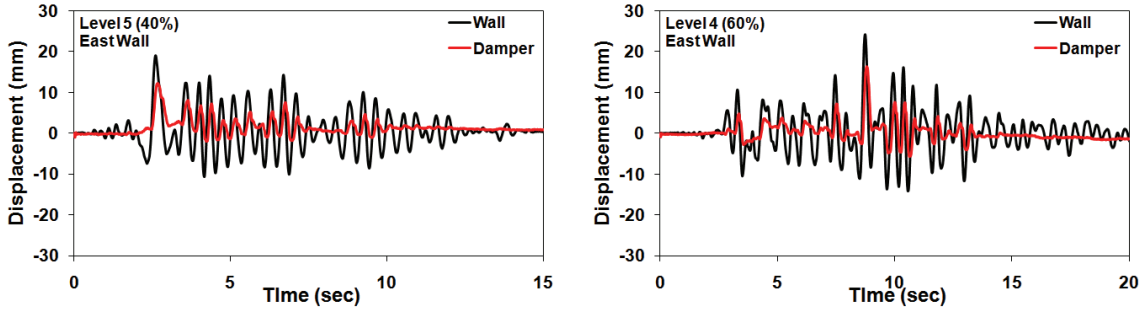

(a) (b)

Figure 3.15 Comparison of Wall and Damper Stroke Response History: (a) Level 5 (40%) Excitation and (b) Level 4 (60%) Excitation

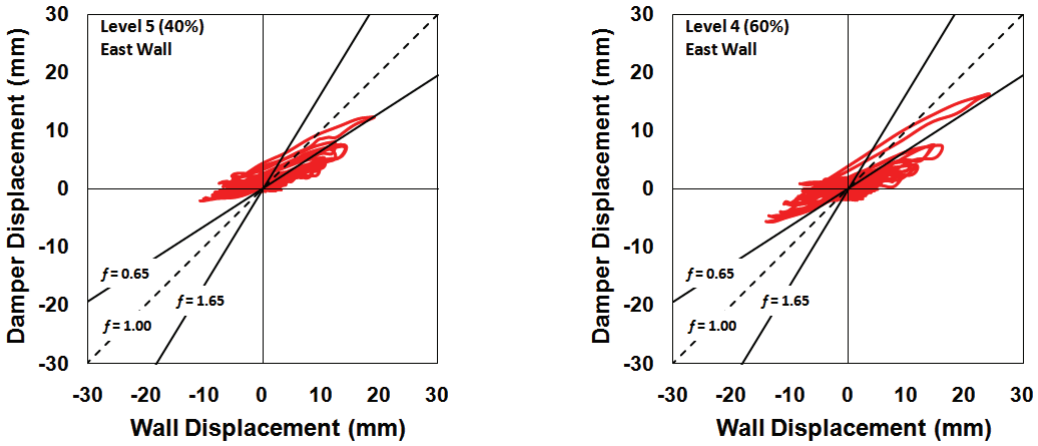

(a) (b)

Figure 3.16 Evaluation of Displacement Transmission Losses: (a) Level 5 (40%) Excitation (b) Level 4 (60%) Excitation

Equation 23-2 in IBC 2006 provides an analytical expression to predict the total deflection experienced by a shearwall during an earthquake by combining the following four types of deflection: bending (Δ_b), shear (Δ_v), nail slip (Δ_n), and anchorage slip (Δ_a). Breyer et al. (2007) provides a detailed explanation of these deflection components. The damper only has the ability to respond to shear deformations and thus the deformation of the damper is only due to the direct shear term and the shear deflection component of the nail slip deflection. Note that nail slip reduces the overall stiffness of the shearwall and thus results in additional deflection of the shearwall. This

additional deflection may include bending and anchorage slip deflections which are not transferred to the dampers. Using the aforementioned analytical expression, shearwall deflection calculations were performed for the Level 4 (33%), Level 5 (40%), and Level 4 (60%) tests for the retrofitted walls (see Section D.6 for details). The total deflection was known from the displacement data collected during the tests, and the measured acceleration at the top of shearwall (corresponding to the maximum deflection) was used to calculate the base shear. Note that the analytical expression for the nail slip contribution was not used herein as it is the most difficult quantity to predict accurately and thus, as compared to the other deflection components, its analytical expression is primarily empirical in nature. Instead, this contribution was computed by subtracting the deflection due to bending, shear and anchorage slip from the total measured displacement. The maximum shear force per unit length at the top of the shearwall is determined from:

$$v = \frac{a_{top}\, m_{top}}{L} \tag{3.1}$$

where a_{top} is the measured acceleration at the top of the wall, m is the seismic mass at the top of the wall, and L is the length of the shearwall. The elongation of the Simpson HD6A hold down, d_a ,was equal to 1.04 mm (0.041 in) for the chord force of 16.37 kN (3.68 kips). The deflection due to anchorage slip Δ_a was then calculated by determining the chord force for the computed shear at the top of the shearwall (see Section D.6 for details).

The percentage contribution of each deflection component was then used to determine the amount of deflection that was transferred to the damper and the amount that was lost within the shearwall. It is assumed that only 30% of the deflection due to nail slip will be lost within the shearwall, leaving 70% to be transmitted in pure shear to the dampers (see Table D.6 for details). The 30% value was selected such that it will give reasonable contribution of losses within the shearwalls to the total displacement transmission loss observed (about 60%). Based on these assumptions, the total displacement loss within the shearwall was estimated to be within the range of 30 to 40%. The additional displacement loss observed (i.e., 20 to 30%) may be due to gaps in joints of the toggle-assembly, gaps created due to crushing of holes in wooden top plates

due to bolt bearing stress, high aspect ratio of the damper assembly (higher height than conventional toggle assemblies used/tested in the past) and gaps in the wall to damper assembly connections. Note that the losses within the shearwall may be used advantageously to dissipate energy by employing a distributed energy dissipation system [e.g., using visco-elastic material directly bonded to wood (Dinehart and Lewicki (2001)].

Another important contributor to the additional displacement loss is the deformation (elongation or contraction) of the bracing members in the toggle-braced assembly. Huang (2004) concluded that the magnification factor derived assuming rigid brace members overpredicts the damper stroke significantly. Huang (2004) also developed a theoretical expression to include the effect of brace elongation. Recall that the magnification factor of 1.65 was derived assuming small deformations with rigid brace members. Thus, losses due to elongation of the bracing members may be significant. Also, Hwang et al. (2005) reported displacement transmission losses on the order of 40% in the second story of a three-story scale-model steel-framed structure with toggle-braced dampers. Thus, it is apparent that some amount of displacement loss of the same or higher order is expected in woodframed structures, given that woodframed structures have more flexible framing members and joints than steel-framed structures.

3.7.1 Influence of Displacement Transmission Loss on Peak Drift

Table 3.8 shows the influence of displacement transmission loss on peak drift. Note that the values were obtained by comparing the experimental results of the conventional test specimen and the numerical simulations of the retrofitted test specimen using the ideal and actual displacement magnification factor (f). Recall that a good match of numerical simulations with actual displacement magnification factor and experimental results of the retrofitted test specimen indicates the correct measurement of damper stroke during experiments and thus the values shown in Table 3.8 will be very close to the peak drift reduction values computed by comparing experimental results. It is apparent that there is a significant seismic performance improvement in the retrofitted test specimen as compared to the conventional test specimen even with 60% loss in the

displacement transmission. The percentage reduction in the peak drift is in fact good enough to recommend the tested configuration for a practical implementation.

Table 3.8 Influence of Displacement Transmission Loss on Peak Drift

	Peak Drift Reduction	
	Level 4 (33%)	**Level 5 (40%)**
Ideal Toggle braced Damper (f = 1.65)	86%	93%
Actual Toggle-braced Damper (f = 0.65)	63%	78%
Actual / Ideal	0.73	0.84

3.8 Influence of Retrofit on Test Specimen

3.8.1 Influence of Retrofit on Supplemental Damping in Test Specimen

The influence of the toggle-braced damper assembly on the damping within the retrofitted test specimen can be estimated by computing the supplemental (linear viscous) damping ratio, ξ_d , as follows:

$$\xi_d = \frac{C_d f^2}{2m\omega_n} \tag{3.2}$$

where C_d is the damping coefficient of the damper, f is the displacement amplification factor, m is the seismic mass of the test specimen, and ω_n is the natural frequency of the retrofitted test specimen. Figure 3.17 shows the supplemental damping ratio ξ_d for the retrofitted wall with the ideal chevron-braced configuration, ideal toggle-braced configuration, and actual toggle-braced configuration based on the observed displacement magnification factor. Note that the inherent damping was obtained from low amplitude system identification tests and the supplemental damping was calculated under the assumption that the retrofitted wall has the same natural frequency for all 3 cases and is equal to the value from low amplitude system identification testing (4.50 Hz). Thus, both the inherent and supplemental damping shown in Figure 3.17 do not include hysteretic damping from non-linear material behavior. It is evident that the loss of damper stroke significantly reduces the damping ratio and thus reduces the seismic resistance from supplemental damping.

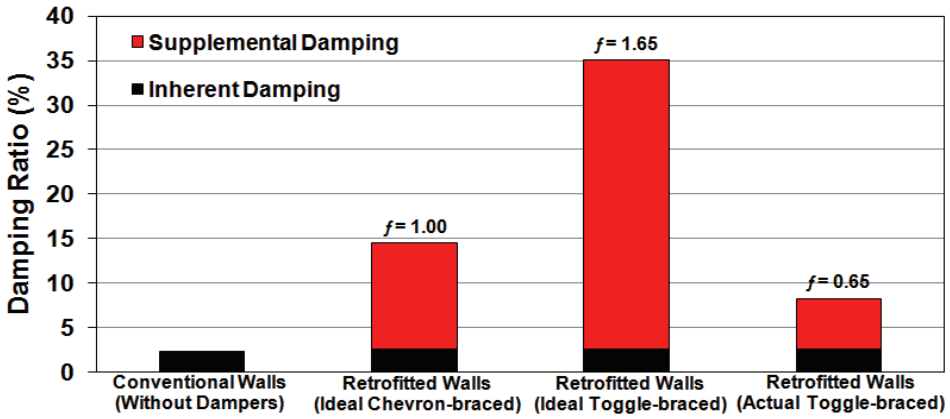

Figure 3.17 Influence of Retrofit on Supplemental Damping in Test Structure

3.8.2 Influence of Retrofit on Performance of Test Specimen

Table 3.9 shows the influence of retrofit on the performance of the test specimen by evaluating the stiffness and the damping contribution to the peak drift reduction. It also shows the hysteretic energy demand reduction and the contribution of energy dissipation of dampers to the total input energy. Note that the results presented herein are obtained by comparing the results of numerical analyses using trains of motions and thus peak drift reduction values do not match those given in Table 3.8. The results for the added stiffness case were obtained by using the Initial Numerical Model (INM) of the convnetional walls without the dampers (i.e., only added stiffness from the toggle-assembly was used by using a different configuration of the wood framing system). The added stiffness reduced the peak drift by 43%. However, it should be noted that the ability of the retrofitted walls to resist repeated seismic excitation without any significant damage will not be present in the wall with just added stiffness given the small reduction in hysteretic energy demand (30%). For the retrofitted walls, the contribution to the drift reduction from the stiffness was assumed equal to the drift reduction obtained from the case where only added stiffness was considered [added stiffness associated with different configuration of the wood framing system (i.e. rotated inner studs and different field nailing) along with the toggle-brace framing], although this contribution would be actually higher for the retrofitted walls as they respond with smaller displacements and thus the secant stiffness is higher (i.e., peak drift was 0.77% for the retrofitted test specimen compared to 3.48% for the conventional test specimen). Note that the inclusion of the damping system results in significant energy dissipation by the dampers

and corresponding reduction in the hysteretic energy demand on the framing system (see Table 3.9). Additionally, since the perimeter nailing of the conventional and retrofitted walls was same, the added stiffness of the retrofitted walls is mainly due to the stiffness of the bracing system of the toggle-assembly (i.e., the elastic portion of the visco-elastic behavior of damper assembly).

Table 3.9 Influence of Retrofit on Performance of Test Specimen

	Level 5 (40%) Excitation				
	Peak Drift Reduction (%)			Hysteretic Energy Demand Reduction (%)	Cumulative Energy Dissipated by Dampers (%)
	Total	Stiffness Contribution (%)	Damper Contribution (%)		
Ideal (f = 1.65)	92	47	53	97	86
Actual (f = 0.65)	77	56	44	77	48
Added Stiffness	43	100	0	30	0

3.9 Test Specimen Modification to Reduce Displacement Transmission Loss

Since the retrofitted test specimen was in good condition after the final shake table test, it was decided to perform one additional seismic test in which a simple modification was made to the test set-up in an effort to reduce the displacement transmission loss to the damper. The modification was made at the connection between the wood top plate and the top steel channel of the damper assembly. Specifically, from the inside of the shear walls, two steel shear plates (9.53 mm (3/8 in) thick) were welded to each top channel and screwed to the top plate (see Figure 3.18), the intent of the shear plates being to more directly transfer shear forces from the wood top plate to the steel top channel and thus to reduce displacement transmission losses at that location.

The effect of the modified design is shown in Figure 3.19 for the east wall of the test specimen for Level 4 (60%) excitation. The damper stroke is significantly increased, particularly for small displacement response (see Figure 3.19a), as compared to the test specimen prior to addition of the shear plates (see Figure 3.15b). The increased damper stroke corresponds to a displacement magnification factor (f) that is increased by about 10% (from 0.65 to 0.72). Also note that the time lag between the damper stroke and wall displacement during seismic excitation was reduced by approximately 60% (compare Figure 3.19a and Figure 3.15b). Further, energy dissipation in the dampers, particularly near zero displacement, is increased significantly (compare Figure 3.19b and 3.11b),

resulting in reduced hysteretic energy dissipation demand on the framing system and thus a peak drift reduction of about 10% (from 0.97% to 0.89%).

Figure 3.18 Close-Up View of Steel Shear Plates for Reducing Displacement Transmission Losses

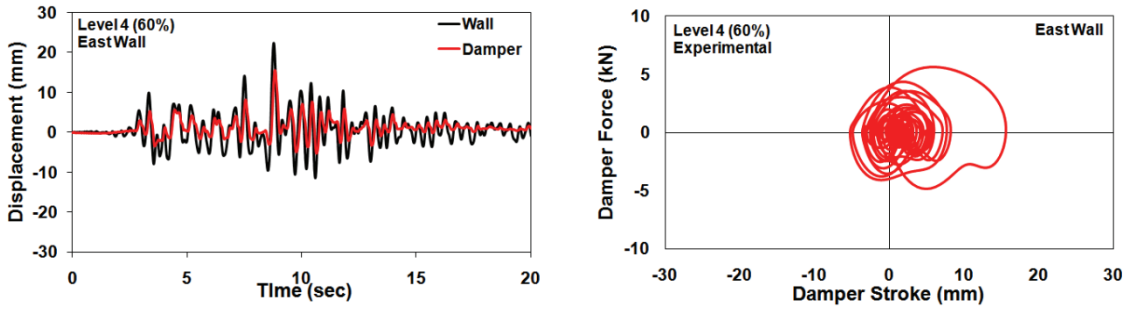

(a) (b)

Figure 3.19 Effect of Modified Design on Performance of East Wall of Test Specimen for Level 4 (60%) Excitation: (a) Wall and Damper Stroke Response History and (b) Damper Hysteretic Response

3.10 Summary and Concluding Remarks

The research presented herein demonstrated the feasibility of implementing modular damper walls within a full-scale shearwall. The modular damper walls contained fluid viscous dampers within a wood framing system. Such dampers can readily fit within the dimensional restrictions of a conventional wood shearwalls. Thus, the modular damper walls can be constructed off-site and delivered to the job site for "drop-in" installation.

The performance of the retrofitted walls with the toggle-braced assembly was significantly improved as compared to the conventional walls. The improvement in performance can be attributed to both added stiffness and additional energy dissipation capacity due to the damper assembly (i.e., visco-elastic behavior). The ability of the retrofitted walls to resist repeated seismic excitation without any significant damage was clear. Due to a number of factors, including the inherent flexibility in the connections of wood framing systems, engagement of the dampers was limited and thus the full effectiveness of the dampers was not realized. Significant loss of displacement transmission (about 60%) was observed. Evaluation of loss of displacement transmission revealed that there are additional possible sources of displacement loss in woodframed structures as compared to steel and concrete structures. These losses can be on the order of 30% to 40%. Additionally, there will be losses within the damper assembly itself. The toggle-braced assembly is a promising design for modular damper walls since the losses in displacement transmission to dampers is compensated to some extent by its displacement amplification properties. However, there can be significant losses due to elongation of the bracing members. These losses should be taken into consideration during the design process via reduction of the ideal displacement amplification factor by some loss factor. Additionally, the added stiffness due to the toggle brace should be accounted for in the design process. Clearly, there is potential for improvement in modular damper wall design via improved connections between the toggle-assembly and shearwall to increase displacement transfer to the toggle-assembly.

4. DISPLACEMENT-BASED DESIGN OF SEISMICALLY-ISOLATED WOODFRAMED STRUCTURES

Seismic isolation systems have been implemented in numerous structures worldwide but with relatively few applications to woodframed buildings, in spite of the fact that recent shaking table tests demonstrate significant improvement in their performance when they are isolated. To facilitate future applications to woodframed buildings, this chapter discusses the development of two displacement-based methods for seismic design of light-framed wood structures with base isolation systems. One method involves a conventional direct displacement-based design procedure in which a new approach has been taken to define an equivalent single-degree-of-freedom (SDOF) model for an isolated building structure with the computation of its design inter-story drift based on

the relative contribution of the isolation system displacement and the effective displacement of the equivalent SDOF fixed-base superstructure, all without the need for modal analysis. In addition, a simple and quick design procedure based on normalized modal analysis and generation of inter-story drift spectra has been developed. These more practical approaches have been developed with the objective of enabling designers to efficiently evaluate various options before making the final selection of isolation system parameters. The validity of both displacement-based procedures is confirmed using results from nonlinear dynamic response-history analyses and experimental results from shaking table tests of a half-scale, two-story, woodframed building supported on a sliding isolation system.

4.1 Introduction

The 1994 Northridge Earthquake (Moment Magnitude = 6.8) clearly demonstrated the seismic vulnerability of woodframed construction in the U.S (Kircher et al. 1997). The estimated property losses in woodframed buildings were approximately $20 billion and 24 of the 25 fatalities occurred in such buildings. Prior to this earthquake, woodframed construction in the U.S. had generally been considered to perform well during earthquakes. However, this earthquake underscored the fact that conventionally designed woodframed structures can become uninhabitable due to significant structural and non-structural damage, although they generally do not collapse and thus relatively few lives are lost in such structures. As such, the NEESWood project sought to develop a performance-based seismic design (PBSD) philosophy that considers multiple levels of performance (van de Lindt et al. 2006). As part of this project, the application of seismic protection systems (seismic damping and isolation systems) to woodframed buildings was also investigated via a comprehensive experimental and numerical study.

One approach to increase the performance reliability of woodframed structures in regions of high seismic intensity is to incorporate an advanced seismic protection system. Seismic protection systems reduce the response of the structure during seismic excitations either by changing fundamental characteristics of structure (e.g., a base isolation system increases the fundamental natural period of the supported structure) or by providing additional means to absorb seismic input energy (e.g., an energy dissipation

provides supplemental damping). A comprehensive literature review on the application of advanced seismic protection systems (both base isolation and supplemental damping systems) to woodframed structures is presented by Symans et al. (2002). Therein, the only known application of a base isolation system to a light-wood framed building is presented (a residential structure on a sliding isolation system). This study clearly identified the various challenges of the application of seismic protection systems to woodframed structures. Some of these challenges for the application of base isolation systems are:

1) Low weight of woodframed structures (Lateral stiffness of isolation systems must be very low to sufficiently extend period. For elastomeric bearings, the requirement of low stiffness leads to potential bearing instability. Also, low weight on sliding bearings leads to high and unstable friction coefficients and the potential for undesirable sliding during strong windstorms).
2) Absence of stiff diaphragm at the first floor in woodframed structures (The introduction of a stiff diaphragm is important to ensure the transfer of base shear to the isolation system while maintaining uniform motion across all bearings and thus maintaining the effectiveness of isolation).
3) A need for flexible utility connections (e.g., gas, electric, telecommunications, etc.) which limit the displacement capacity of the isolation system and thus the isolation effect.

In addition to these technical challenges, some important challenges are cost control, a lack of technical and construction expertise, the need for simple and practical design methods and social awareness among owners about the benefits of using such systems to protect their houses.

There have been continuing research efforts to develop or implement base isolation systems in woodframed buildings, particularly in Japan where different base isolation systems have been applied to residential structures. Recently, Wetzel (2006) developed a friction bearing device to limit damage in lightweight structures. Kubo et al. (1998) proposed a seismic isolation bearing (rubber combined with steel plates) that is configured such that it is particularly suitable for lightweight structures. Yamnouchi et al. (1998) demonstrated the usefulness of base isolation through testing with various

isolation systems using different masses of superstructure. Finally, a number of implementations of base isolation systems consisting of low-friction sliding bearings combined with elastomeric bearings have been implemented in Japan for single family houses (e.g., see http://www.ichijo.co.jp).

The design of seismic isolation systems within the context of PBSD procedures has been discussed within the literature. PBSD with isolation systems have been proposed by Priestley et al. (1998, 2007) in which direct displacement-based design (DDD) of seismically isolated bridges and isolated buildings (assuming both rigid and flexible behavior of superstructure) were covered. Cardone et al. (2008) proposed a new approach for DDD of seismically isolated bridges using the guidelines of Priestley et al. (2007). Direct Displacement-Based Design (DDD) is a method in which a nonlinear system is modeled as an equivalent linear system where the stiffness is represented by the secant stiffness at the design displacement. In addition, the displacement-induced damage (inelastic strain energy) is accounted for via an equivalent linear viscous damping model. This approach to modeling is also applicable to isolated structures since such a structure can be considered to be a conventional structure but with a short first story having high flexibility and energy dissipation capacity. Equivalent viscous damping used in the DDD is often difficult to quantify for structures subjected to damage. Including isolation systems enables the designer to quantify damping more accurately by combining the inherent superstructure damping (typically 5% considering the nearly elastic response of the superstructure with base isolation effect during seismic excitation) and damping of the isolation system based on its hysteretic behavior (which can be based on experimental data), and thus it improves the reliability of the DDD procedure. The advantages of displacement-based approaches over force-based approaches for analysis and design of isolated structures are discussed by Priestley (2007).

Within the NEESWood project, shaking table tests have been recently completed on a half-scale woodframed building with Friction Pendulum System (FPS) bearings (Zayas et al. 1987). The results from the tests clearly demonstrated the effectiveness of sliding isolation bearings for seismic protection of light wood-framed buildings. To facilitate future applications to woodframed buildings, this chapter discusses the development of

two displacement-based methods for seismic design of light-framed wood structures with base isolation systems. One method involves a conventional direct displacement-based design procedure in which a new approach has been taken to define an equivalent single-degree-of-freedom (SDOF) model for an isolated building structure with the computation of its design inter-story drift based on the relative contribution of the isolation system displacement and the effective displacement of the equivalent SDOF fixed-base superstructure, all without the need for modal analysis. In addition, a simple and quick design procedure based on normalized modal analysis and generation of inter-story drift spectra has been developed. These practical approaches have been developed with the objective of enabling designers to efficiently evaluate various options before making the final selection of isolation system parameters. The validity of both displacement-based procedures is confirmed using results from nonlinear dynamic response-history analyses and experimental results from shaking table tests of a half-scale woodframed building supported on a sliding isolation system.

4.2 Half-Scale Seismic Isolation Test

Seismic shaking table tests were performed at Colorado State University on a half-scale woodframed building supported on Friction Pendulum System (FPS) bearings. The tests were conducted as part of the NEESWood project. A half-scale woodframed test structure was designed based on the available plan dimensions of the shake table (see Figure 4.1). The building is assumed to have been located in either Northern or Southern California and may be regarded as a single family home with three bedrooms and an attached one-car garage. The total living area for the full-scale prototype would be approximately 107 m^2 (1150 ft^2) which is relatively small compared to typical houses. The half-scale test specimen had a total living area of 26.7 m^2. The height of the first and second story, H_{SS}, was equal to 1.32 m, thus making the total height of the superstructure (foundation to roof eave) equal to 2.64 m. Note that the shaking table tests were conducted with motion imposed only along the longitudinal direction (i.e., stronger direction) of the test structure.

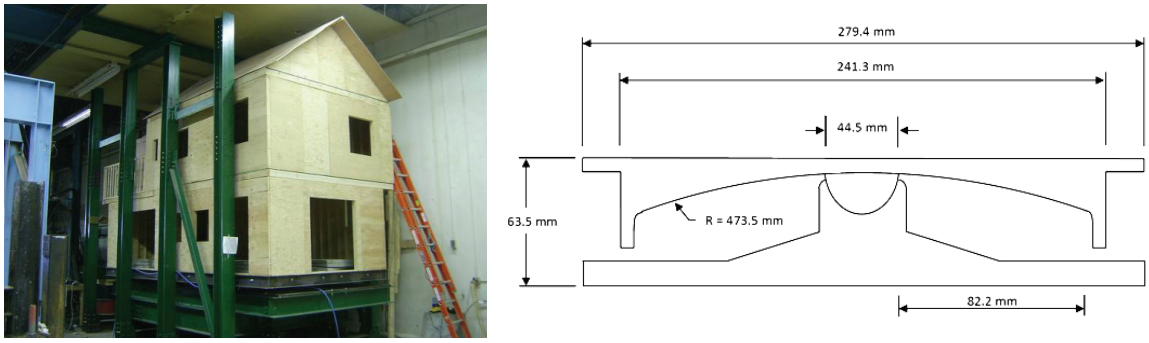

(a) **(b)**

Figure 4.1 (a) Half-Scale Isolated Test Structure and (b) Geometry of FPS Bearing used for Testing

The seismic weight at the first and second floor level and the roof level was 14.23 kN, 23.06 kN and 16.45 kN, respectively. The total weight of the superstructure (second floor and roof levels), W_{SS}, was 39.51 kN and the total weight of the isolated structure (first, second and roof levels), W_{IS}, was 53.74 kN. The radius of curvature, R, of the FPS bearings used for testing was 473.5 mm with a displacement capacity, Δ_{IS}, equal to +/-82.2 mm (see Figure 4.1 for details). Thus, the natural period of a rigid mass supported on the FPS bearings, T_{IS}, is 1.38 sec as given by the natural period of a pendulum:

$$T_{IS} = 2\pi\sqrt{\frac{R}{g}} \tag{4.1}$$

4.3 Displacement-Based Design using Inter-Story Drift Spectra

The simple displacement-based design (DBD) procedure presented herein is based on the generation of inter-story drift spectra and has the potential to be used as a simple and expeditious PBSD approach for design of isolated structures. This method was conceptualized based on the important observation that inter-story drifts are more sensitive than mode shape values to isolation system parameter values (Shinde et.al. 2010). The general method for generating inter-story drift spectra for use within a DBD procedure was adapted from Pang and Rosowsky (2007). This approach provides a reasonably accurate solution and thus serves as a suitable tool for preliminary analysis of isolated buildings. This DBD procedure involves the following steps (see Figure 4.2):

1) For given seismic hazard levels, define desired performance level in terms of limiting inter-story drifts.
2) Select isolation system properties and model the isolation system as a separate story while assuming a suitable height of the isolation story and inter-story drift at the isolation level. Estimate the mass and stiffness ratios for each story [relative to the first story (i.e., story above isolation story)].
3) Perform normalized modal analysis to obtain inter-story drift factors and natural frequency parameters.
4) Assume a suitable value of equivalent damping (based on selected isolation system parameters) and construct design inter-story drift spectra for the given hazard level. From design inter-story spectra obtain estimate of design inter-story drift in each story of superstructure for the defined value of isolation inter-story drift ratio.
5) Compare results with design inter-story drift. Revise isolation design if necessary and repeat steps 2-5.

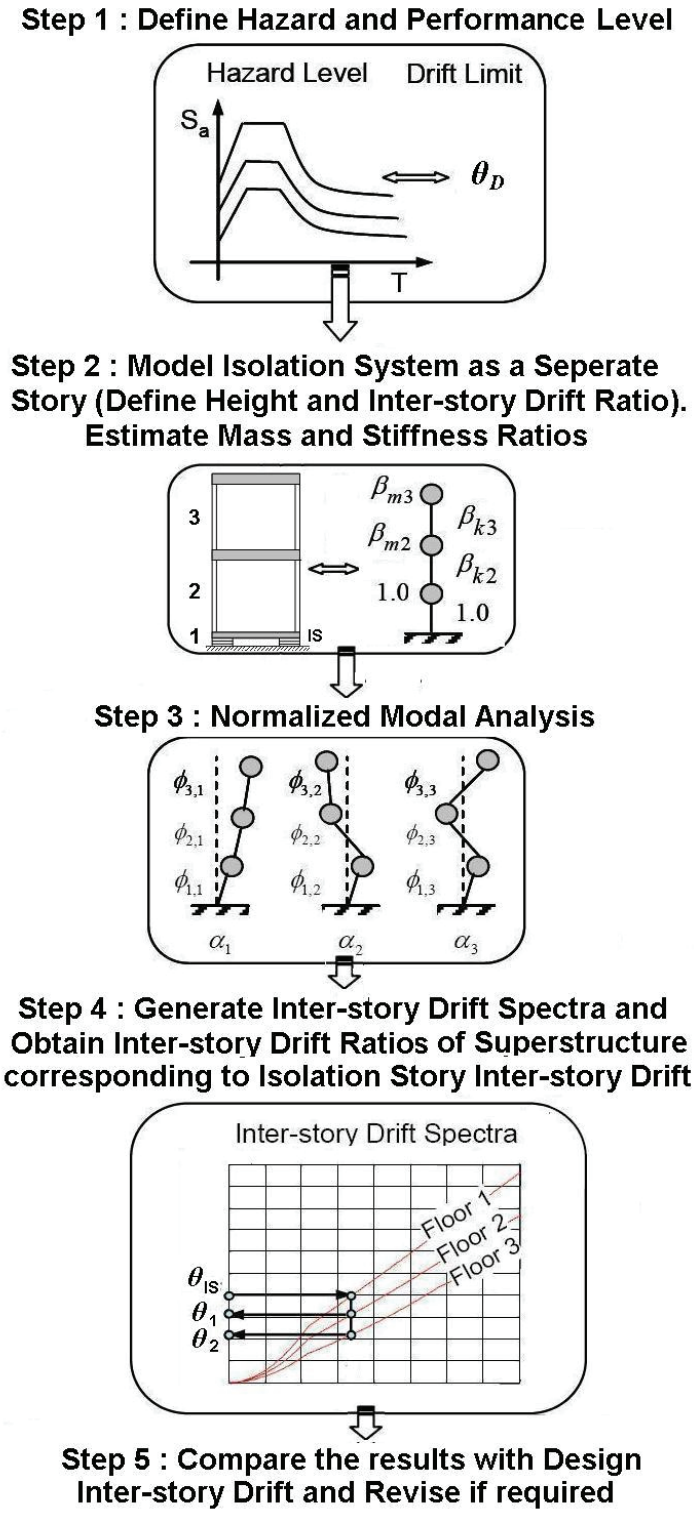

Figure 4.2 Displacement-Based Design using Inter-Story Drift Spectra (Adapted from Pang and Rosowsky, 2007)

4.3.1 Design Process

4.3.1.1 Target Performance Levels and Seismic Hazard Levels (Step 1 in Figure 4.2)

Base isolation can be used to achieve higher design performance levels for high seismic hazard (e.g., Maximum Considered Earthquake (MCE) which has a 2% probability of occurrence for a design life of 50 years). The test structure is designed for a location in Southern California with stiff soil conditions (Site Class D). The design 5%-damped spectral acceleration values for MCE hazard Level were determined in accordance with ASCE/SEI-41 (2006). The MCE spectral response acceleration for short-period, S_{MS}, was taken equal to 1.5g and its value for one-second period, S_{M1}, was taken as 0.9g. The design performance level was chosen as an operational level (0.5% design inter-story drift limit θ_D).

4.3.1.2 Modeling of Isolation System and Estimation of Mass and Stiffness Ratios (Step 2 in Figure 4.2)

Since the isolation system is modeled as an individual story, the height of the isolation story, H_{IS}, must be established. One approach to establishing the height is to base it on the geometry of the FPS bearings such that the resulting height is on the order of 5-10% of the typical height of the stories within the superstructure (H_{IS}).In the case of the isolated test structure, the isolation story height was taken as ten times the depth, D_B, of the FPS bearings (corresponding to the lowest point of the curved surface) which is equal to about 5.4% of the typical height of the stories within the superstructure. Since inter-story drift (actually, inter-story drift ratio) is inversely proportional to the height of the story, an expression for the isolation story drift limit, θ_{IS}, as defined by the following empirical relation:

$$\theta_{IS} = \frac{\eta H_{SS}}{D_B} = \frac{\eta H_{SS}}{R\left(1-\cos\sigma\right)} \tag{4.2}$$

where σ is one-half of the central angle made by the FPS arc (10 degrees for the bearings used in the testing) and η is a calibration factor which was taken equal to 0.013 for the two-story test structure. For different numbers of stories in the

superstructure, a parametric study would be needed to determine a suitable value for the calibration factor. In addition, for other types of isolation systems, the depth of the bearing in Equation 4.2 would need to be defined differently (e.g., for elastomeric bearings, the height of the bearing could be used). Note that Equation 4.2 gives drift expressed as a percentage. As shown in Equation 4.2, the inter-story drift limit for the isolation story, the inter-story drift limit for the isolation story, θ_{IS}, is inversely proportional to the radius, R ,and, therefore, to the square of the natural period of the isolated structure, T_{IS} . Introducing the height of the stories of the superstructure, H_{SS} , in Equation 4.2 allows for a connection to be established between the stiffness of the superstructure and that of the isolation system, that relation being important as it controls the degree of isolation effect.

The mass ratios, β_m , (relative to the isolation story) were computed as 1.62 and 1.16 for the first and second stories, respectively. For initial design purposes, a uniform distribution of inter-story drift can be assumed. A preliminary estimate of the stiffness ratio for each story within the superstructure is given by:

$$\beta_{kj} = \frac{k_{SS}}{k_{IS}} \tag{4.3}$$

where k_{IS} is the secant stiffness of the isolation system and k_{SS} is the stiffness of each story in the superstructure (assumed to be equal for initial design purposes) as given by:

$$k_{IS} = \frac{W_{IS}}{R} + \frac{\mu W_{IS}}{\Delta_{IS}} \tag{4.4}$$

$$k_{SS} = \frac{F_t}{\Delta_{SS}} \tag{4.5}$$

where Δ_{SS} is the displacement at the top (roof-level) of the fixed-base superstructure and F_t is the total lateral force applied at the roof level as given by:

$$F_t = C_c W_{SS} \tag{4.6}$$

where C_c is the design base shear coefficient. Note that this method uses a simple concept of computing the stiffness of superstructure stories by representing the structure as an equivalent SDOF system and applying the total lateral force F_t at the top of the

superstructure which displaces by Δ_{SS} (in this simplified approach, the SDOF model is defined by the total weight, total height, and total displacement at the top of the structure when subjected to the force F_t). To obtain a better estimate of the inter-story drifts, a non-uniform distribution of design inter-story drifts can be assumed in accordance with the seismic mass distribution within the structure. Note that the substitute structure approach used in the classical DDD method developed by Priestley (2007) can also be used herein to define the effective stiffness of the superstructure and compute the stiffness ratio. The method described herein is meant to simplify the calculations. Note that this method results in a smaller value of story stiffness than the effective stiffness (using substitute structure approach) and thus results in a conservative estimate of peak inter-story drifts in the superstructure.

Also note that, due to the relatively low pressure on the bearings for light weight woodframed structures, the value of the coefficient of friction, μ, was taken as 0.10. The design base shear coefficient, C_c, is obtained from:

$$C_c = \frac{S_{MS}}{B_\xi} \tag{4.7}$$

where B_ξ is the damping reduction factor determined in accordance with (ASCE/SEI-41, 2006):

$$B_\xi = \frac{4}{5.6 - \ln\left(100\xi_{SS}\right)} \tag{4.8}$$

where ξ_{SS} is the equivalent damping of the superstructure and is assumed equal in all modes of vibration. The value of B_ξ is equal to unity as an equivalent viscous damping of 5% is assumed for the superstructure (considering that elastic or nearly elastic response of the superstructure is expected).

4.3.1.3 Normalized Modal Analysis and Construction of Inter-story Drift Spectra (Step 3 and 4 of Figure 4.2)

After the mass and stiffness ratios have been determined, a normalized modal analysis is performed to compute frequency parameters, α_n, and mode shapes, ϕ_n, as given by:

$$\alpha_n^2 M\phi_n = K\phi_n \tag{4.9}$$

Knowing these parameters, the inter-story drift factors for the j-th story in the n-th mode, γ_{jn}, is obtained as follows:

$$\gamma_{jn} = \Gamma_n \left(\phi_{jn} - \phi_{j-1,n}\right) \tag{4.10}$$

where Γ_n is the modal participation factor corresponding to the n-th mode. The design inter-story drift spectra are then generated from the design acceleration response spectrum (Pang and Rosowsky, 2007) using:

$$\Delta_j\left(\overline{T}\right) = \frac{1}{H_j}\sqrt{\sum_n \left[\gamma_{jn}\left(\frac{\overline{T}}{2\pi\alpha_n}\right)^2 S_a\left(\frac{\overline{T}}{\alpha_n}\right)\right]^2} \tag{4.11}$$

where $\Delta_j\left(\overline{T}\right)$ is the inter-story drift for the j-th story (with contributions from all modes), H_j is the height of the j-th story, $S_a\left(\overline{T}/\alpha_n\right)$ is the interpolated design acceleration response spectra value, and $\overline{T}$ is the normalized first-story period. Note that the inter-story drift spectra should be further adjusted for equivalent damping of the isolated structure, ξ_{eq}, as given by (Priestley, 2007):

$$\xi_{eq} = \frac{\Delta_{SS}\ \xi_{SS} + \Delta_{IS}\ \xi_{IS}}{\Delta_D} \tag{4.12}$$

where Δ_D is the design displacement of the isolated structure which is equal to the sum of the top structural displacement, Δ_{SS}, and the displacement capacity of the isolation bearings, Δ_{IS}. The derivation of Equation 4.12 involves the assumption that the ratio of equivalent damping of the structure and isolation system is equal to the ratio of the corresponding hysteretic areas used to compute them. Note that the damping reduction factor B_ξ defined in Equation 4.8 is used to scale down the inter-story drift spectra by additional equivalent damping of the isolated structure, ξ_{eq}, by replacing the ξ_{SS} term in Equation 4.8 with ξ_{eq}. The damping ratio associated with the FPS isolation system, ξ_{IS}, is calculated based on Jacobsen's Equation (Cardone et al. 2008) which involves the ratio of the total energy dissipated by the isolation system to the strain energy stored at the maximum displacement as given by:

$$\xi_{IS} = \frac{2}{\pi}\frac{\mu}{\mu + \Delta_{IS}/R} \tag{4.13}$$

After generating the design inter-story drift spectra, the estimate of the peak inter-story drift in each story of the superstructure was obtained at the defined value of isolation inter-story drift ratio (239%) calculated using Equation 4.2 (see Figure 4.3). The first and second story will experience only 0.40% and 0.17% drift, respectively. These values are less than the design inter-story drift limit, θ_D, of 0.5% and thus there is no need to redesign the isolation system.

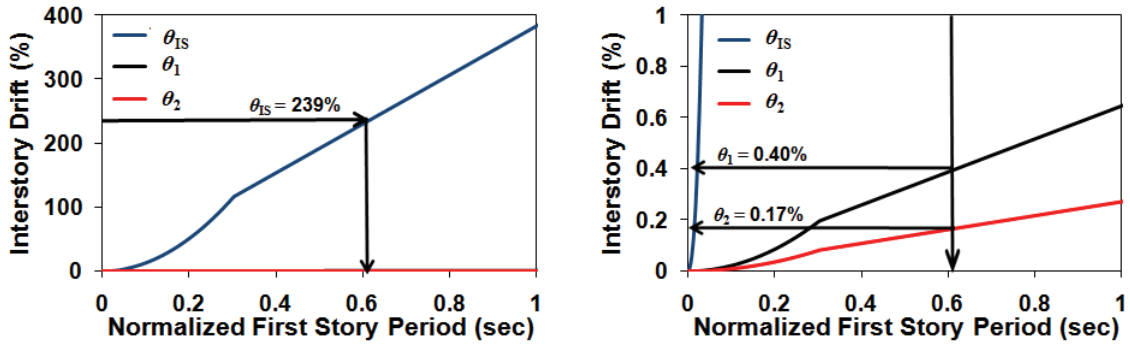

Figure 4.3 Inter-Story Drifts for Test Superstructure from Isolation Story Inter-Story Drift

4.3.2 Advantages of Proposed Displacement-Based Design Procedure

The advantages of the displacement-based design procedure based on using the inter-story drift spectra are:

1) It is simple and thus saves time and effort while maintaining reasonable accuracy of results.
2) It is easy to define the inter-story drift capacity for different isolation systems by performing a parametric study.
3) The use of more sensitive inter-story drifts in the analysis allows better fine-tuning while selecting isolation parameters values than an analysis based on the less sensitive mode shape values.
4) The substitute structure approach to define effective stiffness can be easily incorporated within the design procedure.

5) In the proposed procedure, the isolation story height is directly related to the isolation system parameters (for FPS bearing it is related to the height of the curved surface). Note that this is a better approach than using an assumed value of the isolation story height which is not strongly correlated to the isolation system geometry (e.g., using a percentage of the story height).
6) The proposed procedure gives an estimate of the peak inter-story drift in all the stories of the superstructure which may be useful to make the final design of the superstructure economical (e.g., by modifying the structural properties to avoid excess drift in any one particular story).
7) For fine-tuning the design, a single analysis with the selected isolation system parameters can be used directly as the inter-story drifts in the superstructure are constant for the given isolation inter-story drift generated from the elastic response spectra (i.e., the isolation story drift can be recalculated using Equation 4.2 and the inter-story drift spectra generated in the initial analysis can be directly used to estimate the peak inter-story drifts in the stories of the superstructure for subsequent changes in the isolation system parameter values). Note that this approach does not consider the change in the equivalent damping of the isolated structure and thus results will be approximate. Thus, it is recommended to use it only if the isolation system parameters are changing within a small range with an insignificant change in the equivalent damping.

4.4 Direct Displacement-Based Design

The procedure described herein involves a conventional direct displacement-based design procedure (Priestley et al. 2007) in which a new approach has been taken to define an equivalent single-degree-of-freedom (SDOF) model for the isolated building structure with the computation of its design inter-story drift based on the relative contribution of the isolation system displacement and the effective displacement of the equivalent SDOF fixed-base superstructure, all without the need for modal analysis. This DDD procedure involves the following steps:

1) For given seismic hazard levels, define desired performance level in terms of limiting inter-story drifts.

2) Define equivalent SDOF model for a fixed-base superstructure using substitute structure approach.
3) Select isolation system properties and model isolation system as a separate story. Define an equivalent SDOF model for the isolated superstructure (note that the superstructure is converted to an equivalent SDOF model in the previous step) and determine its actual effective stiffness.
4) Enter displacement response spectra (modified with equivalent viscous damping of equivalent SDOF model of isolated structure) with the design displacement of isolated structure to determine the required effective stiffness.
5) Estimate approximate peak inter-story drift by dividing the design inter-story drift ratio by the ratio of actual to required effective stiffness.
6) Compare results with design inter-story drift. If necessary, revise isolation system design and repeat steps 2-6.

4.4.1 Design Process

DBD of the half-scale test structure presented previously is also used herein to explain the steps of the DDD procedure. Note that target performance levels and hazard levels are the same as defined previously in displacement-based design using inter-story drift spectra.

4.4.1.1 Equivalent SDOF Model of Superstructure

An equivalent SDOF model for a fixed-base superstructure based on DDD guidelines (Pang et al. 2009) is developed herein. Note that the procedure used to define the effective weight and height of the structure is the same as the substitute structure approach discussed by Priestley et al. (2007). Table 4.1 shows the design parameters for the equivalent SDOF model of the superstructure which are defined in Figure 4.4. Note that the design inter-story drift limit for each story, θ_j, is the same as the design inter-story drift limit, θ_D, defined previously. A uniform distribution of inter-story drift is assumed. Alternatively, non-uniform distribution can be assumed based on relative stiffness of stories and the inertial masses associated with them.

Table 4.1 Design Parameters for Equivalent SDOF Model of Half-Scale Test Superstructure

Story	h_j (m)	h_j^t (m)	W_j (kN)	θ_j (%)	Δ_j (mm)	Δ_j^t (mm)	C_{vj}
1	1.32	1.32	23.06	0.50	6.60	6.60	0.41
2	1.32	2.64	16.45	0.50	6.60	13.20	0.59

The vertical distribution factors for base shear, C_{vj}, is computed using:

$$C_{vj} = \frac{W_j \Delta_j^t}{\sum_j W_j \Delta_j^t} \tag{4.14}$$

The effective height, h_{eff}^{SS}, is determined as follows:

$$h_{eff}^{SS} = \sum_j C_{vj} h_j^t \tag{4.15}$$

The target displacement at the effective height, Δ_{eff}^{SS}, is obtained by interpolation at the effective height h_{eff}^{SS}. The effective seismic weight, W_{eff}^{SS}, is computed as follows:

$$W_{eff}^{SS} = \frac{\sum_j \left(W_j \Delta_j^t\right)^2}{\sum_j W_j \left(\Delta_j^t\right)^2} \tag{4.16}$$

Note that, in Figure 4.4, the effective seismic mass, m_{eff}^{SS}, is shown instead of the effective seismic weight W_{eff}^{SS}. The design lateral force, F_t^{SS}, is given by:

$$F_t^{SS} = C_c W_{eff}^{SS} \tag{4.17}$$

where C_c is the design base shear coefficient which is adjusted in accordance with the damping reduction factor B_ξ (see Equation 4.7 and 4.8). As mentioned previously, the value of B_ξ can be taken as unity if it is assumed that the equivalent viscous damping in the superstructure is 5%. Finally, the effective stiffness of the superstructure, k_{eff}^{SS}, is determined as follows:

$$k_{eff}^{SS} = \frac{F_t^{SS}}{\Delta_{eff}^{SS}} \tag{4.18}$$

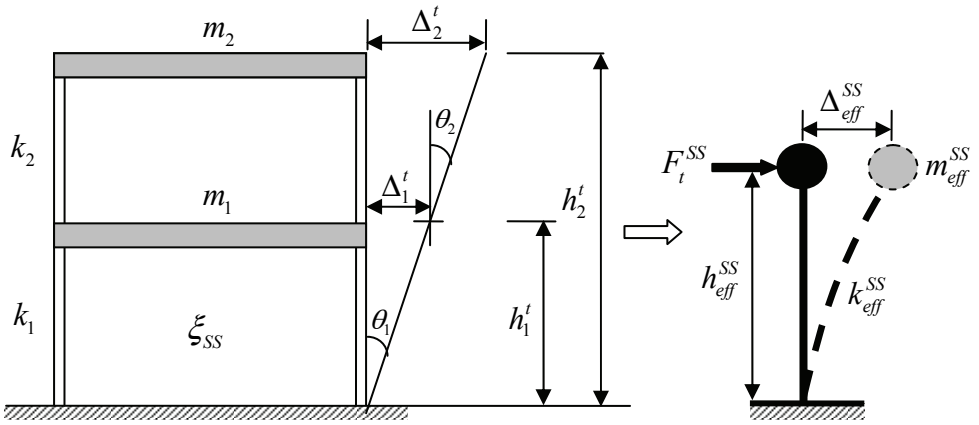

Figure 4.4 Equivalent SDOF Model of Superstructure

4.4.1.2 Equivalent SDOF Model for Isolated Superstructure

An equivalent SDOF model for the isolated structure can also be defined as shown in Figure 4.5 wherein the isolation system is combined with the equivalent SDOF model of the superstructure.

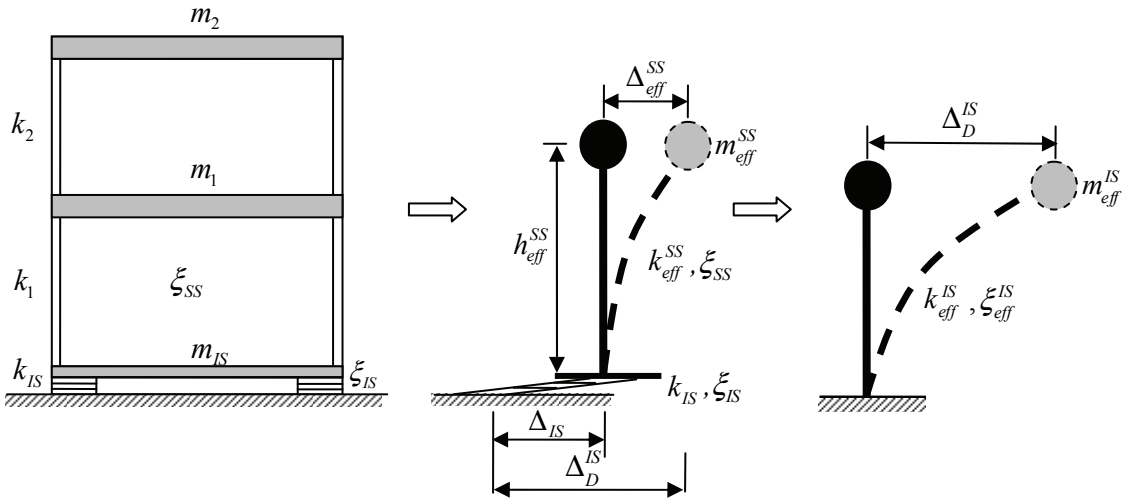

Figure 4.5 Equivalent SDOF Model of Isolated Structure

The design displacement of the isolated structure, Δ_D^{IS}, is determined using:

$$\Delta_D^{IS} = \Delta_{eff}^{SS} + \Delta_{IS} \tag{4.19}$$

The effective mass of the equivalent isolated structure, m_{eff}^{IS}, is obtained as follows:

$$m_{eff}^{IS} = \frac{m_{eff}^{SS}\ \Delta_{eff}^{SS} + m_{IS}\ \Delta_{IS}}{\Delta_D^{IS}} \tag{4.20}$$

The displacement response spectra in step 4 should be further adjusted for the equivalent damping of the isolated structure. The effective damping of the equivalent isolated structure, ξ_{eff}^{IS}, is determined using (Priestley, 2007):

$$\xi_{eff}^{IS} = \frac{\xi_{SS}\Delta_{eff}^{SS} + \xi_{IS}\Delta_{IS}}{\Delta_{D}^{IS}} \tag{4.21}$$

Note that the above equation is the same as Equation 4.12 except with some different notation as used in the DDD procedure described herein. Finally, the actual effective stiffness of the equivalent isolated structure, k_{eff}^{IS}, is determined as follows (equivalent to combining two springs in series):

$$k_{eff}^{IS} = \frac{k_{eff}^{SS}k_{IS}}{k_{eff}^{SS} + k_{IS}} \tag{4.22}$$

4.4.1.3 Required Effective Stiffness using Displacement Response Spectra

Displacement response spectra (adjusted with damping reduction factor B_{ξ}) are used to determine the required effective period, T_{reff}^{IS}, corresponding to the design displacement of the isolated structure, Δ_{D}^{IS} (see Figure 4.6). Next, the required effective stiffness, k_{reff}^{IS}, of the equivalent isolated structure is obtained:

$$k_{reff}^{IS} = \left(\frac{2\pi}{T_{reff}^{IS}}\right)^2 m_{eff}^{IS} \tag{4.23}$$

Note that, for the given design example, the displacement response spectrum for the full-scale test structure (i.e., prototype) is determined as follows:

$$S_d\left(T_p\right) = \left(\frac{T_p}{2\pi}\right)^2 S_a\left(T_p\right) \tag{4.24}$$

where $S_d\left(T_p\right)$ is the spectral displacement of the prototype, $S_a\left(T_p\right)$ is the spectral acceleration of the prototype and T_p is the natural period of the prototype. The spectral displacement for the half-scale test structure is also given by Equation 4.24 except that the values at model scale are used instead of at prototype scale. In that case, the natural period at model scale, T_m, is obtained by invoking similitude principles and results in:

$$T_m = \frac{T_p}{\sqrt{2}} \tag{4.25}$$

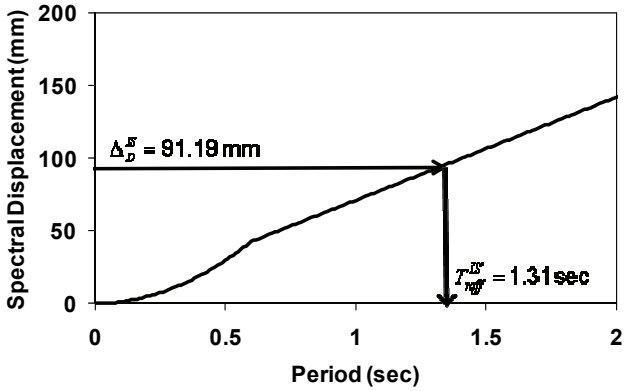

Figure 4.6 Displacement Response Spectra for Half-Scale Isolated Test Structure

4.4.1.4 Estimation of Peak Inter-Story Drift

The ratio of actual to required effective stiffness of the equivalent isolated structure, r_k, is given by:

$$r_k = \frac{k_{eff}^{IS}}{k_{reff}^{IS}} \tag{4.26}$$

and an approximation of the expected peak inter-story drift, θ_E, can be obtained from:

$$\theta_E = \frac{\theta_{ij}}{r_k} \tag{4.27}$$

The expected peak inter-story drift was computed as 0.35% for the half-scale test structure using the DDD procedure described herein. This value is less than the 0.5 % design inter-story drift limit and thus there is no need to redesign the isolation system. Note that this estimated value is almost identical to the peak inter-story drift prediction (i.e., 0.40% in first story; see Figure 4.3) from the displacement-based design procedure using the inter-story drift spectra.

The expected value of peak inter-story drift obtained by imposing different performance levels make sense only when the actual isolated structure is subjected to a similar magnitude of drift demand for the given hazard level. Thus, for accurate predictions, it is important in the DDD procedure to select the performance levels and the isolation system parameters carefully for the given hazard level.

4.4.2 Advantages of Proposed Direct Displacement-Based Design Procedure

The advantages of the proposed DDD procedure are:

1) This procedure is more PBSD oriented (similar to the displacement-based design using the inter-story drift spectra) in which the design inter-story drift is explicitly defined at the start of design and results are obtained in terms of the inter-story drifts which are then directly compared with the design value.
2) The use of isolation story height is eliminated in the proposed procedure. The iterations focus on changing the isolation system parameters to achieve the desired performance, thus saving time and effort. (Note that in Priestley's DDD method for the flexible isolated structure (Priestley et al. 2007), the substitute structure approach (similar to fixed-base structure) is used to define the equivalent SDOF model of the flexible isolated structure. The effective height of the equivalent isolated structure is assumed at the start and iterations may be needed for getting accurate results for the chosen isolation system parameters. Additionally, the height of the isolation floor needs to be defined which includes the assumed value of the thickness of the rigid base diaphragm.)
3) Similar to Priestley's DDD method for flexible isolated structures (Priestley et al. 2007), the proposed procedure does not require modal analysis.

4.5 Comparison of Proposed Displacement-Based Procedures

Figure 4.7 shows a comparison of the proposed displacement-based procedures in terms of the peak inter-story drift prediction for different values of the radius of the FPS bearing. Note that the displacement-based design using inter-story drift spectra is indicated by the red line whereas the direct displacement-based design is indicated by the blue line. The range of radii values is chosen such that the peak inter-story drift varies from a very rigid response of the isolated superstructure (peak drift close to 0.25%) to a maximum value that is deemed acceptable (peak drift close to 1%). It is evident from Figure 4.7 that both displacement-based procedures gives essentially the same prediction for more rigid behavior of the superstructure [i.e., peak drift less than 0.5% (operational performance level)] which might be considered as an acceptable upperbound performance objective for most isolated structures. A possible reason for the

deviation of the two displacement-based procedures at low values of the radii (see Figure 4.7) may be due to the rapid variation of the isolation story drift used in the displacement-based design using inter-story drift spectra at those values. Some of the differences between the two methods are clear from the previous discussions on the advantages of these procedures. It is evident that the displacement-based design procedure using the inter-story drift spectra is better than the conventional DDD approach in terms of time and effort expended relative to the accuracy of results.

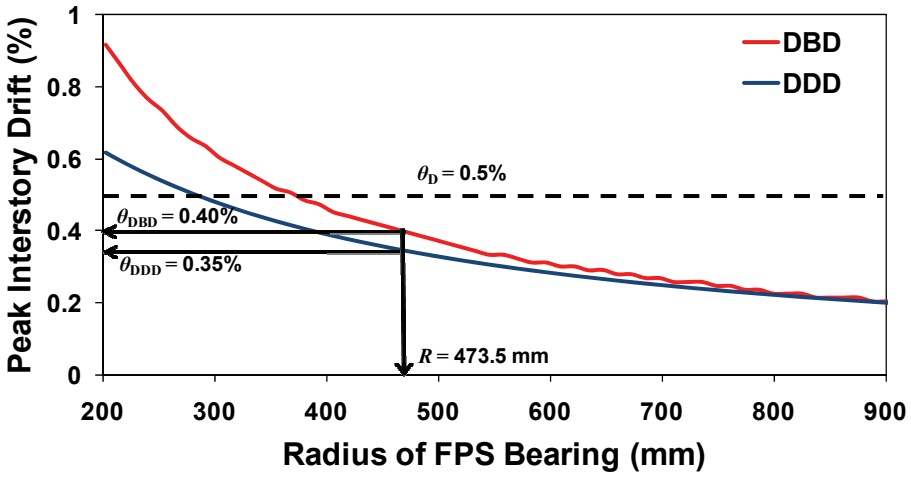

Figure 4.7 Comparison of Proposed Displacement-Based Procedures

4.6 Design Appraisal

4.6.1 Design Appraisal via Nonlinear Response-History Analysis

4.6.1.1 Numerical Modeling

The numerical model that was developed during testing of the half-scale isolated woodframed building was used herein for the design appraisal. In this model, the FPS bearing element was modeled as a three-dimensional element with coupled horizontal stiffnesses and restoring forces. The model also included a time-varying vertical force component and a pressure- and velocity-dependent dynamic coefficient of friction. The FPS bearing model was integrated into the SAPWood software package (Pei and van de Lindt, 2007) wherein it was combined with a non-linear flexible model of the woodframed superstructure. Complete details regarding the numerical model are available in Liu et al. (2008).

4.6.1.2 Nonlinear Response-History Analysis

The optimal design of the isolation system was determined based on the displacement-based design procedure and, as a verification step in the PBSD procedure, earthquake simulations using a suite of twenty earthquake ground motions (Krawinkler et al. 2000) were performed using SAPWood. Similar to the work by Krawinkler et al. (2000), these earthquake ground motions were scaled such that their mean 5%-damped spectral values over a period range from 0.1 to 0.6 seconds is equal to 1.5g, corresponding to the flat region of the response spectrum for the Southern California region for a 2%/50 yr hazard level (see Table 4.2). The approach used in the present study is consistent with ground motion scaling described in FEMA 302 (BSSC 1997) and FEMA 356 (ASCE 2000).

Table 4.2 Suite of Ground Motion Records Used for Design Appraisal

Earthquake Event/Year	Notation	Peak Ground Acceleration (g)	
		Actual	Scaled for Collapse Prevention
Cape Mendocino 1992	Cm1	0.116	0.795
	Cm2	0.385	0.798
Landers 1992	Lan1	0.154	0.813
	Lan2	0.152	0.599
Loma Prieta 1989	Lp1	0.529	0.635
	Lp2	0.555	0.710
	Lp3	0.417	0.780
	Lp4	0.226	0.615
	Lp5	0.279	0.623
	Lp6	0.332	0.900
Northridge 1994	Nor2	0.416	0.705
	Nor3	0.356	0.899
	Nor4	0.357	0.708
	Nor5	0.231	0.723
	Nor6	0.273	0.914
	Nor9	0.271	0.728
	Nor10	0.157	0.708
Superstition Hills 1987	Sup1	0.116	0.906
	Sup2	0.258	0.876
	Sup3	0.186	0.597

In Figure 4.8, the simulation results (with and without isolation) for the suite of 20 motions are plotted in terms of cumulative probability. Note that the simulations are

carried out only in the longitudinal direction (i.e., stronger direction) to be consistent with the experimental tests (see Figure 4.1a).

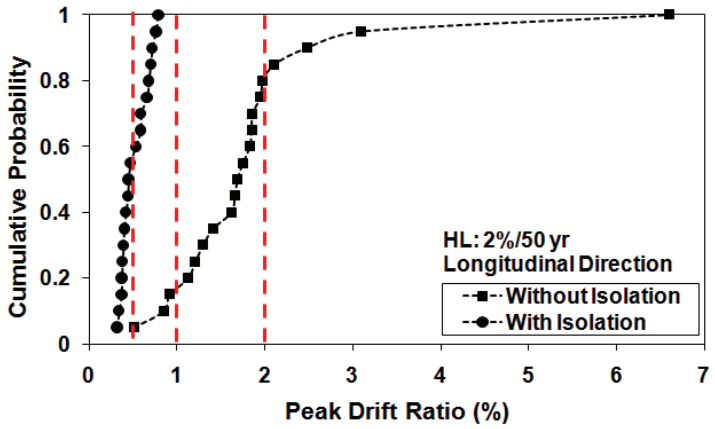

Figure 4.8 Peak Drift Distributions from Nonlinear Dynamic Analysis of Half-Scale Structure With and Without Isolation

As shown in Figure 4.8, the first story drift ratio (which corresponds to the peak drift ratio of the structure) for the no isolation case exceeds the 2% drift limit corresponding to the Life Safety (LS) performance level for four out of twenty earthquakes scaled for a 2%/50 yr hazard level. Since the test structure is stronger in the longitudinal direction, the LS performance level is achieved for most of the earthquakes (median value = 1.72% and probability of nonexceedance (P_{NE}) = 81%) in spite of the strong hazard level (2%/50 year). Although the code criterion for design is well satisfied, the results indicate the possibility of damage to the structure that could render it nonrepairable or uninhabitable. For the isolated structure, it is apparent that the specified performance objective (i.e, operational performance level with a design inter-story drift of 0.5%) can be achieved for a 2%/50 yr hazard level (median value = 0.46% and probability of nonexceedance (P_{NE}) = 57.5%). Also note that the degree of isolation effect would have been even more pronounced for earthquake loading along the weaker direction of the test structure.

The reasonably good agreement between the design inter-story drifts (based on displacement-based design procedures) and the median peak drifts obtained from response-history analyses serves to validate both displacement-based design procedures and thus suggests that they are suitable for design of isolated structures.

4.6.2 Design Appraisal via Experimental Results

Historical ground motions from three different earthquakes were used for the seismic shaking table tests: 1989 Loma Prieta, 1994 Northridge, and 1987 Superstition Hills. The peak interstory drift obtained from experimental testing of the isolated half-scale test structure is shown in Table 4.3 for the three earthquake motions scaled to the same hazard level (2%/50 year) that was used in the displacement-based design presented previously. As an example, the isolated test structure experienced a peak inter-story drift of 0.44% for the Northridge ground motion scaled to a 2%/50 yr hazard level, indicating that, for a hazard level associated with a collapse prevention performance level for conventional structures, an operational performance level was achieved without any significant damage. For the fixed-base test structure, the peak inter-story drift was more than 5% for the same motion, indicating severe damage and a near-collapse condition for the test structure. Note that, for this particular experimental test (Northridge ground motion applied to isolated test structure), the measured peak drift of 0.44% is reasonably close to the design inter-story drifts (i.e., 0.40% and 0.35% based on DBD and DDD, respectively) and thus the proposed displacement-based design procedures are further validated. Also note that, for the other ground motions, the measured peak drift exceeded the design inter-story drift limit (i.e., 0.5%) by about 20%. This may be due to some accumulated damage as the half-scale test structure was also tested with ground motions scaled to 50%/50 year and 10%/50 year hazard levels. The experimental measured drift also includes the effect of overturning of the test structure and shaking table, uplift of shearwalls, bending deformation of shearwalls, and slippage at sill plates. Thus, the actual inter-story drifts (which are directly correlated to damage) may be lower than the values shown in the Table 4.3.

Table 4.3 Peak Drifts from Shaking Table Tests of Half-Scale Test Structure with Motions Scaled to 2%/50 Year Hazard Level

Earthquake Event	Year	Station	PGA (2%/50)	Peak Drift (%)
Loma Prieta	1989	Capitola	0.683	0.61
Northridge	1994	LA – Hollywood Storage	0.778	0.44
Superstition Hills	1987	Plaster City	0.643	0.63

4.7 Summary and Concluding Remarks

Displacement-based PBSD procedures for design of multi-story buildings supported on sliding isolation systems have been presented. These methods were applied to the design of a half-scale woodframed test structure. The final design was evaluated using results from experimental testing and nonlinear response-history analyses. The results demonstrated that the predicted design inter-story drifts based on the selected operational performance level were in reasonable agreement with the median peak inter-story drifts obtained from nonlinear response-history analyses and the peak inter-story drifts from experimental testing, thus validating the proposed displacement-based design procedures. These practical approaches enable designers to efficiently evaluate various options before making the final selection of isolation system parameters.

The isolated half-scale test structure was designed such that the superstructure would respond essentially as a rigid body (the design peak inter-story drift was 0.50%). Thus, treating the superstructure as a rigid mass and performing a simple displacement-based design using only the isolation system properties would be acceptable for practical purposes. However, as the design peak inter-story drift increases, it becomes more important to consider the superstructure flexibility. In such cases, lower performance levels would be expected (e.g., Immediate Occupancy or Life Safety rather than Operational) but might be advantageous in terms of reducing the cost of the isolation system (e.g., by reducing the required bearing displacement capacity).

5. SUMMARY, CONCLUSIONS AND FUTURE WORK

5.1 Summary

Conventionally designed woodframed structures perform well with regard to life safety but suffer significant structural and non-structural damage making them uninhabitable during severe seismic events. Advanced seismic protection systems (e.g., a seismic isolation or damping system) can be employed to effectively protect woodframed buildings during a large seismic event. There are additional challenges in the application of seismic protection systems to woodframed structures as compared to steel and concrete structures. The study presented herein focused on the unique characteristics of woodframed structures that affect the design and implementation of seismic protection

systems and approaches used to increase their performance and their performance reliability in regions of high seismic intensity.

The feasibility of implementing modular damper walls within a full-scale, three-dimensional, woodframed building was demonstrated via Phase 2 benchmark testing. The modular damper walls contained fluid dampers within a wood framing system. Such dampers can readily fit within the dimensional restrictions of a conventional wood shearwall. Thus, the modular damper walls can be constructed off-site and delivered to the job site for "drop-in" installation.

An improved modular damper wall was designed based on experience gained from the benchmark testing, with particular attention given to increasing the damper displacements by employing a toggle-braced damper assembly. The toggle-braced damper assembly was tested within full-scale shearwalls on a seismic shaking table. The performance of the retrofitted walls with the toggle-braced assembly was significantly improved as compared to the conventional walls. The improvement in performance can be attributed to both added stiffness and additional energy dissipation capacity due to the damper assembly (i.e., visco-elastic behavior). The ability of the retrofitted walls to resist repeated seismic excitation without any significant damage was apparent, both from the measured response and from visual inspection of the walls after each test.

Due to a number of factors, including the inherent flexibility in the connections of wood framing systems, engagement of the dampers was limited in both the benchmark structure testing and the shear wall testing (especially in the benchmark testing) and thus the full effectiveness of the dampers was not realized. A detailed evaluation revealed that displacement transmission losses within the woodframed shearwall itself can be on the order of 30 to 40%. Additionally, there will be losses within the damper assembly due to its inherent flexibility. Although there is potential for improvement of the modular damper wall design to minimize the displacement transmission losses, there will always be some losses due to the flexibility of both the woodframing system and the damper framing assembly.

A displacement-based PBSD procedure for design of multi-story woodframed buildings with supplemental linear viscous dampers was presented. The proposed method can be applied to the retrofit of existing structures or to the design of new

structures. The method was applied to the retrofit of the NEESWood Benchmark Structure (with and without interior finish materials) with the final design being evaluated using nonlinear response-history analyses. The results demonstrated that the design inter-story drifts based on selected performance levels were in reasonable agreement with median peak inter-story drifts obtained from the nonlinear response-history analyses, thus validating the proposed displacement-based design procedure.

New displacement-based PBSD procedures for design of multi-story buildings supported on sliding isolation systems were presented. These methods were applied to the design of a half-scale woodframed test structure. The final design was evaluated using results from experimental testing and nonlinear response-history analyses. The results demonstrated that the predicted design inter-story drifts based on the selected operational performance level were in reasonable agreement with the median peak inter-story drifts obtained from nonlinear response-history analyses and the peak inter-story drifts from experimental testing, thus validating the proposed displacement-based design procedures. These practical approaches enable designers to efficiently evaluate various options before making the final selection of isolation system parameters.

5.2 Conclusions

The main conclusions of this study can be summarized as follows:

1) Sliding isolation systems are very effective for protecting lightweight woodframed structures during earthquakes and offer some advantages over energy dissipation systems as they are largely independent of the structural response whereas the energy dissipation provided by dampers is directly related to the displacement and velocity response of the structure (note that a high damping coefficient of the dampers, or a displacement amplification system, is often needed in stiff structures to dissipate significant energy in spite of the low displacement and velocity response of such structures). Additionally, losses in the displacement transmission to the dampers are difficult to control in woodframed structures and thus it is more challenging to achieve the desired performance. On the other hand, sliding isolation systems can be effective in the seismic protection of woodframed structures due to their reliable performance.

However, there may be cases where isolation is not possible or desirable and thus suitably designed energy dissipation systems (i.e., with low displacement transmission losses) may offer a good solution.

2) The implementation of modular damper walls within a full-scale, three-dimensional, woodframed building is feasible but displacement transmission losses to the dampers should be carefully considered in the design of the modular damper walls.
3) Displacement transmission losses can be considered to originate from the structural framing system itself and the damper framing assembly. The losses in the damper framing assembly can be considered to be independent of the type of structural framing system. Compared to steel and concrete structures, in woodframed structures the displacement transmission losses within the woodframed shearwall can be relatively high due to the inherent flexibility of wood framing system and its connections. These additional losses in wood framing systems can be on the order of 30 to 40%. The losses in both the structural framing system and the damper framing assembly should be taken into consideration during the design process via reduction of the ideal displacement amplification factor.
4) The hysteretic energy dissipation demand on the wood framing system can be significantly reduced with implementation of modular damper walls, especially those that employ displacement amplification framing systems. The reduction in hysteretic energy dissipation demand results in reduced structural damage as compared to conventional woodframed structures.
5) The toggle-braced assembly is a promising design for the modular damper walls as the losses in the displacement transmission to the dampers are compensated to some extent by its displacement amplification properties. However, there can be significant amount of losses due to the deformation of the bracing members and these losses should be considered in the design process.
6) The bracing systems within modular damper walls add stiffness to the structural system and thus their visco-elastic behavior should be accounted for during the design process.

7) The proposed displacement-based procedure offers a simplified nonlinear analysis tool for including fluid viscous dampers in woodframed buildings and can be applied in both retrofit applications and the design of new structures. Other types of energy dissipation devices can also be included in the proposed procedure.
8) The proposed displacement-based procedure using the inter-story drift spectra for isolated structures overcomes various problems associated with the conventional DDD procedure while providing a reasonably accurate solution and thus serves as a suitable tool for preliminary analysis of isolated buildings
9) The proposed displacement-based procedures for isolated structures are practical for preliminary design and fulfill the objective of enabling designers to efficiently evaluate various options before making the final selection of isolation system parameters.

5.3 Contributions of Research

The major contributions of this research to the field of structural/earthquake engineering are summarized as follows:

- Development of new PBSD procedures, and integration within existing PBSD procedures, for woodframed structures that incorporate seismic protection systems.
- Development of experimental database for benchmarking future numerical models of woodframed structures with and without seismic protection systems.
- Development of simple and complex numerical models and analysis tools for woodframed structures with and without seismic protection systems.
- Development of new concepts for integrating seismic protection systems within woodframed structure construction.
- An improved understanding of global and local behavior of woodframed structures with and without seismic protection systems.
- Development of systems that provide increased performance reliability for woodframed structures in high seismic regions.

5.4 Recommendations for Future Study

Future research could be directed toward improving the energy dissipation and base isolation systems presented herein. The performance of modular damper walls can be further improved by designing a more effective system in terms of minimizing displacement transmission losses. A numerical (and possibly experimental) parametric study should be carried out to evaluate the optimal damping coefficient for fluid viscous dampers to maximize the energy dissipation for a given woodframed building configuration. The study presented herein focused on fluid viscous dampers but other cost-effective and simple energy dissipation systems could also be evaluated. Although the toggle-braced fluid viscous damper tests showed significant improvement in the performance of the retrofitted shearwalls in the component level testing, the implications for full-scale, three-dimensional buildings are unclear. Thus, their performance should be further verified via testing of a full-scale, three-dimensional woodframed building. This could be done in a shake table laboratory or by retrofitting (or constructing) a woodframed building in an active seismic zone. Another possible improvement that could be explored involves hybrid woodframed construction (e.g., steel and wood) where the modular damper assembly is installed in portions of the woodframed building where displacement transmission losses would be minimized (e.g., portions where steel framing is used rather than wood framing).

The proposed displacement-based design procedure for structures with dampers uses the equivalent stiffness of the shearwall segments derived from the hysteretic parameters of connections (i.e., sheathing-to-framing connectors). There is a need to develop a more comprehensive database from experimental testing of connections to further improve the reliability of the proposed method. The database could include the effect of different finishing materials, different types of wood framing materials, and different environmental and workmanship conditions. Since a poor correlation between experimental and numerical results, especially beyond the peak response, is generally observed for woodframed structures, a comprehensive database will also help to improve numerical predictions such as those obtained with the SAWS program. In addition, there is a need to incorporate the proposed displacement-based procedures in a single comprehensive numerical analysis package (such as the “SAPWood” program developed

within the NEESWood project). A numerical (and possibly experimental) parametric study and testing of a full-scale building with toggle-braced damper walls will also aid in the further validation of the proposed displacement-based design procedures.

The proposed displacement-based design procedures for isolated buildings offer simple and reliable analysis tools. There is a need for a full-scale numerical (and possibly experimental) parametric study to further validate these procedures, including consideration of different sliding isolation systems (e.g., flat sliding bearings combined with elastomeric bearings) with varying isolation system parameters. Other simple and cost-effective isolation systems can also be evaluated. New concepts for stiffening the floor system above the isolation plane could also be explored with emphasis given to reducing the cost of the isolation system.

6. REFERENCES

APA (2007a). "Diaphragms and Shear Walls: Design/Construction Guide," APA-The Engineered Wood Association, Form No. L350A.

APA (2007b). "Engineered Wood Construction Guide," APA-The Engineered Wood Association, Form No. E30U.

ASCE (2006). "Seismic Rehabilitation of Existing Buildings," *ASCE/SEI 41-06*, American Society of Civil Engineers, Reston, VA.

ASCE (2005). "Minimum Design Loads for Buildings and Other Structures," *ASCE/SEI 7-05*, American Society of Civil Engineers, Reston, VA.

ASCE (2000). "Prestandard and Commentary for the Seismic Rehabilitation of Buildings," *Report No. FEMA-356*, Federal Emergency Management Agency, Washington, D.C.

ATC (1996). "Seismic Evaluation and Retrofit of Concrete Buildings," *ATC-40*, Applied Technology Council, Redwood City, CA.

Berton, S. and Bolander, E.B. (2005). "Amplification System for Supplemental Damping Devices in Seismic Applications," *Journal of Structural Engineering*, 131(6), 979-983.

Breyer, D., Fridley, K., Pollock, D. and Cobeen, K. (2006). "Design of Wood Structures-ASD/LRFD," McGraw-Hill Professional, 6th edition, 1025 p.

BSSC (1997). "NEHRP Recommended Provisions for Seismic Regulations for New Buildings and Other Structures," *Report No. FEMA-302*, Federal Emergency Management Agency, Washington, D.C.

Cardone, D., Dolce, M. and Palermo, G. (2008). "Direct Displacement-Based Design of Seismically Isolated Bridges," *Bulletin of Earthquake Eng.*, DOI 10.1007/s10518-008-9069-2.

Christovasilis, I., Filiatrault, A. and Wanitkorkul, A. (2007). "Seismic Testing of a Full-Scale Two-Story Wood Light-Frame Building: NEESWood Benchmark Test," *NEESWood Project Report NW-01*.

Constantinou, M.C., Tsopelas, P., Hammel, W. and Sigaher, A.N. (2001). "Toggle-Brace-Damper Seismic Energy Dissipation Systems." *Journal of Structural Engineering*, 127(2), 105–112.

Dinehart, D.W. and Lewicki, D.E. (2001). "Viscoelastic Material as a Seismic Protection System for Wood-Framed Buildings," *Proc. of 2001 Structures Congress and Exposition*, ASCE, Edited by P.C. Chang, Washington, D.C., May.

Dutil, D.A. and Symans. M.D. (2004). "Experimental Investigation of Seismic Behavior of Light-Framed Wood Shear Walls with Supplemental Energy Dissipation," *13th World Conference on Earthquake Engineering*, Vancouver, B.C., Canada.

Ekiert, C. and Hong, J. (2006). "Framing-to-Sheathing Connection Tests in Support of NEESWood Project," Technical Report, University at Buffalo, Buffalo, NY, 28 p.

Filiatrault, A., Wanitkorkul, A., Christovasilis, I., van de Lindt, J.W., Symans, M.D., Rosowsky, D.V. and Davidson, R. (2007). "Experimental Seismic Performance Evaluation of a Full-Scale Woodframe Building," *Proc. of 2007 ASCE Structures Congress*, Long Beach, CA, May.

Filiatrault, A., Christovasilis, I., Wanitkorkul, A. and Folz, B. (2006). "Displacement-Based Seismic Design of Light-Frame Wood Buildings," *Proceedings of the 9th World Conference on Timber Engineering*, Portland, OR.

Filiatrault, A. and Folz, B. (2002). "Performance-Based Seismic Design of Wood Framed Buildings," *Journal of Structural Engineering*, 128(1), 39–47.

Folz, B. and Filiatrault, A. (2004a). "Seismic Analysis of Woodframe Structures. I: Model Formulation," *Journal of Structural Engineering*, 130(9), 1353-1360.

Folz, B. and Filiatrault, A. (2004b). "Seismic Analysis of Woodframe Structures. II: Model Implementation and Formulation," *Journal of Structural Engineering*, 130(9), 1361-1370.

Folz, B. and Filiatrault, A. (2001). "Cyclic Analysis of Wood Shear Walls," *Journal of Structural Engineering*, 127(4), 433-441.

Huang, C.H. (2004). "Parametric Study for Motion Amplification Device with Viscous Damper," *13th World Conference on Earthquake Engineering*, Vancouver, B.C., Canada.

Hwang, J. S., Huang, Y. N., Hung, Y. H. and Hung, Y. H. (2005). "Analytical and Experimental Study of Toggle-Brace-Damper Systems," *Journal of Structural Engineering*, 131(7), 1035-1043.

ICBO (1997). "Uniform Building Code," International Conference of Building Officials, Whittier, CA.

ICBO (1988). "Uniform Building Code," International Conference of Building Officials, Whittier, CA.

ICC (2006). "International Building Code," International Code Council, Inc., Falls Church, VA.

Isoda H., Folz B. and Filiatrault A. (2001). "Seismic Modeling of Index Woodframe Buildings," *Structural Systems Research Project Report No. SSRP-2001/12*. Department of Structural Engineering, University of California, San Diego, La Jolla, CA.

Kim, J.K. and Choi, H.H. (2006). "Displacement-Based Design of Supplemental Dampers for Seismic Retrofit of a Framed Structure," *Journal of Structural Engineering*, 132(6), 432-439.

Kim, J.K. and Choi, H.H. (2003). "Performance-Based Design of Added Viscous Dampers using Capacity Spectrum Method," *Journal of Earthquake Eng*., 7(1), 1–24.

Kircher, C., Reitherman, R., Whitman, R., and Arnold, C. (1997). "Estimation of Earthquake Losses to Buildings," *Earthquake Spectra*, 13 (4), 703–720.

Krawinkler, H., Parisi, F., Ibarra, L., Ayoub, A. and Medina, R. (2000). "Development of a Testing Protocol for Woodframe Structures," *CUREE Publication No. W-02*, Richmond, CA.

Kubo, T., Hagiwara, I., Fukahori, Y., Hachioji, Harada, I., Yokusaka (1998). "Seismic Isolation Apparatus," U.S. Patent No. 5765322.

Lin, Y. Y., Tsai, M. H., Hwang, J. S. and Chang, K. C. (2003). "Direct Displacement-Based Design for Building with Passive Energy Dissipation Systems," *Eng. Struct*., 25(1), 25–37.

Liu, H., van de Lindt, J.W. and Symans, M.D. (2008). "Performance-Based Evaluation of Base Isolated Light-Frame Wood Structures," *Proc. of Tenth World Conference on Timber Engineering*, Miyazaki, Japan.

Pang, W.C., Rosowsky, D.V, van de Lindt, J.W and Pei, S. (2009). "Simplified Direct Displacement Design of Six-story NEESWood Capstone building and Pre-test Seismic Performance Assessment," *NEESWood Project Report NW-05*.

Pang, W. and Rosowsky, D. (2007). "Direct Displacement Procedure for Performance-Based Seismic Design of Multistory Woodframe Structures," *NEESWood Project Report NW-02*.

Pei, S. and van de Lindt, J.W. (2007). "SAPWood User's Manual," Released with SAPWood Program. http://www.engr.colostate.edu/NEESWood/sapwood.html.

Porter, K.A., Beck, J.L., Seligson, H.A., Scawthorn, C.R., Tobin, L.T., Young, R. and Boyd, T. (2001). "Improving Loss Estimation for Woodframe Buildings," *CUREE Report No. W-18,* Consortium of Universities for Research in Earthquake Engineering (CUREE), Richmond, CA.

Priestley, M.J.N., Calvi, G.M. and Kowalsky, M.J. (2007). "Displacement-Based Seismic Design of Structures," *IUSS Press*, Pavia, Italy, 720 pp.

Priestley, M.J.N. (1998). "Displacement-based Approaches to Rational Limit States Design of New Structures," Keynote Address, *Proceedings of the 11th European Conference on Earthquake Engineering*, Paris, France.

Shinde, J.K., Symans, M.D. and van de Lindt, J.W. (2010). "Displacement-Based Design of Seismically-Isolated Woodframed Structures," *9th US National & 10th Canadian Conference on Earthquake Engineering*, Toronto, to appear July, 2010.

Shinde, J.K. and Symans, M.D. (2010). "Seismic Performance of Light-Framed Wood Structures with Toggle-Braced Fluid Dampers," *Proc. of 2010 ASCE Structures Congress*, Orlando, FL, to appear May, 2010.

Shinde, J.K., Symans, M.D., Pang, W. and Rosowsky, D. (2008a). "Displacement-Based Design of Woodframed Structures with Linear Viscous Fluid Dampers," *Proceedings. of 14WCEE*, Beijing, China, October, 2008.

Shinde, J.K., Symans, M.D., Liu, H. and van de Lindt, J.W. (2008b). "Seismic Performance Assessment of Woodframed Structures with Energy Dissipation Systems," *Proc. of Eighteenth Conf. on Analysis and Computation held in Conjunction with ASCE/SEI Structures Congress 2008*, Vancouver, Canada, April.

Shinde, J.K., Symans, M.D., van de Lindt, J.W. and Filiatrault, A. (2007). "Application of Seismic Protection Systems to Woodframed Buildings: Full-Scale Testing and Field Implementation," *Proc. of 5th Annual NEES Meeting*, Snowbird, Utah, June.

Symans, M.D., Cofer, W.F., Fridley, K.J. and Du, Y. (2004). "Seismic Behavior of Wood-framed Structures with Viscous Fluid Dampers," *Earthquake Spectra*, 20(2), 451-482.

Symans, M.D., Cofer, W.F. and Fridley, K.J. (2002). "Base Isolation and Supplemental Damping Systems for Seismic Protection of Wood Structures: Literature Review," *Earthquake Spectra*, 18(3), 549-572.

Symans, M.D. and Constantinou, M.C. (1998). "Passive Fluid Viscous Damping Systems for Seismic Energy Dissipation," *J. of Earthquake Technology*, 35(4), 185-206.

Twitchell, B.S. and Symans, M.D. (2003). "Analytical Modeling, System Identification and Tracking Performance of Uniaxial Seismic Simulators," Technical Note, *J. of Engineering Mechanics*, ASCE, 129(12).

van de Lindt, J.W. and Liu, H. (2007). "Nonstructural Elements in Performance-Based Seismic Design of Wood Frame Structures," *Journal of Structural Engineering*, 133(3), 432-439.

van de Lindt, J.W., Rosowsky, D.V., Filiatrault, A., Symans, M.D. and Davidson, R.A. (2006). "The NEESWood Project: Progress on the Development of a Performance-Based Seismic Design Philosophy for Mid-Rise Woodframe Construction," *Proc. of 2006 World Conference on Timber Engineering,* Portland, OR.

Wetzel (2006). "Friction Bearing Device to Limit Service Level Damage of Lightweight Structures," Masters Thesis, California Polytechnic State University, San Louis Obispo, CA.

Yamnouchi, H., Midorikawa, M. and Iiba, M. (1998). "Shaking Table Test on Base Isolated House Model," *Proc. of the 30th Joint Meeting of The U.S.-Japan Cooperative Program in Natural Resources: Panel on Wind and Seismic Effects*, NIST SP 931, Gaithersburg, MD.

APPENDIX A

SAWS

Folz and Filiatrault (2004a) developed a software program for nonlinear dynamic analysis of woodframed structures [SAWS - Seismic Analysis of Wood Structures (Folz and Filiatrault 2004a] in which a three-dimensional woodframed building is degenerated to a two-dimensional "pancake" model. The model consists of the lateral load resisting system (shearwalls in both orthogonal directions) that are modeled as zero-height nonlinear hysteretic spring elements and horizontal diaphragms that are assumed to have infinite in-place stiffness, resulting in three degrees-of-freedom per floor. The structure is assumed to be connected to a rigid foundation.

The hysteretic parameter values that are used to develop the SAWS model can be obtained by using the companion analysis program CASHEW (Folz and Filiatrault 2001). In the CASHEW program, the wall geometry, nail spacing, shear stiffness of the sheathing panels, and hysteretic parameters from sheathing-to-connector tests, are used to generate a SDOF hysteretic model for each shear wall. The resulting hysteretic model includes pinched behavior and strength and stiffness degradation. The framing members are assumed to be rigid with pinned-pinned boundary conditions. Figure A.1 shows the hysteretic response of a sheathing-to-framing connector along with a ten-parameter non-linear model used to define it. For a detailed explanation of these parameters, see Folz and Filiatrault (2001). Note that the hysteretic response of a shearwall is similar to that of the sheathing-to-framing connector and the CASHEW program gives output of zero-height nonlinear hysteretic spring elements for a shearwall with a similar ten-parameter hysteresis model. This model (generated for different configurations of shearwalls in the structure) is directly used in the input file of the SAWS program. The analysis can be performed using shearwall hysteretic parameters for wall configurations with exterior and/or interior finish materials. Inherent rate-dependent damping is accounted for via a Rayleigh damping formulation (based on the initial stiffness matrix). Since energy dissipation due to nonlinear hysteretic response (rate-independent damping) is explicitly

considered in the response-history analysis, a damping ratio of 1% is generally assumed in the first and second modes to account for rate-dependent damping effects.

Modifications to the SAWS program were made to allow for the inclusion of the dampers as a pure viscous element (both linear and non-linear type). In the SAWS model, the viscous damper element is oriented horizontally with its deformation being equal to the difference in horizontal displacement of the top and bottom of the wall. Thus, for analysis of other damper configurations (e.g., a toggle-braced damper), an equivalent damping coefficient must be utilized for the horizontal damper in the SAWS model. Similarly, in the post-processing of the analysis results, the output from the SAWS analysis (displacement and force between the upper and lower nodes of the horizontal viscous damper element) must be modified to obtain the corresponding force and displacement for the actual damper configuration.

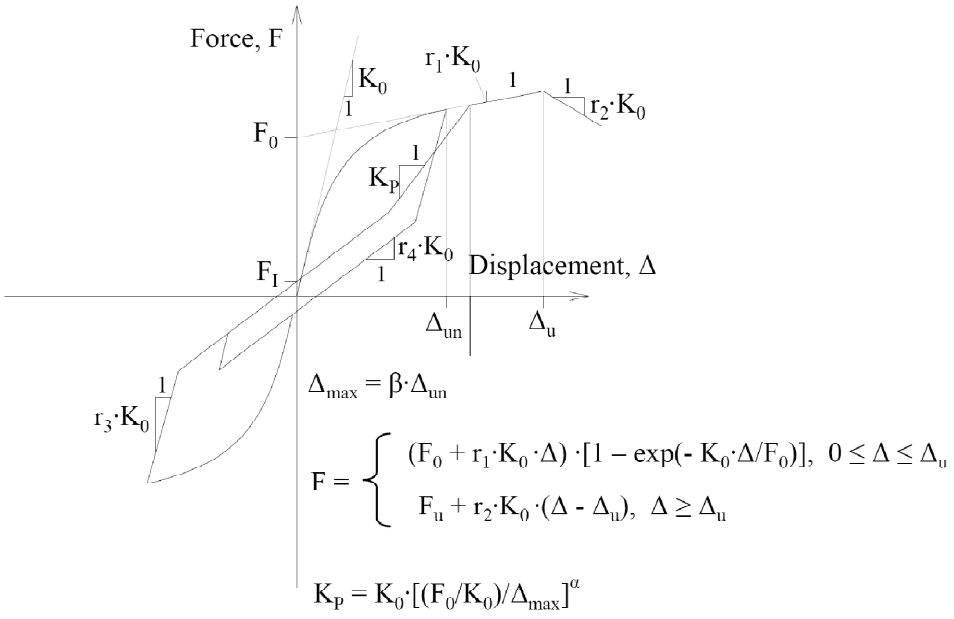

Figure A.1 Hysteretic Response of a Sheathing-to-framing Connector (Adapted from Christovasilis et al. 2007)

A.1 SAWS Analysis Input File Example

```
RPI Toggle-braced Damper Test (Units: kips,in)
2                   ! Nonlinear dynamic analysis
1                   ! Number of diaphragms
1 4 0.0341 106      ! Floor # 1, no. of pts needed to define geometry,
                    ! mass & elevation
0 0                 ! A1 Floor # 1 coordinates
44 0                ! A2
44 96               ! A3
0 96                ! A4
0                   ! Number of discrete masses
0                   ! Number of walls parallel to x-axis
2                   ! Number of walls parallel to y-axis
0     0     1       ! Shear Wall-Y1 (X intercept and connectivity)
2.47  0.338 2.198   ! Ten-parameter hysteretic model from CASHEW
10.00 0.0383      -0.0491     1.0   0.0149
0.6857      1.25

44    0     1       ! Shear Wall-Y2 (X intercept and connectivity)
2.47  0.338 2.198   ! Ten-parameter hysteretic model from CASHEW
10.00 0.0383      -0.0491     1.0   0.0149
0.6857      1.25
0                   ! Number of viscous elements parallel to x-axis
2                   ! Number of viscous elements parallel to y-axis
0 0 1               ! Viscous element 1 (X intercept and connectivity)
0.095 1             ! Damping and velocity coefficient for element 1
44 0 1              ! Viscous element 2 (X intercept and connectivity)
0.095 1             ! Damping and velocity coefficient for element 2
1 0.01 2 0.01       ! Mode no. and corresponding damping ratio
0.001 5 31155 5 6232 0 1 2      ! EQ parameters: DELTA, INTER, NSTEP,
                                ! TOLER, NPDATA, ISCALE, ACCMAX, IEQXY
0     0                         ! Earthquake acceleration data starts
0.005 -3.9485E-05
```

Appendix B

PHASE 2 BENCHMARK TESTING

B.1 Earthquake Motions

Figure B.1 shows the acceleration time histories and absolute acceleration response spectra [true (not pseudo) acceleration] for the east-west component (i.e., the longitudinal X-direction) of the ordinary ground motion [Canoga Park (unscaled)] and near-field ground motion (Rinaldi) used in the Phase 2 benchmark testing. The data in Figure B.1 is for the field recorded motions, not the shake table motions. Also, these motions are the weaker of the two orthogonal components for each ground motion (the stronger north-south components were applied in the transverse Y-direction).

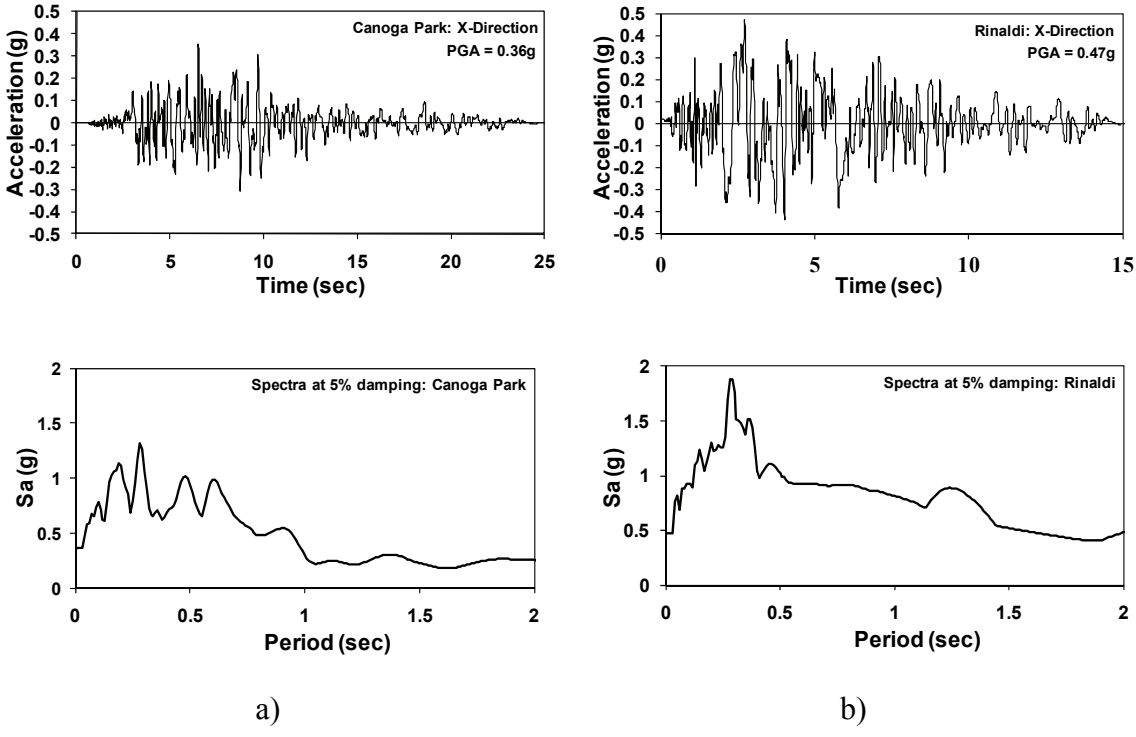

a) b)

Figure B.1 Acceleration Time Histories and Absolute Acceleration Response Spectra for Earthquake Ground Motions in X- direction: (a) Canoga Park (b) Rinaldi Motion

B.2 Shake Table Fidelity

Shake table fidelity can be investigated via comparison of time history response and response spectra of field motion and recorded shaking table motion. A68 and A71 are the acceleration sensors in the X-direction located at the center of the west and east shake table extension frame, respectively. Figure B.2a and B.2b shows the acceleration time history comparison of the field motions and west shake table motion (A68 sensor) for NWP2S14 (Level 4) and NWP2S16 (Level 5) seismic tests, respectively (note that the time lag in the recorded shake table motions was adjusted to approximately match the field motions). Figure B2 also shows the 5%-damped response spectra [true (not pseudo) acceleration] up to a period of two seconds for the same seismic tests. Note that Level 4 (i.e., 1.2 times Canoga Park) and Level 5 excitation was applied in the longitudinal direction of the benchmark structure for the phase 2 testing. From the time-history comparisons, it is evident that the shaking table was capable of reproducing the dominant features of the ground motion. On the other hand, the response spectra comparisons indicate that, for the Level 4 Canoga Park record, the shake table motion will tend to amplify the acceleration response of the test specimen (natural periods of wood structures are relatively low) whereas, for the Level 5 Rinaldi record, the shake table motion may amplify or deamplify the acceleration response. For the Phase 2 benchmark structure, the first three modes had natural periods that ranged from about 0.2 to 0.3 sec, putting it in a range of natural periods where amplification or deamplification of the acceleration response can not be definitively stated prior to the tests.

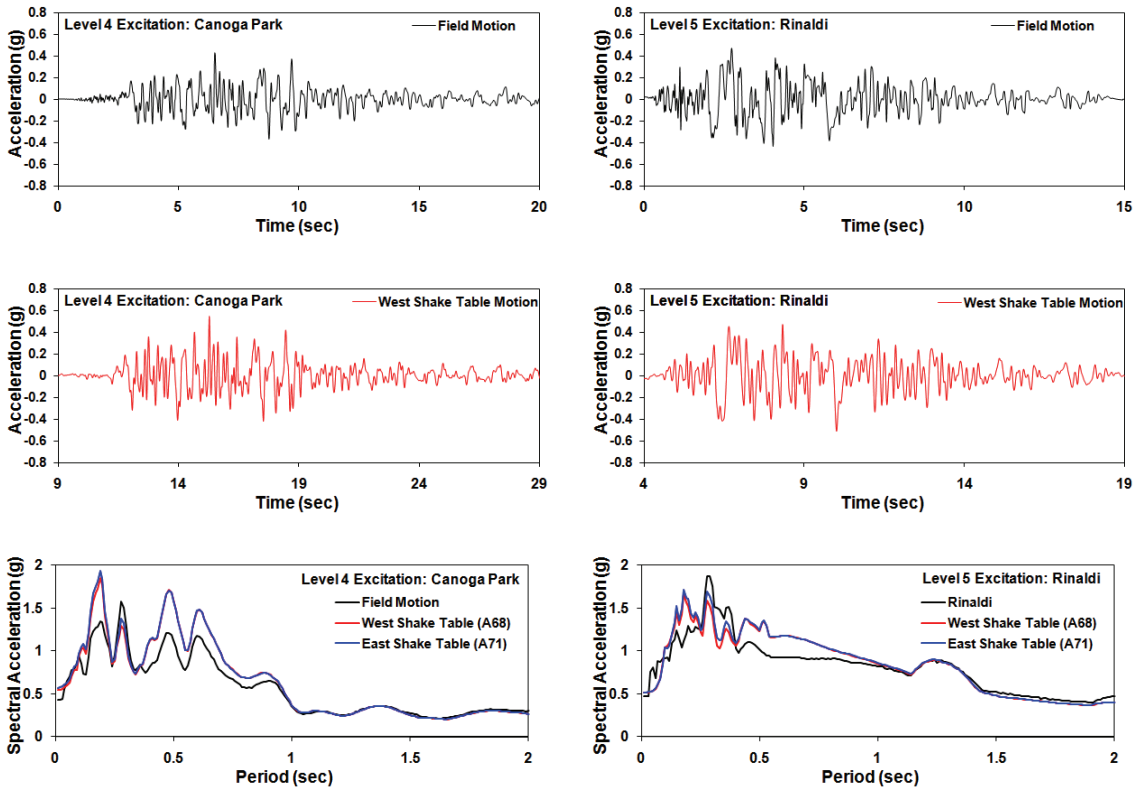

(a) (b)

Figure B.2 Comparison of Field and Shake Table Motion via Acceleration Time History and Response Spectra: (a) Level 4 and (b) Level 5 Excitation

B.3 Description of Fluid Damper

Fluid viscous dampers are one of many alternatives for dissipating energy in structures. A key feature of this type of damper is its high energy dissipation density (i.e., its ability to dissipate significant amounts of energy in comparison to its physical size). Due to its compact size, it can be easily accommodated within the confines of a woodframed shearwall and thus results in a compact, portable, and thus economical, modular damper wall. The damper consists of two major parts, a cylinder filled with a low viscosity silicone fluid and a piston rod that includes a piston head (cylinder) containing orifices (see Figure B.3). Energy is dissipated as the piston head strokes through the fluid-filled chamber, resulting in differential pressure that causes the silicone fluid to pass through the orifices at high speed.

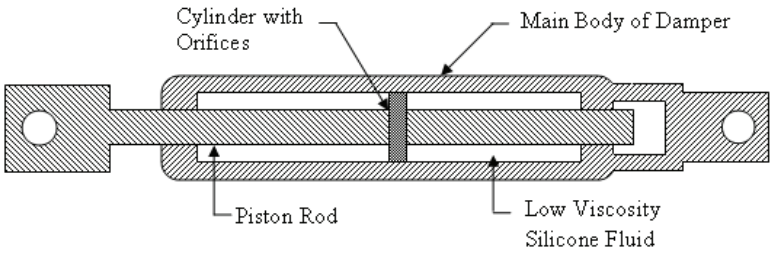

Figure B.3 Cross-Section of Fluid Viscous Damper

B.4 Instrumentation

Table B.1 summarizes the types of sensors (230 in all) that were used to monitor the response of the benchmark test structure during the Phase 2 testing. A detailed description of the sensors and their locations are available in Christovasilis et al. (2007). Accelerometers were used to record the shake table, floor, and roof absolute acceleration at several locations in the benchmark test structure. String potentiometers were used to measure the absolute horizontal displacement at the shake table level and along the North and West walls on each floor level. Thus, the relative displacement of the benchmark test structure with respect to the shake table was obtained by subtracting the shake table displacement from the floor displacements. String potentiometers were also used to measure shear deformations of selected walls in each story. Additionally, uplift and sliding of the sill plate was monitored at several locations using displacement transducers. All anchor bolts along the perimeter of the base of the structure were instrumented with load cells to obtain the distribution of anchor bolt forces. Displacement transducers and load cells were used to measure the stroke and force in each damper.

Table B.1 Sensors used for Benchmark Structure Seismic Tests

Type of sensors	**Qty.**
Accelerometers	71
String potentiometers	38
Displacement transducers	62
Displacement transducers for dampers	4 (or 6)
Load cells for dampers	4
Load cells (for anchor bolts)	50

B.5 Benchmark Results Summary

Table B.2 summarizes the peak response quantities for the Phase 1 and Phase 2 benchmark testing (i.e., without damper and with dampers, respectively). Note that the peak drifts were small [largest corresponds approximately to the Immediate Occupancy performance level (1%)]. The peak drifts are consistently reduced whereas other response quantities (the peak base shear and peak overturning moment) were not consistently increased or decreased. However, the peak acceleration was generally reduced. The base shear was calculated by adding the forces obtained by multiplying the accelerations at each floor of the superstructure (i.e., second floor and roof) by the corresponding portion of the mass assigned to them. The overturning moment was obtained by summing the moments of these forces about the base of the structure. The peak inter-story drifts and accelerations (absolute and in a horizontal direction) represent the maximum values of these quantities throughout the structure. Note that, since uniaxial excitation along the longitudinal direction (N-S direction) was applied during these tests, the North and South walls (Line D or Line A, respectively) produced the maximum response.

Table B.2 Summary of Peak Responses With & Without Dampers

Global Test #	Test ID	Level	Global Peak Drifts (%)	Peak Base Shear (kips)	Overturning Moment (kip-ft)	Peak Acceleration (g)
Without dampers						
1.1	NWP1S03	1	0.061	6.50	95.81	0.111
1.2	NWP1S07	2	0.237	19.02	263.55	0.315
1.3	NWP1S10	3	0.602	32.70	450.38	0.602
2.23	NWP2S29	4	0.865	51.84	735.50	0.952
2.24	NWP2S30	5	1.026	58.77	854.52	1.046
With dampers						
2.12	NWP2S08	1	0.052	5.05	74.53	0.087
2.14	NWP2S10	2	0.218	20.22	282.62	0.357
2.16	NWP2S12	3	0.441	33.36	468.31	0.585
2.18	NWP2S14	4	0.714	48.03	665.89	0.838
2.20	NWP2S16	5	0.996	60.07	850.50	1.045

B.6 Verification of Diaphragm Rigidity

In the numerical simulations using SAWS, in-plane rigidity of diaphragms is assumed. To verify the diaphragm rigidity, the rotational response was obtained by dividing the

difference in response values of sensors (i.e., acceleration and displacement sensors) located at the corners of the North and West walls by the corresponding length of the walls. Figure B.4 and B.5 show the rotational response for the Level 4 test with dampers (NWP2S14) obtained from acceleration and displacement data, respectively. As expected, the roof rotational response is larger than that of the second floor.

Note that the angular acceleration and rotation as measured by response at the North and West walls is similar in terms of frequency content and amplitudes (particularly the peak amplitudes). This suggests that the relative rotation at the floor diaphragm corners is negligible and thus, due to the relatively short transverse direction, any in-plane diaphragm deformations due to longitudinal excitation would be relatively small. Thus, the rigid diaphragm assumption that is used in the numerical simulations (SAWS program) is reasonable.

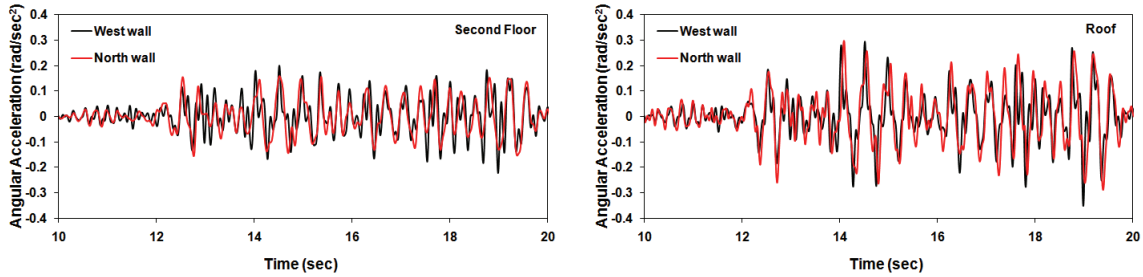

(a) **(b)**

Figure B.4 Comparison of Rotational Response from Acceleration Data: (a) Second Floor and (b) Roof

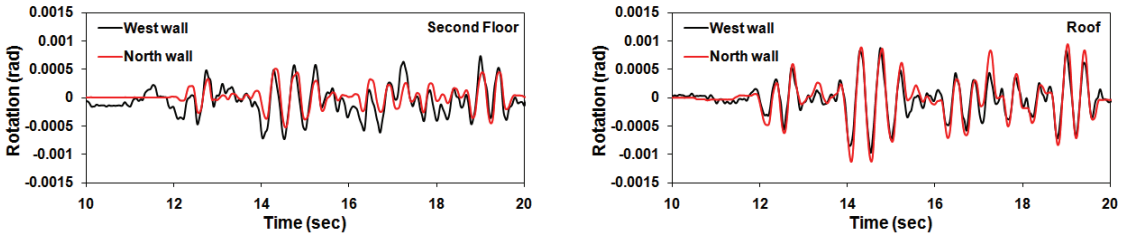

(a) **(b)**

Figure B.5 Comparison of Rotational Response from Displacement Data: (a) Second Floor and (b) Roof

B.7 Torsional Response

The torsional response was evaluated by comparing the displacements at each floor level in the EW and NS directions from the Level 4 test with dampers (NWP2S14) (see Figure B.6). In this Figure, sensors D8, D9, D15 and D16 are the EW direction horizontal displacement sensors located at the corners of the West wall. Also, sensors D10, D13, D17 and D20 are the NS direction horizontal displacement sensors located at the corners of the North wall. Note that the torsional response appears to be minor since the displacements at the corners of the West wall are nearly equal. The displacements at the corners of the North wall are out-of-phase but the motion in that direction is relatively small, again suggesting that the torsional response was minor. Thus, although the structure was asymmetric, primarily with respect to the longitudinal axis, minimal torsional response occurred. This can also be seen in Figure B.5 where the maximum rotation of the North and West Walls was about 0.001 rad (0.06 degrees). The small torsional response is expected since the center of mass and center of rigidity are quite close (about 6 in. apart).

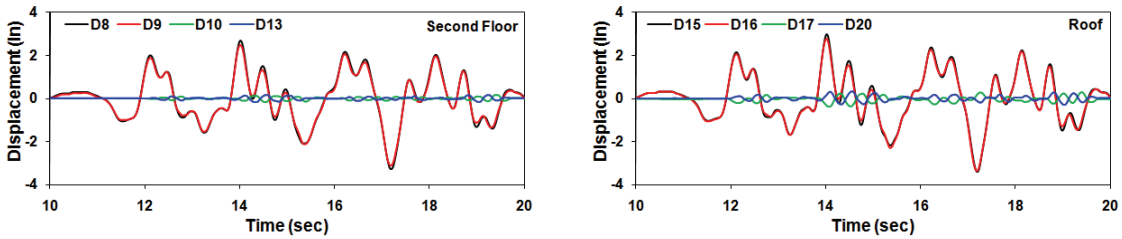

(a) (b)

Figure B.6 Displacement Time Histories for (a) Second Floor (b) Roof

Appendix C

DISPLACEMENT-BASED DESIGN WITH FLUID VISCOUS DAMPERS

C.1 Development of Shearwall Design Table via Equivalent Stiffness Estimation from Shearwall Backbone Curve

The backbone curve parameters used in the proposed displacement-based procedure (Pang and Rosowsky 2007) are defined by following five-parameter nonlinear equation (also see Figure C.1):

$$F_b(\delta) = \left[1 - e^{-\frac{K_0}{F_0}\delta}\right]\left(r_1 K_0 \delta + F_0\right) \quad \text{for} \quad \delta \le \delta_u$$
$$F_b(\delta) = F_u + r_2 K_0 \left(\delta - \delta_u\right) \quad \text{for} \quad \delta > \delta_u \tag{C.1}$$

For a detailed explanation of these parameters, see Pang and Rosowsky (2007). Note that, to reduce the complexity of the numerical model used in the DBD procedure, the five-parameter model defined above is used instead of the ten-parameter model used in the CASHEW program (which defines the full cyclic hysteretic behavior of a wood shearwall). An equivalent stiffness, k_{eq}, is defined such that the energy stored in an actual nonlinear wood shearwall at a design (target) displacement, δ_t, is equal to that of an equivalent linear system (see Figure C.1). Estimation of equivalent viscous damping is not needed as the hysteretic energy dissipation (displacement-dependent energy dissipation) at the design displacement δ_t is used to define the equivalent stiffness associated with non-linear behavior.

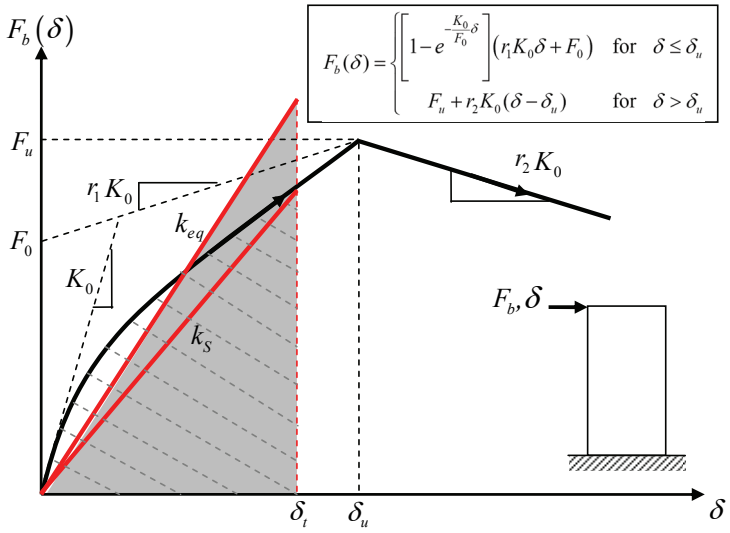

Figure C.1 Shearwall Backbone Curve with Concept of Equivalent Linearization

Backbone parameters for 8 ft high walls with studs spaced at 16 in on-center and OSB attached using 8d common nails is shown in Table C.1 for Phase 1 (OSB only) and Phase 4 (OSB and GWB). The table contains the values of parameters that define the backbone curve for walls constructed with various nailing patterns and panel widths. The CASHEW program (Folz and Filiatrault 2001), along with available shearwall test data from the benchmark test, was used to generate the design table. Table C.2a and C.2b shows the shearwall design table for the same parameters which include the actual equivalent stiffness of shearwall segments.

Table C.1 Backbone Parameters for 8ft High Walls with 16 in Stud Spacing and OSB Attached Using 8d Common Nails

Sheathing (Phase)	Panel Width (ft)	Nail Spacing (in) ext./int.	Panel ID	Backbone Parameters					
				K_0 (kips/in)	r_1	r_2	δ_v(in)	F_0 (kip)	F_u (kip)
OSB (Phase 1)	2.5	2/12	s1	7.65	0.040	-0.083	4.09	4.25	5.51
		3/12	s2	6.40	0.038	-0.070	3.94	2.92	3.89
		4/12	s3	5.42	0.037	-0.062	3.82	2.23	2.99
		6/12	s4	4.17	0.035	-0.055	3.70	1.51	2.05
	3	2/12	s5	9.88	0.042	-0.096	3.58	5.53	7.01
		3/12	s6	8.17	0.042	-0.075	3.35	3.62	4.77
		4/12	s7	6.91	0.041	-0.066	3.27	2.72	3.64
		6/12	s8	5.37	0.039	-0.055	3.15	1.84	2.50
	4	2/12	s9	14.33	0.037	-0.126	2.91	8.34	9.82
		3/12	s10	12.45	0.042	-0.099	2.76	5.58	7.01
		4/12	s11	10.91	0.043	-0.083	2.64	4.20	5.42
		6/12	s12	8.85	0.042	-0.070	2.52	2.90	3.84
OSB & GWB (Phase 4)	2.5	2/12	s13	8.57	0.025	-0.075	4.09	4.65	5.51
		3/12	s14	7.37	0.021	-0.061	3.86	3.33	3.91
		4/12	s15	6.45	0.017	-0.053	3.74	2.63	3.01
		6/12	s16	5.25	0.011	-0.047	3.58	1.91	2.11
	3	2/12	s17	11.42	0.026	-0.084	3.58	6.07	7.10
		3/12	s18	9.88	0.022	-0.064	3.35	4.18	4.90
		4/12	s19	8.68	0.018	-0.054	3.19	3.28	3.78
		6/12	s20	7.19	0.012	-0.044	3.03	2.41	2.65
	4	2/12	s21	16.67	0.023	-0.110	2.95	8.84	9.94
		3/12	s22	15.07	0.021	-0.084	2.76	6.27	7.13
		4/12	s23	13.70	0.017	-0.069	2.64	4.95	5.58
		6/12	s24	11.82	0.012	-0.053	2.48	3.66	4.00

Table C.2a Shearwall Design Table for 8 ft High Walls with Studs Spaced at 16 in On-Center and OSB Attached Using 8d Common Nails

Sheathing (Phase)	Panel Width (ft)	Nail Spacing (in) ext./int.	Panel ID	Equivalent Stiffness k_{eq} (kips/in) at Target Drift Drift (% of Wall Height)							
				0.25	**0.50**	**0.75**	**1.00**	**1.25**	**1.50**	**1.75**	**2.00**
OSB (Phase 1)	2.5	2/12	s1	6.73	5.98	5.36	4.84	4.40	4.04	3.72	3.45
		3/12	s2	5.48	4.76	4.18	3.72	3.34	3.03	2.77	2.55
		4/12	s3	4.57	3.91	3.40	3.00	2.67	2.41	2.19	2.01
		6/12	s4	3.43	2.89	2.48	2.16	1.91	1.71	1.55	1.41
	3	2/12	s5	8.71	7.75	6.95	6.28	5.72	5.25	4.84	4.49
		3/12	s6	6.98	6.04	5.30	4.71	4.23	3.83	3.50	3.22
		4/12	s7	5.79	4.94	4.28	3.76	3.35	3.02	2.74	2.52
		6/12	s8	4.38	3.66	3.13	2.72	2.40	2.14	1.94	1.77
	4	2/12	s9	12.67	11.30	10.16	9.20	8.39	7.70	7.11	6.60
		3/12	s10	10.65	9.24	8.12	7.21	6.48	5.87	5.37	4.94
		4/12	s11	9.11	7.75	6.71	5.89	5.24	4.72	4.29	3.94
		6/12	s12	7.17	5.96	5.07	4.39	3.87	3.46	3.13	2.86
OSB & GWB (Phase 4)	2.5	2/12	s13	7.49	6.61	5.89	5.29	4.79	4.37	4.01	3.70
		3/12	s14	6.27	5.40	4.72	4.17	3.73	3.36	3.06	2.80
		4/12	s15	5.38	4.58	3.95	3.46	3.06	2.74	2.48	2.26
		6/12	s16	4.28	3.57	3.04	2.62	2.30	2.05	1.84	1.67
	3	2/12	s17	9.95	8.77	7.80	6.99	6.32	5.76	5.28	4.88
		3/12	s18	8.32	7.11	6.17	5.43	4.83	4.34	3.94	3.60
		4/12	s19	7.15	6.01	5.15	4.48	3.95	3.52	3.18	2.89
		6/12	s20	5.77	4.75	4.00	3.44	3.00	2.66	2.38	2.15
	4	2/12	s21	14.51	12.77	11.34	10.16	9.18	8.36	7.66	7.07
		3/12	s22	12.64	10.79	9.34	8.20	7.29	6.54	5.93	5.42
		4/12	s23	11.19	9.34	7.95	6.89	6.05	5.39	4.85	4.41
		6/12	s24	9.33	7.59	6.33	5.39	4.68	4.13	3.69	3.33

Table C.2b Shearwall Design Table for 8 ft High Walls with Studs Spaced at 16 in On-Center and OSB Attached Using 8d Common Nails (continuation of Table C.2)

Sheathing (Phase)	Panel Width (ft)	Nail Spacing (in) ext./int.	Panel ID	Equivalent Stiffness k_{eq} (kips/in) at Target Drift							
				Drift (% of Wall Height)							
				2.25	**2.50**	**2.75**	**3.00**	**3.25**	**3.50**	**3.75**	**4.00**
OSB (Phase 1)	2.5	2/12	s1	3.21	3.00	2.83	2.67	2.53	2.40	2.29	2.19
		3/12	s2	2.36	2.20	2.06	1.94	1.83	1.74	1.65	1.58
		4/12	s3	1.86	1.73	1.62	1.52	1.43	1.36	1.29	1.23
		6/12	s4	1.30	1.21	1.13	1.06	1.00	0.94	0.90	0.86
	3	2/12	s5	4.19	3.92	3.69	3.48	3.30	3.14	2.99	2.85
		3/12	s6	2.99	2.78	2.61	2.45	2.32	2.20	2.09	1.99
		4/12	s7	2.33	2.16	2.02	1.90	1.80	1.70	1.62	1.53
		6/12	s8	1.63	1.52	1.42	1.33	1.25	1.19	1.12	1.06
	4	2/12	s9	6.15	5.76	5.42	5.12	4.84	4.56	4.30	4.05
		3/12	s10	4.58	4.27	4.00	3.77	3.54	3.33	3.12	2.94
		4/12	s11	3.64	3.39	3.17	2.97	2.78	2.61	2.44	2.29
		6/12	s12	2.63	2.44	2.28	2.13	1.99	1.86	1.74	1.63
OSB & GWB (Phase 4)	2.5	2/12	s13	3.43	3.20	3.00	2.82	2.67	2.53	2.40	2.29
		3/12	s14	2.59	2.40	2.24	2.10	1.97	1.86	1.77	1.68
		4/12	s15	2.08	1.92	1.79	1.67	1.57	1.48	1.40	1.33
		6/12	s16	1.53	1.41	1.30	1.21	1.14	1.07	1.01	0.96
	3	2/12	s17	4.53	4.22	3.95	3.72	3.51	3.32	3.16	3.00
		3/12	s18	3.32	3.08	2.87	2.68	2.53	2.39	2.26	2.14
		4/12	s19	2.65	2.45	2.28	2.13	2.00	1.88	1.78	1.68
		6/12	s20	1.97	1.81	1.68	1.56	1.46	1.37	1.29	1.21
	4	2/12	s21	6.55	6.10	5.71	5.37	5.06	4.76	4.48	4.22
		3/12	s22	4.99	4.62	4.30	4.03	3.77	3.53	3.30	3.09
		4/12	s23	4.04	3.73	3.46	3.22	3.01	2.81	2.62	2.45
		6/12	s24	3.04	2.79	2.58	2.39	2.22	2.06	1.92	1.79

Appendix D

TESTING OF WOOD SHEARWALLS WITH TOGGLE-BRACED DAMPER

D.1 Code-Based Design of Conventional Shearwalls

Seismic load calculations according to ASCE/SEI-7 (2005):

Assume two story residential building: h_n = 16 ft

Approximate natural period of building: $T = C_t h_n^x$ = 0.020 (16)$^{0.75}$ = 0.16 sec

Maximum spectral accelerations for a site in California:

S_S = Mapped short-period spectral acceleration = 1.5g

S_1 = Mapped one-second spectral acceleration = 0.75g

(Note: Above values are taken from Ch. 2 (Section 2.14) of "Design of Wood Structures" by Breyer et al. (2007))

Site class: D

Site coefficients: F_a = 1.0, F_v = 1.5 (from Table 11.4.1 and 11.4.2, respectively)

Maximum considered earthquake (MCE) spectral response acceleration for short-period:

$S_{MS} = F_a S_S$ = 1.5g

Maximum considered earthquake (MCE) spectral response acceleration for one-second period:

$S_{M1} = F_v S_1$ = 1.125g

Short-period design spectral response acceleration: $S_{DS} = \frac{2}{3} S_{MS}$ = 1.0g

One-second design spectral response acceleration: $S_{D1} = \frac{2}{3} S_{M1} = 0.75\text{g}$

Controlling periods: $T_s = \frac{S_{D1}}{S_{DS}} = 0.75\,\text{sec}$, $T_o = 0.2T_s = 0.15\,\text{sec}$

Design spectral acceleration at zero period: $S_a = 0.4S_{DS} = 0.4(1.0) = 0.4g$

Design response spectrum for considered site:

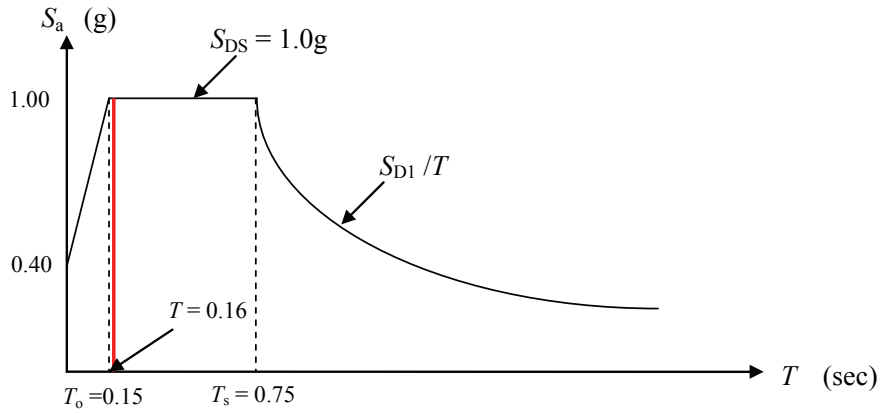

Figure D.1 ASCE/SEI-7 Design Response Spectrum for a California Site

Response modification factor: R = 6.0 (wood bearing wall structure with structural panels rated for shear)

(Note: R = 6.0 was used (instead of R = 6.5 specified in ASCE/SEI-7) since non-structural finish materials were not included in the test specimens whereas they would be present in a complete structural system)

Importance factor: I = 1.0

Superimposed load (weight) on each wall = 825 plf

Combined superimposed load on both walls = 2 x 8 x 825 = 13200 lbs =13.20 kips

Estimated weight of wall = 20 psf (Breyer et al. 2007)

Combined weight of both walls = 2 x 8 x 4 x 20 = 1280 lbs = 1.28 kips
(Note: 8 ft walls are sheathed only over 4 ft center portion)

Total weight on both walls: W = 14.48 kips

Seismic response coefficient (for short period structures):

$$C_S = \frac{S_{DS}}{R/I} = \frac{1.0}{6.0/1.0} = 0.166 \text{ g}$$

Base shear: $V = C_S W$ = 0.166 x 14.48 = 2.40 kips

Base shear on each 4 ft wall segment: v = 2.40/(2*4) = 0.3 k/ft = 300 plf

Shear Force Demand (ASD Level):

The seismic force demand calculated in accordance with ASCE/SEI-7 is at a strength (LRFD level) while IBC Table 2306.4 (IBC 2006) specifies resistance in terms of allowable shear in the wall (ASD level).

Shear demand on wall (ASD): v = (1/1.4) x 300 = 214 plf
(Note: Factor of (1/1.4) used to convert from LRFD to ASD shear demand (i.e. from LRFD level according to APA shear wall design guide (APA 2007a))

Shear Force Capacity (ASD Level):
In accordance with IBC Table 2306.4.1 (IBC 2006), the allowable shears (ASD level) are provided in Table D.1 for different wall configurations with 6 in edge spacing and 12 in field spacing.
(Note: The allowable shears given in Table D.1 are for APA panel shear walls with framing of douglas-fir, larch, or southern pine. The values are reduced by the specific

gravity adjustment factor [1 - (0.5 - SG)] for spruce-pine-fir (SG = 0.42) which gives an adjustment factor of 0.92).

Table D.1 Allowable Shear for Different Wall Specifications

Wall specifications	ASD capacity (plf)
5/16" or ¼" thk OSB, 6d	165.6
3/8" thk OSB, 6d	184.0
3/8" thk OSB, 8d	202.4
7/16" thk OSB, 8d	220.8
15/32" thk OSB, 8d	239.2

Note:

In Table D.1, the allowable shears for 3/8 in and 7/16 in thk OSB are permitted to be increased to the value shown for 15/32 in thk OSB sheathing (for the same nailing schedule) when: (1) studs are spaced a maximum of 16 inch on center or (2) panels are applied with long dimension across studs. Although the first condition is satisfied herein, the permitted increase was not considered in the design of the walls to ensure a conservative design. Also, the APA wood construction guide (APA 2007b) mentions that greater stiffness is required for wall sheathing when stucco (which is commonly used as a finish material in California) is to be applied and recommends a minimum 7/16" thk OSB for 16 in stud spacing with vertical panel orientation. Hence, 7/16" thk OSB with 8d nails and 6/12 spacing was selected (ASD capacity = 220.8 plf > ASD demand = 214 plf).

D.2 Code-Based Design of Retrofitted Shearwalls

Section 11.4.7 of ASCE/SEI-7 (2005) specifies that for seismically isolated structures and for structures with damping systems on sites with S_1 greater than or equal to 0.6g, a ground motion hazard analysis shall be performed in accordance with Section 21.2.

For the assumed location in California:

S_S = Mapped short-period spectral acceleration = 1.5g

S_1 = Mapped one-second spectral acceleration = 0.75g

Site class: D

Site coefficients: $F_a = 1.0$, $F_v = 1.5$

$S_{MS} = F_a S_S = 1.5\text{g}$, $S_{M1} = F_v S_1 = 1.125\text{g}$

(Note: For $S_S \geq 1.25g$ and $S_1 \geq 0.50g$, the values of F_a and F_v obtained from Table 11.4.1 and 11.4.2, respectively, get capped to above mentioned values.)

Section 21.2.2 provides the following response spectra as a lower limit on the deterministic MCE ground motion response spectrum.

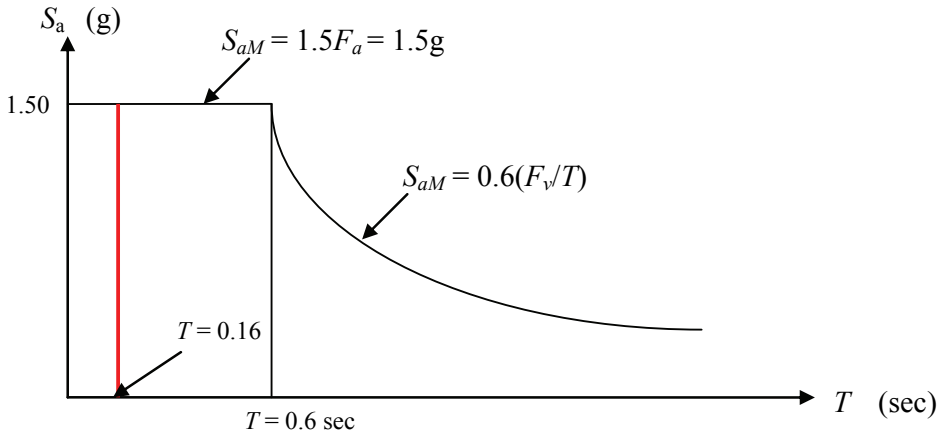

Figure D.2 ASCE/SEI-7 Deterministic Lower Limit on MCE Response Spectra

where S_{aM} = site-specific MCE spectral response acceleration at any period.

The design spectral response acceleration at any period is obtained as follows:

$$S_a = \frac{2}{3} S_{aM}$$

Short-period design spectral response acceleration: $S_{DS} = \frac{2}{3} S_{aM} = 1.0\text{g}$

One-second design spectral response acceleration:

$$S_{D1} = \frac{2}{3} S_{aM} = \frac{2}{3}\left(\frac{0.6 \times 1.5}{1} g \right) = \frac{2}{3}(0.9g) = 0.6\text{g}$$

The above values should not be less than 80 percent of S_a determined in accordance with Section 11.4.5 (i.e., design of conventional wall). Thus,

$$(S_{DS})_{min} = 0.8\left(\frac{2}{3} S_{MS} \right) = 0.8g$$

$$(S_{D1})_{min} = 0.8\left(\frac{2}{3} S_{M1} \right) = 0.6g = 0.6\text{g}$$

Hence, final values of design spectral response acceleration for retrofitted wall are:

$$S_{DS} = 1.0\text{g}$$

$$S_{D1} = 0.6\text{g}$$

Base shear:

Calculations for base shear are identical to those for the conventional walls (i.e., $C_S = 0.166\,\text{g}$) since the design spectral response acceleration is the same (1.0g) and the R-factor is the same (i.e., the basic structural framing is of the same form – light-framed walls with wood sheathing). The reduction in base shear that is permitted (but not required) in Section 18.2-1 of ASCE/SEI-7 was not considered since the focus of this study is on the effectiveness of the damping system when incorporated within a nominally conventional wall design. Thus, the retrofitted wall design was nominally the same as the conventional wall design (7/16" thk OSB with 8d nails and 6/12 spacing) but with some modification to accommodate the toggle-braced framing system.

D.3 Working Drawings of Test Setup

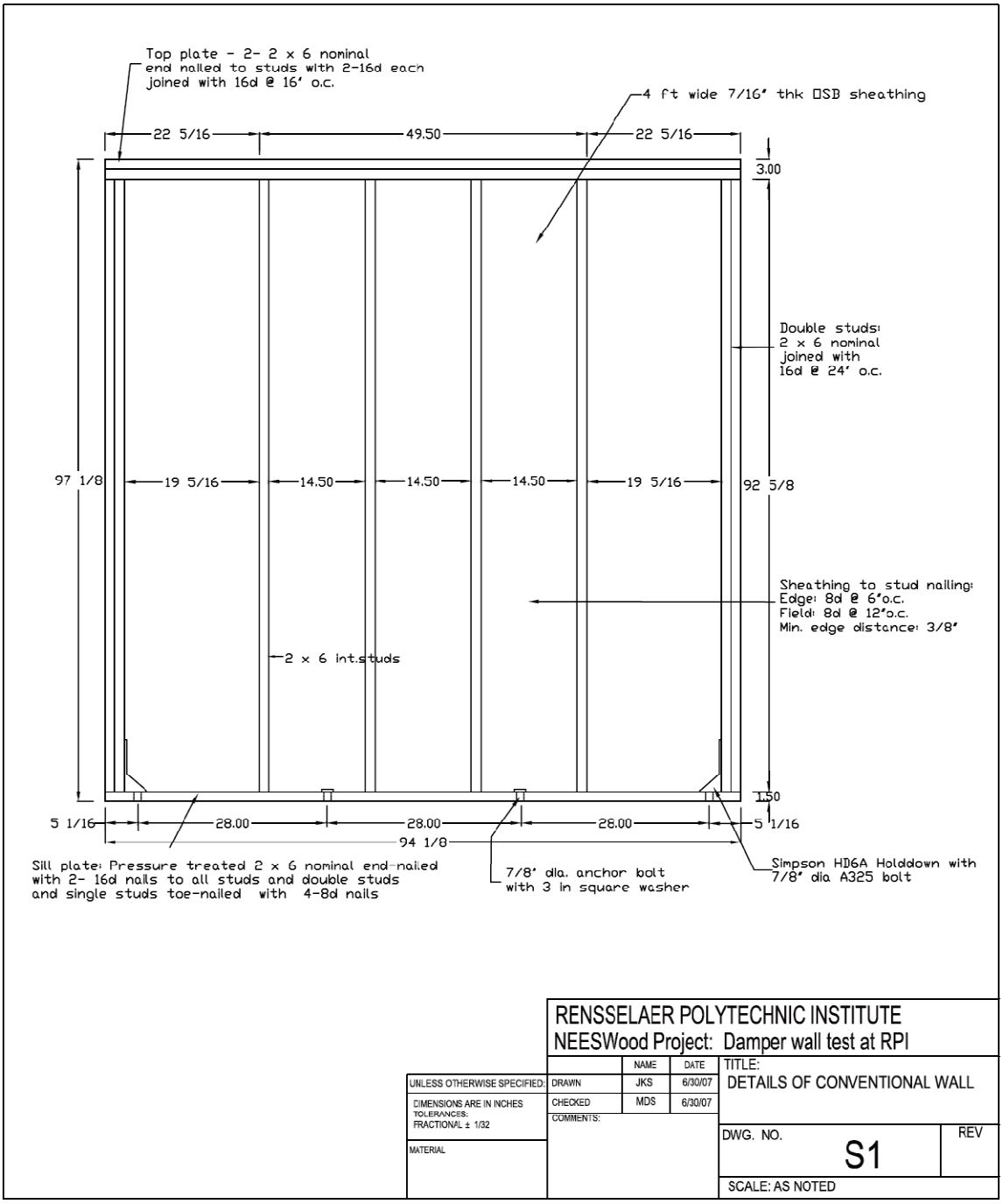

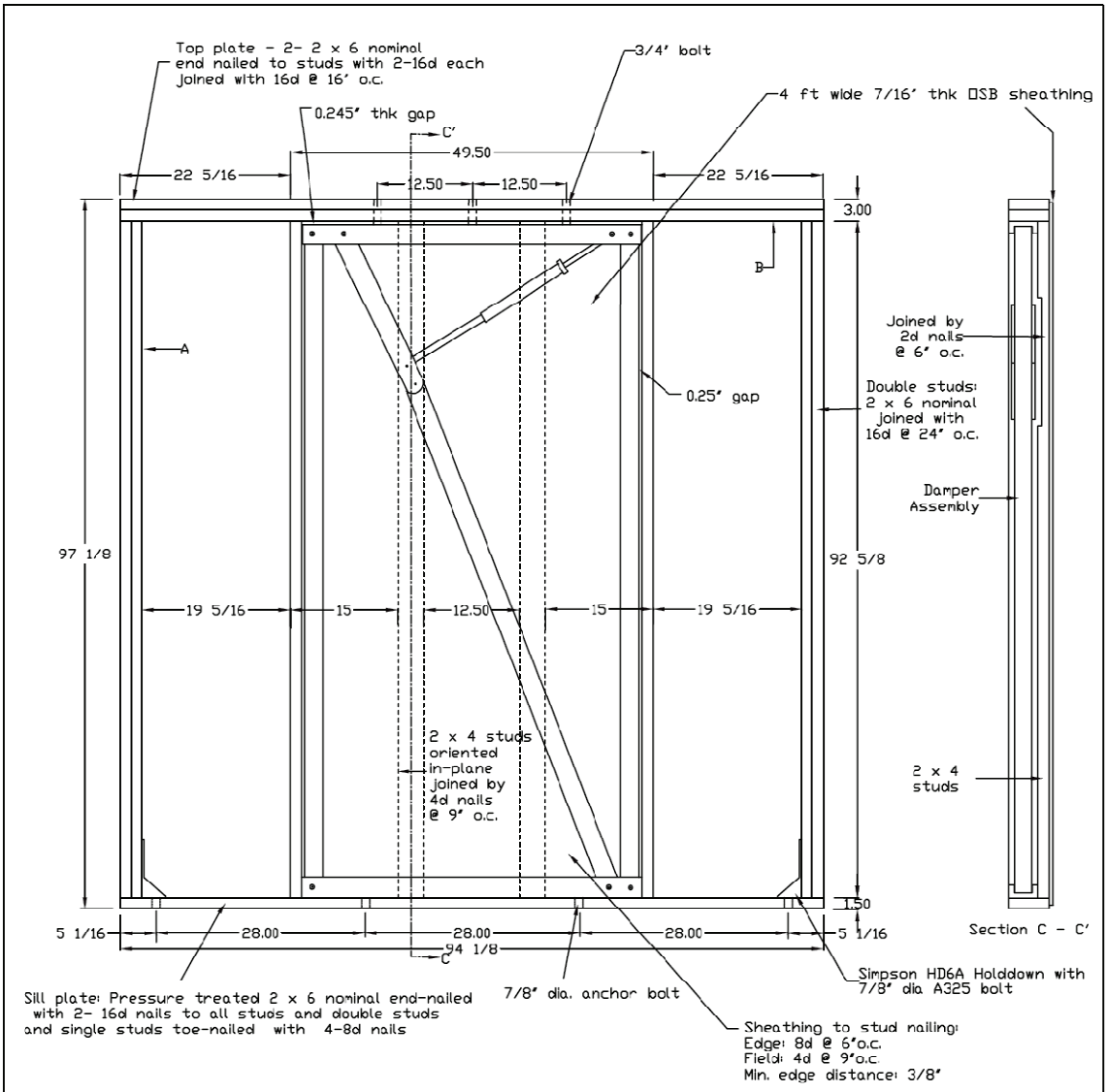

RENSSELAER POLYTECHNIC INSTITUTE
NEESWood Project: Damper wall test at RPI

		NAME	DATE
UNLESS OTHERWISE SPECIFIED:	DRAWN	JKS	6/30/07
DIMENSIONS ARE IN INCHES TOLERANCES: FRACTIONAL ± 1/32	CHECKED	MDS	6/30/07
MATERIAL	COMMENTS:		

TITLE: DETAILS OF DAMPER WALL

DWG. NO. S2-A

REV

SCALE: AS NOTED

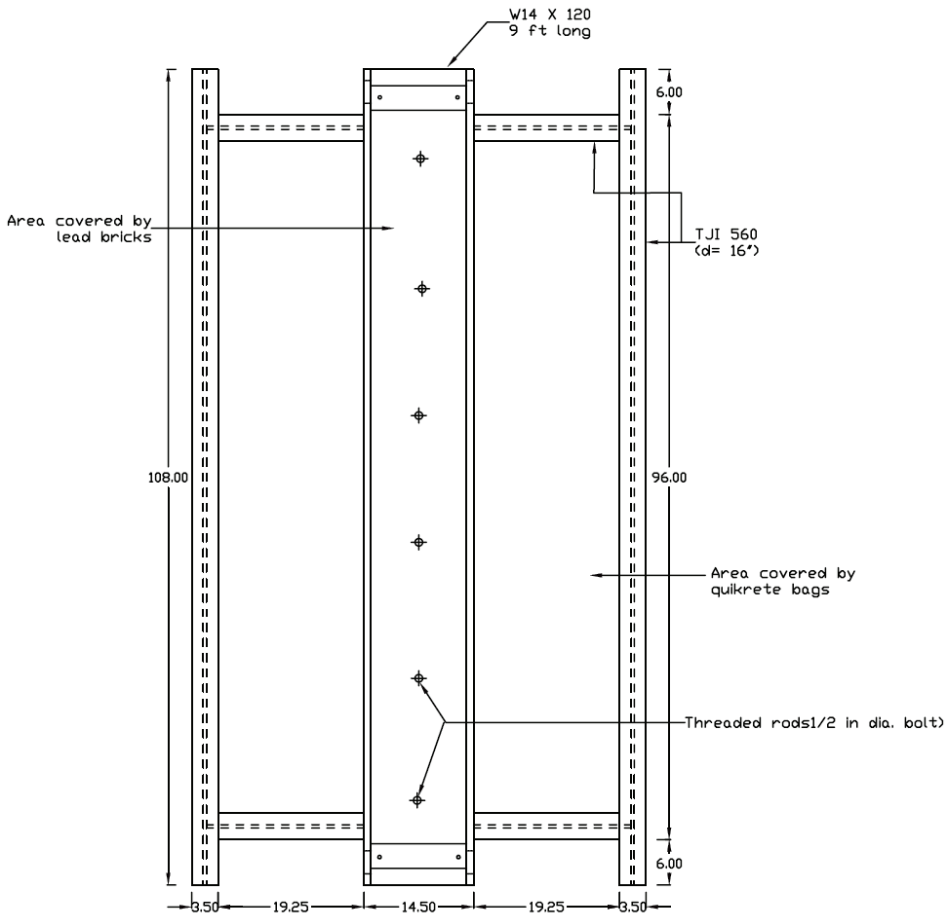

RENSSELAER POLYTECHNIC INSTITUTE NEESWood Project: Damper wall test at RPI			
	NAME	DATE	TITLE:
UNLESS OTHERWISE SPECIFIED:	DRAWN	JKS	6/30/07
DIMENSIONS ARE IN INCHES TOLERANCES: FRACTIONAL ± 1/32	CHECKED	MDS	6/30/07
	COMMENTS:		
MATERIAL			DWG. NO. S3-A / REV
			SCALE: AS NOTED

TOP VIEW OF TEST SETUP

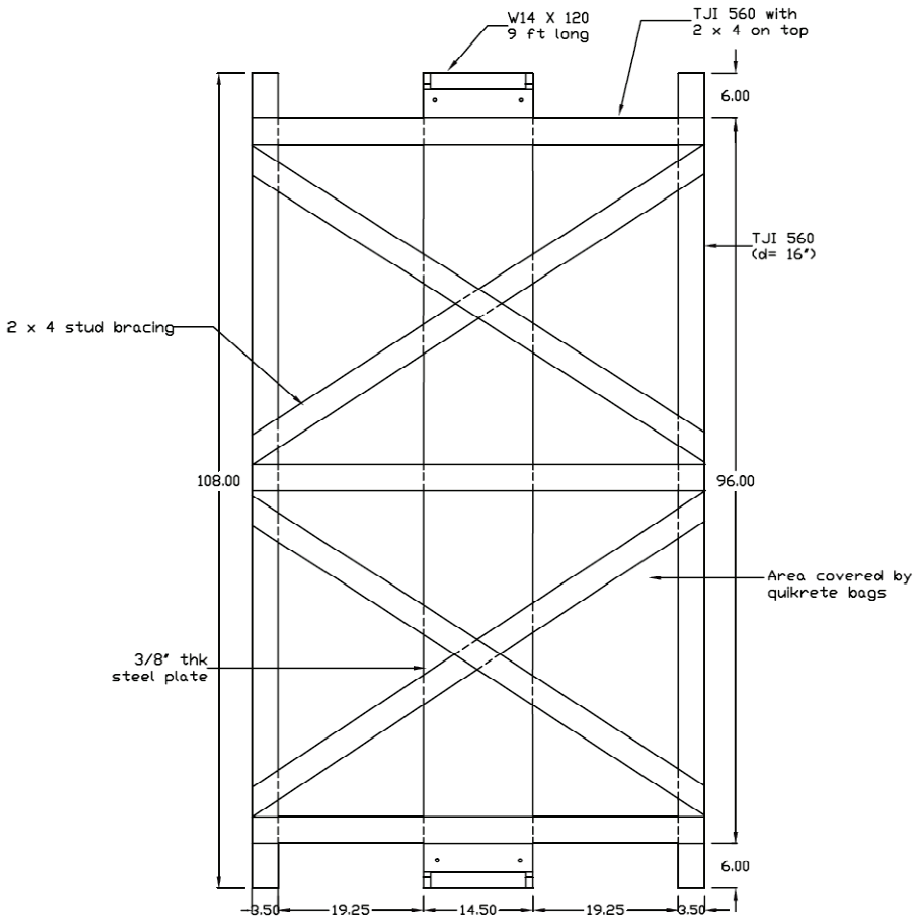

RENSSELAER POLYTECHNIC INSTITUTE NEESWood Project: Damper wall test at RPI			
	NAME	DATE	TITLE: TOP VIEW OF TEST SETUP
UNLESS OTHERWISE SPECIFIED:	DRAWN	JKS	6/30/07
DIMENSIONS ARE IN INCHES TOLERANCES: FRACTIONAL ± 1/32	CHECKED	MDS	6/30/07
MATERIAL	COMMENTS:		DWG. NO. S3-B / REV
			SCALE: AS NOTED

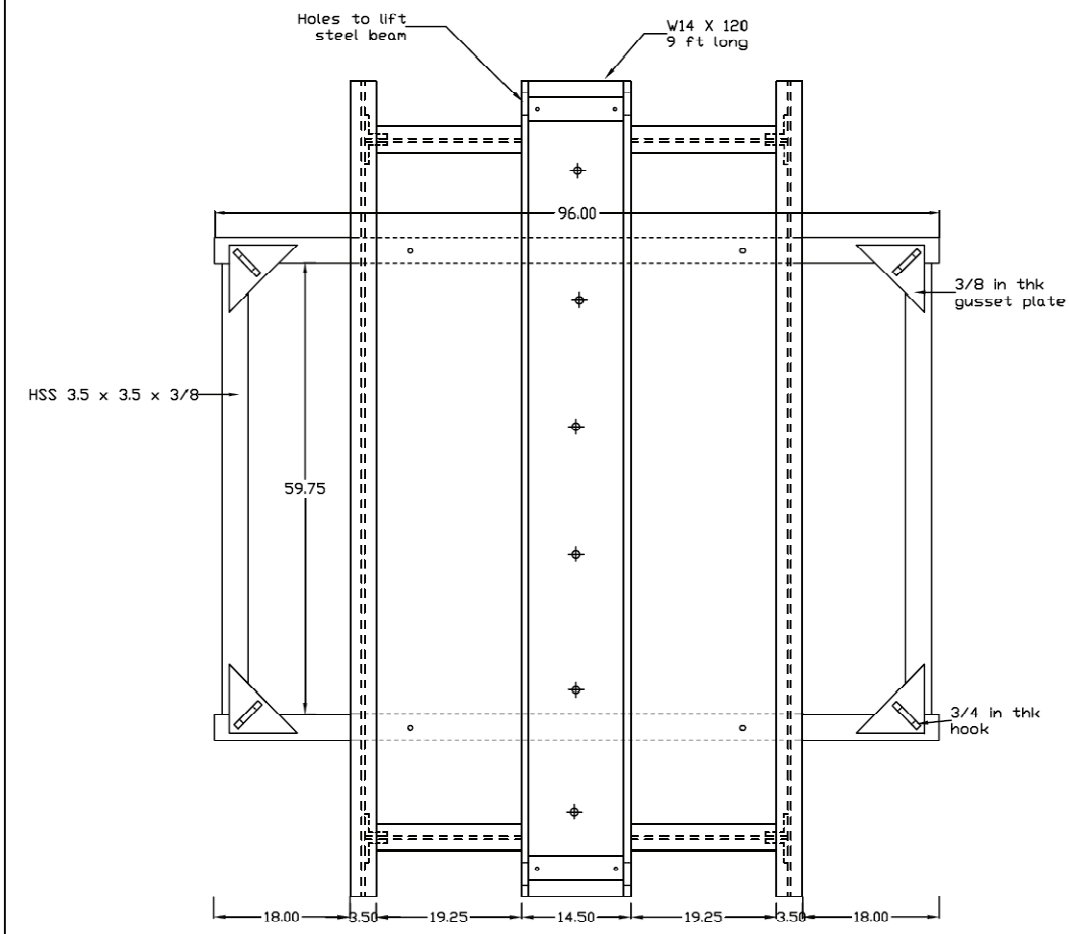

RENSSELAER POLYTECHNIC INSTITUTE
NEESWood Project: Damper wall test at RPI

		NAME	DATE
UNLESS OTHERWISE SPECIFIED:	DRAWN	JKS	6/30/07
DIMENSIONS ARE IN INCHES TOLERANCES: FRACTIONAL ± 1/32	CHECKED	MDS	6/30/07
MATERIAL	COMMENTS:		

TITLE: TOP VIEW - STEEL FRAMEWORK TO SUPPORT WT.

DWG. NO. S3-C

REV

SCALE: AS NOTED

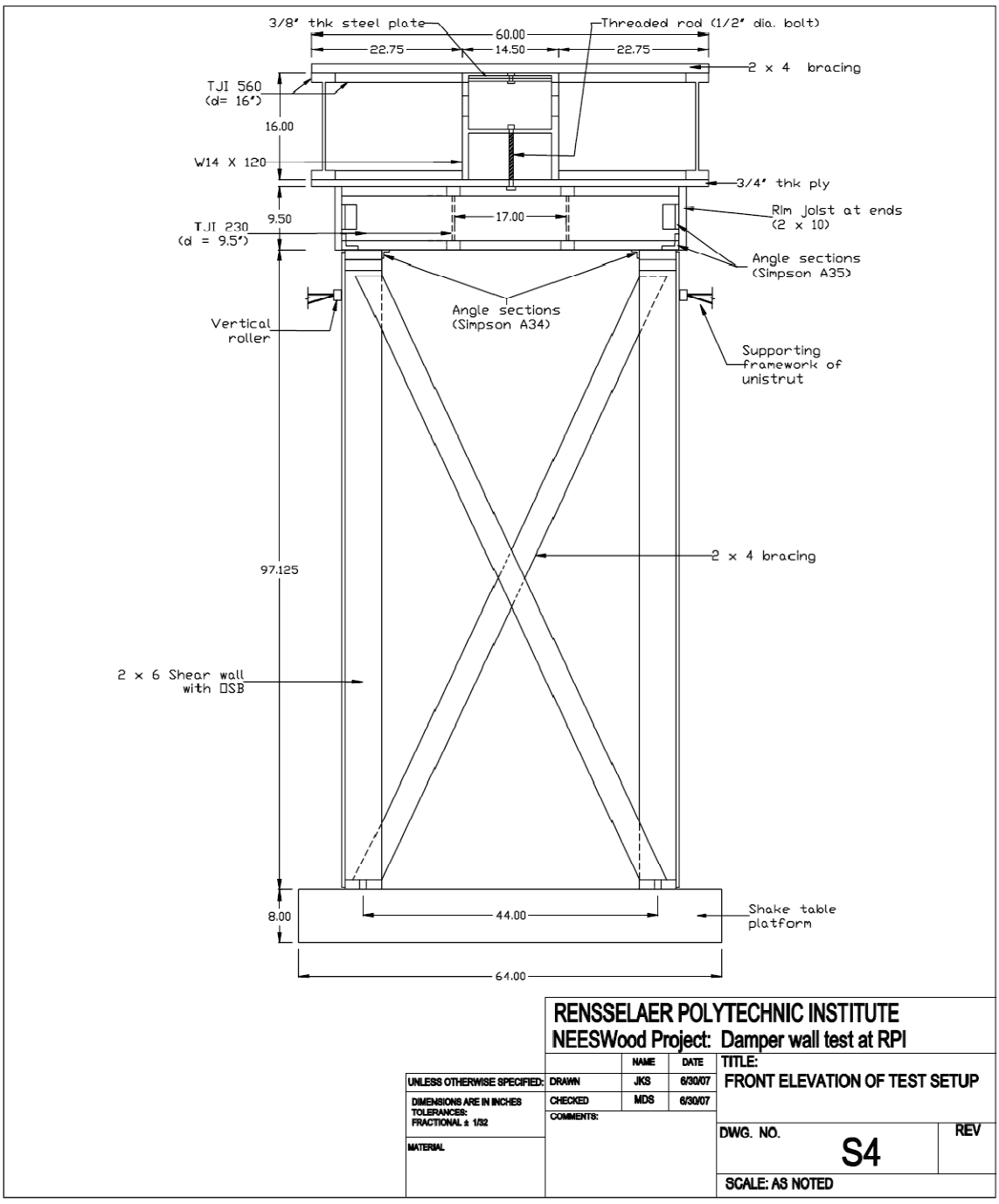

RENSSELAER POLYTECHNIC INSTITUTE NEESWood Project: Damper wall test at RPI			
	NAME	DATE	TITLE: FRONT ELEVATION OF TEST SETUP
UNLESS OTHERWISE SPECIFIED:	DRAWN	JKS	6/30/07
DIMENSIONS ARE IN INCHES TOLERANCES: FRACTIONAL ± 1/32	CHECKED	MDS	6/30/07
	COMMENTS:		DWG. NO. S4 / REV
MATERIAL			SCALE: AS NOTED

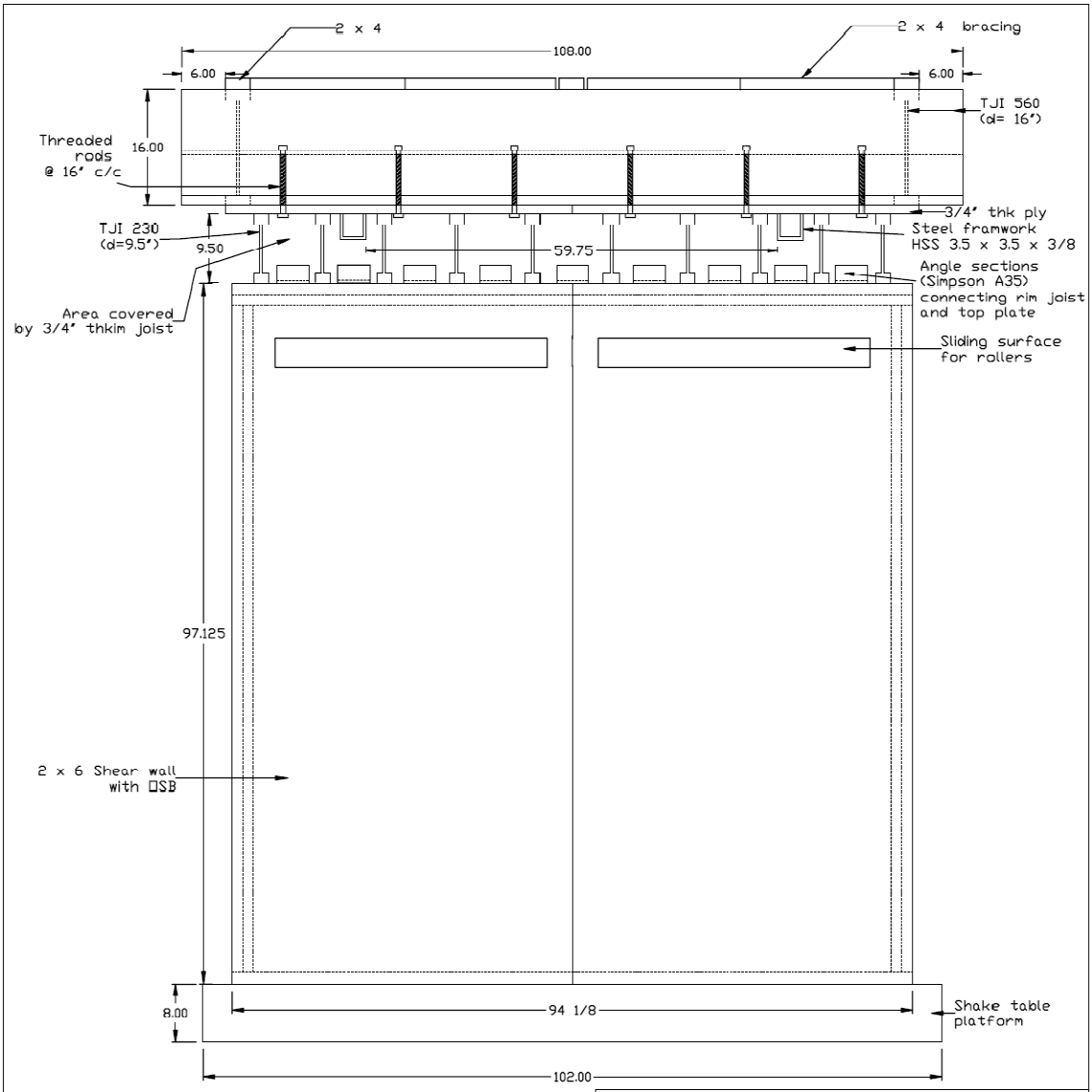
2 x 4
108.00
6.00
2 x 4 bracing
6.00
TJI 560
(d= 16")
Threaded
rods
@ 16" c/c
16.00
3/4" thk ply
Steel framwork
HSS 3.5 x 3.5 x 3/8
TJI 230
(d=9.5")
9.50
59.75
Angle sections
(Simpson A35)
connecting rim joist
and top plate
Area covered
by 3/4" thkim joist
Sliding surface
for rollers
97.125
2 x 6 Shear wall
with OSB
8.00
94 1/8
Shake table
platform
102.00
RENSSELAER POLYTECHNIC INSTITUTE
NEESWood Project: Damper walls test at RPI
NAME
DATE
UNLESS OTHERWISE SPECIFIED:
DRAWN
JKS
6/30/07
DIMENSIONS ARE IN INCHES
TOLERANCES:
FRACTIONAL ± 1/32
CHECKED
MDS
6/30/07
COMMENTS:
MATERIAL
TITLE:
SIDE ELEVATION OF TEST SETUP
DWG. NO.
S5
REV
SCALE: AS NOTED

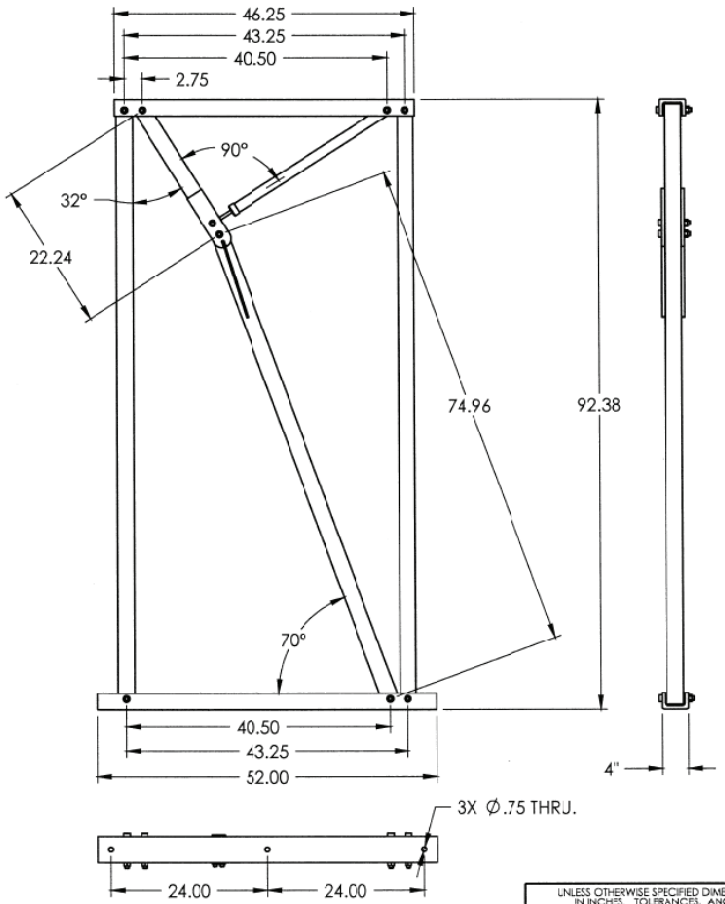

REVISIONS				
ZONE	REV.	DESCRIPTION	DATE	APPROVED

UNLESS OTHERWISE SPECIFIED DIMENSIONS ARE IN INCHES. TOLERANCES: ANGLES ±2°
.XX ±.12 .XXX ±.005
.XXXX ±.0002 X/X ±1/16
ALL CORNERS & EDGES TO BE R .01-.02
√ MAX. ALL SURFACES

B/P COPY NO.
B/P SUBJECT TO RECALL:
B/P & SUBJECT MATTER PROPERTY TAYLOR COMPANIES
REPRODUCTION B/P OR SUBJECT MATTER PROHIBITED
COPYRIGHT 1956
PATENTS { PENDING / APPLIED FOR
FORM 5E

STOCK SIZE (RE⁷):
Ø

PREPARED	K.VARNEY	06/10/12
CHECKED		
Q.A.		
MFG APPR.		
ENGINEER		
APPROVED		
MATERIAL:		

taylor devices inc.
NORTH TONAWANDA, NY
PHONE 716-694-0800
FAX 716-695-5015

FRAME ASSEMBLY

SIZE	CAGE CODE	DRAWING NO:	REV.
B	06742	67DP-18084-01	

SCALE: 1:16 | WEIGHT: 263 | SHEET 1 OF 1

NOTES: UNLESS OTHERWISE NOTED

D.4 Sensors

Table D.2 Location of Sensors

Sensor Number	Units	Location of Sensor
A-1, A-2	g	Attached to End Face of Sill Plate of both Walls to Measure Acceleration Input to the Walls and Monitor Slippage
A-3, A-4	g	Attached to End Face of Top Plate of both Walls to Measure Acceleration Response of Top of Walls
A-5	g	Attached to Shake Table to Measure Acceleration Input
R-1, R-2 (+/- 6 in)	in and in/sec	Attached to End Face of Sill Plate of both the Walls to Measure Slippage Between Sill plate and Shaking Table
DT-12, DT-24	in and in/sec	Connected to End Face of Top plate of Both Walls to Measure Displacement and Velocity of the Top of the Walls
SP-E, SP-W	in	Attached to Damper to Measure Damper Stroke (only used in tests of retrofitted walls)

Table D.3 Selected Accelerometer Specifications as Provided by Manufacturer

Manufacturer	Endevco Corporation
Model Number	7292A-10M1
Type of Accelerometer	Variable Capacitance
Peak Response Range	± 10 g
Sensitivity	200 ± 20 mV/g
Scale Factor	5 g/V
Voltage Output Range	+/- 2 V
Frequency Response (± 5%)	0 to 500 Hz
Excitation	8.5 to 30.0 Vdc

Table D.4 Selected String Potentiometers Specifications as Provided by Manufacturer

Manufacturer	Unimeasure
Model Number	LX-PA25
Input Impedence	100 ohms +/- 10%
Output Impedence	0 to 1000 ohms
Sensitivity	39.282 mv/V/in
Linearity	+/- 0.5% Full Scale
Excitation	25 V maximum AC or DC

Table D.5 Selected Displacement and Velocity Transducer Specifications as Provided by Manufacturer

	DT-12	**DT-24**	**R-1 and R-2**
Manufacturer	MTS Systems Corporation		
Model Number	LHTRB00U01204NO	LHTRB00U02404NO	RHS0120UD601V610200
Type of Sensor	Analog Linear Position Sensor		Analog Magnetostrictive Position Sensor
Displacement Stroke Capacity	±15.24 cm (±6 in.)	±30.48 cm (±12 in.)	±15.24 cm (±6 in.)
Output Voltage Range	±10 Vdc	±10 Vdc	0 - 10 Vdc
Displacement Sensitivity	±0.66 V/cm (±1.67 V/in.)	±0.33 V/cm (±0.83 V/in.)	±0.33 V/cm (±0.83 V/in.)
Displacement Scale Factor	±1.52 cm/V (±0.6 in./V)	±3.05 cm/V (±1.2 in./V)	±3.05 cm/V (±1.2 in./V)
Output	Displacement (Square Wave Neuter)		DC voltage
Resolution	Infinity		10 µm
Operating Voltage	+11.4 to +26.4 Vdc (for Strokes ≤ 152.4 cm (60 in.))		
Corresponding Analog Output Module (AOM) Model Number	315011020RBU0120	315011020RBU0240	Not applicable
Excitation Voltage	24 Vdc		
Velocity Capacity	±50.8 cm/s (±20 in./s)		
Output Voltage Range	±10 Vdc		
Velocity Sensitivity	±0.20 V/cm/s (±0.50 V/in./s)		
Velocity Scale Factor	±5.08 cm/s/V (±2.0 in./s/V)		

D.5 Test Log

Test No.	Date	Input Signal	Table Disp. Amplitude (in)	Frequency (Hz)	Data Sample Rate (Hz)	Filter Frequency (Hz)	Actuator Control Rate (Hz)	Loading on Table	Purpose	Outcome
1	5/16/2008	Sine Wave (Controller)	0.5	0.75	200	100	NA	Pre-test Structure with inertial mass = 7000 pounds	Sensors verification test	A1 and A2 magnet loose:recorded data was not accurate
2	5/23/2008	Sine Wave (Controller)	0.5	0.75	200	100	NA	Pre-test Structure with inertial mass = 7000 pounds	Sensors verification test	A1 and A2 corrected, Input and output is matching well
3	5/23/2008	Sine Wave (Controller)	0.25	1.25	200	100	NA	Pre-test Structure with inertial mass = 7000 pounds	Sensors verification test	Test at higher frequency, Input and output is matching well
4	5/27/2008	No Excitation	NA	NA	200	100	NA	Pre-test Structure with inertial mass = 7000 pounds	Sensors noise test	Sensors noise was observed for no excitation case
5	5/28/2008	Sine Wave (Controller)	0.25	1.25	200	100	NA	Pre-test Structure with inertial mass = 7000 pounds	A1 moved to shake table to confirm actuator frequency	Actuator frequency (~25 Hz) in A1 and A2 output was confirmed
6	11/4/2008	Sine Wave (Controller)	0.5	0.5	200	100	NA	Pre-test Structure with inertial mass = 13200 pounds	Sensors verification test	
7	11/4/2008	Sine Wave (Controller)	0.5	1	200	100	NA	Pre-test Structure with inertial mass = 13200 pounds	Sensors verification test	
8	11/4/2008	Sine Wave (Controller)	0.25	1.5	200	100	NA	Pre-test Structure with inertial mass = 13200 pounds	Sensors verification test	
9	11/4/2008	Sine Wave (Controller)	0.25	2	200	100	NA	Pre-test Structure with inertial mass = 13200 pounds	Sensors verification test	
10	11/4/2008	Sine Wave (Controller)	0.15	2.5	200	100	NA	Pre-test Structure with inertial mass = 13200 pounds	Sensors verification test	

Test No.	Date	Input Signal	Table Disp. Amplitude (in)	Frequency (Hz)	Data Sample Rate (Hz)	Filter Frequency (Hz)	Actuator Control Rate (Hz)	Loading on Table	Purpose	Outcome
11	12/18/2008	White Noise	= 0.02	0-30	200	100	200	Pre-test Structure with inertial mass = 13200 pounds	System idenification test	A1 and A2 were loose (Affected white noise transfer function results of acceleration)
12	12/18/2008	Sine sweep	= 0.03	0-10	200	100	200	Pre-test Structure with inertial mass = 13200 pounds	System idenification test	
13	12/18/2008	Sine sweep	= 0.06	0-10	200	100	200	Pre-test Structure with inertial mass = 13200 pounds	System idenification test	
14	12/18/2008	Canoga park (Corrected 10%)	NA	NA	200	100	200	Pre-test Structure with inertial mass = 13200 pounds	Seismic excitation test	
15	12/18/2008	Canoga park (Corrected 30%)	NA	NA	200	100	200	Pre-test Structure with inertial mass = 13200 pounds	Seismic excitation test	
16	12/18/2008	Canoga park (Corrected 50%)	NA	NA	200	100	200	Pre-test Structure with inertial mass = 13200 pounds	Seismic excitation test	
17	12/18/2008	Canoga park (Corrected 70%)	NA	NA	200	100	200	Pre-test Structure with inertial mass = 13200 pounds	Seismic excitation test	A1 and A2 were loose (Reproduction was correct but considered faulty)
18	12/18/2008	Rinaldi (Corrected 10%)	NA	NA	200	100	200	Pre-test Structure with inertial mass = 13200 pounds	Seismic excitation test	
19	12/18/2008	Rinaldi (Corrected 20%)	NA	NA	200	100	200	Pre-test Structure with inertial mass = 13200 pounds	Seismic excitation test	
20	12/18/2008	Rinaldi (Corrected 25%)	NA	NA	200	100	200	Pre-test Structure with inertial mass = 13200 pounds	Seismic excitation test	Torsion is not significant,Not visibly big damage from outside

Test No.	Date	Input Signal	Table Disp. Amplitude (in)	Frequency (Hz)	Data Sample Rate (Hz)	Filter Frequency (Hz)	Actuator Control Rate (Hz)	Loading on Table	Purpose	Outcome
21	12/18/2008	Rinaldi (Corrected 30%)	NA	NA	200	100	200	Pre-test Structure with inertial mass = 13200 pounds	Seismic excitation test	A1 and A2 were loose (Reproduction was correct but considered faulty)
22	12/18/2008	White Noise	± 0.02	0-30	200	100	200	Pre-test Structure with inertial mass = 13200 pounds	System idenification test	A1 and A2 were loose (Affected white noise transfer function results of acceleration)
23	12/18/2008	Sine sweep	± 0.03	0-10	200	100	200	Pre-test Structure with inertial mass = 13200 pounds	System idenification test	
24	1/29/2009	White Noise	± 0.02	0-30	1000	100	60	Pre-test Structure with inertial mass = 13200 pounds	Tranfser Function Develpoment	A5 moved to the shake table, Command data recording started, A1 and A2 were tightened after finding them loose (earlier test data was affected)
25	1/29/2009	White Noise	± 0.05	0-30	1000	100	60	Pre-test Structure with inertial mass = 13200 pounds	Tranfser Function Develpoment	
26	12/18/2008	Canoga park (Corrected 70%)	NA	NA	200	100	200	Pre-test Structure with inertial mass = 13200 pounds	Seismic excitation test to test ground motion reproduction	Dutil TF (0.10 in amplitude white noise)was used for ground motion correction. Best reproduction is obtained for this case due to its larger amplitude. A1 and A5 senors results also matched well
27	12/18/2008	Canoga park (Corrected 70%)	NA	NA	200	100	200	Pre-test Structure with inertial mass = 13200 pounds	Seismic excitation test to test ground motion reproduction	Test 24 (0.02 in amplitude white noise) was used for ground motion correction. Small change in TF due to additonal mass
28	12/18/2008	Canoga park (Corrected 70%)	NA	NA	200	100	200	Pre-test Structure with inertial mass = 13200 pounds	Seismic excitation test to test ground motion reproduction	Test 25 (0.05 in amplitude white noise) was used for ground motion correction. Small change in TF due to additonal mass
29	2/17/2009	Sine Wave (Controller)	0.15	0.5	200	100	NA	Test Structure without dampers	Sensors verification test	Reference frame movement observed: Need to be fixed before seismic tests
30	2/17/2009	Sine Wave (Controller)	0.15	1	200	100	NA	Test Structure without dampers	Sensors verification test	

Test No.	Date	Input Signal	Table Disp. Amplitude (in)	Frequency (Hz)	Data Sample Rate (Hz)	Filter Frequency (Hz)	Actuator Control Rate (Hz)	Loading on Table	Purpose	Outcome
31	2/17/2009	White Noise	± 0.02	0-30	400	100	60	Test Structure without dampers	System idenification test	f = 3.45 Hz (TF) f = 4.31 Hz (free vibration)
32	2/17/2009	Sine sweep	± 0.01	0-3.70	400	100	200	Test Structure without dampers	System idenification test	f = 3.25 Hz (Sine sweep) f = 3.99 Hz (free vibration)
33	2/23/2009	Sine Wave (Controller)	0.15	1	200	100	NA	Test Structure without dampers	Sensors verification test	
34	2/23/2009	Level 4 -10%	NA	NA	200	100	200	Test Structure without dampers	Seismic excitation test	Torsion is not significant,Not visibly big damage from outside
35	2/23/2009	Level 4 - 33%	NA	NA	200	100	200	Test Structure without dampers	Seismic excitation test	Peak drift = 0.86 %, west shear wall experienced slightly higher drift than east shear wall, Corners of east walls damaged
36	2/26/2009	White Noise	± 0.02	0-30	200	100	60	Test Structure without dampers	System idenification test	f = 2.20 Hz (TF) f = 3.98 Hz (free vibration)
37	2/26/2009	Sine sweep	± 0.01	0-3.70	200	100	200	Test Structure without dampers	System idenification test	f = 2.22 Hz (Sine sweep) f =3.48 Hz (free vibration)
38	2/26/2009	White Noise	± 0.02	0-30	400	100	60	Test Structure without dampers	System idenification test	f = 2.35 Hz(TF) f =3.73 Hz (free vibration)
39	2/26/2009	Sine sweep	± 0.01	0-3.70	400	100	200	Test Structure without dampers	System idenification test	f = 2.26 Hz (Sine sweep) f =3.37 Hz (free vibration)
40	4/8/2009	Sine Wave (Controller)	0.15	1	200	100	NA	Test Structure without dampers	Sensors verification test	R-2 sensor was fixed (wire from voltage meter were out) and 3 lead bricks moved to the east side to have symmetric distribution of overhead mass

Test No.	Date	Input Signal	Table Disp. Amplitude (in)	Frequency (Hz)	Data Sample Rate (Hz)	Filter Frequency (Hz)	Actuator Control Rate (Hz)	Loading or Table	Purpose	Outcome
41	4/8/2009	White Noise	± 0.02	0-30	400	100	60	Test Structure without dampers	System identification test	f = 2.55 Hz (TF) f = 4.02 Hz (free vibration)
42	4/8/2009	Level 5 (40%)	NA	NA	200	100	200	Test Structure without dampers	Seismic excitation test	Peak drift = 3.48%. Big damage from outside (east wall experienced more damge: nail pullout was significant)
43	4/8/2009	White Noise	± 0.02	0-30	400	100	60	Test Structure without dampers	System identification test	f = 1.10 Hz (TF) f = 2.6 Hz (free vibration)
44	4/9/2009	Sine sweep	± 0.02	0-1.47	400	100	200	Test Structure without dampers	System identification test	f = 1.17 Hz (SS) f = 2.1 Hz (free vibration)
45	4/9/2009	Sine sweep	± 0.05	0-1.47	400	100	200	Test Structure without dampers	System identification test	f = 0.96 Hz (SS) f = 1.75 Hz (free vibration)
46	4/13/2009	Sine sweep	± 0.03	0-2.5	400	100	200	Test Structure without dampers	System identification test	f = 1.0 Hz (Sine sweep only)
47	4/13/2009	Sine sweep	± 0.06	0-2.5	400	100	200	Test Structure without dampers	System identification test	f = 0.87 Hz (Sine sweep only)
48	4/13/2009	Sine sweep	± 0.07	0-1.47	400	100	200	Test Structure without dampers	System identification test	f = 0.96 Hz (SS) f = 1.4 Hz (free vibration)
49	5/1/2009	No Excitation	NA	NA	200	100	NA	Test Structure without dampers	Sensors noise test	Sensors noise was observed for no excitation case
50	5/1/2009	Sine Wave (Controller)	0.15	0.5	200	100	NA	Test Structure with dampers	Sensors verification test	More symmetic distribution of mass obtained along long and lateral direction with crane balance

Test No.	Date	Input Signal	Table Disp. Amplitude (in)	Frequency (Hz)	Data Sample Rate (Hz)	Filter Frequency (Hz)	Actuator Control Rate (Hz)	Loading on Table	Purpose	Outcome
51	5/1/2009	White Noise	± 0.02	0-30	400	100	60	Test Structure with dampers	System idenification test	f = 4.35 Hz(TF) f = 4.94 Hz (free vibration)
52	5/1/2009	Sine sweep	± 0.01	0-3.70	400	100	200	Test Structure with dampers	System idenification test	f = 3.42 Hz (Sine sweep) f = 4.61 Hz (free vibration)
53	5/1/2009	Level 4 -10%	NA	NA	200	100	200	Test Structure with dampers	Seismic excitation test	Peak drift = 0.087%
54	5/4/2009	Sine sweep	± 0.01	0-5	400	100	200	Test Structure with dampers	System idenification test	f = 4.6 Hz (Sine sweep only)
55	5/4/2009	Level 4 -33%	NA	NA	200	100	200	Test Structure with dampers	Seismic excitation test	Peak drift 0.32%, not visible damage
56	5/4/2009	White Noise	± 0.02	0-30	400	100	60	Test Structure with dampers	System idenification test	f = 4.06 Hz(TF) f = 4.64 Hz (free vibration)
57	5/4/2009	Sine sweep	± 0.01	0-3.70	400	100	200	Test Structure with dampers	System idenification test	f = 3.38 Hz (Sine sweep) f = 4.30 Hz (free vibration)
58	5/4/2009	Level 5 -40%	NA	NA	200	100	200	Test Structure with dampers	Seismic excitation test	Peak drift = 0.77%, not visible damage
59	5/4/2009	White Noise	± 0.02	0-30	400	100	60	Test Structure with dampers	System idenification test	f = 3.55 Hz(TF) f = 4.64 Hz (free vibration)
60	5/4/2009	Sine sweep	± 0.01	0-3.70	400	100	200	Test Structure with dampers	System idenification test	f = 3.29 Hz (Sine sweep) f = 4.30 Hz (free vibration)
61	5/4/2009	Level 4 -60%	NA	NA	200	100	200	Test Structure with dampers	Seismic excitation test	Peak drift = 0.98%, not visible damage yet
62	5/4/2009	White Noise	± 0.02	0-30	400	100	60	Test Structure with dampers	System idenification test	f = 3.35 Hz(TF) f = 4.64 Hz (free vibration)
63	5/4/2009	Sine sweep	± 0.01	0-3.70	400	100	200	Test Structure with dampers	System idenification test	f = 3.38 Hz (Sine sweep) f = 4.30 Hz (free vibration)

Test No.	Date	Input Signal	Table Disp. Amplitude (in)	Frequency (Hz)	Data Sample Rate (Hz)	Filter Frequency (Hz)	Actuator Control Rate (Hz)	Loading on Table	Purpose	Outcome
64	12/2/2009	White Noise	± 0.02	0-30	400	100	60	Test Structure with dampers	System idenification test	f = 3.35 Hz(TF) f = 4.64 Hz (free vibration)
65	12/2/2009	Sine sweep	± 0.01	0-3.70	400	100	200	Test Structure with dampers	System idenification test	f = 3.38 Hz (Sine sweep) f = 4.30 Hz (free vibration)
66	12/2/2009	Level 4 -60%	NA	NA	200	100	200	Test Structure with dampers	Seismic excitation test	Peak drift 0.89%, some visible damage
69	12/2/2009	White Noise	± 0.02	0-30	400	100	60	Test Structure with dampers	System idenification test	f = 3.1 Hz(TF) f = 4.02 Hz (free vibration)
68	12/2/2009	Level 4 -75%	NA	NA	200	100	200	Test Structure with dampers	Seismic excitation test	Peak drift 1.08%, some visible damage
69	12/2/2009	White Noise	± 0.02	0-30	400	100	60	Test Structure with dampers	System idenification test	f = 3.1 Hz(TF) f = 3.95 Hz (free vibration)
70	12/12/2009	Level 5 -50%	NA	NA	200	100	200	Test Structure with dampers	Seismic excitation test	Peak drift 1.03%, some visible damage
71	12/12/2009	White Noise	± 0.02	0-30	400	100	60	Test Structure with dampers	System idenification test	f = 3.0 Hz(TF) f = 3.90 Hz (free vibration)

D.6 Evaluation of Loss of Displacement Transmission to Damper via Code-Based Analytical Equations

IBC 2006 provides an equation to predict the total deflection, Δ, experienced by shearwalls during earthquakes. The equation includes deformation due to bending (Δ_b), shear (Δ_v), nail slip (Δ_n) and anchorage slip (Δ_a) and is given by (see Breyer et al. (2007) and APA (2007a) for further explanations of each component):

$$\Delta = \Delta_b + \Delta_v + \Delta_n + \Delta_a = \frac{8vh^3}{EAb} + \frac{vh}{Gt} + 0.75he_n + \frac{d_a\ h}{b} \tag{D.1}$$

where A is the area of the boundary element cross-section (vertical member of shear wall boundary) in square inches, b is the shearwall length in feet, d_a is the vertical displacement (elongation) of the overturning anchorage or the hold-down slip in inches, E is the elastic modulus of the boundary element [vertical member at shearwall boundary (chord)] in psi, e_n is the nail slip in inches, G is the shear modulus of the sheathing in psi, t is the thickness of the sheathing in inches (and thus Gt is the sheathing panel rigidity in lb/in), h is the shearwall height in feet, and v is the maximum shear due to the design loads at the top of the shearwall, in lb/ft.

The calculation of displacement components for the Level 5 (40% Rinaldi) shaking table test with toggle-braced dampers (Test No. 58) is shown below:

Experimentally measured data: a_{top} = 0.44g Δ = 0.74 in

$$v = \frac{V}{L} = \frac{m_{top}a_{top}}{L} = \frac{W_{top}a_{top}(g)}{L} = \frac{(13200\ lb)(0.44)}{(2)(4\ ft)} = \frac{5808\ lb}{8\ ft} = 726\ plf$$

Assuming hold-down displacement increases linearly with hold-down tensile force, T:

$$d_a = \frac{(d_a)_{max}}{T_{max}}T = \frac{(d_a)_{max}}{T_{max}}vh = \frac{0.041\ in}{3680\ lb}(726\ plf)(8\ ft) = \ 0.0647 \text{ in}$$

For two 2 x 6 vertical end studs at boundary of shear wall:

$$A = 2(1.5\ in)(5.5\ in) = \ 16.5 \text{ in}^2$$

$$\Delta_b = \frac{8vh^3}{EAb} = \frac{(8)(726\ plf)(8\ ft)^3}{(1{,}200{,}000\ psi)(16.5\ in^2)(8\ ft)} = 0.0188\ in$$

$$\Delta_v = \frac{vh}{Gt} = \frac{(726\ plf)(8\ ft)}{(83500\ lbf/in)} = 0.0696\ in$$

$$\Delta_a = \frac{d_a h}{b} = \frac{(0.0647\ in)(8\ ft)}{(8\ ft)} = 0.0647\ in$$

$$\Delta_n = \Delta - \Delta_b - \Delta_v - \Delta_a = 0.74\ in - 0.0188\ in - 0.0696\ in - 0.0647\ in = 0.587\ in$$

$$\%\Delta_b = \frac{0.0188\ in}{0.74\ in} \times 100 = 2.54\%$$

$$\%\Delta_v = \frac{0.0696\ in}{0.74\ in} \times 100 = 9.41\%$$

$$\%\Delta_a = \frac{0.0647\ in}{0.74\ in} \times 100 = 8.74\%$$

$$\%\Delta_n = \frac{0.587\ in}{0.74\ in} \times 100 = 79.32\%$$

The shearing component (9.41%) is directly transmitted to the damper. A portion of the nail slip component contributes to displacement transfer in that, as the nails slip, the wall is more flexible, and thus the damper is stroked. Herein, it is assumed that 70% of the nail slip component is transmitted to the damper. Thus, the displacement transmitted to the damper assembly is:

$$\%\ Displacement\ Transmitted\ to\ Damper\ Assembly = 9.41\% + (0.7)(79.32\%) = 64.93\%$$

and the displacement transmission loss within the wood framing of the shearwall (displacement that does not get transmitted to the damper assembly) is then:

$$\%\ Displacement\ Loss\ within\ Wood\ Framing = 2.54\% + 8.74\% + (0.3)(79.32\%) = 35.08\%$$

An evaluation of displacement transmission losses based on the above code-based analytical equations is provided in Table D.6 for the toggle-braced test specimens. Note that the losses within the wood framing and within the damper assembly (see last two

rows of table) are essentially the same for the three different cases shown. Thus, the losses may be regarded as independent of the level of excitation. Recall that significant loss of displacement transmission (about 60% loss from ideal magnification of 165% to actual magnification of 65%) occurred in the shaking table tests. As noted previously, it is assumed that 30% of the deflection due to nail slip will be lost within the wood framing of the shearwall, The 30% value was selected such that it will give reasonable contribution of losses within the wood framing of the shearwalls to the total displacement transmission loss observed (about 60%). Based on these assumptions, the total displacement loss within the wood framing of the shearwall was estimated to be in the range of 30 to 40% (see second to last row in Table D.6). The additional displacement loss observed (i.e., 20 to 30%) is assumed to be due to losses within the steel damper assembly (e.g., due to tolerances in the joints of the toggle-brace assembly, flexibility of bracing, and other losses with unknown origin (see Section 3.7 for details)).

Table D.6 Summary of Displacement Transmission Losses

	Test # 55 Level 4 (33%)	**Test # 58 Level 5 (40%)**	**Test # 61 Level 4 (60%)**
Maximum Total Deflection (in)	0.31	0.74	0.94
Acceleration (g) (at time of maximum total deflection)	0.25	0.44	0.38
Unit Load (plf)	412.5	726	627
Hold-Down Slip (in)	0.0368	0.0647	0.0559
Deflection due to Bending, Δ_b (in)	0.0107	0.0188	0.0162
Deflection due to Shear, Δ_v (in)	0.0395	0.0696	0.0601
Deflection due to Anchorage Slip, Δ_a (in)	0.0368	0.0647	0.0559
Deflection due to Nail Slip, Δ_n (in)	0.2257	0.587	0.808
$\%\Delta_b$	3.45	2.54	1.72
$\%\Delta_v$	12.74	9.41	6.40
$\%\Delta_a$	11.87	8.74	5.95
$\%\Delta_n$	72.81	79.32	85.96
% Transmitted to Damper Assembly ($\%\Delta_v + \%\Delta_n(0.7)$)	63.71	64.93	66.57
% Displacement Loss within Wood Framing ($\%\Delta_b + \%\Delta_a + \%\Delta_n(0.3)$)	37.16	35.08	33.46
% Displacement Loss within Damper Assembly (connection of wood framing to damper assembly, deformation of bracing members, and other unknown losses) = 60% minus losses within wood framing	23.71	24.93	26.57

D.7 Photographs of Experimental Test Setup

Roof Diaphragm

Anchor Bolts with 3 in. Square Washer

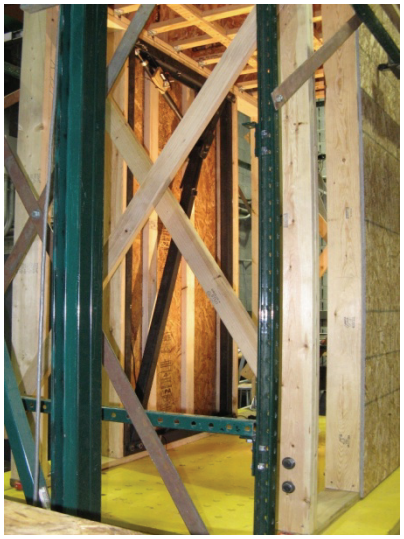

Toggle Assembly Installed inside Retrofitted Wall

Simpson HD6A Hold-Down Installed in Test Walls

Top Channel Connected to Top Plate with Three A325 Structural Bolts

Bottom Channel Anchored to Shake Table with Two A325 Structural Bolts

Fluid Viscous Damper Installed with String Potentiometer

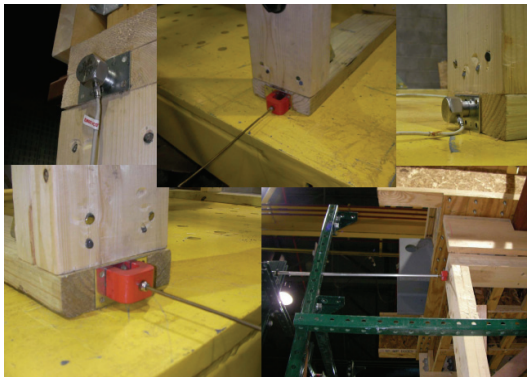

Sensors Installed at Various Locations

MCEER Technical Reports

MCEER publishes technical reports on a variety of subjects written by authors funded through MCEER. These reports are available from both MCEER Publications and the National Technical Information Service (NTIS). Requests for reports should be directed to MCEER Publications, MCEER, University at Buffalo, State University of New York, 133A Ketter Hall, Buffalo, New York 14260. Reports can also be requested through NTIS, P.O. Box 1425, Springfield, Virginia 22151. NTIS accession numbers are shown in parenthesis, if available.

NCEER-87-0001 "First-Year Program in Research, Education and Technology Transfer," 3/5/87, (PB88-134275, A04, MF-A01).

NCEER-87-0002 "Experimental Evaluation of Instantaneous Optimal Algorithms for Structural Control," by R.C. Lin, T.T. Soong and A.M. Reinhorn, 4/20/87, (PB88-134341, A04, MF-A01).

NCEER-87-0003 "Experimentation Using the Earthquake Simulation Facilities at University at Buffalo," by A.M. Reinhorn and R.L. Ketter, to be published.

NCEER-87-0004 "The System Characteristics and Performance of a Shaking Table," by J.S. Hwang, K.C. Chang and G.C. Lee, 6/1/87, (PB88-134259, A03, MF-A01). This report is available only through NTIS (see address given above).

NCEER-87-0005 "A Finite Element Formulation for Nonlinear Viscoplastic Material Using a Q Model," by O. Gyebi and G. Dasgupta, 11/2/87, (PB88-213764, A08, MF-A01).

NCEER-87-0006 "Symbolic Manipulation Program (SMP) - Algebraic Codes for Two and Three Dimensional Finite Element Formulations," by X. Lee and G. Dasgupta, 11/9/87, (PB88-218522, A05, MF-A01).

NCEER-87-0007 "Instantaneous Optimal Control Laws for Tall Buildings Under Seismic Excitations," by J.N. Yang, A. Akbarpour and P. Ghaemmaghami, 6/10/87, (PB88-134333, A06, MF-A01). This report is only available through NTIS (see address given above).

NCEER-87-0008 "IDARC: Inelastic Damage Analysis of Reinforced Concrete Frame - Shear-Wall Structures," by Y.J. Park, A.M. Reinhorn and S.K. Kunnath, 7/20/87, (PB88-134325, A09, MF-A01). This report is only available through NTIS (see address given above).

NCEER-87-0009 "Liquefaction Potential for New York State: A Preliminary Report on Sites in Manhattan and Buffalo," by M. Budhu, V. Vijayakumar, R.F. Giese and L. Baumgras, 8/31/87, (PB88-163704, A03, MF-A01). This report is available only through NTIS (see address given above).

NCEER-87-0010 "Vertical and Torsional Vibration of Foundations in Inhomogeneous Media," by A.S. Veletsos and K.W. Dotson, 6/1/87, (PB88-134291, A03, MF-A01). This report is only available through NTIS (see address given above).

NCEER-87-0011 "Seismic Probabilistic Risk Assessment and Seismic Margins Studies for Nuclear Power Plants," by Howard H.M. Hwang, 6/15/87, (PB88-134267, A03, MF-A01). This report is only available through NTIS (see address given above).

NCEER-87-0012 "Parametric Studies of Frequency Response of Secondary Systems Under Ground-Acceleration Excitations," by Y. Yong and Y.K. Lin, 6/10/87, (PB88-134309, A03, MF-A01). This report is only available through NTIS (see address given above).

NCEER-87-0013 "Frequency Response of Secondary Systems Under Seismic Excitation," by J.A. HoLung, J. Cai and Y.K. Lin, 7/31/87, (PB88-134317, A05, MF-A01). This report is only available through NTIS (see address given above).

NCEER-87-0014 "Modelling Earthquake Ground Motions in Seismically Active Regions Using Parametric Time Series Methods," by G.W. Ellis and A.S. Cakmak, 8/25/87, (PB88-134283, A08, MF-A01). This report is only available through NTIS (see address given above).

NCEER-87-0015 "Detection and Assessment of Seismic Structural Damage," by E. DiPasquale and A.S. Cakmak, 8/25/87, (PB88-163712, A05, MF-A01). This report is only available through NTIS (see address given above).

NCEER-87-0016 "Pipeline Experiment at Parkfield, California," by J. Isenberg and E. Richardson, 9/15/87, (PB88-163720, A03, MF-A01). This report is available only through NTIS (see address given above).

NCEER-87-0017 "Digital Simulation of Seismic Ground Motion," by M. Shinozuka, G. Deodatis and T. Harada, 8/31/87, (PB88-155197, A04, MF-A01). This report is available only through NTIS (see address given above).

NCEER-87-0018 "Practical Considerations for Structural Control: System Uncertainty, System Time Delay and Truncation of Small Control Forces," J.N. Yang and A. Akbarpour, 8/10/87, (PB88-163738, A08, MF-A01). This report is only available through NTIS (see address given above).

NCEER-87-0019 "Modal Analysis of Nonclassically Damped Structural Systems Using Canonical Transformation," by J.N. Yang, S. Sarkani and F.X. Long, 9/27/87, (PB88-187851, A04, MF-A01).

NCEER-87-0020 "A Nonstationary Solution in Random Vibration Theory," by J.R. Red-Horse and P.D. Spanos, 11/3/87, (PB88-163746, A03, MF-A01).

NCEER-87-0021 "Horizontal Impedances for Radially Inhomogeneous Viscoelastic Soil Layers," by A.S. Veletsos and K.W. Dotson, 10/15/87, (PB88-150859, A04, MF-A01).

NCEER-87-0022 "Seismic Damage Assessment of Reinforced Concrete Members," by Y.S. Chung, C. Meyer and M. Shinozuka, 10/9/87, (PB88-150867, A05, MF-A01). This report is available only through NTIS (see address given above).

NCEER-87-0023 "Active Structural Control in Civil Engineering," by T.T. Soong, 11/11/87, (PB88-187778, A03, MF-A01).

NCEER-87-0024 "Vertical and Torsional Impedances for Radially Inhomogeneous Viscoelastic Soil Layers," by K.W. Dotson and A.S. Veletsos, 12/87, (PB88-187786, A03, MF-A01).

NCEER-87-0025 "Proceedings from the Symposium on Seismic Hazards, Ground Motions, Soil-Liquefaction and Engineering Practice in Eastern North America," October 20-22, 1987, edited by K.H. Jacob, 12/87, (PB88-188115, A23, MF-A01). This report is available only through NTIS (see address given above).

NCEER-87-0026 "Report on the Whittier-Narrows, California, Earthquake of October 1, 1987," by J. Pantelic and A. Reinhorn, 11/87, (PB88-187752, A03, MF-A01). This report is available only through NTIS (see address given above).

NCEER-87-0027 "Design of a Modular Program for Transient Nonlinear Analysis of Large 3-D Building Structures," by S. Srivastav and J.F. Abel, 12/30/87, (PB88-187950, A05, MF-A01). This report is only available through NTIS (see address given above).

NCEER-87-0028 "Second-Year Program in Research, Education and Technology Transfer," 3/8/88, (PB88-219480, A04, MF-A01).

NCEER-88-0001 "Workshop on Seismic Computer Analysis and Design of Buildings With Interactive Graphics," by W. McGuire, J.F. Abel and C.H. Conley, 1/18/88, (PB88-187760, A03, MF-A01). This report is only available through NTIS (see address given above).

NCEER-88-0002 "Optimal Control of Nonlinear Flexible Structures," by J.N. Yang, F.X. Long and D. Wong, 1/22/88, (PB88-213772, A06, MF-A01).

NCEER-88-0003 "Substructuring Techniques in the Time Domain for Primary-Secondary Structural Systems," by G.D. Manolis and G. Juhn, 2/10/88, (PB88-213780, A04, MF-A01).

NCEER-88-0004 "Iterative Seismic Analysis of Primary-Secondary Systems," by A. Singhal, L.D. Lutes and P.D. Spanos, 2/23/88, (PB88-213798, A04, MF-A01).

NCEER-88-0005 "Stochastic Finite Element Expansion for Random Media," by P.D. Spanos and R. Ghanem, 3/14/88, (PB88-213806, A03, MF-A01).

NCEER-88-0006 "Combining Structural Optimization and Structural Control," by F.Y. Cheng and C.P. Pantelides, 1/10/88, (PB88-213814, A05, MF-A01).

NCEER-88-0007 "Seismic Performance Assessment of Code-Designed Structures," by H.H-M. Hwang, J-W. Jaw and H-J. Shau, 3/20/88, (PB88-219423, A04, MF-A01). This report is only available through NTIS (see address given above).

NCEER-88-0008 "Reliability Analysis of Code-Designed Structures Under Natural Hazards," by H.H-M. Hwang, H. Ushiba and M. Shinozuka, 2/29/88, (PB88-229471, A07, MF-A01). This report is only available through NTIS (see address given above).

NCEER-88-0009 "Seismic Fragility Analysis of Shear Wall Structures," by J-W Jaw and H.H-M. Hwang, 4/30/88, (PB89-102867, A04, MF-A01).

NCEER-88-0010 "Base Isolation of a Multi-Story Building Under a Harmonic Ground Motion - A Comparison of Performances of Various Systems," by F-G Fan, G. Ahmadi and I.G. Tadjbakhsh, 5/18/88, (PB89-122238, A06, MF-A01). This report is only available through NTIS (see address given above).

NCEER-88-0011 "Seismic Floor Response Spectra for a Combined System by Green's Functions," by F.M. Lavelle, L.A. Bergman and P.D. Spanos, 5/1/88, (PB89-102875, A03, MF-A01).

NCEER-88-0012 "A New Solution Technique for Randomly Excited Hysteretic Structures," by G.Q. Cai and Y.K. Lin, 5/16/88, (PB89-102883, A03, MF-A01).

NCEER-88-0013 "A Study of Radiation Damping and Soil-Structure Interaction Effects in the Centrifuge," by K. Weissman, supervised by J.H. Prevost, 5/24/88, (PB89-144703, A06, MF-A01).

NCEER-88-0014 "Parameter Identification and Implementation of a Kinematic Plasticity Model for Frictional Soils," by J.H. Prevost and D.V. Griffiths, to be published.

NCEER-88-0015 "Two- and Three- Dimensional Dynamic Finite Element Analyses of the Long Valley Dam," by D.V. Griffiths and J.H. Prevost, 6/17/88, (PB89-144711, A04, MF-A01).

NCEER-88-0016 "Damage Assessment of Reinforced Concrete Structures in Eastern United States," by A.M. Reinhorn, M.J. Seidel, S.K. Kunnath and Y.J. Park, 6/15/88, (PB89-122220, A04, MF-A01). This report is only available through NTIS (see address given above).

NCEER-88-0017 "Dynamic Compliance of Vertically Loaded Strip Foundations in Multilayered Viscoelastic Soils," by S. Ahmad and A.S.M. Israil, 6/17/88, (PB89-102891, A04, MF-A01).

NCEER-88-0018 "An Experimental Study of Seismic Structural Response With Added Viscoelastic Dampers," by R.C. Lin, Z. Liang, T.T. Soong and R.H. Zhang, 6/30/88, (PB89-122212, A05, MF-A01). This report is available only through NTIS (see address given above).

NCEER-88-0019 "Experimental Investigation of Primary - Secondary System Interaction," by G.D. Manolis, G. Juhn and A.M. Reinhorn, 5/27/88, (PB89-122204, A04, MF-A01).

NCEER-88-0020 "A Response Spectrum Approach For Analysis of Nonclassically Damped Structures," by J.N. Yang, S. Sarkani and F.X. Long, 4/22/88, (PB89-102909, A04, MF-A01).

NCEER-88-0021 "Seismic Interaction of Structures and Soils: Stochastic Approach," by A.S. Veletsos and A.M. Prasad, 7/21/88, (PB89-122196, A04, MF-A01). This report is only available through NTIS (see address given above).

NCEER-88-0022 "Identification of the Serviceability Limit State and Detection of Seismic Structural Damage," by E. DiPasquale and A.S. Cakmak, 6/15/88, (PB89-122188, A05, MF-A01). This report is available only through NTIS (see address given above).

NCEER-88-0023 "Multi-Hazard Risk Analysis: Case of a Simple Offshore Structure," by B.K. Bhartia and E.H. Vanmarcke, 7/21/88, (PB89-145213, A05, MF-A01).

NCEER-88-0024 "Automated Seismic Design of Reinforced Concrete Buildings," by Y.S. Chung, C. Meyer and M. Shinozuka, 7/5/88, (PB89-122170, A06, MF-A01). This report is available only through NTIS (see address given above).

NCEER-88-0025 "Experimental Study of Active Control of MDOF Structures Under Seismic Excitations," by L.L. Chung, R.C. Lin, T.T. Soong and A.M. Reinhorn, 7/10/88, (PB89-122600, A04, MF-A01).

NCEER-88-0026 "Earthquake Simulation Tests of a Low-Rise Metal Structure," by J.S. Hwang, K.C. Chang, G.C. Lee and R.L. Ketter, 8/1/88, (PB89-102917, A04, MF-A01).

NCEER-88-0027 "Systems Study of Urban Response and Reconstruction Due to Catastrophic Earthquakes," by F. Kozin and H.K. Zhou, 9/22/88, (PB90-162348, A04, MF-A01).

NCEER-88-0028 "Seismic Fragility Analysis of Plane Frame Structures," by H.H-M. Hwang and Y.K. Low, 7/31/88, (PB89-131445, A06, MF-A01).

NCEER-88-0029 "Response Analysis of Stochastic Structures," by A. Kardara, C. Bucher and M. Shinozuka, 9/22/88, (PB89-174429, A04, MF-A01).

NCEER-88-0030 "Nonnormal Accelerations Due to Yielding in a Primary Structure," by D.C.K. Chen and L.D. Lutes, 9/19/88, (PB89-131437, A04, MF-A01).

NCEER-88-0031 "Design Approaches for Soil-Structure Interaction," by A.S. Veletsos, A.M. Prasad and Y. Tang, 12/30/88, (PB89-174437, A03, MF-A01). This report is available only through NTIS (see address given above).

NCEER-88-0032 "A Re-evaluation of Design Spectra for Seismic Damage Control," by C.J. Turkstra and A.G. Tallin, 11/7/88, (PB89-145221, A05, MF-A01).

NCEER-88-0033 "The Behavior and Design of Noncontact Lap Splices Subjected to Repeated Inelastic Tensile Loading," by V.E. Sagan, P. Gergely and R.N. White, 12/8/88, (PB89-163737, A08, MF-A01).

NCEER-88-0034 "Seismic Response of Pile Foundations," by S.M. Mamoon, P.K. Banerjee and S. Ahmad, 11/1/88, (PB89-145239, A04, MF-A01).

NCEER-88-0035 "Modeling of R/C Building Structures With Flexible Floor Diaphragms (IDARC2)," by A.M. Reinhorn, S.K. Kunnath and N. Panahshahi, 9/7/88, (PB89-207153, A07, MF-A01).

NCEER-88-0036 "Solution of the Dam-Reservoir Interaction Problem Using a Combination of FEM, BEM with Particular Integrals, Modal Analysis, and Substructuring," by C-S. Tsai, G.C. Lee and R.L. Ketter, 12/31/88, (PB89-207146, A04, MF-A01).

NCEER-88-0037 "Optimal Placement of Actuators for Structural Control," by F.Y. Cheng and C.P. Pantelides, 8/15/88, (PB89-162846, A05, MF-A01).

NCEER-88-0038 "Teflon Bearings in Aseismic Base Isolation: Experimental Studies and Mathematical Modeling," by A. Mokha, M.C. Constantinou and A.M. Reinhorn, 12/5/88, (PB89-218457, A10, MF-A01). This report is available only through NTIS (see address given above).

NCEER-88-0039 "Seismic Behavior of Flat Slab High-Rise Buildings in the New York City Area," by P. Weidlinger and M. Ettouney, 10/15/88, (PB90-145681, A04, MF-A01).

NCEER-88-0040 "Evaluation of the Earthquake Resistance of Existing Buildings in New York City," by P. Weidlinger and M. Ettouney, 10/15/88, to be published.

NCEER-88-0041 "Small-Scale Modeling Techniques for Reinforced Concrete Structures Subjected to Seismic Loads," by W. Kim, A. El-Attar and R.N. White, 11/22/88, (PB89-189625, A05, MF-A01).

NCEER-88-0042 "Modeling Strong Ground Motion from Multiple Event Earthquakes," by G.W. Ellis and A.S. Cakmak, 10/15/88, (PB89-174445, A03, MF-A01).

NCEER-88-0043 "Nonstationary Models of Seismic Ground Acceleration," by M. Grigoriu, S.E. Ruiz and E. Rosenblueth, 7/15/88, (PB89-189617, A04, MF-A01).

NCEER-88-0044 "SARCF User's Guide: Seismic Analysis of Reinforced Concrete Frames," by Y.S. Chung, C. Meyer and M. Shinozuka, 11/9/88, (PB89-174452, A08, MF-A01).

NCEER-88-0045 "First Expert Panel Meeting on Disaster Research and Planning," edited by J. Pantelic and J. Stoyle, 9/15/88, (PB89-174460, A05, MF-A01).

NCEER-88-0046 "Preliminary Studies of the Effect of Degrading Infill Walls on the Nonlinear Seismic Response of Steel Frames," by C.Z. Chrysostomou, P. Gergely and J.F. Abel, 12/19/88, (PB89-208383, A05, MF-A01).

NCEER-88-0047 "Reinforced Concrete Frame Component Testing Facility - Design, Construction, Instrumentation and Operation," by S.P. Pessiki, C. Conley, T. Bond, P. Gergely and R.N. White, 12/16/88, (PB89-174478, A04, MF-A01).

NCEER-89-0001 "Effects of Protective Cushion and Soil Compliancy on the Response of Equipment Within a Seismically Excited Building," by J.A. HoLung, 2/16/89, (PB89-207179, A04, MF-A01).

NCEER-89-0002 "Statistical Evaluation of Response Modification Factors for Reinforced Concrete Structures," by H.H-M. Hwang and J-W. Jaw, 2/17/89, (PB89-207187, A05, MF-A01).

NCEER-89-0003 "Hysteretic Columns Under Random Excitation," by G-Q. Cai and Y.K. Lin, 1/9/89, (PB89-196513, A03, MF-A01).

NCEER-89-0004 "Experimental Study of `Elephant Foot Bulge' Instability of Thin-Walled Metal Tanks," by Z-H. Jia and R.L. Ketter, 2/22/89, (PB89-207195, A03, MF-A01).

NCEER-89-0005 "Experiment on Performance of Buried Pipelines Across San Andreas Fault," by J. Isenberg, E. Richardson and T.D. O'Rourke, 3/10/89, (PB89-218440, A04, MF-A01). This report is available only through NTIS (see address given above).

NCEER-89-0006 "A Knowledge-Based Approach to Structural Design of Earthquake-Resistant Buildings," by M. Subramani, P. Gergely, C.H. Conley, J.F. Abel and A.H. Zaghw, 1/15/89, (PB89-218465, A06, MF-A01).

NCEER-89-0007 "Liquefaction Hazards and Their Effects on Buried Pipelines," by T.D. O'Rourke and P.A. Lane, 2/1/89, (PB89-218481, A09, MF-A01).

NCEER-89-0008 "Fundamentals of System Identification in Structural Dynamics," by H. Imai, C-B. Yun, O. Maruyama and M. Shinozuka, 1/26/89, (PB89-207211, A04, MF-A01).

NCEER-89-0009 "Effects of the 1985 Michoacan Earthquake on Water Systems and Other Buried Lifelines in Mexico," by A.G. Ayala and M.J. O'Rourke, 3/8/89, (PB89-207229, A06, MF-A01).

NCEER-89-R010 "NCEER Bibliography of Earthquake Education Materials," by K.E.K. Ross, Second Revision, 9/1/89, (PB90-125352, A05, MF-A01). This report is replaced by NCEER-92-0018.

NCEER-89-0011 "Inelastic Three-Dimensional Response Analysis of Reinforced Concrete Building Structures (IDARC-3D), Part I - Modeling," by S.K. Kunnath and A.M. Reinhorn, 4/17/89, (PB90-114612, A07, MF-A01). This report is available only through NTIS (see address given above).

NCEER-89-0012 "Recommended Modifications to ATC-14," by C.D. Poland and J.O. Malley, 4/12/89, (PB90-108648, A15, MF-A01).

NCEER-89-0013 "Repair and Strengthening of Beam-to-Column Connections Subjected to Earthquake Loading," by M. Corazao and A.J. Durrani, 2/28/89, (PB90-109885, A06, MF-A01).

NCEER-89-0014 "Program EXKAL2 for Identification of Structural Dynamic Systems," by O. Maruyama, C-B. Yun, M. Hoshiya and M. Shinozuka, 5/19/89, (PB90-109877, A09, MF-A01).

NCEER-89-0015 "Response of Frames With Bolted Semi-Rigid Connections, Part I - Experimental Study and Analytical Predictions," by P.J. DiCorso, A.M. Reinhorn, J.R. Dickerson, J.B. Radziminski and W.L. Harper, 6/1/89, to be published.

NCEER-89-0016 "ARMA Monte Carlo Simulation in Probabilistic Structural Analysis," by P.D. Spanos and M.P. Mignolet, 7/10/89, (PB90-109893, A03, MF-A01).

NCEER-89-P017 "Preliminary Proceedings from the Conference on Disaster Preparedness - The Place of Earthquake Education in Our Schools," Edited by K.E.K. Ross, 6/23/89, (PB90-108606, A03, MF-A01).

NCEER-89-0017 "Proceedings from the Conference on Disaster Preparedness - The Place of Earthquake Education in Our Schools," Edited by K.E.K. Ross, 12/31/89, (PB90-207895, A012, MF-A02). This report is available only through NTIS (see address given above).

NCEER-89-0018 "Multidimensional Models of Hysteretic Material Behavior for Vibration Analysis of Shape Memory Energy Absorbing Devices, by E.J. Graesser and F.A. Cozzarelli, 6/7/89, (PB90-164146, A04, MF-A01).

NCEER-89-0019 "Nonlinear Dynamic Analysis of Three-Dimensional Base Isolated Structures (3D-BASIS)," by S. Nagarajaiah, A.M. Reinhorn and M.C. Constantinou, 8/3/89, (PB90-161936, A06, MF-A01). This report has been replaced by NCEER-93-0011.

NCEER-89-0020 "Structural Control Considering Time-Rate of Control Forces and Control Rate Constraints," by F.Y. Cheng and C.P. Pantelides, 8/3/89, (PB90-120445, A04, MF-A01).

NCEER-89-0021 "Subsurface Conditions of Memphis and Shelby County," by K.W. Ng, T-S. Chang and H-H.M. Hwang, 7/26/89, (PB90-120437, A03, MF-A01).

NCEER-89-0022 "Seismic Wave Propagation Effects on Straight Jointed Buried Pipelines," by K. Elhmadi and M.J. O'Rourke, 8/24/89, (PB90-162322, A10, MF-A02).

NCEER-89-0023 "Workshop on Serviceability Analysis of Water Delivery Systems," edited by M. Grigoriu, 3/6/89, (PB90-127424, A03, MF-A01).

NCEER-89-0024 "Shaking Table Study of a 1/5 Scale Steel Frame Composed of Tapered Members," by K.C. Chang, J.S. Hwang and G.C. Lee, 9/18/89, (PB90-160169, A04, MF-A01).

NCEER-89-0025 "DYNA1D: A Computer Program for Nonlinear Seismic Site Response Analysis - Technical Documentation," by Jean H. Prevost, 9/14/89, (PB90-161944, A07, MF-A01). This report is available only through NTIS (see address given above).

NCEER-89-0026 "1:4 Scale Model Studies of Active Tendon Systems and Active Mass Dampers for Aseismic Protection," by A.M. Reinhorn, T.T. Soong, R.C. Lin, Y.P. Yang, Y. Fukao, H. Abe and M. Nakai, 9/15/89, (PB90-173246, A10, MF-A02). This report is available only through NTIS (see address given above).

NCEER-89-0027 "Scattering of Waves by Inclusions in a Nonhomogeneous Elastic Half Space Solved by Boundary Element Methods," by P.K. Hadley, A. Askar and A.S. Cakmak, 6/15/89, (PB90-145699, A07, MF-A01).

NCEER-89-0028 "Statistical Evaluation of Deflection Amplification Factors for Reinforced Concrete Structures," by H.H.M. Hwang, J-W. Jaw and A.L. Ch'ng, 8/31/89, (PB90-164633, A05, MF-A01).

NCEER-89-0029 "Bedrock Accelerations in Memphis Area Due to Large New Madrid Earthquakes," by H.H.M. Hwang, C.H.S. Chen and G. Yu, 11/7/89, (PB90-162330, A04, MF-A01).

NCEER-89-0030 "Seismic Behavior and Response Sensitivity of Secondary Structural Systems," by Y.Q. Chen and T.T. Soong, 10/23/89, (PB90-164658, A08, MF-A01).

NCEER-89-0031 "Random Vibration and Reliability Analysis of Primary-Secondary Structural Systems," by Y. Ibrahim, M. Grigoriu and T.T. Soong, 11/10/89, (PB90-161951, A04, MF-A01).

NCEER-89-0032 "Proceedings from the Second U.S. - Japan Workshop on Liquefaction, Large Ground Deformation and Their Effects on Lifelines, September 26-29, 1989," Edited by T.D. O'Rourke and M. Hamada, 12/1/89, (PB90-209388, A22, MF-A03).

NCEER-89-0033 "Deterministic Model for Seismic Damage Evaluation of Reinforced Concrete Structures," by J.M. Bracci, A.M. Reinhorn, J.B. Mander and S.K. Kunnath, 9/27/89, (PB91-108803, A06, MF-A01).

NCEER-89-0034 "On the Relation Between Local and Global Damage Indices," by E. DiPasquale and A.S. Cakmak, 8/15/89, (PB90-173865, A05, MF-A01).

NCEER-89-0035 "Cyclic Undrained Behavior of Nonplastic and Low Plasticity Silts," by A.J. Walker and H.E. Stewart, 7/26/89, (PB90-183518, A10, MF-A01).

NCEER-89-0036 "Liquefaction Potential of Surficial Deposits in the City of Buffalo, New York," by M. Budhu, R. Giese and L. Baumgrass, 1/17/89, (PB90-208455, A04, MF-A01).

NCEER-89-0037 "A Deterministic Assessment of Effects of Ground Motion Incoherence," by A.S. Veletsos and Y. Tang, 7/15/89, (PB90-164294, A03, MF-A01).

NCEER-89-0038 "Workshop on Ground Motion Parameters for Seismic Hazard Mapping," July 17-18, 1989, edited by R.V. Whitman, 12/1/89, (PB90-173923, A04, MF-A01).

NCEER-89-0039 "Seismic Effects on Elevated Transit Lines of the New York City Transit Authority," by C.J. Costantino, C.A. Miller and E. Heymsfield, 12/26/89, (PB90-207887, A06, MF-A01).

NCEER-89-0040 "Centrifugal Modeling of Dynamic Soil-Structure Interaction," by K. Weissman, Supervised by J.H. Prevost, 5/10/89, (PB90-207879, A07, MF-A01).

NCEER-89-0041 "Linearized Identification of Buildings With Cores for Seismic Vulnerability Assessment," by I-K. Ho and A.E. Aktan, 11/1/89, (PB90-251943, A07, MF-A01).

NCEER-90-0001 "Geotechnical and Lifeline Aspects of the October 17, 1989 Loma Prieta Earthquake in San Francisco," by T.D. O'Rourke, H.E. Stewart, F.T. Blackburn and T.S. Dickerman, 1/90, (PB90-208596, A05, MF-A01).

NCEER-90-0002 "Nonnormal Secondary Response Due to Yielding in a Primary Structure," by D.C.K. Chen and L.D. Lutes, 2/28/90, (PB90-251976, A07, MF-A01).

NCEER-90-0003 "Earthquake Education Materials for Grades K-12," by K.E.K. Ross, 4/16/90, (PB91-251984, A05, MF-A05). This report has been replaced by NCEER-92-0018.

NCEER-90-0004 "Catalog of Strong Motion Stations in Eastern North America," by R.W. Busby, 4/3/90, (PB90-251984, A05, MF-A01).

NCEER-90-0005 "NCEER Strong-Motion Data Base: A User Manual for the GeoBase Release (Version 1.0 for the Sun3)," by P. Friberg and K. Jacob, 3/31/90 (PB90-258062, A04, MF-A01).

NCEER-90-0006 "Seismic Hazard Along a Crude Oil Pipeline in the Event of an 1811-1812 Type New Madrid Earthquake," by H.H.M. Hwang and C-H.S. Chen, 4/16/90, (PB90-258054, A04, MF-A01).

NCEER-90-0007 "Site-Specific Response Spectra for Memphis Sheahan Pumping Station," by H.H.M. Hwang and C.S. Lee, 5/15/90, (PB91-108811, A05, MF-A01).

NCEER-90-0008 "Pilot Study on Seismic Vulnerability of Crude Oil Transmission Systems," by T. Ariman, R. Dobry, M. Grigoriu, F. Kozin, M. O'Rourke, T. O'Rourke and M. Shinozuka, 5/25/90, (PB91-108837, A06, MF-A01).

NCEER-90-0009 "A Program to Generate Site Dependent Time Histories: EQGEN," by G.W. Ellis, M. Srinivasan and A.S. Cakmak, 1/30/90, (PB91-108829, A04, MF-A01).

NCEER-90-0010 "Active Isolation for Seismic Protection of Operating Rooms," by M.E. Talbott, Supervised by M. Shinozuka, 6/8/9, (PB91-110205, A05, MF-A01).

NCEER-90-0011 "Program LINEARID for Identification of Linear Structural Dynamic Systems," by C-B. Yun and M. Shinozuka, 6/25/90, (PB91-110312, A08, MF-A01).

NCEER-90-0012 "Two-Dimensional Two-Phase Elasto-Plastic Seismic Response of Earth Dams," by A.N. Yiagos, Supervised by J.H. Prevost, 6/20/90, (PB91-110197, A13, MF-A02).

NCEER-90-0013 "Secondary Systems in Base-Isolated Structures: Experimental Investigation, Stochastic Response and Stochastic Sensitivity," by G.D. Manolis, G. Juhn, M.C. Constantinou and A.M. Reinhorn, 7/1/90, (PB91-110320, A08, MF-A01).

NCEER-90-0014 "Seismic Behavior of Lightly-Reinforced Concrete Column and Beam-Column Joint Details," by S.P. Pessiki, C.H. Conley, P. Gergely and R.N. White, 8/22/90, (PB91-108795, A11, MF-A02).

NCEER-90-0015 "Two Hybrid Control Systems for Building Structures Under Strong Earthquakes," by J.N. Yang and A. Danielians, 6/29/90, (PB91-125393, A04, MF-A01).

NCEER-90-0016 "Instantaneous Optimal Control with Acceleration and Velocity Feedback," by J.N. Yang and Z. Li, 6/29/90, (PB91-125401, A03, MF-A01).

NCEER-90-0017 "Reconnaissance Report on the Northern Iran Earthquake of June 21, 1990," by M. Mehrain, 10/4/90, (PB91-125377, A03, MF-A01).

NCEER-90-0018 "Evaluation of Liquefaction Potential in Memphis and Shelby County," by T.S. Chang, P.S. Tang, C.S. Lee and H. Hwang, 8/10/90, (PB91-125427, A09, MF-A01).

NCEER-90-0019 "Experimental and Analytical Study of a Combined Sliding Disc Bearing and Helical Steel Spring Isolation System," by M.C. Constantinou, A.S. Mokha and A.M. Reinhorn, 10/4/90, (PB91-125385, A06, MF-A01). This report is available only through NTIS (see address given above).

NCEER-90-0020 "Experimental Study and Analytical Prediction of Earthquake Response of a Sliding Isolation System with a Spherical Surface," by A.S. Mokha, M.C. Constantinou and A.M. Reinhorn, 10/11/90, (PB91-125419, A05, MF-A01).

NCEER-90-0021 "Dynamic Interaction Factors for Floating Pile Groups," by G. Gazetas, K. Fan, A. Kaynia and E. Kausel, 9/10/90, (PB91-170381, A05, MF-A01).

NCEER-90-0022 "Evaluation of Seismic Damage Indices for Reinforced Concrete Structures," by S. Rodriguez-Gomez and A.S. Cakmak, 9/30/90, PB91-171322, A06, MF-A01).

NCEER-90-0023 "Study of Site Response at a Selected Memphis Site," by H. Desai, S. Ahmad, E.S. Gazetas and M.R. Oh, 10/11/90, (PB91-196857, A03, MF-A01).

NCEER-90-0024 "A User's Guide to Strongmo: Version 1.0 of NCEER's Strong-Motion Data Access Tool for PCs and Terminals," by P.A. Friberg and C.A.T. Susch, 11/15/90, (PB91-171272, A03, MF-A01).

NCEER-90-0025 "A Three-Dimensional Analytical Study of Spatial Variability of Seismic Ground Motions," by L-L. Hong and A.H.-S. Ang, 10/30/90, (PB91-170399, A09, MF-A01).

NCEER-90-0026 "MUMOID User's Guide - A Program for the Identification of Modal Parameters," by S. Rodriguez-Gomez and E. DiPasquale, 9/30/90, (PB91-171298, A04, MF-A01).

NCEER-90-0027 "SARCF-II User's Guide - Seismic Analysis of Reinforced Concrete Frames," by S. Rodriguez-Gomez, Y.S. Chung and C. Meyer, 9/30/90, (PB91-171280, A05, MF-A01).

NCEER-90-0028 "Viscous Dampers: Testing, Modeling and Application in Vibration and Seismic Isolation," by N. Makris and M.C. Constantinou, 12/20/90 (PB91-190561, A06, MF-A01).

NCEER-90-0029 "Soil Effects on Earthquake Ground Motions in the Memphis Area," by H. Hwang, C.S. Lee, K.W. Ng and T.S. Chang, 8/2/90, (PB91-190751, A05, MF-A01).

NCEER-91-0001 "Proceedings from the Third Japan-U.S. Workshop on Earthquake Resistant Design of Lifeline Facilities and Countermeasures for Soil Liquefaction, December 17-19, 1990," edited by T.D. O'Rourke and M. Hamada, 2/1/91, (PB91-179259, A99, MF-A04).

NCEER-91-0002 "Physical Space Solutions of Non-Proportionally Damped Systems," by M. Tong, Z. Liang and G.C. Lee, 1/15/91, (PB91-179242, A04, MF-A01).

NCEER-91-0003 "Seismic Response of Single Piles and Pile Groups," by K. Fan and G. Gazetas, 1/10/91, (PB92-174994, A04, MF-A01).

NCEER-91-0004 "Damping of Structures: Part 1 - Theory of Complex Damping," by Z. Liang and G. Lee, 10/10/91, (PB92-197235, A12, MF-A03).

NCEER-91-0005 "3D-BASIS - Nonlinear Dynamic Analysis of Three Dimensional Base Isolated Structures: Part II," by S. Nagarajaiah, A.M. Reinhorn and M.C. Constantinou, 2/28/91, (PB91-190553, A07, MF-A01). This report has been replaced by NCEER-93-0011.

NCEER-91-0006 "A Multidimensional Hysteretic Model for Plasticity Deforming Metals in Energy Absorbing Devices," by E.J. Graesser and F.A. Cozzarelli, 4/9/91, (PB92-108364, A04, MF-A01).

NCEER-91-0007 "A Framework for Customizable Knowledge-Based Expert Systems with an Application to a KBES for Evaluating the Seismic Resistance of Existing Buildings," by E.G. Ibarra-Anaya and S.J. Fenves, 4/9/91, (PB91-210930, A08, MF-A01).

NCEER-91-0008 "Nonlinear Analysis of Steel Frames with Semi-Rigid Connections Using the Capacity Spectrum Method," by G.G. Deierlein, S-H. Hsieh, Y-J. Shen and J.F. Abel, 7/2/91, (PB92-113828, A05, MF-A01).

NCEER-91-0009 "Earthquake Education Materials for Grades K-12," by K.E.K. Ross, 4/30/91, (PB91-212142, A06, MF-A01). This report has been replaced by NCEER-92-0018.

NCEER-91-0010 "Phase Wave Velocities and Displacement Phase Differences in a Harmonically Oscillating Pile," by N. Makris and G. Gazetas, 7/8/91, (PB92-108356, A04, MF-A01).

NCEER-91-0011 "Dynamic Characteristics of a Full-Size Five-Story Steel Structure and a 2/5 Scale Model," by K.C. Chang, G.C. Yao, G.C. Lee, D.S. Hao and Y.C. Yeh," 7/2/91, (PB93-116648, A06, MF-A02).

NCEER-91-0012 "Seismic Response of a 2/5 Scale Steel Structure with Added Viscoelastic Dampers," by K.C. Chang, T.T. Soong, S-T. Oh and M.L. Lai, 5/17/91, (PB92-110816, A05, MF-A01).

NCEER-91-0013 "Earthquake Response of Retaining Walls; Full-Scale Testing and Computational Modeling," by S. Alampalli and A-W.M. Elgamal, 6/20/91, to be published.

NCEER-91-0014 "3D-BASIS-M: Nonlinear Dynamic Analysis of Multiple Building Base Isolated Structures," by P.C. Tsopelas, S. Nagarajaiah, M.C. Constantinou and A.M. Reinhorn, 5/28/91, (PB92-113885, A09, MF-A02).

NCEER-91-0015 "Evaluation of SEAOC Design Requirements for Sliding Isolated Structures," by D. Theodossiou and M.C. Constantinou, 6/10/91, (PB92-114602, A11, MF-A03).

NCEER-91-0016 "Closed-Loop Modal Testing of a 27-Story Reinforced Concrete Flat Plate-Core Building," by H.R. Somaprasad, T. Toksoy, H. Yoshiyuki and A.E. Aktan, 7/15/91, (PB92-129980, A07, MF-A02).

NCEER-91-0017 "Shake Table Test of a 1/6 Scale Two-Story Lightly Reinforced Concrete Building," by A.G. El-Attar, R.N. White and P. Gergely, 2/28/91, (PB92-222447, A06, MF-A02).

NCEER-91-0018 "Shake Table Test of a 1/8 Scale Three-Story Lightly Reinforced Concrete Building," by A.G. El-Attar, R.N. White and P. Gergely, 2/28/91, (PB93-116630, A08, MF-A02).

NCEER-91-0019 "Transfer Functions for Rigid Rectangular Foundations," by A.S. Veletsos, A.M. Prasad and W.H. Wu, 7/31/91, to be published.

NCEER-91-0020 "Hybrid Control of Seismic-Excited Nonlinear and Inelastic Structural Systems," by J.N. Yang, Z. Li and A. Danielians, 8/1/91, (PB92-143171, A06, MF-A02).

NCEER-91-0021 "The NCEER-91 Earthquake Catalog: Improved Intensity-Based Magnitudes and Recurrence Relations for U.S. Earthquakes East of New Madrid," by L. Seeber and J.G. Armbruster, 8/28/91, (PB92-176742, A06, MF-A02).

NCEER-91-0022 "Proceedings from the Implementation of Earthquake Planning and Education in Schools: The Need for Change - The Roles of the Changemakers," by K.E.K. Ross and F. Winslow, 7/23/91, (PB92-129998, A12, MF-A03).

NCEER-91-0023 "A Study of Reliability-Based Criteria for Seismic Design of Reinforced Concrete Frame Buildings," by H.H.M. Hwang and H-M. Hsu, 8/10/91, (PB92-140235, A09, MF-A02).

NCEER-91-0024 "Experimental Verification of a Number of Structural System Identification Algorithms," by R.G. Ghanem, H. Gavin and M. Shinozuka, 9/18/91, (PB92-176577, A18, MF-A04).

NCEER-91-0025 "Probabilistic Evaluation of Liquefaction Potential," by H.H.M. Hwang and C.S. Lee," 11/25/91, (PB92-143429, A05, MF-A01).

NCEER-91-0026 "Instantaneous Optimal Control for Linear, Nonlinear and Hysteretic Structures - Stable Controllers," by J.N. Yang and Z. Li, 11/15/91, (PB92-163807, A04, MF-A01).

NCEER-91-0027 "Experimental and Theoretical Study of a Sliding Isolation System for Bridges," by M.C. Constantinou, A. Kartoum, A.M. Reinhorn and P. Bradford, 11/15/91, (PB92-176973, A10, MF-A03).

NCEER-92-0001 "Case Studies of Liquefaction and Lifeline Performance During Past Earthquakes, Volume 1: Japanese Case Studies," Edited by M. Hamada and T. O'Rourke, 2/17/92, (PB92-197243, A18, MF-A04).

NCEER-92-0002 "Case Studies of Liquefaction and Lifeline Performance During Past Earthquakes, Volume 2: United States Case Studies," Edited by T. O'Rourke and M. Hamada, 2/17/92, (PB92-197250, A20, MF-A04).

NCEER-92-0003 "Issues in Earthquake Education," Edited by K. Ross, 2/3/92, (PB92-222389, A07, MF-A02).

NCEER-92-0004 "Proceedings from the First U.S. - Japan Workshop on Earthquake Protective Systems for Bridges," Edited by I.G. Buckle, 2/4/92, (PB94-142239, A99, MF-A06).

NCEER-92-0005 "Seismic Ground Motion from a Haskell-Type Source in a Multiple-Layered Half-Space," A.P. Theoharis, G. Deodatis and M. Shinozuka, 1/2/92, to be published.

NCEER-92-0006 "Proceedings from the Site Effects Workshop," Edited by R. Whitman, 2/29/92, (PB92-197201, A04, MF-A01).

NCEER-92-0007 "Engineering Evaluation of Permanent Ground Deformations Due to Seismically-Induced Liquefaction," by M.H. Baziar, R. Dobry and A-W.M. Elgamal, 3/24/92, (PB92-222421, A13, MF-A03).

NCEER-92-0008 "A Procedure for the Seismic Evaluation of Buildings in the Central and Eastern United States," by C.D. Poland and J.O. Malley, 4/2/92, (PB92-222439, A20, MF-A04).

NCEER-92-0009 "Experimental and Analytical Study of a Hybrid Isolation System Using Friction Controllable Sliding Bearings," by M.Q. Feng, S. Fujii and M. Shinozuka, 5/15/92, (PB93-150282, A06, MF-A02).

NCEER-92-0010 "Seismic Resistance of Slab-Column Connections in Existing Non-Ductile Flat-Plate Buildings," by A.J. Durrani and Y. Du, 5/18/92, (PB93-116812, A06, MF-A02).

NCEER-92-0011 "The Hysteretic and Dynamic Behavior of Brick Masonry Walls Upgraded by Ferrocement Coatings Under Cyclic Loading and Strong Simulated Ground Motion," by H. Lee and S.P. Prawel, 5/11/92, to be published.

NCEER-92-0012 "Study of Wire Rope Systems for Seismic Protection of Equipment in Buildings," by G.F. Demetriades, M.C. Constantinou and A.M. Reinhorn, 5/20/92, (PB93-116655, A08, MF-A02).

NCEER-92-0013 "Shape Memory Structural Dampers: Material Properties, Design and Seismic Testing," by P.R. Witting and F.A. Cozzarelli, 5/26/92, (PB93-116663, A05, MF-A01).

NCEER-92-0014 "Longitudinal Permanent Ground Deformation Effects on Buried Continuous Pipelines," by M.J. O'Rourke, and C. Nordberg, 6/15/92, (PB93-116671, A08, MF-A02).

NCEER-92-0015 "A Simulation Method for Stationary Gaussian Random Functions Based on the Sampling Theorem," by M. Grigoriu and S. Balopoulou, 6/11/92, (PB93-127496, A05, MF-A01).

NCEER-92-0016 "Gravity-Load-Designed Reinforced Concrete Buildings: Seismic Evaluation of Existing Construction and Detailing Strategies for Improved Seismic Resistance," by G.W. Hoffmann, S.K. Kunnath, A.M. Reinhorn and J.B. Mander, 7/15/92, (PB94-142007, A08, MF-A02).

NCEER-92-0017 "Observations on Water System and Pipeline Performance in the Limón Area of Costa Rica Due to the April 22, 1991 Earthquake," by M. O'Rourke and D. Ballantyne, 6/30/92, (PB93-126811, A06, MF-A02).

NCEER-92-0018 "Fourth Edition of Earthquake Education Materials for Grades K-12," Edited by K.E.K. Ross, 8/10/92, (PB93-114023, A07, MF-A02).

NCEER-92-0019 "Proceedings from the Fourth Japan-U.S. Workshop on Earthquake Resistant Design of Lifeline Facilities and Countermeasures for Soil Liquefaction," Edited by M. Hamada and T.D. O'Rourke, 8/12/92, (PB93-163939, A99, MF-E11).

NCEER-92-0020 "Active Bracing System: A Full Scale Implementation of Active Control," by A.M. Reinhorn, T.T. Soong, R.C. Lin, M.A. Riley, Y.P. Wang, S. Aizawa and M. Higashino, 8/14/92, (PB93-127512, A06, MF-A02).

NCEER-92-0021 "Empirical Analysis of Horizontal Ground Displacement Generated by Liquefaction-Induced Lateral Spreads," by S.F. Bartlett and T.L. Youd, 8/17/92, (PB93-188241, A06, MF-A02).

NCEER-92-0022 "IDARC Version 3.0: Inelastic Damage Analysis of Reinforced Concrete Structures," by S.K. Kunnath, A.M. Reinhorn and R.F. Lobo, 8/31/92, (PB93-227502, A07, MF-A02).

NCEER-92-0023 "A Semi-Empirical Analysis of Strong-Motion Peaks in Terms of Seismic Source, Propagation Path and Local Site Conditions, by M. Kamiyama, M.J. O'Rourke and R. Flores-Berrones, 9/9/92, (PB93-150266, A08, MF-A02).

NCEER-92-0024 "Seismic Behavior of Reinforced Concrete Frame Structures with Nonductile Details, Part I: Summary of Experimental Findings of Full Scale Beam-Column Joint Tests," by A. Beres, R.N. White and P. Gergely, 9/30/92, (PB93-227783, A05, MF-A01).

NCEER-92-0025 "Experimental Results of Repaired and Retrofitted Beam-Column Joint Tests in Lightly Reinforced Concrete Frame Buildings," by A. Beres, S. El-Borgi, R.N. White and P. Gergely, 10/29/92, (PB93-227791, A05, MF-A01).

NCEER-92-0026 "A Generalization of Optimal Control Theory: Linear and Nonlinear Structures," by J.N. Yang, Z. Li and S. Vongchavalitkul, 11/2/92, (PB93-188621, A05, MF-A01).

NCEER-92-0027 "Seismic Resistance of Reinforced Concrete Frame Structures Designed Only for Gravity Loads: Part I - Design and Properties of a One-Third Scale Model Structure," by J.M. Bracci, A.M. Reinhorn and J.B. Mander, 12/1/92, (PB94-104502, A08, MF-A02).

NCEER-92-0028 "Seismic Resistance of Reinforced Concrete Frame Structures Designed Only for Gravity Loads: Part II - Experimental Performance of Subassemblages," by L.E. Aycardi, J.B. Mander and A.M. Reinhorn, 12/1/92, (PB94-104510, A08, MF-A02).

NCEER-92-0029 "Seismic Resistance of Reinforced Concrete Frame Structures Designed Only for Gravity Loads: Part III - Experimental Performance and Analytical Study of a Structural Model," by J.M. Bracci, A.M. Reinhorn and J.B. Mander, 12/1/92, (PB93-227528, A09, MF-A01).

NCEER-92-0030 "Evaluation of Seismic Retrofit of Reinforced Concrete Frame Structures: Part I - Experimental Performance of Retrofitted Subassemblages," by D. Choudhuri, J.B. Mander and A.M. Reinhorn, 12/8/92, (PB93-198307, A07, MF-A02).

NCEER-92-0031 "Evaluation of Seismic Retrofit of Reinforced Concrete Frame Structures: Part II - Experimental Performance and Analytical Study of a Retrofitted Structural Model," by J.M. Bracci, A.M. Reinhorn and J.B. Mander, 12/8/92, (PB93-198315, A09, MF-A03).

NCEER-92-0032 "Experimental and Analytical Investigation of Seismic Response of Structures with Supplemental Fluid Viscous Dampers," by M.C. Constantinou and M.D. Symans, 12/21/92, (PB93-191435, A10, MF-A03). This report is available only through NTIS (see address given above).

NCEER-92-0033 "Reconnaissance Report on the Cairo, Egypt Earthquake of October 12, 1992," by M. Khater, 12/23/92, (PB93-188621, A03, MF-A01).

NCEER-92-0034 "Low-Level Dynamic Characteristics of Four Tall Flat-Plate Buildings in New York City," by H. Gavin, S. Yuan, J. Grossman, E. Pekelis and K. Jacob, 12/28/92, (PB93-188217, A07, MF-A02).

NCEER-93-0001 "An Experimental Study on the Seismic Performance of Brick-Infilled Steel Frames With and Without Retrofit," by J.B. Mander, B. Nair, K. Wojtkowski and J. Ma, 1/29/93, (PB93-227510, A07, MF-A02).

NCEER-93-0002 "Social Accounting for Disaster Preparedness and Recovery Planning," by S. Cole, E. Pantoja and V. Razak, 2/22/93, (PB94-142114, A12, MF-A03).

NCEER-93-0003 "Assessment of 1991 NEHRP Provisions for Nonstructural Components and Recommended Revisions," by T.T. Soong, G. Chen, Z. Wu, R-H. Zhang and M. Grigoriu, 3/1/93, (PB93-188639, A06, MF-A02).

NCEER-93-0004 "Evaluation of Static and Response Spectrum Analysis Procedures of SEAOC/UBC for Seismic Isolated Structures," by C.W. Winters and M.C. Constantinou, 3/23/93, (PB93-198299, A10, MF-A03).

NCEER-93-0005 "Earthquakes in the Northeast - Are We Ignoring the Hazard? A Workshop on Earthquake Science and Safety for Educators," edited by K.E.K. Ross, 4/2/93, (PB94-103066, A09, MF-A02).

NCEER-93-0006 "Inelastic Response of Reinforced Concrete Structures with Viscoelastic Braces," by R.F. Lobo, J.M. Bracci, K.L. Shen, A.M. Reinhorn and T.T. Soong, 4/5/93, (PB93-227486, A05, MF-A02).

NCEER-93-0007 "Seismic Testing of Installation Methods for Computers and Data Processing Equipment," by K. Kosar, T.T. Soong, K.L. Shen, J.A. HoLung and Y.K. Lin, 4/12/93, (PB93-198299, A07, MF-A02).

NCEER-93-0008 "Retrofit of Reinforced Concrete Frames Using Added Dampers," by A. Reinhorn, M. Constantinou and C. Li, to be published.

NCEER-93-0009 "Seismic Behavior and Design Guidelines for Steel Frame Structures with Added Viscoelastic Dampers," by K.C. Chang, M.L. Lai, T.T. Soong, D.S. Hao and Y.C. Yeh, 5/1/93, (PB94-141959, A07, MF-A02).

NCEER-93-0010 "Seismic Performance of Shear-Critical Reinforced Concrete Bridge Piers," by J.B. Mander, S.M. Waheed, M.T.A. Chaudhary and S.S. Chen, 5/12/93, (PB93-227494, A08, MF-A02).

NCEER-93-0011 "3D-BASIS-TABS: Computer Program for Nonlinear Dynamic Analysis of Three Dimensional Base Isolated Structures," by S. Nagarajaiah, C. Li, A.M. Reinhorn and M.C. Constantinou, 8/2/93, (PB94-141819, A09, MF-A02).

NCEER-93-0012 "Effects of Hydrocarbon Spills from an Oil Pipeline Break on Ground Water," by O.J. Helweg and H.H.M. Hwang, 8/3/93, (PB94-141942, A06, MF-A02).

NCEER-93-0013 "Simplified Procedures for Seismic Design of Nonstructural Components and Assessment of Current Code Provisions," by M.P. Singh, L.E. Suarez, E.E. Matheu and G.O. Maldonado, 8/4/93, (PB94-141827, A09, MF-A02).

NCEER-93-0014 "An Energy Approach to Seismic Analysis and Design of Secondary Systems," by G. Chen and T.T. Soong, 8/6/93, (PB94-142767, A11, MF-A03).

NCEER-93-0015 "Proceedings from School Sites: Becoming Prepared for Earthquakes - Commemorating the Third Anniversary of the Loma Prieta Earthquake," Edited by F.E. Winslow and K.E.K. Ross, 8/16/93, (PB94-154275, A16, MF-A02).

NCEER-93-0016 "Reconnaissance Report of Damage to Historic Monuments in Cairo, Egypt Following the October 12, 1992 Dahshur Earthquake," by D. Sykora, D. Look, G. Croci, E. Karaesmen and E. Karaesmen, 8/19/93, (PB94-142221, A08, MF-A02).

NCEER-93-0017 "The Island of Guam Earthquake of August 8, 1993," by S.W. Swan and S.K. Harris, 9/30/93, (PB94-141843, A04, MF-A01).

NCEER-93-0018 "Engineering Aspects of the October 12, 1992 Egyptian Earthquake," by A.W. Elgamal, M. Amer, K. Adalier and A. Abul-Fadl, 10/7/93, (PB94-141983, A05, MF-A01).

NCEER-93-0019 "Development of an Earthquake Motion Simulator and its Application in Dynamic Centrifuge Testing," by I. Krstelj, Supervised by J.H. Prevost, 10/23/93, (PB94-181773, A-10, MF-A03).

NCEER-93-0020 "NCEER-Taisei Corporation Research Program on Sliding Seismic Isolation Systems for Bridges: Experimental and Analytical Study of a Friction Pendulum System (FPS)," by M.C. Constantinou, P. Tsopelas, Y-S. Kim and S. Okamoto, 11/1/93, (PB94-142775, A08, MF-A02).

NCEER-93-0021 "Finite Element Modeling of Elastomeric Seismic Isolation Bearings," by L.J. Billings, Supervised by R. Shepherd, 11/8/93, to be published.

NCEER-93-0022 "Seismic Vulnerability of Equipment in Critical Facilities: Life-Safety and Operational Consequences," by K. Porter, G.S. Johnson, M.M. Zadeh, C. Scawthorn and S. Eder, 11/24/93, (PB94-181765, A16, MF-A03).

NCEER-93-0023 "Hokkaido Nansei-oki, Japan Earthquake of July 12, 1993, by P.I. Yanev and C.R. Scawthorn, 12/23/93, (PB94-181500, A07, MF-A01).

NCEER-94-0001 "An Evaluation of Seismic Serviceability of Water Supply Networks with Application to the San Francisco Auxiliary Water Supply System," by I. Markov, Supervised by M. Grigoriu and T. O'Rourke, 1/21/94, (PB94-204013, A07, MF-A02).

NCEER-94-0002 "NCEER-Taisei Corporation Research Program on Sliding Seismic Isolation Systems for Bridges: Experimental and Analytical Study of Systems Consisting of Sliding Bearings, Rubber Restoring Force Devices and Fluid Dampers," Volumes I and II, by P. Tsopelas, S. Okamoto, M.C. Constantinou, D. Ozaki and S. Fujii, 2/4/94, (PB94-181740, A09, MF-A02 and PB94-181757, A12, MF-A03).

NCEER-94-0003 "A Markov Model for Local and Global Damage Indices in Seismic Analysis," by S. Rahman and M. Grigoriu, 2/18/94, (PB94-206000, A12, MF-A03).

NCEER-94-0004 "Proceedings from the NCEER Workshop on Seismic Response of Masonry Infills," edited by D.P. Abrams, 3/1/94, (PB94-180783, A07, MF-A02).

NCEER-94-0005 "The Northridge, California Earthquake of January 17, 1994: General Reconnaissance Report," edited by J.D. Goltz, 3/11/94, (PB94-193943, A10, MF-A03).

NCEER-94-0006 "Seismic Energy Based Fatigue Damage Analysis of Bridge Columns: Part I - Evaluation of Seismic Capacity," by G.A. Chang and J.B. Mander, 3/14/94, (PB94-219185, A11, MF-A03).

NCEER-94-0007 "Seismic Isolation of Multi-Story Frame Structures Using Spherical Sliding Isolation Systems," by T.M. Al-Hussaini, V.A. Zayas and M.C. Constantinou, 3/17/94, (PB94-193745, A09, MF-A02).

NCEER-94-0008 "The Northridge, California Earthquake of January 17, 1994: Performance of Highway Bridges," edited by I.G. Buckle, 3/24/94, (PB94-193851, A06, MF-A02).

NCEER-94-0009 "Proceedings of the Third U.S.-Japan Workshop on Earthquake Protective Systems for Bridges," edited by I.G. Buckle and I. Friedland, 3/31/94, (PB94-195815, A99, MF-A06).

NCEER-94-0010 "3D-BASIS-ME: Computer Program for Nonlinear Dynamic Analysis of Seismically Isolated Single and Multiple Structures and Liquid Storage Tanks," by P.C. Tsopelas, M.C. Constantinou and A.M. Reinhorn, 4/12/94, (PB94-204922, A09, MF-A02).

NCEER-94-0011 "The Northridge, California Earthquake of January 17, 1994: Performance of Gas Transmission Pipelines," by T.D. O'Rourke and M.C. Palmer, 5/16/94, (PB94-204989, A05, MF-A01).

NCEER-94-0012 "Feasibility Study of Replacement Procedures and Earthquake Performance Related to Gas Transmission Pipelines," by T.D. O'Rourke and M.C. Palmer, 5/25/94, (PB94-206638, A09, MF-A02).

NCEER-94-0013 "Seismic Energy Based Fatigue Damage Analysis of Bridge Columns: Part II - Evaluation of Seismic Demand," by G.A. Chang and J.B. Mander, 6/1/94, (PB95-18106, A08, MF-A02).

NCEER-94-0014 "NCEER-Taisei Corporation Research Program on Sliding Seismic Isolation Systems for Bridges: Experimental and Analytical Study of a System Consisting of Sliding Bearings and Fluid Restoring Force/Damping Devices," by P. Tsopelas and M.C. Constantinou, 6/13/94, (PB94-219144, A10, MF-A03).

NCEER-94-0015 "Generation of Hazard-Consistent Fragility Curves for Seismic Loss Estimation Studies," by H. Hwang and J-R. Huo, 6/14/94, (PB95-181996, A09, MF-A02).

NCEER-94-0016 "Seismic Study of Building Frames with Added Energy-Absorbing Devices," by W.S. Pong, C.S. Tsai and G.C. Lee, 6/20/94, (PB94-219136, A10, A03).

NCEER-94-0017 "Sliding Mode Control for Seismic-Excited Linear and Nonlinear Civil Engineering Structures," by J. Yang, J. Wu, A. Agrawal and Z. Li, 6/21/94, (PB95-138483, A06, MF-A02).

NCEER-94-0018 "3D-BASIS-TABS Version 2.0: Computer Program for Nonlinear Dynamic Analysis of Three Dimensional Base Isolated Structures," by A.M. Reinhorn, S. Nagarajaiah, M.C. Constantinou, P. Tsopelas and R. Li, 6/22/94, (PB95-182176, A08, MF-A02).

NCEER-94-0019 "Proceedings of the International Workshop on Civil Infrastructure Systems: Application of Intelligent Systems and Advanced Materials on Bridge Systems," Edited by G.C. Lee and K.C. Chang, 7/18/94, (PB95-252474, A20, MF-A04).

NCEER-94-0020 "Study of Seismic Isolation Systems for Computer Floors," by V. Lambrou and M.C. Constantinou, 7/19/94, (PB95-138533, A10, MF-A03).

NCEER-94-0021 "Proceedings of the U.S.-Italian Workshop on Guidelines for Seismic Evaluation and Rehabilitation of Unreinforced Masonry Buildings," Edited by D.P. Abrams and G.M. Calvi, 7/20/94, (PB95-138749, A13, MF-A03).

NCEER-94-0022 "NCEER-Taisei Corporation Research Program on Sliding Seismic Isolation Systems for Bridges: Experimental and Analytical Study of a System Consisting of Lubricated PTFE Sliding Bearings and Mild Steel Dampers," by P. Tsopelas and M.C. Constantinou, 7/22/94, (PB95-182184, A08, MF-A02).

NCEER-94-0023 “Development of Reliability-Based Design Criteria for Buildings Under Seismic Load,” by Y.K. Wen, H. Hwang and M. Shinozuka, 8/1/94, (PB95-211934, A08, MF-A02).

NCEER-94-0024 “Experimental Verification of Acceleration Feedback Control Strategies for an Active Tendon System,” by S.J. Dyke, B.F. Spencer, Jr., P. Quast, M.K. Sain, D.C. Kaspari, Jr. and T.T. Soong, 8/29/94, (PB95-212320, A05, MF-A01).

NCEER-94-0025 “Seismic Retrofitting Manual for Highway Bridges,” Edited by I.G. Buckle and I.F. Friedland, published by the Federal Highway Administration (PB95-212676, A15, MF-A03).

NCEER-94-0026 “Proceedings from the Fifth U.S.-Japan Workshop on Earthquake Resistant Design of Lifeline Facilities and Countermeasures Against Soil Liquefaction,” Edited by T.D. O’Rourke and M. Hamada, 11/7/94, (PB95-220802, A99, MF-E08).

NCEER-95-0001 "Experimental and Analytical Investigation of Seismic Retrofit of Structures with Supplemental Damping: Part 1 - Fluid Viscous Damping Devices," by A.M. Reinhorn, C. Li and M.C. Constantinou, 1/3/95, (PB95-266599, A09, MF-A02).

NCEER-95-0002 "Experimental and Analytical Study of Low-Cycle Fatigue Behavior of Semi-Rigid Top-And-Seat Angle Connections," by G. Pekcan, J.B. Mander and S.S. Chen, 1/5/95, (PB95-220042, A07, MF-A02).

NCEER-95-0003 "NCEER-ATC Joint Study on Fragility of Buildings," by T. Anagnos, C. Rojahn and A.S. Kiremidjian, 1/20/95, (PB95-220026, A06, MF-A02).

NCEER-95-0004 "Nonlinear Control Algorithms for Peak Response Reduction," by Z. Wu, T.T. Soong, V. Gattulli and R.C. Lin, 2/16/95, (PB95-220349, A05, MF-A01).

NCEER-95-0005 "Pipeline Replacement Feasibility Study: A Methodology for Minimizing Seismic and Corrosion Risks to Underground Natural Gas Pipelines," by R.T. Eguchi, H.A. Seligson and D.G. Honegger, 3/2/95, (PB95-252326, A06, MF-A02).

NCEER-95-0006 "Evaluation of Seismic Performance of an 11-Story Frame Building During the 1994 Northridge Earthquake," by F. Naeim, R. DiSulio, K. Benuska, A. Reinhorn and C. Li, to be published.

NCEER-95-0007 "Prioritization of Bridges for Seismic Retrofitting," by N. Basöz and A.S. Kiremidjian, 4/24/95, (PB95-252300, A08, MF-A02).

NCEER-95-0008 "Method for Developing Motion Damage Relationships for Reinforced Concrete Frames," by A. Singhal and A.S. Kiremidjian, 5/11/95, (PB95-266607, A06, MF-A02).

NCEER-95-0009 "Experimental and Analytical Investigation of Seismic Retrofit of Structures with Supplemental Damping: Part II - Friction Devices," by C. Li and A.M. Reinhorn, 7/6/95, (PB96-128087, A11, MF-A03).

NCEER-95-0010 "Experimental Performance and Analytical Study of a Non-Ductile Reinforced Concrete Frame Structure Retrofitted with Elastomeric Spring Dampers," by G. Pekcan, J.B. Mander and S.S. Chen, 7/14/95, (PB96-137161, A08, MF-A02).

NCEER-95-0011 "Development and Experimental Study of Semi-Active Fluid Damping Devices for Seismic Protection of Structures," by M.D. Symans and M.C. Constantinou, 8/3/95, (PB96-136940, A23, MF-A04).

NCEER-95-0012 "Real-Time Structural Parameter Modification (RSPM): Development of Innervated Structures," by Z. Liang, M. Tong and G.C. Lee, 4/11/95, (PB96-137153, A06, MF-A01).

NCEER-95-0013 "Experimental and Analytical Investigation of Seismic Retrofit of Structures with Supplemental Damping: Part III - Viscous Damping Walls," by A.M. Reinhorn and C. Li, 10/1/95, (PB96-176409, A11, MF-A03).

NCEER-95-0014 "Seismic Fragility Analysis of Equipment and Structures in a Memphis Electric Substation," by J-R. Huo and H.H.M. Hwang, 8/10/95, (PB96-128087, A09, MF-A02).

NCEER-95-0015 "The Hanshin-Awaji Earthquake of January 17, 1995: Performance of Lifelines," Edited by M. Shinozuka, 11/3/95, (PB96-176383, A15, MF-A03).

NCEER-95-0016 "Highway Culvert Performance During Earthquakes," by T.L. Youd and C.J. Beckman, available as NCEER-96-0015.

NCEER-95-0017 "The Hanshin-Awaji Earthquake of January 17, 1995: Performance of Highway Bridges," Edited by I.G. Buckle, 12/1/95, to be published.

NCEER-95-0018 "Modeling of Masonry Infill Panels for Structural Analysis," by A.M. Reinhorn, A. Madan, R.E. Valles, Y. Reichmann and J.B. Mander, 12/8/95, (PB97-110886, MF-A01, A06).

NCEER-95-0019 "Optimal Polynomial Control for Linear and Nonlinear Structures," by A.K. Agrawal and J.N. Yang, 12/11/95, (PB96-168737, A07, MF-A02).

NCEER-95-0020 "Retrofit of Non-Ductile Reinforced Concrete Frames Using Friction Dampers," by R.S. Rao, P. Gergely and R.N. White, 12/22/95, (PB97-133508, A10, MF-A02).

NCEER-95-0021 "Parametric Results for Seismic Response of Pile-Supported Bridge Bents," by G. Mylonakis, A. Nikolaou and G. Gazetas, 12/22/95, (PB97-100242, A12, MF-A03).

NCEER-95-0022 "Kinematic Bending Moments in Seismically Stressed Piles," by A. Nikolaou, G. Mylonakis and G. Gazetas, 12/23/95, (PB97-113914, MF-A03, A13).

NCEER-96-0001 "Dynamic Response of Unreinforced Masonry Buildings with Flexible Diaphragms," by A.C. Costley and D.P. Abrams," 10/10/96, (PB97-133573, MF-A03, A15).

NCEER-96-0002 "State of the Art Review: Foundations and Retaining Structures," by I. Po Lam, to be published.

NCEER-96-0003 "Ductility of Rectangular Reinforced Concrete Bridge Columns with Moderate Confinement," by N. Wehbe, M. Saiidi, D. Sanders and B. Douglas, 11/7/96, (PB97-133557, A06, MF-A02).

NCEER-96-0004 "Proceedings of the Long-Span Bridge Seismic Research Workshop," edited by I.G. Buckle and I.M. Friedland, to be published.

NCEER-96-0005 "Establish Representative Pier Types for Comprehensive Study: Eastern United States," by J. Kulicki and Z. Prucz, 5/28/96, (PB98-119217, A07, MF-A02).

NCEER-96-0006 "Establish Representative Pier Types for Comprehensive Study: Western United States," by R. Imbsen, R.A. Schamber and T.A. Osterkamp, 5/28/96, (PB98-118607, A07, MF-A02).

NCEER-96-0007 "Nonlinear Control Techniques for Dynamical Systems with Uncertain Parameters," by R.G. Ghanem and M.I. Bujakov, 5/27/96, (PB97-100259, A17, MF-A03).

NCEER-96-0008 "Seismic Evaluation of a 30-Year Old Non-Ductile Highway Bridge Pier and Its Retrofit," by J.B. Mander, B. Mahmoodzadegan, S. Bhadra and S.S. Chen, 5/31/96, (PB97-110902, MF-A03, A10).

NCEER-96-0009 "Seismic Performance of a Model Reinforced Concrete Bridge Pier Before and After Retrofit," by J.B. Mander, J.H. Kim and C.A. Ligozio, 5/31/96, (PB97-110910, MF-A02, A10).

NCEER-96-0010 "IDARC2D Version 4.0: A Computer Program for the Inelastic Damage Analysis of Buildings," by R.E. Valles, A.M. Reinhorn, S.K. Kunnath, C. Li and A. Madan, 6/3/96, (PB97-100234, A17, MF-A03).

NCEER-96-0011 "Estimation of the Economic Impact of Multiple Lifeline Disruption: Memphis Light, Gas and Water Division Case Study," by S.E. Chang, H.A. Seligson and R.T. Eguchi, 8/16/96, (PB97-133490, A11, MF-A03).

NCEER-96-0012 "Proceedings from the Sixth Japan-U.S. Workshop on Earthquake Resistant Design of Lifeline Facilities and Countermeasures Against Soil Liquefaction, Edited by M. Hamada and T. O'Rourke, 9/11/96, (PB97-133581, A99, MF-A06).

NCEER-96-0013 "Chemical Hazards, Mitigation and Preparedness in Areas of High Seismic Risk: A Methodology for Estimating the Risk of Post-Earthquake Hazardous Materials Release," by H.A. Seligson, R.T. Eguchi, K.J. Tierney and K. Richmond, 11/7/96, (PB97-133565, MF-A02, A08).

NCEER-96-0014 "Response of Steel Bridge Bearings to Reversed Cyclic Loading," by J.B. Mander, D-K. Kim, S.S. Chen and G.J. Premus, 11/13/96, (PB97-140735, A12, MF-A03).

NCEER-96-0015 "Highway Culvert Performance During Past Earthquakes," by T.L. Youd and C.J. Beckman, 11/25/96, (PB97-133532, A06, MF-A01).

NCEER-97-0001 "Evaluation, Prevention and Mitigation of Pounding Effects in Building Structures," by R.E. Valles and A.M. Reinhorn, 2/20/97, (PB97-159552, A14, MF-A03).

NCEER-97-0002 "Seismic Design Criteria for Bridges and Other Highway Structures," by C. Rojahn, R. Mayes, D.G. Anderson, J. Clark, J.H. Hom, R.V. Nutt and M.J. O'Rourke, 4/30/97, (PB97-194658, A06, MF-A03).

NCEER-97-0003 “Proceedings of the U.S.-Italian Workshop on Seismic Evaluation and Retrofit,” Edited by D.P. Abrams and G.M. Calvi, 3/19/97, (PB97-194666, A13, MF-A03).

NCEER-97-0004 "Investigation of Seismic Response of Buildings with Linear and Nonlinear Fluid Viscous Dampers," by A.A. Seleemah and M.C. Constantinou, 5/21/97, (PB98-109002, A15, MF-A03).

NCEER-97-0005 "Proceedings of the Workshop on Earthquake Engineering Frontiers in Transportation Facilities," edited by G.C. Lee and I.M. Friedland, 8/29/97, (PB98-128911, A25, MR-A04).

NCEER-97-0006 "Cumulative Seismic Damage of Reinforced Concrete Bridge Piers," by S.K. Kunnath, A. El-Bahy, A. Taylor and W. Stone, 9/2/97, (PB98-108814, A11, MF-A03).

NCEER-97-0007 "Structural Details to Accommodate Seismic Movements of Highway Bridges and Retaining Walls," by R.A. Imbsen, R.A. Schamber, E. Thorkildsen, A. Kartoum, B.T. Martin, T.N. Rosser and J.M. Kulicki, 9/3/97, (PB98-108996, A09, MF-A02).

NCEER-97-0008 "A Method for Earthquake Motion-Damage Relationships with Application to Reinforced Concrete Frames," by A. Singhal and A.S. Kiremidjian, 9/10/97, (PB98-108988, A13, MF-A03).

NCEER-97-0009 "Seismic Analysis and Design of Bridge Abutments Considering Sliding and Rotation," by K. Fishman and R. Richards, Jr., 9/15/97, (PB98-108897, A06, MF-A02).

NCEER-97-0010 "Proceedings of the FHWA/NCEER Workshop on the National Representation of Seismic Ground Motion for New and Existing Highway Facilities," edited by I.M. Friedland, M.S. Power and R.L. Mayes, 9/22/97, (PB98-128903, A21, MF-A04).

NCEER-97-0011 "Seismic Analysis for Design or Retrofit of Gravity Bridge Abutments," by K.L. Fishman, R. Richards, Jr. and R.C. Divito, 10/2/97, (PB98-128937, A08, MF-A02).

NCEER-97-0012 "Evaluation of Simplified Methods of Analysis for Yielding Structures," by P. Tsopelas, M.C. Constantinou, C.A. Kircher and A.S. Whittaker, 10/31/97, (PB98-128929, A10, MF-A03).

NCEER-97-0013 "Seismic Design of Bridge Columns Based on Control and Repairability of Damage," by C-T. Cheng and J.B. Mander, 12/8/97, (PB98-144249, A11, MF-A03).

NCEER-97-0014 "Seismic Resistance of Bridge Piers Based on Damage Avoidance Design," by J.B. Mander and C-T. Cheng, 12/10/97, (PB98-144223, A09, MF-A02).

NCEER-97-0015 “Seismic Response of Nominally Symmetric Systems with Strength Uncertainty,” by S. Balopoulou and M. Grigoriu, 12/23/97, (PB98-153422, A11, MF-A03).

NCEER-97-0016 “Evaluation of Seismic Retrofit Methods for Reinforced Concrete Bridge Columns,” by T.J. Wipf, F.W. Klaiber and F.M. Russo, 12/28/97, (PB98-144215, A12, MF-A03).

NCEER-97-0017 “Seismic Fragility of Existing Conventional Reinforced Concrete Highway Bridges,” by C.L. Mullen and A.S. Cakmak, 12/30/97, (PB98-153406, A08, MF-A02).

NCEER-97-0018 “Loss Asssessment of Memphis Buildings,” edited by D.P. Abrams and M. Shinozuka, 12/31/97, (PB98-144231, A13, MF-A03).

NCEER-97-0019 “Seismic Evaluation of Frames with Infill Walls Using Quasi-static Experiments,” by K.M. Mosalam, R.N. White and P. Gergely, 12/31/97, (PB98-153455, A07, MF-A02).

NCEER-97-0020 “Seismic Evaluation of Frames with Infill Walls Using Pseudo-dynamic Experiments,” by K.M. Mosalam, R.N. White and P. Gergely, 12/31/97, (PB98-153430, A07, MF-A02).

NCEER-97-0021 “Computational Strategies for Frames with Infill Walls: Discrete and Smeared Crack Analyses and Seismic Fragility,” by K.M. Mosalam, R.N. White and P. Gergely, 12/31/97, (PB98-153414, A10, MF-A02).

NCEER-97-0022 "Proceedings of the NCEER Workshop on Evaluation of Liquefaction Resistance of Soils," edited by T.L. Youd and I.M. Idriss, 12/31/97, (PB98-155617, A15, MF-A03).

MCEER-98-0001 "Extraction of Nonlinear Hysteretic Properties of Seismically Isolated Bridges from Quick-Release Field Tests," by Q. Chen, B.M. Douglas, E.M. Maragakis and I.G. Buckle, 5/26/98, (PB99-118838, A06, MF-A01).

MCEER-98-0002 "Methodologies for Evaluating the Importance of Highway Bridges," by A. Thomas, S. Eshenaur and J. Kulicki, 5/29/98, (PB99-118846, A10, MF-A02).

MCEER-98-0003 "Capacity Design of Bridge Piers and the Analysis of Overstrength," by J.B. Mander, A. Dutta and P. Goel, 6/1/98, (PB99-118853, A09, MF-A02).

MCEER-98-0004 "Evaluation of Bridge Damage Data from the Loma Prieta and Northridge, California Earthquakes," by N. Basoz and A. Kiremidjian, 6/2/98, (PB99-118861, A15, MF-A03).

MCEER-98-0005 "Screening Guide for Rapid Assessment of Liquefaction Hazard at Highway Bridge Sites," by T. L. Youd, 6/16/98, (PB99-118879, A06, not available on microfiche).

MCEER-98-0006 "Structural Steel and Steel/Concrete Interface Details for Bridges," by P. Ritchie, N. Kauhl and J. Kulicki, 7/13/98, (PB99-118945, A06, MF-A01).

MCEER-98-0007 "Capacity Design and Fatigue Analysis of Confined Concrete Columns," by A. Dutta and J.B. Mander, 7/14/98, (PB99-118960, A14, MF-A03).

MCEER-98-0008 "Proceedings of the Workshop on Performance Criteria for Telecommunication Services Under Earthquake Conditions," edited by A.J. Schiff, 7/15/98, (PB99-118952, A08, MF-A02).

MCEER-98-0009 "Fatigue Analysis of Unconfined Concrete Columns," by J.B. Mander, A. Dutta and J.H. Kim, 9/12/98, (PB99-123655, A10, MF-A02).

MCEER-98-0010 "Centrifuge Modeling of Cyclic Lateral Response of Pile-Cap Systems and Seat-Type Abutments in Dry Sands," by A.D. Gadre and R. Dobry, 10/2/98, (PB99-123606, A13, MF-A03).

MCEER-98-0011 "IDARC-BRIDGE: A Computational Platform for Seismic Damage Assessment of Bridge Structures," by A.M. Reinhorn, V. Simeonov, G. Mylonakis and Y. Reichman, 10/2/98, (PB99-162919, A15, MF-A03).

MCEER-98-0012 "Experimental Investigation of the Dynamic Response of Two Bridges Before and After Retrofitting with Elastomeric Bearings," by D.A. Wendichansky, S.S. Chen and J.B. Mander, 10/2/98, (PB99-162927, A15, MF-A03).

MCEER-98-0013 "Design Procedures for Hinge Restrainers and Hinge Sear Width for Multiple-Frame Bridges," by R. Des Roches and G.L. Fenves, 11/3/98, (PB99-140477, A13, MF-A03).

MCEER-98-0014 "Response Modification Factors for Seismically Isolated Bridges," by M.C. Constantinou and J.K. Quarshie, 11/3/98, (PB99-140485, A14, MF-A03).

MCEER-98-0015 "Proceedings of the U.S.-Italy Workshop on Seismic Protective Systems for Bridges," edited by I.M. Friedland and M.C. Constantinou, 11/3/98, (PB2000-101711, A22, MF-A04).

MCEER-98-0016 "Appropriate Seismic Reliability for Critical Equipment Systems: Recommendations Based on Regional Analysis of Financial and Life Loss," by K. Porter, C. Scawthorn, C. Taylor and N. Blais, 11/10/98, (PB99-157265, A08, MF-A02).

MCEER-98-0017 "Proceedings of the U.S. Japan Joint Seminar on Civil Infrastructure Systems Research," edited by M. Shinozuka and A. Rose, 11/12/98, (PB99-156713, A16, MF-A03).

MCEER-98-0018 "Modeling of Pile Footings and Drilled Shafts for Seismic Design," by I. PoLam, M. Kapuskar and D. Chaudhuri, 12/21/98, (PB99-157257, A09, MF-A02).

MCEER-99-0001 "Seismic Evaluation of a Masonry Infilled Reinforced Concrete Frame by Pseudodynamic Testing," by S.G. Buonopane and R.N. White, 2/16/99, (PB99-162851, A09, MF-A02).

MCEER-99-0002 "Response History Analysis of Structures with Seismic Isolation and Energy Dissipation Systems: Verification Examples for Program SAP2000," by J. Scheller and M.C. Constantinou, 2/22/99, (PB99-162869, A08, MF-A02).

MCEER-99-0003 "Experimental Study on the Seismic Design and Retrofit of Bridge Columns Including Axial Load Effects," by A. Dutta, T. Kokorina and J.B. Mander, 2/22/99, (PB99-162877, A09, MF-A02).

MCEER-99-0004 "Experimental Study of Bridge Elastomeric and Other Isolation and Energy Dissipation Systems with Emphasis on Uplift Prevention and High Velocity Near-source Seismic Excitation," by A. Kasalanati and M. C. Constantinou, 2/26/99, (PB99-162885, A12, MF-A03).

MCEER-99-0005 "Truss Modeling of Reinforced Concrete Shear-flexure Behavior," by J.H. Kim and J.B. Mander, 3/8/99, (PB99-163693, A12, MF-A03).

MCEER-99-0006 "Experimental Investigation and Computational Modeling of Seismic Response of a 1:4 Scale Model Steel Structure with a Load Balancing Supplemental Damping System," by G. Pekcan, J.B. Mander and S.S. Chen, 4/2/99, (PB99-162893, A11, MF-A03).

MCEER-99-0007 "Effect of Vertical Ground Motions on the Structural Response of Highway Bridges," by M.R. Button, C.J. Cronin and R.L. Mayes, 4/10/99, (PB2000-101411, A10, MF-A03).

MCEER-99-0008 "Seismic Reliability Assessment of Critical Facilities: A Handbook, Supporting Documentation, and Model Code Provisions," by G.S. Johnson, R.E. Sheppard, M.D. Quilici, S.J. Eder and C.R. Scawthorn, 4/12/99, (PB2000-101701, A18, MF-A04).

MCEER-99-0009 "Impact Assessment of Selected MCEER Highway Project Research on the Seismic Design of Highway Structures," by C. Rojahn, R. Mayes, D.G. Anderson, J.H. Clark, D'Appolonia Engineering, S. Gloyd and R.V. Nutt, 4/14/99, (PB99-162901, A10, MF-A02).

MCEER-99-0010 "Site Factors and Site Categories in Seismic Codes," by R. Dobry, R. Ramos and M.S. Power, 7/19/99, (PB2000-101705, A08, MF-A02).

MCEER-99-0011 "Restrainer Design Procedures for Multi-Span Simply-Supported Bridges," by M.J. Randall, M. Saiidi, E. Maragakis and T. Isakovic, 7/20/99, (PB2000-101702, A10, MF-A02).

MCEER-99-0012 "Property Modification Factors for Seismic Isolation Bearings," by M.C. Constantinou, P. Tsopelas, A. Kasalanati and E. Wolff, 7/20/99, (PB2000-103387, A11, MF-A03).

MCEER-99-0013 "Critical Seismic Issues for Existing Steel Bridges," by P. Ritchie, N. Kauhl and J. Kulicki, 7/20/99, (PB2000-101697, A09, MF-A02).

MCEER-99-0014 "Nonstructural Damage Database," by A. Kao, T.T. Soong and A. Vender, 7/24/99, (PB2000-101407, A06, MF-A01).

MCEER-99-0015 "Guide to Remedial Measures for Liquefaction Mitigation at Existing Highway Bridge Sites," by H.G. Cooke and J. K. Mitchell, 7/26/99, (PB2000-101703, A11, MF-A03).

MCEER-99-0016 "Proceedings of the MCEER Workshop on Ground Motion Methodologies for the Eastern United States," edited by N. Abrahamson and A. Becker, 8/11/99, (PB2000-103385, A07, MF-A02).

MCEER-99-0017 "Quindío, Colombia Earthquake of January 25, 1999: Reconnaissance Report," by A.P. Asfura and P.J. Flores, 10/4/99, (PB2000-106893, A06, MF-A01).

MCEER-99-0018 "Hysteretic Models for Cyclic Behavior of Deteriorating Inelastic Structures," by M.V. Sivaselvan and A.M. Reinhorn, 11/5/99, (PB2000-103386, A08, MF-A02).

MCEER-99-0019 "Proceedings of the 7th U.S.- Japan Workshop on Earthquake Resistant Design of Lifeline Facilities and Countermeasures Against Soil Liquefaction," edited by T.D. O'Rourke, J.P. Bardet and M. Hamada, 11/19/99, (PB2000-103354, A99, MF-A06).

MCEER-99-0020 "Development of Measurement Capability for Micro-Vibration Evaluations with Application to Chip Fabrication Facilities," by G.C. Lee, Z. Liang, J.W. Song, J.D. Shen and W.C. Liu, 12/1/99, (PB2000-105993, A08, MF-A02).

MCEER-99-0021 "Design and Retrofit Methodology for Building Structures with Supplemental Energy Dissipating Systems," by G. Pekcan, J.B. Mander and S.S. Chen, 12/31/99, (PB2000-105994, A11, MF-A03).

MCEER-00-0001 "The Marmara, Turkey Earthquake of August 17, 1999: Reconnaissance Report," edited by C. Scawthorn; with major contributions by M. Bruneau, R. Eguchi, T. Holzer, G. Johnson, J. Mander, J. Mitchell, W. Mitchell, A. Papageorgiou, C. Scaethorn, and G. Webb, 3/23/00, (PB2000-106200, A11, MF-A03).

MCEER-00-0002 "Proceedings of the MCEER Workshop for Seismic Hazard Mitigation of Health Care Facilities," edited by G.C. Lee, M. Ettouney, M. Grigoriu, J. Hauer and J. Nigg, 3/29/00, (PB2000-106892, A08, MF-A02).

MCEER-00-0003 "The Chi-Chi, Taiwan Earthquake of September 21, 1999: Reconnaissance Report," edited by G.C. Lee and C.H. Loh, with major contributions by G.C. Lee, M. Bruneau, I.G. Buckle, S.E. Chang, P.J. Flores, T.D. O'Rourke, M. Shinozuka, T.T. Soong, C-H. Loh, K-C. Chang, Z-J. Chen, J-S. Hwang, M-L. Lin, G-Y. Liu, K-C. Tsai, G.C. Yao and C-L. Yen, 4/30/00, (PB2001-100980, A10, MF-A02).

MCEER-00-0004 "Seismic Retrofit of End-Sway Frames of Steel Deck-Truss Bridges with a Supplemental Tendon System: Experimental and Analytical Investigation," by G. Pekcan, J.B. Mander and S.S. Chen, 7/1/00, (PB2001-100982, A10, MF-A02).

MCEER-00-0005 "Sliding Fragility of Unrestrained Equipment in Critical Facilities," by W.H. Chong and T.T. Soong, 7/5/00, (PB2001-100983, A08, MF-A02).

MCEER-00-0006 "Seismic Response of Reinforced Concrete Bridge Pier Walls in the Weak Direction," by N. Abo-Shadi, M. Saiidi and D. Sanders, 7/17/00, (PB2001-100981, A17, MF-A03).

MCEER-00-0007 "Low-Cycle Fatigue Behavior of Longitudinal Reinforcement in Reinforced Concrete Bridge Columns," by J. Brown and S.K. Kunnath, 7/23/00, (PB2001-104392, A08, MF-A02).

MCEER-00-0008 "Soil Structure Interaction of Bridges for Seismic Analysis," I. PoLam and H. Law, 9/25/00, (PB2001-105397, A08, MF-A02).

MCEER-00-0009 "Proceedings of the First MCEER Workshop on Mitigation of Earthquake Disaster by Advanced Technologies (MEDAT-1), edited by M. Shinozuka, D.J. Inman and T.D. O'Rourke, 11/10/00, (PB2001-105399, A14, MF-A03).

MCEER-00-0010 "Development and Evaluation of Simplified Procedures for Analysis and Design of Buildings with Passive Energy Dissipation Systems, Revision 01," by O.M. Ramirez, M.C. Constantinou, C.A. Kircher, A.S. Whittaker, M.W. Johnson, J.D. Gomez and C. Chrysostomou, 11/16/01, (PB2001-105523, A23, MF-A04).

MCEER-00-0011 "Dynamic Soil-Foundation-Structure Interaction Analyses of Large Caissons," by C-Y. Chang, C-M. Mok, Z-L. Wang, R. Settgast, F. Waggoner, M.A. Ketchum, H.M. Gonnermann and C-C. Chin, 12/30/00, (PB2001-104373, A07, MF-A02).

MCEER-00-0012 "Experimental Evaluation of Seismic Performance of Bridge Restrainers," by A.G. Vlassis, E.M. Maragakis and M. Saiid Saiidi, 12/30/00, (PB2001-104354, A09, MF-A02).

MCEER-00-0013 "Effect of Spatial Variation of Ground Motion on Highway Structures," by M. Shinozuka, V. Saxena and G. Deodatis, 12/31/00, (PB2001-108755, A13, MF-A03).

MCEER-00-0014 "A Risk-Based Methodology for Assessing the Seismic Performance of Highway Systems," by S.D. Werner, C.E. Taylor, J.E. Moore, II, J.S. Walton and S. Cho, 12/31/00, (PB2001-108756, A14, MF-A03).

MCEER-01-0001 "Experimental Investigation of P-Delta Effects to Collapse During Earthquakes," by D. Vian and M. Bruneau, 6/25/01, (PB2002-100534, A17, MF-A03).

MCEER-01-0002 "Proceedings of the Second MCEER Workshop on Mitigation of Earthquake Disaster by Advanced Technologies (MEDAT-2)," edited by M. Bruneau and D.J. Inman, 7/23/01, (PB2002-100434, A16, MF-A03).

MCEER-01-0003 "Sensitivity Analysis of Dynamic Systems Subjected to Seismic Loads," by C. Roth and M. Grigoriu, 9/18/01, (PB2003-100884, A12, MF-A03).

MCEER-01-0004 "Overcoming Obstacles to Implementing Earthquake Hazard Mitigation Policies: Stage 1 Report," by D.J. Alesch and W.J. Petak, 12/17/01, (PB2002-107949, A07, MF-A02).

MCEER-01-0005 "Updating Real-Time Earthquake Loss Estimates: Methods, Problems and Insights," by C.E. Taylor, S.E. Chang and R.T. Eguchi, 12/17/01, (PB2002-107948, A05, MF-A01).

MCEER-01-0006 "Experimental Investigation and Retrofit of Steel Pile Foundations and Pile Bents Under Cyclic Lateral Loadings," by A. Shama, J. Mander, B. Blabac and S. Chen, 12/31/01, (PB2002-107950, A13, MF-A03).

MCEER-02-0001 "Assessment of Performance of Bolu Viaduct in the 1999 Duzce Earthquake in Turkey" by P.C. Roussis, M.C. Constantinou, M. Erdik, E. Durukal and M. Dicleli, 5/8/02, (PB2003-100883, A08, MF-A02).

MCEER-02-0002 "Seismic Behavior of Rail Counterweight Systems of Elevators in Buildings," by M.P. Singh, Rildova and L.E. Suarez, 5/27/02. (PB2003-100882, A11, MF-A03).

MCEER-02-0003 "Development of Analysis and Design Procedures for Spread Footings," by G. Mylonakis, G. Gazetas, S. Nikolaou and A. Chauncey, 10/02/02, (PB2004-101636, A13, MF-A03, CD-A13).

MCEER-02-0004 "Bare-Earth Algorithms for Use with SAR and LIDAR Digital Elevation Models," by C.K. Huyck, R.T. Eguchi and B. Houshmand, 10/16/02, (PB2004-101637, A07, CD-A07).

MCEER-02-0005 "Review of Energy Dissipation of Compression Members in Concentrically Braced Frames," by K.Lee and M. Bruneau, 10/18/02, (PB2004-101638, A10, CD-A10).

MCEER-03-0001 "Experimental Investigation of Light-Gauge Steel Plate Shear Walls for the Seismic Retrofit of Buildings" by J. Berman and M. Bruneau, 5/2/03, (PB2004-101622, A10, MF-A03, CD-A10).

MCEER-03-0002 "Statistical Analysis of Fragility Curves," by M. Shinozuka, M.Q. Feng, H. Kim, T. Uzawa and T. Ueda, 6/16/03, (PB2004-101849, A09, CD-A09).

MCEER-03-0003 "Proceedings of the Eighth U.S.-Japan Workshop on Earthquake Resistant Design f Lifeline Facilities and Countermeasures Against Liquefaction," edited by M. Hamada, J.P. Bardet and T.D. O'Rourke, 6/30/03, (PB2004-104386, A99, CD-A99).

MCEER-03-0004 "Proceedings of the PRC-US Workshop on Seismic Analysis and Design of Special Bridges," edited by L.C. Fan and G.C. Lee, 7/15/03, (PB2004-104387, A14, CD-A14).

MCEER-03-0005 "Urban Disaster Recovery: A Framework and Simulation Model," by S.B. Miles and S.E. Chang, 7/25/03, (PB2004-104388, A07, CD-A07).

MCEER-03-0006 "Behavior of Underground Piping Joints Due to Static and Dynamic Loading," by R.D. Meis, M. Maragakis and R. Siddharthan, 11/17/03, (PB2005-102194, A13, MF-A03, CD-A00).

MCEER-04-0001 "Experimental Study of Seismic Isolation Systems with Emphasis on Secondary System Response and Verification of Accuracy of Dynamic Response History Analysis Methods," by E. Wolff and M. Constantinou, 1/16/04 (PB2005-102195, A99, MF-E08, CD-A00).

MCEER-04-0002 "Tension, Compression and Cyclic Testing of Engineered Cementitious Composite Materials," by K. Kesner and S.L. Billington, 3/1/04, (PB2005-102196, A08, CD-A08).

MCEER-04-0003 "Cyclic Testing of Braces Laterally Restrained by Steel Studs to Enhance Performance During Earthquakes," by O.C. Celik, J.W. Berman and M. Bruneau, 3/16/04, (PB2005-102197, A13, MF-A03, CD-A00).

MCEER-04-0004 "Methodologies for Post Earthquake Building Damage Detection Using SAR and Optical Remote Sensing: Application to the August 17, 1999 Marmara, Turkey Earthquake," by C.K. Huyck, B.J. Adams, S. Cho, R.T. Eguchi, B. Mansouri and B. Houshmand, 6/15/04, (PB2005-104888, A10, CD-A00).

MCEER-04-0005 "Nonlinear Structural Analysis Towards Collapse Simulation: A Dynamical Systems Approach," by M.V. Sivaselvan and A.M. Reinhorn, 6/16/04, (PB2005-104889, A11, MF-A03, CD-A00).

MCEER-04-0006 "Proceedings of the Second PRC-US Workshop on Seismic Analysis and Design of Special Bridges," edited by G.C. Lee and L.C. Fan, 6/25/04, (PB2005-104890, A16, CD-A00).

MCEER-04-0007 "Seismic Vulnerability Evaluation of Axially Loaded Steel Built-up Laced Members," by K. Lee and M. Bruneau, 6/30/04, (PB2005-104891, A16, CD-A00).

MCEER-04-0008 "Evaluation of Accuracy of Simplified Methods of Analysis and Design of Buildings with Damping Systems for Near-Fault and for Soft-Soil Seismic Motions," by E.A. Pavlou and M.C. Constantinou, 8/16/04, (PB2005-104892, A08, MF-A02, CD-A00).

MCEER-04-0009 "Assessment of Geotechnical Issues in Acute Care Facilities in California," by M. Lew, T.D. O'Rourke, R. Dobry and M. Koch, 9/15/04, (PB2005-104893, A08, CD-A00).

MCEER-04-0010 "Scissor-Jack-Damper Energy Dissipation System," by A.N. Sigaher-Boyle and M.C. Constantinou, 12/1/04 (PB2005-108221).

MCEER-04-0011 "Seismic Retrofit of Bridge Steel Truss Piers Using a Controlled Rocking Approach," by M. Pollino and M. Bruneau, 12/20/04 (PB2006-105795).

MCEER-05-0001 "Experimental and Analytical Studies of Structures Seismically Isolated with an Uplift-Restraint Isolation System," by P.C. Roussis and M.C. Constantinou, 1/10/05 (PB2005-108222).

MCEER-05-0002 "A Versatile Experimentation Model for Study of Structures Near Collapse Applied to Seismic Evaluation of Irregular Structures," by D. Kusumastuti, A.M. Reinhorn and A. Rutenberg, 3/31/05 (PB2006-101523).

MCEER-05-0003 "Proceedings of the Third PRC-US Workshop on Seismic Analysis and Design of Special Bridges," edited by L.C. Fan and G.C. Lee, 4/20/05, (PB2006-105796).

MCEER-05-0004 "Approaches for the Seismic Retrofit of Braced Steel Bridge Piers and Proof-of-Concept Testing of an Eccentrically Braced Frame with Tubular Link," by J.W. Berman and M. Bruneau, 4/21/05 (PB2006-101524).

MCEER-05-0005 "Simulation of Strong Ground Motions for Seismic Fragility Evaluation of Nonstructural Components in Hospitals," by A. Wanitkorkul and A. Filiatrault, 5/26/05 (PB2006-500027).

MCEER-05-0006 "Seismic Safety in California Hospitals: Assessing an Attempt to Accelerate the Replacement or Seismic Retrofit of Older Hospital Facilities," by D.J. Alesch, L.A. Arendt and W.J. Petak, 6/6/05 (PB2006-105794).

MCEER-05-0007 "Development of Seismic Strengthening and Retrofit Strategies for Critical Facilities Using Engineered Cementitious Composite Materials," by K. Kesner and S.L. Billington, 8/29/05 (PB2006-111701).

MCEER-05-0008 "Experimental and Analytical Studies of Base Isolation Systems for Seismic Protection of Power Transformers," by N. Murota, M.Q. Feng and G-Y. Liu, 9/30/05 (PB2006-111702).

MCEER-05-0009 "3D-BASIS-ME-MB: Computer Program for Nonlinear Dynamic Analysis of Seismically Isolated Structures," by P.C. Tsopelas, P.C. Roussis, M.C. Constantinou, R. Buchanan and A.M. Reinhorn, 10/3/05 (PB2006-111703).

MCEER-05-0010 "Steel Plate Shear Walls for Seismic Design and Retrofit of Building Structures," by D. Vian and M. Bruneau, 12/15/05 (PB2006-111704).

MCEER-05-0011 "The Performance-Based Design Paradigm," by M.J. Astrella and A. Whittaker, 12/15/05 (PB2006-111705).

MCEER-06-0001 "Seismic Fragility of Suspended Ceiling Systems," H. Badillo-Almaraz, A.S. Whittaker, A.M. Reinhorn and G.P. Cimellaro, 2/4/06 (PB2006-111706).

MCEER-06-0002 "Multi-Dimensional Fragility of Structures," by G.P. Cimellaro, A.M. Reinhorn and M. Bruneau, 3/1/06 (PB2007-106974, A09, MF-A02, CD A00).

MCEER-06-0003 "Built-Up Shear Links as Energy Dissipators for Seismic Protection of Bridges," by P. Dusicka, A.M. Itani and I.G. Buckle, 3/15/06 (PB2006-111708).

MCEER-06-0004 "Analytical Investigation of the Structural Fuse Concept," by R.E. Vargas and M. Bruneau, 3/16/06 (PB2006-111709).

MCEER-06-0005 "Experimental Investigation of the Structural Fuse Concept," by R.E. Vargas and M. Bruneau, 3/17/06 (PB2006-111710).

MCEER-06-0006 "Further Development of Tubular Eccentrically Braced Frame Links for the Seismic Retrofit of Braced Steel Truss Bridge Piers," by J.W. Berman and M. Bruneau, 3/27/06 (PB2007-105147).

MCEER-06-0007 "REDARS Validation Report," by S. Cho, C.K. Huyck, S. Ghosh and R.T. Eguchi, 8/8/06 (PB2007-106983).

MCEER-06-0008 "Review of Current NDE Technologies for Post-Earthquake Assessment of Retrofitted Bridge Columns," by J.W. Song, Z. Liang and G.C. Lee, 8/21/06 (PB2007-106984).

MCEER-06-0009 "Liquefaction Remediation in Silty Soils Using Dynamic Compaction and Stone Columns," by S. Thevanayagam, G.R. Martin, R. Nashed, T. Shenthan, T. Kanagalingam and N. Ecemis, 8/28/06 (PB2007-106985).

MCEER-06-0010 "Conceptual Design and Experimental Investigation of Polymer Matrix Composite Infill Panels for Seismic Retrofitting," by W. Jung, M. Chiewanichakorn and A.J. Aref, 9/21/06 (PB2007-106986).

MCEER-06-0011 "A Study of the Coupled Horizontal-Vertical Behavior of Elastomeric and Lead-Rubber Seismic Isolation Bearings," by G.P. Warn and A.S. Whittaker, 9/22/06 (PB2007-108679).

MCEER-06-0012 "Proceedings of the Fourth PRC-US Workshop on Seismic Analysis and Design of Special Bridges: Advancing Bridge Technologies in Research, Design, Construction and Preservation," Edited by L.C. Fan, G.C. Lee and L. Ziang, 10/12/06 (PB2007-109042).

MCEER-06-0013 "Cyclic Response and Low Cycle Fatigue Characteristics of Plate Steels," by P. Dusicka, A.M. Itani and I.G. Buckle, 11/1/06 06 (PB2007-106987).

MCEER-06-0014 "Proceedings of the Second US-Taiwan Bridge Engineering Workshop," edited by W.P. Yen, J. Shen, J-Y. Chen and M. Wang, 11/15/06 (PB2008-500041).

MCEER-06-0015 "User Manual and Technical Documentation for the REDARS^{TM} Import Wizard," by S. Cho, S. Ghosh, C.K. Huyck and S.D. Werner, 11/30/06 (PB2007-114766).

MCEER-06-0016 "Hazard Mitigation Strategy and Monitoring Technologies for Urban and Infrastructure Public Buildings: Proceedings of the China-US Workshops," edited by X.Y. Zhou, A.L. Zhang, G.C. Lee and M. Tong, 12/12/06 (PB2008-500018).

MCEER-07-0001 "Static and Kinetic Coefficients of Friction for Rigid Blocks," by C. Kafali, S. Fathali, M. Grigoriu and A.S. Whittaker, 3/20/07 (PB2007-114767).

MCEER-07-0002 "Hazard Mitigation Investment Decision Making: Organizational Response to Legislative Mandate," by L.A. Arendt, D.J. Alesch and W.J. Petak, 4/9/07 (PB2007-114768).

MCEER-07-0003 "Seismic Behavior of Bidirectional-Resistant Ductile End Diaphragms with Unbonded Braces in Straight or Skewed Steel Bridges," by O. Celik and M. Bruneau, 4/11/07 (PB2008-105141).

MCEER-07-0004 "Modeling Pile Behavior in Large Pile Groups Under Lateral Loading," by A.M. Dodds and G.R. Martin, 4/16/07(PB2008-105142).

MCEER-07-0005 "Experimental Investigation of Blast Performance of Seismically Resistant Concrete-Filled Steel Tube Bridge Piers," by S. Fujikura, M. Bruneau and D. Lopez-Garcia, 4/20/07 (PB2008-105143).

MCEER-07-0006 "Seismic Analysis of Conventional and Isolated Liquefied Natural Gas Tanks Using Mechanical Analogs," by I.P. Christovasilis and A.S. Whittaker, 5/1/07.

MCEER-07-0007 "Experimental Seismic Performance Evaluation of Isolation/Restraint Systems for Mechanical Equipment – Part 1: Heavy Equipment Study," by S. Fathali and A. Filiatrault, 6/6/07 (PB2008-105144).

MCEER-07-0008 "Seismic Vulnerability of Timber Bridges and Timber Substructures," by A.A. Sharma, J.B. Mander, I.M. Friedland and D.R. Allicock, 6/7/07 (PB2008-105145).

MCEER-07-0009 "Experimental and Analytical Study of the XY-Friction Pendulum (XY-FP) Bearing for Bridge Applications," by C.C. Marin-Artieda, A.S. Whittaker and M.C. Constantinou, 6/7/07 (PB2008-105191).

MCEER-07-0010 "Proceedings of the PRC-US Earthquake Engineering Forum for Young Researchers," Edited by G.C. Lee and X.Z. Qi, 6/8/07 (PB2008-500058).

MCEER-07-0011 "Design Recommendations for Perforated Steel Plate Shear Walls," by R. Purba and M. Bruneau, 6/18/07, (PB2008-105192).

MCEER-07-0012 "Performance of Seismic Isolation Hardware Under Service and Seismic Loading," by M.C. Constantinou, A.S. Whittaker, Y. Kalpakidis, D.M. Fenz and G.P. Warn, 8/27/07, (PB2008-105193).

MCEER-07-0013 "Experimental Evaluation of the Seismic Performance of Hospital Piping Subassemblies," by E.R. Goodwin, E. Maragakis and A.M. Itani, 9/4/07, (PB2008-105194).

MCEER-07-0014 "A Simulation Model of Urban Disaster Recovery and Resilience: Implementation for the 1994 Northridge Earthquake," by S. Miles and S.E. Chang, 9/7/07, (PB2008-106426).

MCEER-07-0015 "Statistical and Mechanistic Fragility Analysis of Concrete Bridges," by M. Shinozuka, S. Banerjee and S-H. Kim, 9/10/07, (PB2008-106427).

MCEER-07-0016 "Three-Dimensional Modeling of Inelastic Buckling in Frame Structures," by M. Schachter and AM. Reinhorn, 9/13/07, (PB2008-108125).

MCEER-07-0017 "Modeling of Seismic Wave Scattering on Pile Groups and Caissons," by I. Po Lam, H. Law and C.T. Yang, 9/17/07 (PB2008-108150).

MCEER-07-0018 "Bridge Foundations: Modeling Large Pile Groups and Caissons for Seismic Design," by I. Po Lam, H. Law and G.R. Martin (Coordinating Author), 12/1/07 (PB2008-111190).

MCEER-07-0019 "Principles and Performance of Roller Seismic Isolation Bearings for Highway Bridges," by G.C. Lee, Y.C. Ou, Z. Liang, T.C. Niu and J. Song, 12/10/07 (PB2009-110466).

MCEER-07-0020 "Centrifuge Modeling of Permeability and Pinning Reinforcement Effects on Pile Response to Lateral Spreading," by L.L Gonzalez-Lagos, T. Abdoun and R. Dobry, 12/10/07 (PB2008-111191).

MCEER-07-0021 "Damage to the Highway System from the Pisco, Perú Earthquake of August 15, 2007," by J.S. O'Connor, L. Mesa and M. Nykamp, 12/10/07, (PB2008-108126).

MCEER-07-0022 "Experimental Seismic Performance Evaluation of Isolation/Restraint Systems for Mechanical Equipment – Part 2: Light Equipment Study," by S. Fathali and A. Filiatrault, 12/13/07 (PB2008-111192).

MCEER-07-0023 "Fragility Considerations in Highway Bridge Design," by M. Shinozuka, S. Banerjee and S.H. Kim, 12/14/07 (PB2008-111193).

MCEER-07-0024 "Performance Estimates for Seismically Isolated Bridges," by G.P. Warn and A.S. Whittaker, 12/30/07 (PB2008-112230).

MCEER-08-0001 "Seismic Performance of Steel Girder Bridge Superstructures with Conventional Cross Frames," by L.P. Carden, A.M. Itani and I.G. Buckle, 1/7/08, (PB2008-112231).

MCEER-08-0002 "Seismic Performance of Steel Girder Bridge Superstructures with Ductile End Cross Frames with Seismic Isolators," by L.P. Carden, A.M. Itani and I.G. Buckle, 1/7/08 (PB2008-112232).

MCEER-08-0003 "Analytical and Experimental Investigation of a Controlled Rocking Approach for Seismic Protection of Bridge Steel Truss Piers," by M. Pollino and M. Bruneau, 1/21/08 (PB2008-112233).

MCEER-08-0004 "Linking Lifeline Infrastructure Performance and Community Disaster Resilience: Models and Multi-Stakeholder Processes," by S.E. Chang, C. Pasion, K. Tatebe and R. Ahmad, 3/3/08 (PB2008-112234).

MCEER-08-0005 "Modal Analysis of Generally Damped Linear Structures Subjected to Seismic Excitations," by J. Song, Y-L. Chu, Z. Liang and G.C. Lee, 3/4/08 (PB2009-102311).

MCEER-08-0006 "System Performance Under Multi-Hazard Environments," by C. Kafali and M. Grigoriu, 3/4/08 (PB2008-112235).

MCEER-08-0007 "Mechanical Behavior of Multi-Spherical Sliding Bearings," by D.M. Fenz and M.C. Constantinou, 3/6/08 (PB2008-112236).

MCEER-08-0008 "Post-Earthquake Restoration of the Los Angeles Water Supply System," by T.H.P. Tabucchi and R.A. Davidson, 3/7/08 (PB2008-112237).

MCEER-08-0009 "Fragility Analysis of Water Supply Systems," by A. Jacobson and M. Grigoriu, 3/10/08 (PB2009-105545).

MCEER-08-0010 "Experimental Investigation of Full-Scale Two-Story Steel Plate Shear Walls with Reduced Beam Section Connections," by B. Qu, M. Bruneau, C-H. Lin and K-C. Tsai, 3/17/08 (PB2009-106368).

MCEER-08-0011 "Seismic Evaluation and Rehabilitation of Critical Components of Electrical Power Systems," S. Ersoy, B. Feizi, A. Ashrafi and M. Ala Saadeghvaziri, 3/17/08 (PB2009-105546).

MCEER-08-0012 "Seismic Behavior and Design of Boundary Frame Members of Steel Plate Shear Walls," by B. Qu and M. Bruneau, 4/26/08 . (PB2009-106744).

MCEER-08-0013 "Development and Appraisal of a Numerical Cyclic Loading Protocol for Quantifying Building System Performance," by A. Filiatrault, A. Wanitkorkul and M. Constantinou, 4/27/08 (PB2009-107906).

MCEER-08-0014 "Structural and Nonstructural Earthquake Design: The Challenge of Integrating Specialty Areas in Designing Complex, Critical Facilities," by W.J. Petak and D.J. Alesch, 4/30/08 (PB2009-107907).

MCEER-08-0015 "Seismic Performance Evaluation of Water Systems," by Y. Wang and T.D. O'Rourke, 5/5/08 (PB2009-107908).

MCEER-08-0016 "Seismic Response Modeling of Water Supply Systems," by P. Shi and T.D. O'Rourke, 5/5/08 (PB2009-107910).

MCEER-08-0017 "Numerical and Experimental Studies of Self-Centering Post-Tensioned Steel Frames," by D. Wang and A. Filiatrault, 5/12/08 (PB2009-110479).

MCEER-08-0018 "Development, Implementation and Verification of Dynamic Analysis Models for Multi-Spherical Sliding Bearings," by D.M. Fenz and M.C. Constantinou, 8/15/08 (PB2009-107911).

MCEER-08-0019 "Performance Assessment of Conventional and Base Isolated Nuclear Power Plants for Earthquake Blast Loadings," by Y.N. Huang, A.S. Whittaker and N. Luco, 10/28/08 (PB2009-107912).

MCEER-08-0020 "Remote Sensing for Resilient Multi-Hazard Disaster Response – Volume I: Introduction to Damage Assessment Methodologies," by B.J. Adams and R.T. Eguchi, 11/17/08 (PB2010-102695).

MCEER-08-0021 "Remote Sensing for Resilient Multi-Hazard Disaster Response – Volume II: Counting the Number of Collapsed Buildings Using an Object-Oriented Analysis: Case Study of the 2003 Bam Earthquake," by L. Gusella, C.K. Huyck and B.J. Adams, 11/17/08 (PB2010-100925).

MCEER-08-0022 "Remote Sensing for Resilient Multi-Hazard Disaster Response – Volume III: Multi-Sensor Image Fusion Techniques for Robust Neighborhood-Scale Urban Damage Assessment," by B.J. Adams and A. McMillan, 11/17/08 (PB2010-100926).

MCEER-08-0023 "Remote Sensing for Resilient Multi-Hazard Disaster Response – Volume IV: A Study of Multi-Temporal and Multi-Resolution SAR Imagery for Post-Katrina Flood Monitoring in New Orleans," by A. McMillan, J.G. Morley, B.J. Adams and S. Chesworth, 11/17/08 (PB2010-100927).

MCEER-08-0024 "Remote Sensing for Resilient Multi-Hazard Disaster Response – Volume V: Integration of Remote Sensing Imagery and VIEWS^{TM} Field Data for Post-Hurricane Charley Building Damage Assessment," by J.A. Womble, K. Mehta and B.J. Adams, 11/17/08 (PB2009-115532).

MCEER-08-0025 "Building Inventory Compilation for Disaster Management: Application of Remote Sensing and Statistical Modeling," by P. Sarabandi, A.S. Kiremidjian, R.T. Eguchi and B. J. Adams, 11/20/08 (PB2009-110484).

MCEER-08-0026 "New Experimental Capabilities and Loading Protocols for Seismic Qualification and Fragility Assessment of Nonstructural Systems," by R. Retamales, G. Mosqueda, A. Filiatrault and A. Reinhorn, 11/24/08 (PB2009-110485).

MCEER-08-0027 "Effects of Heating and Load History on the Behavior of Lead-Rubber Bearings," by I.V. Kalpakidis and M.C. Constantinou, 12/1/08 (PB2009-115533).

MCEER-08-0028 "Experimental and Analytical Investigation of Blast Performance of Seismically Resistant Bridge Piers," by S.Fujikura and M. Bruneau, 12/8/08 (PB2009-115534).

MCEER-08-0029 "Evolutionary Methodology for Aseismic Decision Support," by Y. Hu and G. Dargush, 12/15/08.

MCEER-08-0030 "Development of a Steel Plate Shear Wall Bridge Pier System Conceived from a Multi-Hazard Perspective," by D. Keller and M. Bruneau, 12/19/08 (PB2010-102696).

MCEER-09-0001 "Modal Analysis of Arbitrarily Damped Three-Dimensional Linear Structures Subjected to Seismic Excitations," by Y.L. Chu, J. Song and G.C. Lee, 1/31/09 (PB2010-100922).

MCEER-09-0002 "Air-Blast Effects on Structural Shapes," by G. Ballantyne, A.S. Whittaker, A.J. Aref and G.F. Dargush, 2/2/09 (PB2010-102697).

MCEER-09-0003 "Water Supply Performance During Earthquakes and Extreme Events," by A.L. Bonneau and T.D. O'Rourke, 2/16/09 (PB2010-100923).

MCEER-09-0004 "Generalized Linear (Mixed) Models of Post-Earthquake Ignitions," by R.A. Davidson, 7/20/09 (PB2010-102698).

MCEER-09-0005 "Seismic Testing of a Full-Scale Two-Story Light-Frame Wood Building: NEESWood Benchmark Test," by I.P. Christovasilis, A. Filiatrault and A. Wanitkorkul, 7/22/09.

MCEER-09-0006 "IDARC2D Version 7.0: A Program for the Inelastic Damage Analysis of Structures," by A.M. Reinhorn, H. Roh, M. Sivaselvan, S.K. Kunnath, R.E. Valles, A. Madan, C. Li, R. Lobo and Y.J. Park, 7/28/09 (PB2010-103199).

MCEER-09-0007 "Enhancements to Hospital Resiliency: Improving Emergency Planning for and Response to Hurricanes," by D.B. Hess and L.A. Arendt, 7/30/09 (PB2010-100924).

MCEER-09-0008 "Assessment of Base-Isolated Nuclear Structures for Design and Beyond-Design Basis Earthquake Shaking," by Y.N. Huang, A.S. Whittaker, R.P. Kennedy and R.L. Mayes, 8/20/09 (PB2010-102699).

MCEER-09-0009 "Quantification of Disaster Resilience of Health Care Facilities," by G.P. Cimellaro, C. Fumo, A.M Reinhorn and M. Bruneau, 9/14/09.

MCEER-09-0010 "Performance-Based Assessment and Design of Squat Reinforced Concrete Shear Walls," by C.K. Gulec and A.S. Whittaker, 9/15/09 (PB2010-102700).

MCEER-09-0011 "Proceedings of the Fourth US-Taiwan Bridge Engineering Workshop," edited by W.P. Yen, J.J. Shen, T.M. Lee and R.B. Zheng, 10/27/09 (PB2010-500009).

MCEER-09-0012 "Proceedings of the Special International Workshop on Seismic Connection Details for Segmental Bridge Construction," edited by W. Phillip Yen and George C. Lee, 12/21/09.

MCEER-10-0001 "Direct Displacement Procedure for Performance-Based Seismic Design of Multistory Woodframe Structures," by W. Pang and D. Rosowsky, 4/26/10.

MCEER-10-0002 "Simplified Direct Displacement Design of Six-Story NEESWood Capstone Building and Pre-Test Seismic Performance Assessment," by W. Pang, D. Rosowsky, J. van de Lindt and S. Pei, 5/28/10.

MCEER-10-0003 "Integration of Seismic Protection Systems in Performance-Based Seismic Design of Woodframed Structures," by J.K. Shinde and M.D. Symans, 6/18/10.

MCEER
EARTHQUAKE ENGINEERING TO EXTREME EVENTS
University at Buffalo, The State University of New York
Red Jacket Quadrangle ▪ Buffalo, New York 14261
Phone: (716) 645-3391 ▪ Fax: (716) 645-3399
E-mail: *mceer@buffalo.edu* ▪ WWW Site *http://mceer.buffalo.edu*
University at Buffalo *The State University of New York*
ISSN 1520-295X